Technical Report Documentation Page

| 1. Report No. | 2. Government Accession No. | 3. Recipient's Catalog No. |
|---|---|---|
| FHWA/TX-1995/1243-2 | | |

| 4. Title and Subtitle | 5. Report Date |
|---|---|
| EFFECTS OF IRREGULARITIES ON THE DYNAMIC RESPONSE OF PAVEMENTS IN NON-DESTRUCTIVE TESTING | December 1994 |
| | 6. Performing Organization Code |

| 7. Author(s) | 8. Performing Organization Report No. |
|---|---|
| Chine Chung Chiang, Jose M. Roesset, and Kenneth H. Stokoe, II | Research Report 1243-2 |

| 9. Performing Organization Name and Address | 10. Work Unit No. (TRAIS) |
|---|---|
| Center for Transportation Research<br>The University of Texas at Austin<br>3208 Red River, Suite 200<br>Austin, Texas 78705-2650 | 11. Contract or Grant No.<br>Research Study 0-1243 |
| | 13. Type of Report and Period Covered<br>Interim |
| 12. Sponsoring Agency Name and Address<br>Texas Department of Transportation<br>Research and Technology Transfer Office<br>P. O. Box 5080<br>Austin, Texas 78763-5080 | 14. Sponsoring Agency Code |

15. Supplementary Notes

Study conducted in cooperation with the U.S. Department of Transportation, Federal Highway Administration. Research study title: "Automated Equipment for Characterizing the Properties and Thicknesses of Pavements"

16. Abstract

A computer program using finite elements was developed to simulate the response of defective pavements (i.e., pavements with horizontal delaminations, voids of different sizes, and vertical cracks) to dynamic loads applied at the surface. The solution of the finite element model is carried out in the time domain to obtain transient responses and steady-state amplitudes. These are easily obtained by applying the Fast Fourier Transform to the transient responses. The results obtained with this procedure were compared with those computed directly in the frequency domain with a boundary element formulation. The effect of horizontal delaminations, voids, and vertical cracks on the motions that would be recorded at the surface when an impulse is applied (also at the surface) was investigated. It was found that voids and delaminations can be easily recognized, if they are not too deep or at the interface of two layers with very different elastic properties. The impulse excites frequencies in one of two ranges: the first range corresponds to flexural waves traveling along the surface; the second to more traditional P waves traveling up and down. Each range offers some advantages and disadvantages. The flexural range provides a larger contrast and, therefore, easier identification when applicable. Vertical cracks have also a clear signature when they are surface piercing; they are, however, difficult to detect with the methods explored here when they are at depth and do not reach the surface.

| 17. Key Words | 18. Distribution Statement |
|---|---|
| Non-destructive pavement testing, voids, delaminations, finite element modeling | No restrictions. This document is available to the public through the National Technical Information Service, Springfield, Virginia 22161. |

| 19. Security Classif. (of this report) | 20. Security Classif. (of this page) | 21. No. of Pages | 22. Price |
|---|---|---|---|
| Unclassified | Unclassified | 230 | |

# EFFECTS OF IRREGULARITIES ON THE DYNAMIC RESPONSE OF PAVEMENTS IN NON-DESTRUCTIVE TESTING

by

Chine Chung Chiang
Jose M. Roesset
Kenneth H. Stokoe, II

Research Report 1243-2

Research Project 0-1243
Automated Equipment for Characterizing the
Properties and Thicknesses of Pavements

conducted for the

**Texas Department of Transportation**

in cooperation with the

**U.S. Department of Transportation**
**Federal Highway Administration**

by the

**CENTER FOR TRANSPORTATION RESEARCH**
**Bureau of Engineering Research**
**THE UNIVERSITY OF TEXAS AT AUSTIN**

December 1994

## IMPLEMENTATION STATEMENT

The results of parametric studies conducted under this project indicate the possibility of detecting voids or delaminations within a pavement from recordings of motions at the surface. If an impulse is applied at the surface by moving equipment, the records obtained by a receiver adjacent to the load, at a distance of 8 to 15 cm (3 to 6 inches) will exhibit clear changes as the receiver moves over a zone with a delamination. These changes are apparent both in the time records and in their frequency spectra obtained applying the Fast Fourier Transform. They are particularly noticeable in two ranges of frequencies: one related to P waves traveling up and down and reflecting at the interface of the delamination, the other associated with flexural waves. The P frequency changes with the depth of the defect but is independent of the horizontal extent. The flexural frequency, on the other hand, is a function of the horizontal dimension of the irregularity but insensitive to its depth. In general, the flexural wave frequency range provides clearer images (more distinct variations due to the presence of the void or delamination). This implies that the duration of the applied pulse should be selected so as to excite the particular range of frequencies of interest. As the depth increases, the effects become less pronounced and more difficult to distinguish. It is also difficult to detect delaminations that would occur at the interface between two layers with very different elastic properties (particularly a stiff layer over a softer one). Vertical cracks that extend to the surface have again a clear and easily recognized signature on recorded signals as the receiver approaches and moves over the crack; however, vertical cracks at some depth that are not surface piercing are difficult to identify using the methods explored here.

Prepared in cooperation with the Texas Department of Transportation and the U.S. Department of Transportation, Federal Highway Administration.

## DISCLAIMERS

The content of this report reflect the views of the authors, who are responsible for the facts and the accuracy of the data presented herein. The contents do not necessarily reflect the official views or policies of the Federal Highway Administration or the Texas Department of Transportation. This report does not constitute a standard, specification, or regulation.

NOT INTENDED FOR CONSTRUCTION, BIDDING, OR PERMIT PURPOSES

Kenneth H. Stokoe, II (Texas No. 49095)
*Research Supervisor*

## TABLE OF CONTENTS

## SUMMARY

A computer program using finite elements was developed to simulate the response of defective pavements (i.e., pavements with horizontal delaminations, voids of different sizes, and vertical cracks) to dynamic loads applied at the surface. The solution of the finite element model is carried out in the time domain to obtain transient responses and steady-state amplitudes. These are easily obtained by applying the Fast Fourier Transform to the transient responses. The results obtained with this procedure were compared with those computed directly in the frequency domain with a boundary element formulation. The effect of horizontal delaminations, voids, and vertical cracks on the motions that would be recorded at the surface when an impulse is applied (also at the surface) was investigated. It was found that voids and delaminations can be easily recognized, if they are not too deep or at the interface of two layers with very different elastic properties. The impulse excites frequencies in one of two ranges: the first range corresponds to flexural waves traveling along the surface; the second to more traditional P waves traveling up and down. Each range offers some advantages and disadvantages. The flexural range provides a larger contrast and, therefore, easier identification when applicable. Vertical cracks have also a clear signature when they are surface piercing; they are, however, difficult to detect with the methods explored here when they are at depth and do not reach the surface.

# CHAPTER ONE

# INTRODUCTION

## 1.1 BACKGROUND

Maintenance is an important issue in the management of pavement systems because of the cost involved in the rehabilitation of these facilities. Several methods have been developed to assess in a non-destructive way the condition of pavements or the need for repairs. Among these are the Falling Weight Deflectometer (FWD) and the Dynaflect. The Dynaflect applies a harmonic load at a fixed frequency (normally 8 Hz) on the surface of the pavement and records the amplitudes of the steady state displacements at several receivers also along the surface. The Falling Weight Deflectometer applies instead an impulse with a nearly triangular shape in time and a duration of approximately 30 msec. The time histories of the displacements at several stations (with equal spacings) are recorded, but normally only the maximum displacements (which do not occur exactly at the same time at the various receivers) are used to construct a deflection basin. From the deflection basins the elastic properties (Young's modulus) of the surface layer, the base and the subgrade are obtained through a trial and error procedure (changing the values until the theoretical results agree with the experimental data) or through a more formal inversion algorithm (based in most cases on a least squares fit).

The approximations introduced in these procedures by using static analyses to match the results of dynamic tests, ways to account for the dynamic

effects, and other improvements have been the subject of a number of research projects conducted at the University of Texas at Austin. Computer programs have been developed to perform the dynamic analysis of layered systems subjected to the loads imposed by the Dynaflect and the Falling Weight Deflectometer, accounting, if so desired, for the finite width of the pavement (by opposition to the assumption of horizontal layers of infinite extent) and for nonlinear behavior (which may occur for the largest drop weights used in conjunction with the Falling Weight Deflectometer).

An improved inversion procedure which takes into account the dynamic effects and makes use of the experience obtained from a large number of parametric studies has also been developed. With these modifications, these procedures and the Falling Weight Deflectometer in particular can provide very reasonable estimates of the material moduli. Neither of these two techniques is well equipped, however, for identification of delaminations, debonding, voids, or cracks in pavement systems, although these are very important features which should be discovered early for a good maintenance program.

In this work a computer model using finite elements was developed to simulate the response of pavements with horizontal delaminations, voids or vertical cracks of different sizes to dynamic loads applied at the free surface. The solution of the finite element model was carried out in the time domain to obtain both transient responses and steady state amplitudes of displacements. From the transient responses computed in the time domain, the steady state amplitudes could be predicted using the Fast Fourier Transform (FFT). The effects of different irregularities on various response quantities were investigated for

variable dimensions and locations in order to determine optimum ways to detect them.

## 1.2 OBJECTIVES AND ORGANIZATION

The objectives of this research are to develop model of a pavement with irregularities, to study the effect of irregularities on the motions caused by a surface load, and to determine optimum ways of detecting delaminations, voids and vertical cracks in pavement systems.

This dissertation consists of seven chapters.

In Chapter Two, the formulation used in the finite element model in the time domain is presented. This includes the description of the model for the irregularities (delaminations, voids and vertical cracks) and the way the lateral and bottom boundaries are treated in the model.

Chapter Three includes a series of validation studies to verify the accuracy of the model. The three different approaches are used and their results compared. They include a boundary element formulation in the frequency domain, a finite element model solution in the time domain under a steady state load, and the finite element model subjected to a transient impulse with a step by step integration of the equations of motion in the time domain.

In Chapter Four, a number of studies are reported to find the largest possible ratios of response of delaminated pavements to those of intact pavements and the optimum ways to determine the depth and size of the delamination. The effect of load duration, material damping, depth and size of the delaminations, and

position of the delamination with respect to the edge are discussed. The two dimensional, plane strain, formulation is complemented with an axisymmetric model used to investigate three dimensional effects. The moving source-receiver testing was also simulated to investigate the effect of the position of the source-receiver system with respect to the delamination, and the feasibility of testing with an automated vehicle in motion.

Chapter Five includes the investigation on pavements with a void and the comparison with some experimental work. In addition to motion amplitudes, the phase and phase velocities were studied.

In Chapter Six, the effect of vertical cracks on the phases and displacement amplitudes are discussed as the source-receiver system moves over the surface and across the cracks. Both surface-piercing cracks and the subsurface cracks are considered.

Chapter Seven contains a summary of the major findings, conclusions and recommendations for future research.

# CHAPTER TWO

# ANALYTICAL FORMULATION IN TIME DOMAIN

## 2.1 INTRODUCTION

For analysis purposes the pavement system was considered as a horizontally layered medium and was discretized using conventional finite elements. The equations of motion were solved through direct step by step integration in the time domain using the central difference formula. A two dimensional, plane strain, formulation was used to simulate the propagation of plane waves, as a first approximation. In reality the solution near the area of application of the load, whether a harmonic excitation or a transient impact, can be strongly influenced by three dimensional effects. It was felt, however, that the two dimensional model could provide a reasonable assessment of whether it is feasible or not to detect voids, cracks and delaminations, and of the types of loads and measurements which will provide a clearer indication of their existence.

## 2.2 GOVERNING EQUATIONS

The governing equations of the model were formulated with the standard finite element approach using the principle of virtual work. Since the internal virtual work is equal to the external virtual work, for a body with forces f per unit of volume, tractions t per unit of surface, displacements u, strains $\varepsilon$, and stresses $\sigma$, one can obtain the following equation:

$$\int_v \delta\varepsilon^T \sigma \, dV = \int_v \delta u^T f \, dV + \int_s \delta u^T t \, dS \qquad (2.1)$$

where $\delta\varepsilon$ represents the virtual strain vector, and $\delta u$ is the vector of virtual displacements.

In addition,

$$f = b - \rho \ddot{u} - c \dot{u} \qquad (2.2)$$

where b are body forces, $\rho$ is the mass density of the material, and c is the viscosity coefficient. Thus, $\rho \ddot{u}$ stands for inertia forces and $c\dot{u}$ represents damping forces.

## 2.3 SPACE DISCRETIZATION

The displacement vector u, velocity vector $\dot{u}$, and acceleration vector $\ddot{u}$ in an element are interpolated from the vector of nodal displacements U, the vector of nodal velocities $\dot{U}$, and the nodal acceleration vector $\ddot{U}$ respectively.

$$u = N^T U ; \quad \dot{u} = N^T \dot{U}; \quad \ddot{u} = N^T \ddot{U} \qquad (2.3)$$

where N is the vector of shape functions.

The virtual components of displacement, velocity, and acceleration are

$$\delta u = N^T \delta U ; \quad \delta\dot{u} = N^T \delta\dot{U} ; \quad \delta\ddot{u} = N^T \delta\ddot{U} \qquad (2.4)$$

Similarly, the strains $\varepsilon$ in an element are interpolated from the nodal displacement vector U.

$$\varepsilon = A\,u = A\,N^T\,U = B^T\,U \tag{2.5}$$

where A is the matrix of differential operators, and B is the strain-displacement matrix.

Thus, the virtual component of strain is

$$\delta\varepsilon = B^T\,\delta U \tag{2.6}$$

Substituting Eqs. 2.2, 2.4, 2.6 and $\sigma = E\,\varepsilon$ into the dynamic equilibrium equation, Eq. 2.1, we obtain

$$\left(\int_v N^T \rho\, N\, dV\right) \ddot{U} + \left(\int_v N^T c\, N\, dV\right) \dot{U} + \left(\int_v B^T E\, B\, dV\right) U$$

$$= \int_v N^T b\, dV + \int_s N^T t\, dS \tag{2.7}$$

This equation can be simplified as

$$M\,\ddot{U} + C\,\dot{U} + K\,U = P \tag{2.8}$$

where M, C, and K are the element mass, damping, and stiffness matrices and P is the force vector.

$$M = \int_v N^T \rho N \, dV \tag{2.9}$$

$$C = \int_v N^T c N \, dV \tag{2.10}$$

$$K = \int_v B^T E B \, dV \tag{2.11}$$

$$P = \int_v N^T b \, dV + \int_s N^T t \, dS \tag{2.12}$$

Two dimensional, plane strain, linear isoparametric 4 noded elements were mainly used in this study. Eight noded elements were only used to validate the accuracy of the solutions. Axisymmetric 4 noded elements were used to simulate the disk-shaped delaminations (horizontal cracks). For 4 noded elements, the vector of shape functions N is defined as:

$$N = \begin{bmatrix} f_1 & 0 & f_2 & 0 & f_3 & 0 & f_4 & 0 \\ 0 & f_1 & 0 & f_2 & 0 & f_3 & 0 & f_4 \end{bmatrix} \tag{2.13}$$

The shape functions are defined below in terms of the natural coordinates.

$$f_1 = \frac{1}{4}(1-\xi)\,(1-\eta)$$

$$f_2 = \frac{1}{4}(1+\xi)\,(1-\eta)$$

$$f_3 = \frac{1}{4}(1+\xi)\,(1+\eta) \qquad (2.14)$$

$$f_4 = \frac{1}{4}(1-\xi)\,(1+\eta)$$

The subscripts of the shape functions refer to the node numbers.

## 2.4 LUMPED MASS MATRIX

Because the central difference formula were to be used for the time integration, it was desirable to have lumped masses which would allow to solve the equations of motion independently at each node, without the need to assemble the matrices of the complete system. As a result, relatively small computer storage and less computer time are required to obtain the results without solving a system of simultaneous equations in each time step.

For a four noded rectangular element the masses to be lumped at each node would be simply one fourth of the total mass of the element in each of the two coordinate directions. For the more general case of isoparametric elements of arbitrary shape (and for the eight noded elements even if they were rectangular), the procedure proposed by Hinton *et al.* (1976) was used to obtain a diagonal mass matrix from the consistent mass matrix by taking the consistent mass matrix and scaling the diagonal terms to preserve the total mass. Letting $M_{ij}$ be a general term of the consistent mass matrix

$$M_T = \sum_{i=1}^{n} \sum_{j=1}^{n} M_{ij} \tag{2.15}$$

$$M_D = \sum_{i=1}^{n} M_{ii} \tag{2.16}$$

where $M_T$ is the summation of all elements of the consistent mass matrix, $M_D$ is the summation of all the diagonal elements and n is the number of total degrees of freedom in an element.

An element of the diagonal lumped mass matrix is then expressed as

$$M_{ii}^{*} = M_{ii} \frac{M_T}{M_D} \tag{2.17}$$

## 2.5 RAYLEIGH DAMPING MATRIX

The internal dissipation of energy in soils is generally through hysteretic type damping which depends on the magnitude of the strains but is independent of frequency (Christian *et al.,* 1977). There is in addition a loss of energy due to propagation of waves away from the source, so called radiation damping, which depends on the frequency of the waves.

The amount of internal damping that could be expected during a non-destructive test should be very small since the main source of energy dissipation would take place through nonlinear behavior and the strains induced by the test should be very small. To simulate a small amount of damping a Rayleigh type damping was considered. The damping matrix is a combination of mass and stiffness proportional damping and is then of the form

$$C = \alpha M + \beta K \tag{2.18}$$

where M is the mass matrix and K is the stiffness matrix.

The values of the two parameters $\alpha$ and $\beta$ were selected as $D_1\Omega_1$ and $D_1/\Omega_1$ respectively. The resulting damping varies with frequency as shown in Fig. 2.1. It will have the value $D_1$ at the selected frequency $\Omega_1$ but it will increase for smaller or larger frequencies. When one performs dynamic analyses with a steady state harmonic excitation in order to obtain the steady state response, this feature of the damping will contribute to filter out the free vibration terms decreasing the time necessary to reach a steady state condition and providing the desired damping in this state. When one considers, on the other hand, the response to a transient triangular impulse the amplitudes in the low and high frequency ranges, relative to a frequency $\Omega_1$ equal to $2\pi$ / $t_d$ (where $t_d$ is the duration of the pulse), will be distorted. One must thus make sure that the values of damping are within a reasonable range for the frequencies of interest.

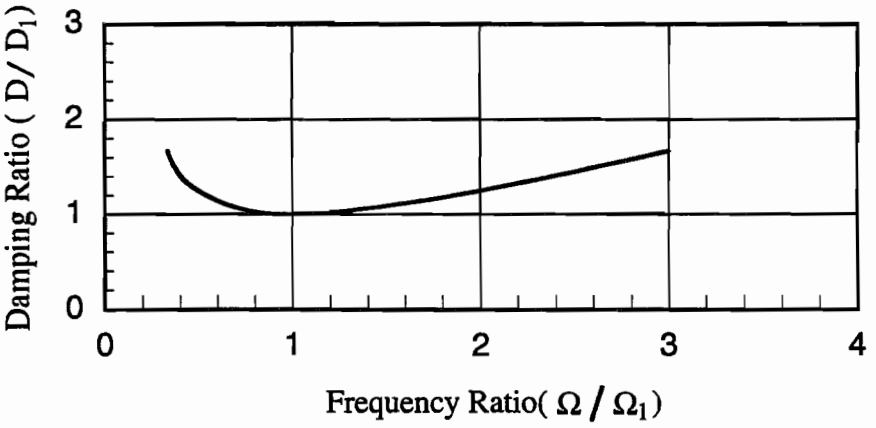


Fig. 2.1 Rayleigh Damping at Different Frequencies in Transient Excitation

## 2.6 LATERAL AND BOTTOM BOUNDARIES

To prevent the reflection of waves at the edges of the discretized domain and to simulate a medium that extends to infinity in the horizontal direction as well as vertically (if there is not a much stiffer rock-like material at a finite depth), the finite element domain was expanded at each time step. Initially the model had two elements contiguous to the node where the load is applied. For the second step, six elements were added surrounding the initial two. Unless rock was encountered the number of active elements for the $n$th time step of integration would be $2n^2$. When the limit in the maximum number of elements desired was reached viscous dashpots were placed at the edge nodes. In the area of rigid base, all the degrees of freedom were assumed to be fixed.

In Fig. 2.2 viscous boundaries consist of viscous dashpots placed along the edges of the elements on these boundaries. These viscous constants are determined to absorb plane body waves propagating perpendicular to the boundaries. Since this is not the actual condition (in fact the solution is composed mostly of surface waves at some distance from the load) the dashpots must be placed at a sufficient distance from the source and the zone of interest to obtain reasonable results (Roësset 1980). A minimum of four wavelengths was imposed with the wavelength computed for each frequency using the shear wave velocity of the material.

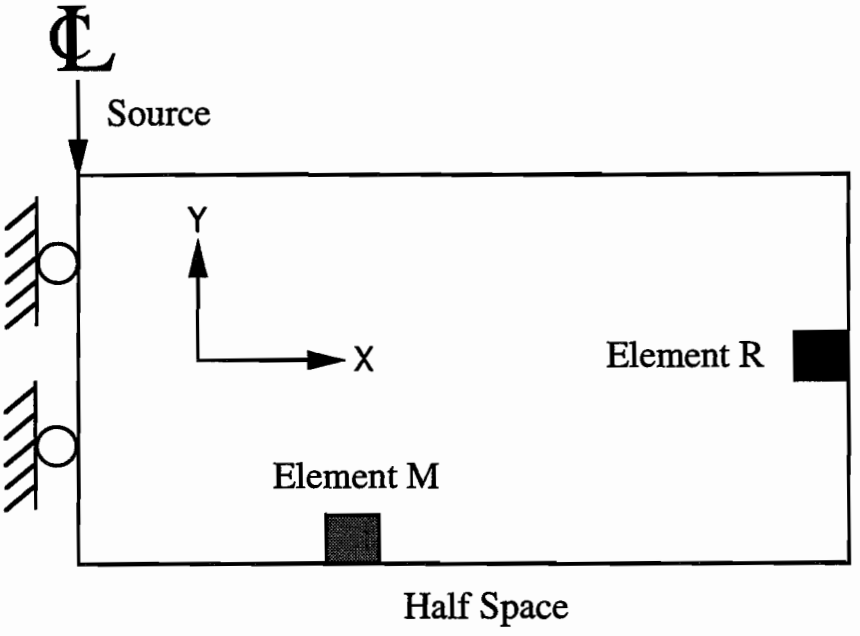


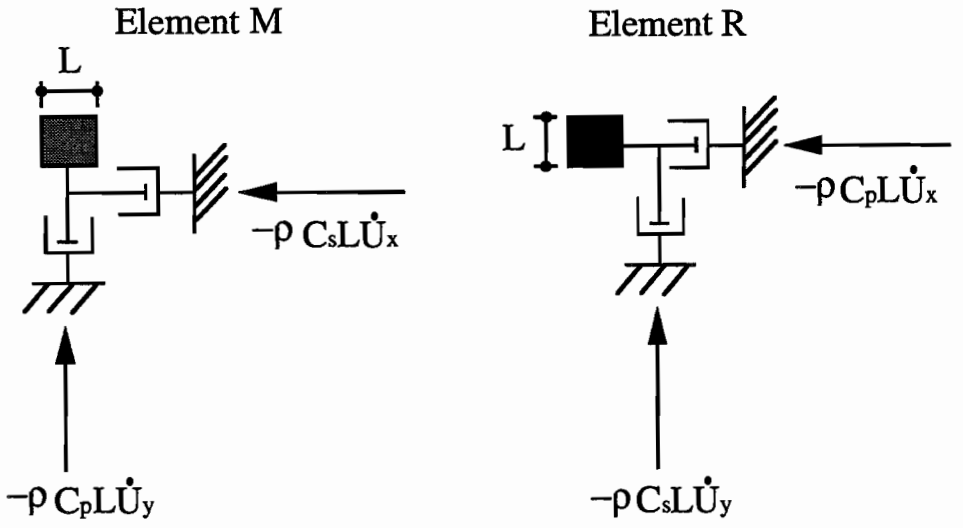


Fig. 2.2 Viscous Boundaries in Half Space

## 2.7 IRREGULARITY SIMULATION

The way that the different irregularities (a square or rectangular void or cavity), a horizontal crack or delamination and a vertical crack were simulated is shown in Fig. 2.3. The boundary conditions of irregularities are zero stresses along their boundaries. For a horizontal crack (delamination), the depth of the crack is assumed to be zero so that the top and bottom faces of the crack are at the same location initially. Likewise, for a vertical crack, the left and right faces of the crack are assumed to be at the same location before the loading is applied to the system.

In order to obtain good results the size of elements around irregularities should be at most one eighth of the wavelength and there should be at least two elements per face of an irregularity.

## 2.8 STEADY STATE AND TRANSIENT EXCITATION

The analyses can be performed to obtain directly the steady state response to a harmonic excitation or to compute the transient response to an impact type load. In the latter case one can obtain the steady state responses as a function of frequency computing the Fourier transforms of the response and the excitation and dividing them, determining the transfer function. One obtains thus the steady state responses over a whole set of frequencies from a single analysis. The second procedure is much more efficient, requiring a shorter duration of integration and also a smaller domain. Using a triangular pulse with a duration $t_d$ the predominant frequency is $f = 1 / t_d$ (in Hz). The results will be valid over a range of

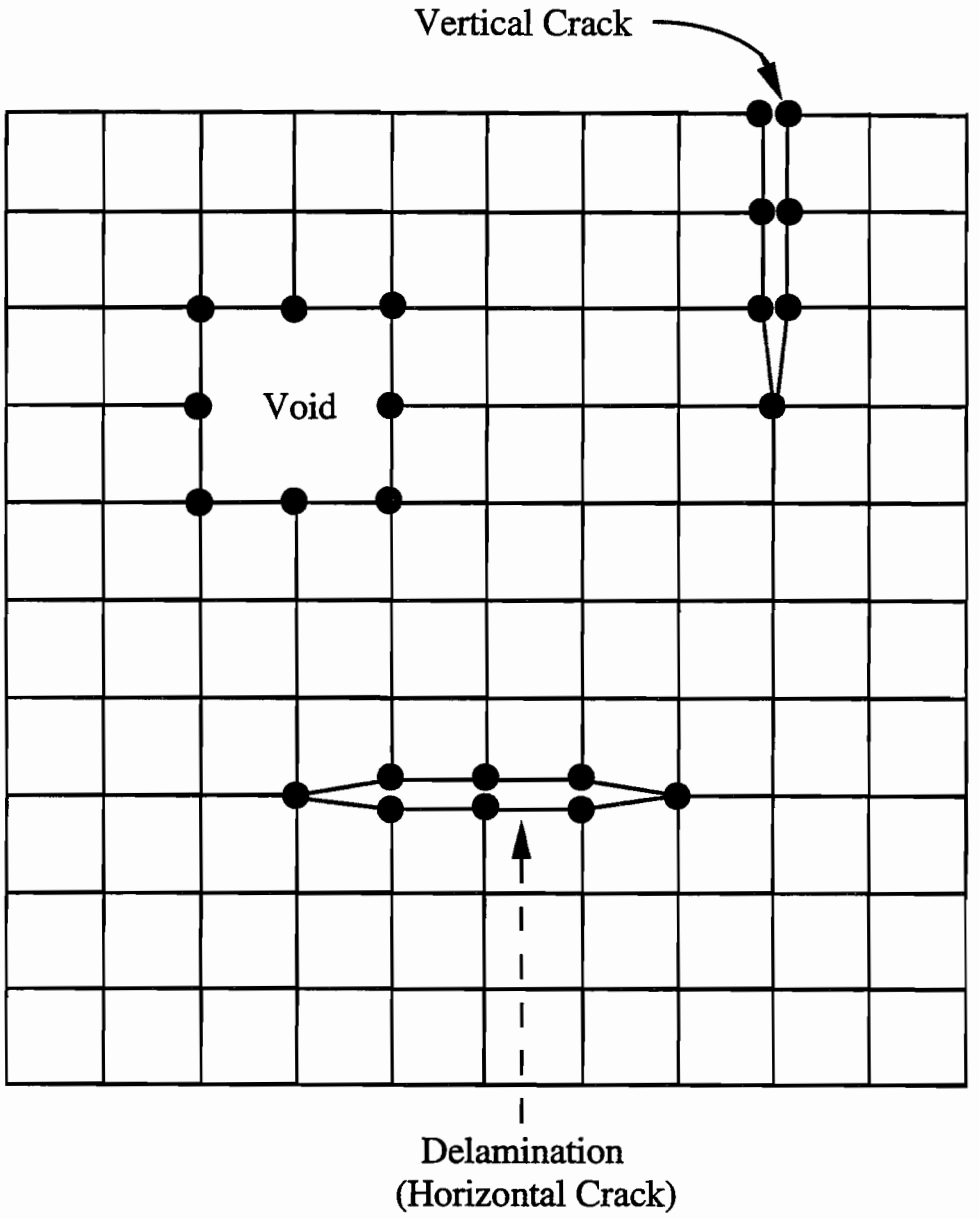


Fig. 2.3 Simulation of Irregularities

frequencies centered at this value. If one desires results over an extended range of frequencies it may be necessary to perform these analyses for a set of pulses with different duration.

For any given analysis the frequency f, inverse of the time duration of the pulse, is used to select the minimum distances to the viscous boundaries as well as the size of the finite elements. For linear (four noded) elements the maximum size should be less than one eighth of the wavelength (much smaller values, of the order of 1/40 of the wavelength were used for some of the runs). For the eight noded elements the size should be less than one quarter to one third of the wavelength.

## 2.9 DIRECT INTEGRATION METHOD

In order to solve the dynamic equilibrium equations, an explicit integration scheme, the central difference method, was used. The displacement vector at time $t+\Delta t$ is directly solved in terms of the displacements at the two previous time steps with the equilibrium conditions established at time t.

Using the central difference method, one obtains the velocity and acceleration expressed as

$$\dot{u}_t = \frac{1}{2\,\Delta t}( u_{t+\Delta t} - u_{t-\Delta t} ) \tag{2.19}$$

$$\ddot{u}_t = \frac{1}{\Delta t^2}( u_{t+\Delta t} - 2u_t + u_{t-\Delta t} ) \tag{2.20}$$

where $\Delta t$ is the time step.

Substituting these two equations and Rayleigh damping, $C = \alpha M + \beta K$, into the governing equation (Eq. 2.8), one obtains

$$(M + \alpha M \frac{\Delta t}{2}) u_{t+\Delta t}$$

$$= 2Mu_t - (M - \alpha M \frac{\Delta t}{2}) u_{t-\Delta t} + \Delta t^2[P - Ku_t - \beta K(u_t - u_{t-\Delta t})/\Delta t] \qquad (2.21)$$

It should be noticed that in order to maintain a diagonal matrix of coefficients the velocity term associated with the $\beta$ K part of Rayleigh damping was reproduced by a backward difference rather than the central difference formula 2.19. Then

$$\dot{u}_t = \frac{1}{\Delta t}(u_t - u_{t-\Delta t}) \qquad (2.22)$$

The central difference formula is a conditionally stable integration algorithm. For square, or nearly square, linear elements with lumped masses the time step of integration used was selected so that

$$\Delta t \leq \frac{h}{c_s} \sqrt{0.5 - \nu} \qquad (2.23)$$

where h is the minimum element side , $c_s$ is the shear wave velocity of the material and $\nu$ is Poisson's ratio.

# CHAPTER THREE

# VALIDATION

## 3.1 INTRODUCTION

A number of parametric studies were carried out first to validate the accuracy of the solutions obtained with the three different approaches: the boundary element method (BEM) in the frequency domain, the finite element model (FEM) with a solution in the time domain under a steady state load, and the finite element model subjected to a transient impulse with a step by step integration of the equations of motion in the time domain. From the transient responses computed in the time domain for the impact load the steady state amplitudes were predicted using the Fast Fourier Transform (FFT). Five cases were considered for these studies: a uniform stratum on rigid base, a uniform half-space, a uniform half-space with a cavity, a layered medium with a void, and a layered medium with a horizontal crack (delamination).

## 3.2 UNIFORM LAYER ON RIGID BASE

The first sample problems is shown schematically in Fig. 3.1. It is a homogeneous soil layer resting on a rigid base. The total thickness H, the shear modulus, the mass density, and the amplitude of the sinusoidal exciting force are all taken as unity. A value of Poisson's ratio of 0.3 was assumed.

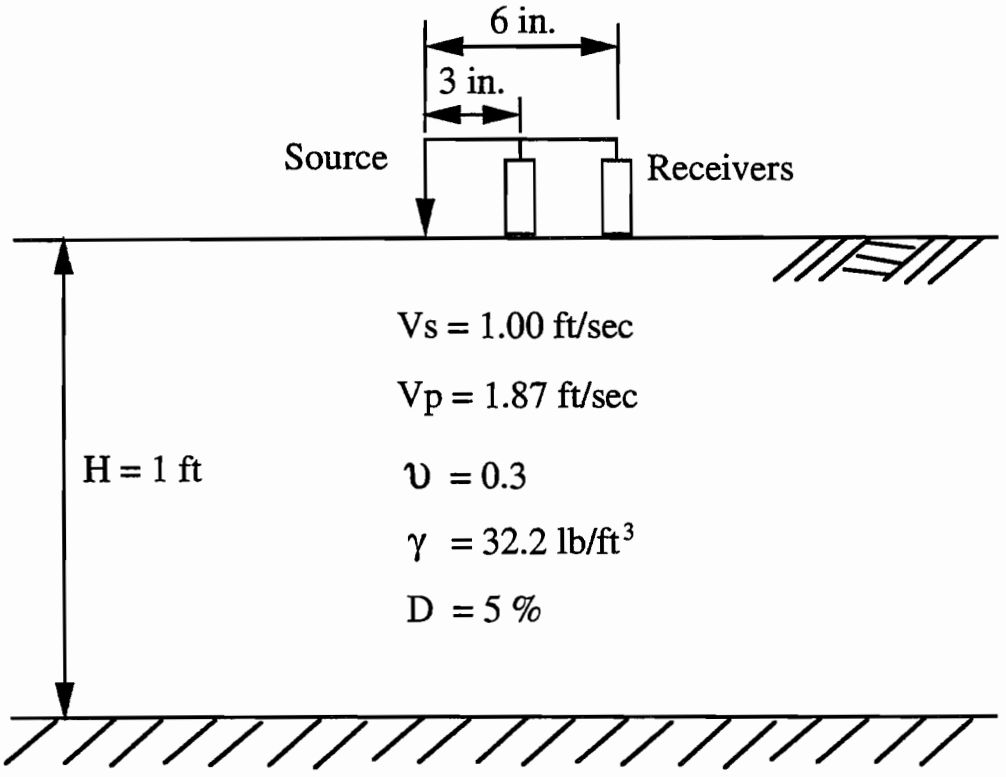


Fig. 3.1 Schematic Diagram of the Uniform Layer on Rigid Base

Even though viscous boundaries were used to eliminate unwanted reflections from the lateral boundaries, a horizontal distance of four wavelengths (based on shear waves) was used between the source and the lateral boundaries of finite element model to guarantee acceptable results.

The amplitude of the steady state vertical displacements at two points (3 and 6 inches) from a concentrated vertical load are plotted versus mesh size in Fig. 3.2. The abscissa in these figures is the ratio of the wavelength to the size of the finite elements or the layer thickness in the discrete Green's function solution. It is interesting to notice that the two solutions approach the limit from opposite directions at a frequency of 1 Hz and the same direction for 10 Hz. It should be remembered that lumped masses rather than consistent masses were used in the FEM approach. The computer program with discrete Green's function used in this study, was developed by Nogueira (1986).

A wavelength to discretized-size ratio of 16 was selected for most results shown later in this study (16 elements or sublayers per wavelength).

The time histories of the displacement at a point 3 inches from the load for frequencies of 0.1, 1 and 10 Hz are shown in Figs. 3.3 and 3.4. The results in Fig. 3.3 correspond to a case without damping. For the lowest frequency (0.1 Hz) the solution seems to reach a steady state condition with a harmonic type response at the frequency of the excitation although there is no damping in the system. For frequencies of 1 Hz and 10 Hz there is radiation damping but the system has not reached a steady state condition after 24 cycles. Figure 3.4 shows the results for a soil with 5% internal damping of a linear hysteretic nature. The response reaches already a harmonic steady state condition in all cases. The effect of the damping

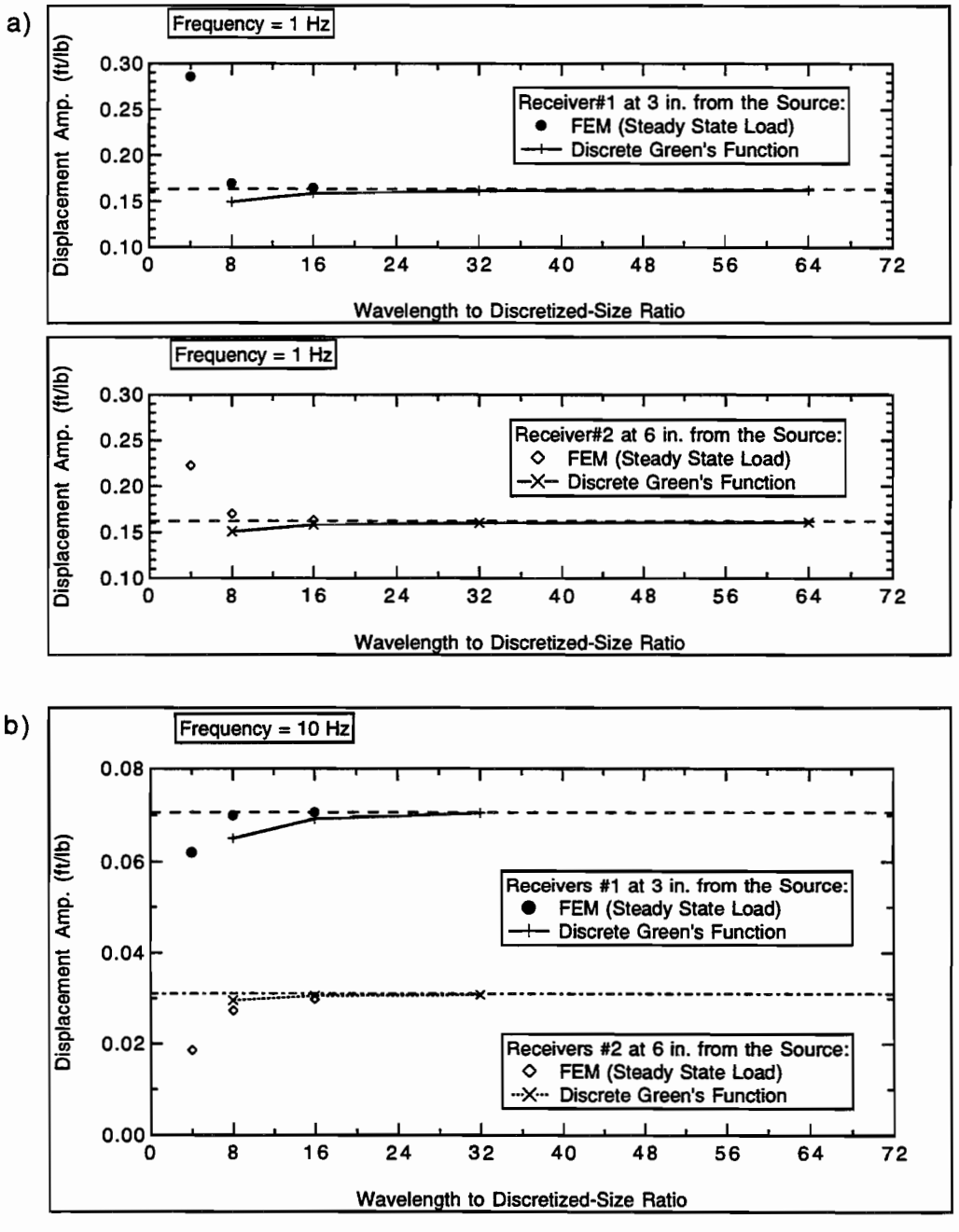


Fig. 3.2 Convergence of Results for 1 ft Medium with Rigid Base under the Excitation of Unit Point Load

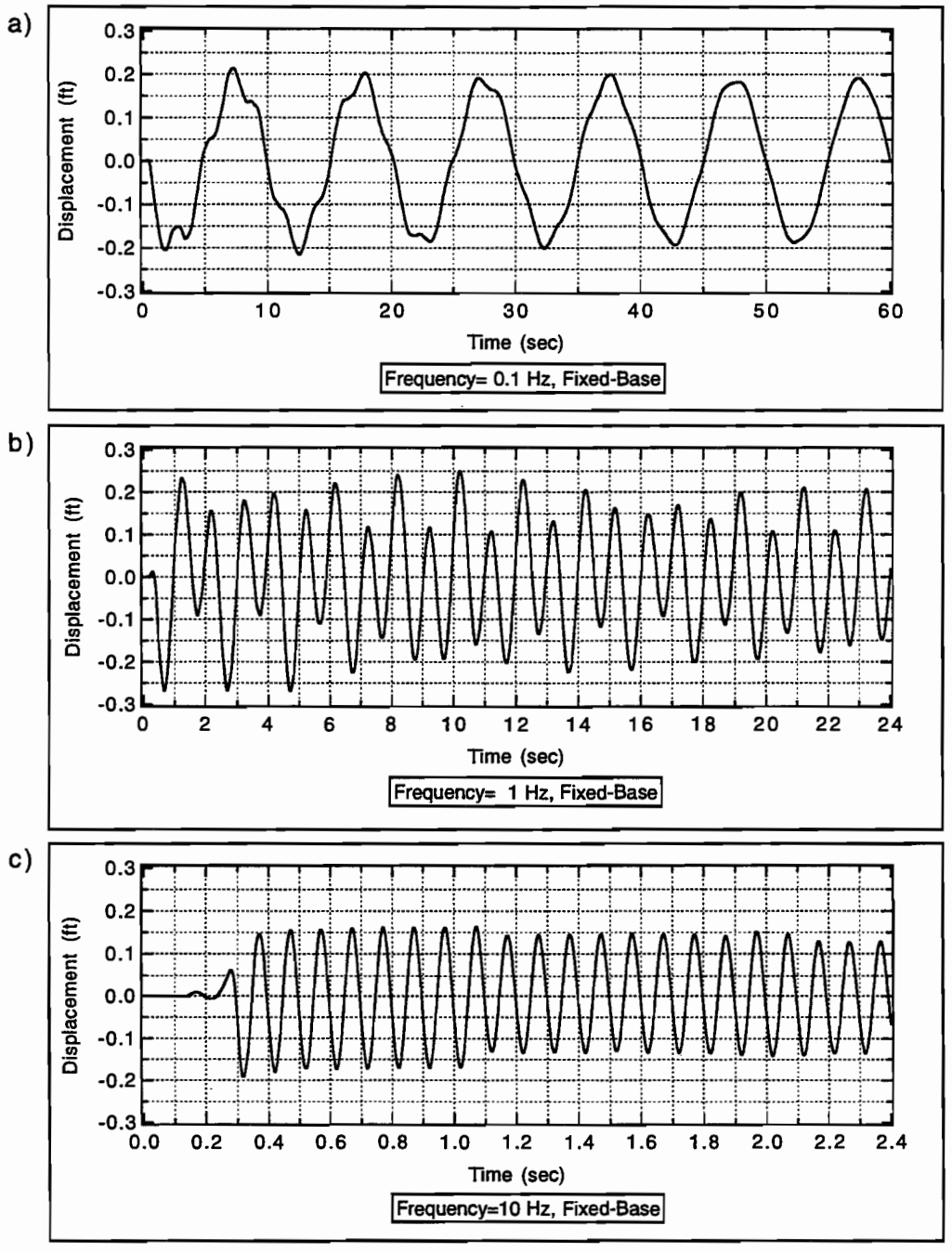


Fig. 3.3 Surface Displacement Histories at 3 inches from the Source for a 1 ft Medium Having No Damping and Overlying a Rigid Base

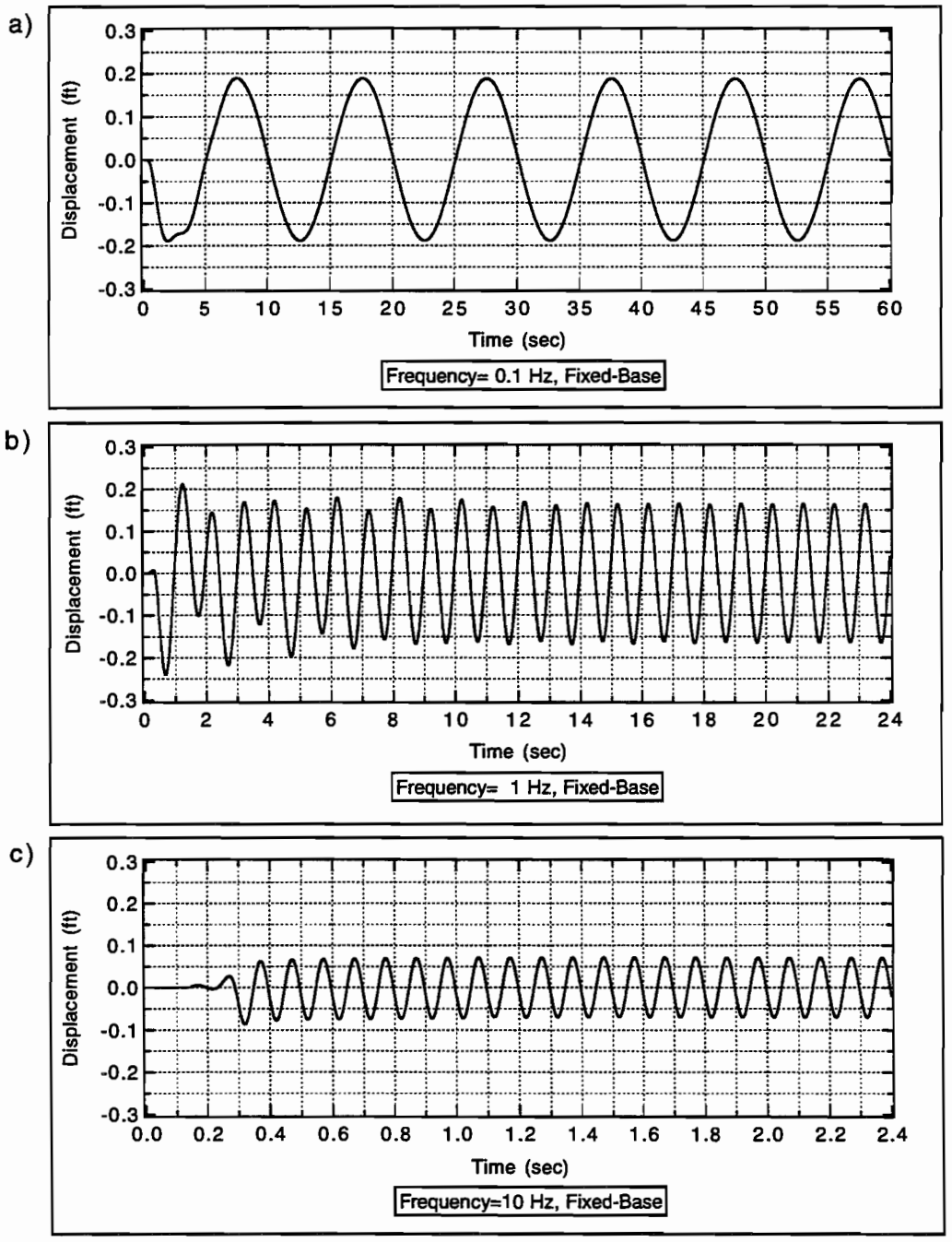


Fig. 3.4 Surface Displacement Histories at 3 inches from the Source for a 1 ft Medium Having 5% Damping and Overlying a Rigid Base

is small for the 0.1 and 1 Hz cases as far as the amplitude of the motions is concerned. It is very substantial, however, for the 10 Hz excitation.

The corresponding results at a distance of 6 inches from the load are shown in Figs. 3.5 and 3.6. The same trends are observed. It is interesting to notice that while the amplitudes of the displacement at 6 inches are considerably smaller than those recorded at 3 inches for the 0.1 and 10 Hz frequencies, there are nearly the same at 1 Hz.

To save computation time in the comparative studies among different approaches, five percent damping was used to decrease the time needed to reach steady state.

The results obtained using the finite element model with a steady state load are compared with those provided by discrete Green's function solution (Nogueira, 1986) and a Fourier expansion solution developed by Kang (1990) in Fig. 3.7. It can be seen that they are all in excellent agreement.

The determination of the steady state amplitudes from a time domain analysis is, however, very time-consuming since only one result is obtained from each run for a given frequency. Using instead an impact load and then the Fast Fourier transform (FFT) the displacement amplitudes can be obtained at one shot over a range of frequencies. The displacement amplitudes from these two approaches are compared in Fig. 3.8. For an impact duration of 2.17 seconds the predominant frequency would be 0.46 Hz (the duration was selected based on the location of the peak in Fig. 3.7). For the transient load case the damping was defined at the predominant frequency. It can be seen that the agreement between

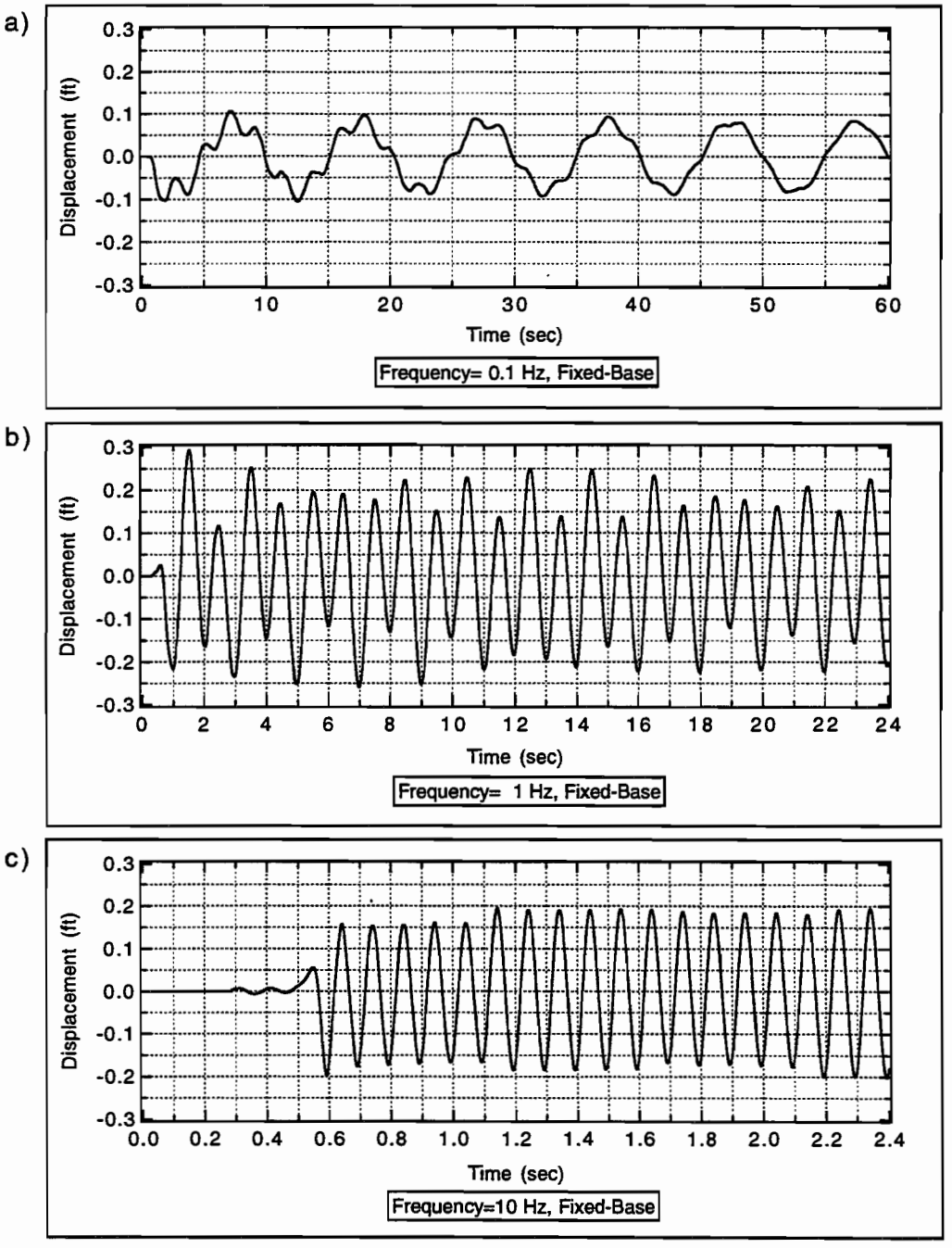


Fig. 3.5 Surface Displacement Histories at 6 inches from the Source for a 1 ft Medium Having No Damping and Overlying a Rigid Base

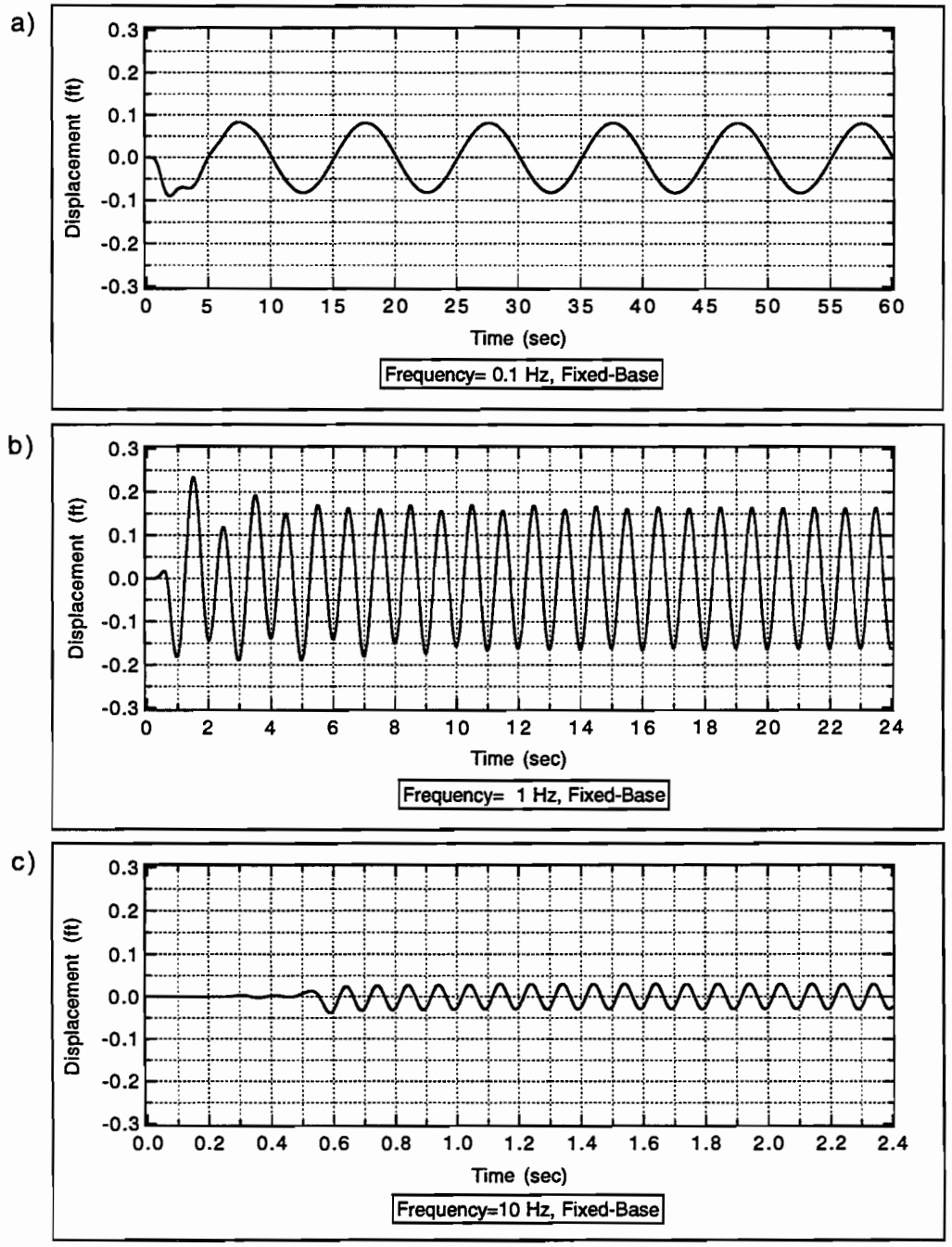


Fig. 3.6 Surface Displacement Histories at 6 inches from the Source for a 1 ft Medium Having 5% Damping and Overlying a Rigid Base

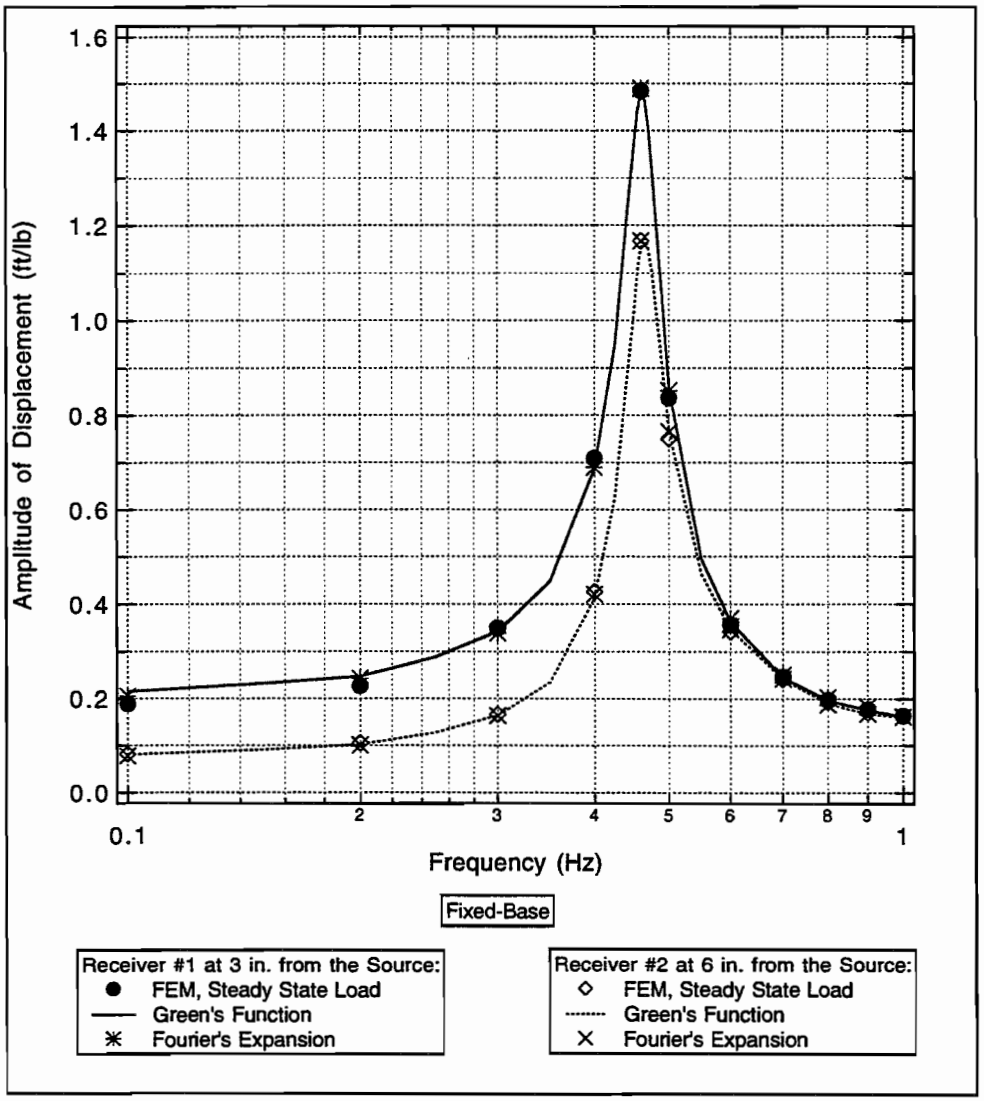


Fig. 3.7 Comparison of the Finite Element Solutions with the other Solutions Using 5 Percent Damping at Various Frequencies in 1 ft Medium on Rigid Base

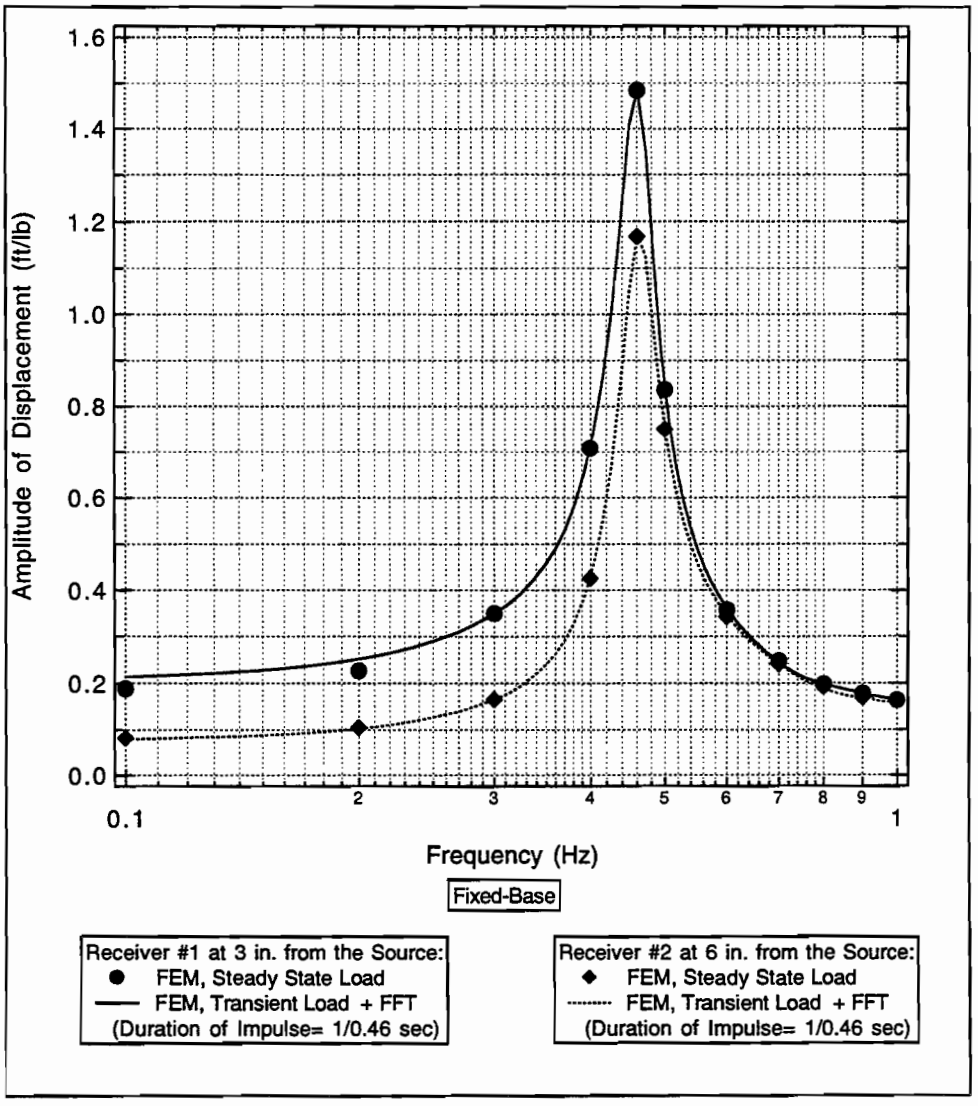


Fig. 3.8 Comparison of the Transient Solutions with the Steady-State Solutions Using 5 Percent Damping at Various Frequencies for a 1 ft Medium on Rigid Base

the two solutions is excellent over the range of frequencies from 0.2 Hz (or even 0.1 Hz) and 1 Hz corresponding to half and double the predominant frequency.

## 3.3 UNIFORM HALF SPACE

The homogeneous half-space considered for the second series of comparative studies is shown in Fig. 3.9.

Similar to the case of fixed base, the shear modulus, the mass density, and the amplitude of the sinusoidal exciting force were all given a value of one. And the Poisson's ratio was assumed to be 0.3. The viscous boundaries were applied not only to the lateral boundary but also at the bottom of the model at a distance of four wavelengths (shear wave wavelengths).

The variation of the displacement amplitudes obtained by the FEM and discrete Green's function approach as a function of the mesh size (ratio of wavelength to size of elements or layer thickness) is shown in Fig. 3.10. The two solutions approach the limit again from opposite directions for a frequency of 1 Hz.

Again, a wavelength to discretized-size ratio of 16 was selected for most of the later studies (16 elements or sublayers per wavelength).

Figures 3.11 and 3.12 show the time histories of the displacement that would be recorded at the receiver 3 inches from the load for frequencies of 0.1, 1 and 10 Hz, as in the case of the soil layer of finite depth. The results in Fig. 3.11 correspond to a soil layer without any internal damping. In this case, however, there is radiation damping for all frequencies. It can be seen that a steady state,

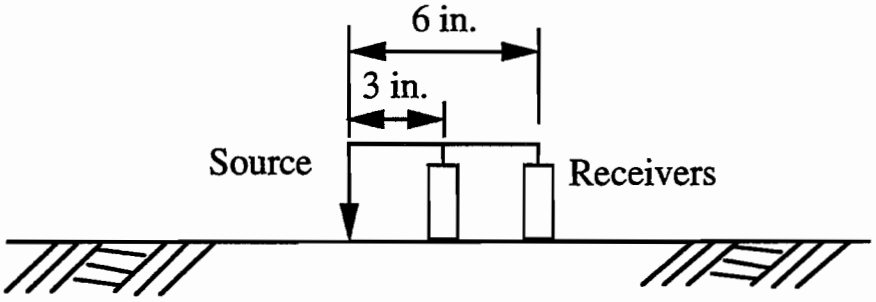


Vs = 1.00 ft/sec

Vp = 1.87 ft/sec

$\upsilon$ = 0.3

$\gamma$ = 32.2 lb/ft$^3$

D = 5 %

Half Space

Fig. 3.9 Schematic Diagram of the Uniform Medium in Half Space

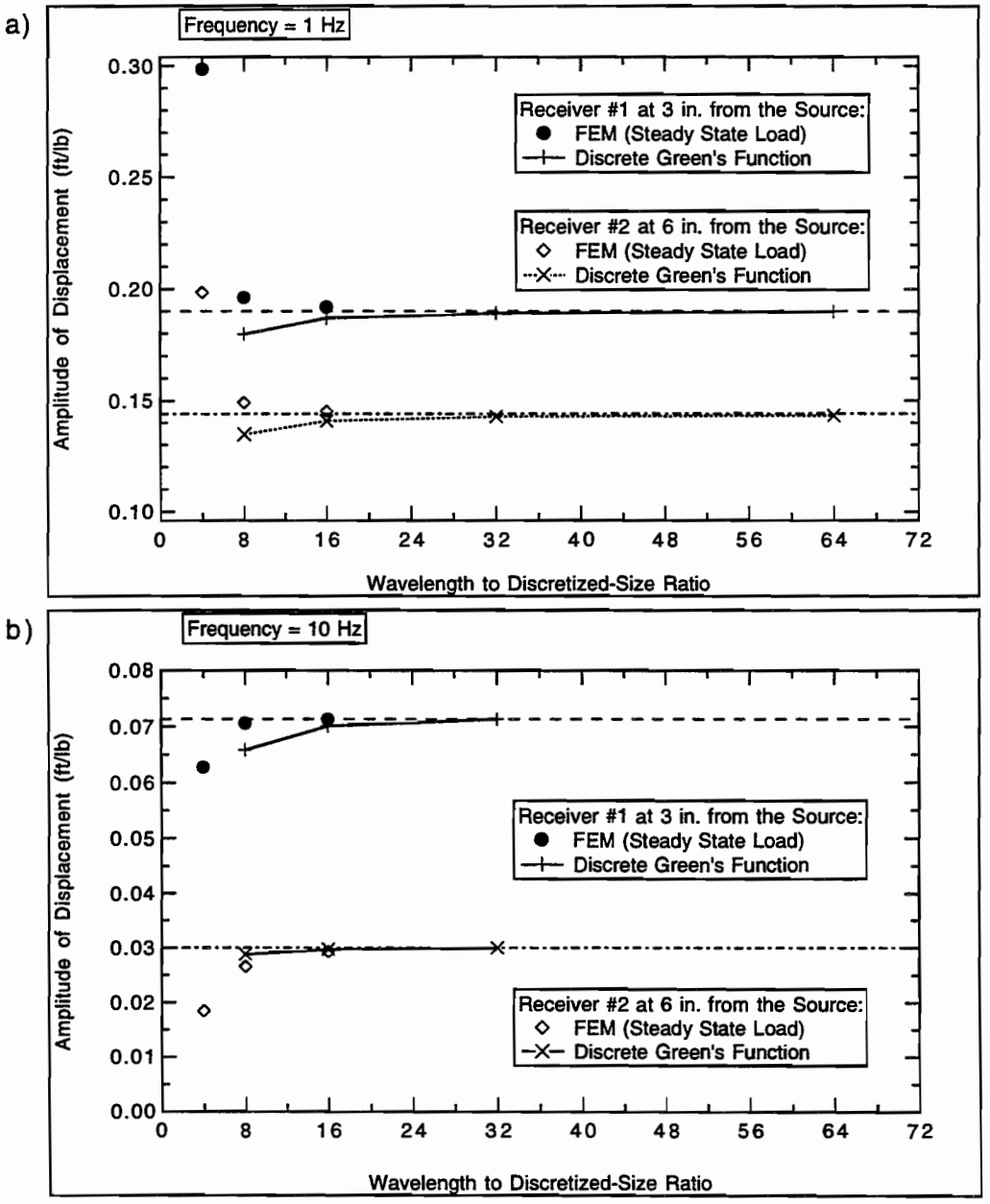


Fig. 3.10 Convergence of Results for Half-Space under the Excitation of Unit Point Load

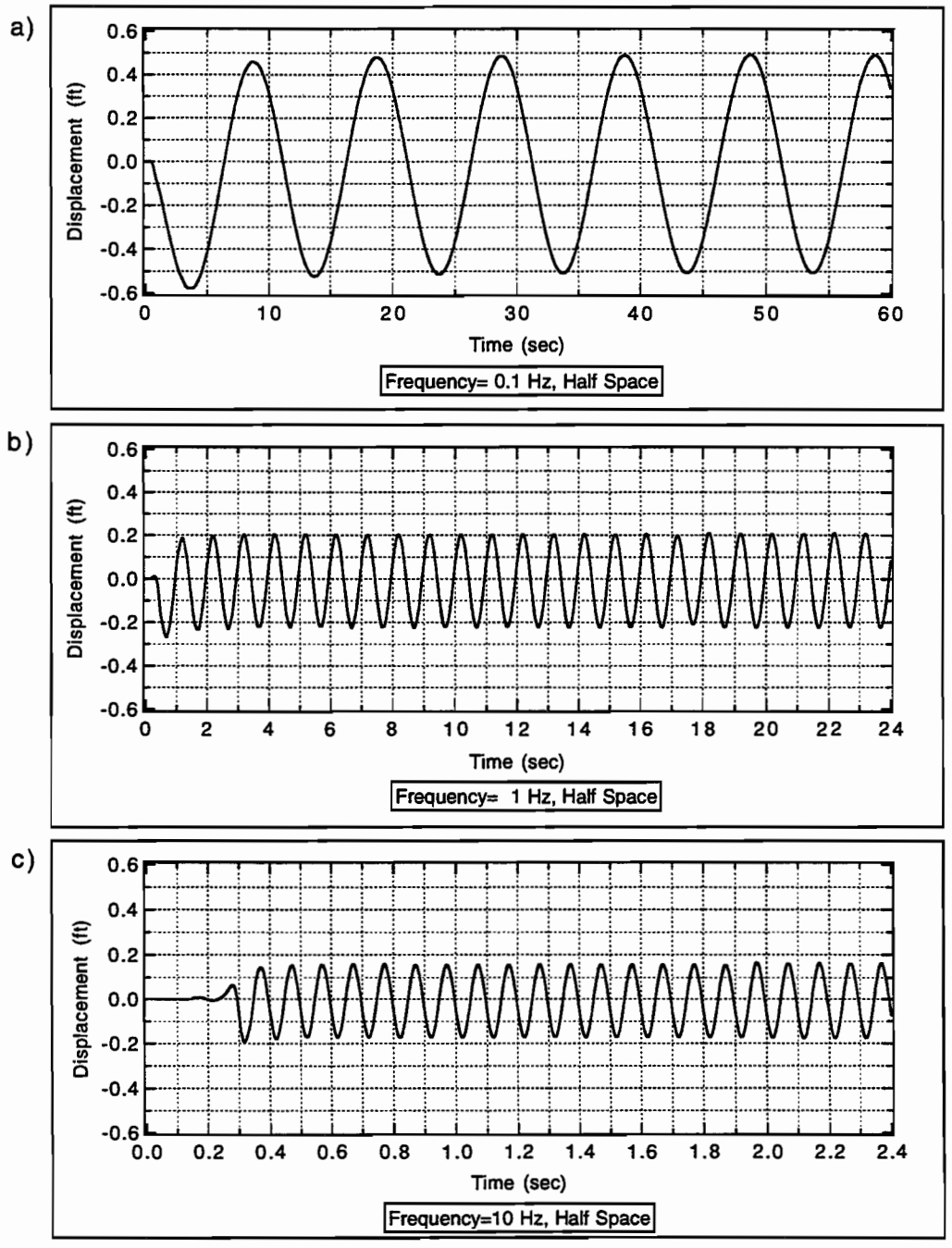


Fig. 3.11 Surface Displacement Histories at 3 inches from the Source for a Half Space without Damping

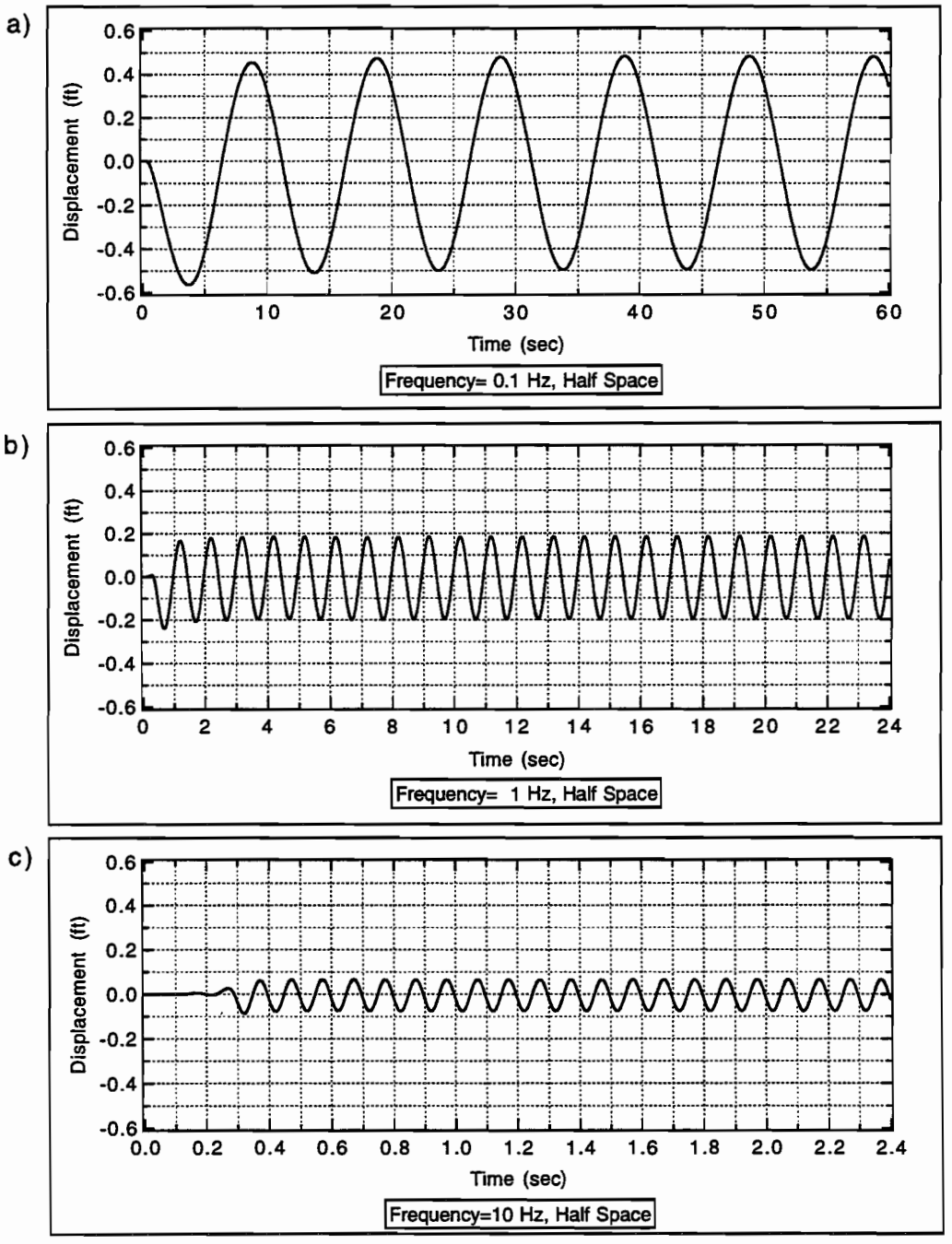


Fig. 3.12 Surface Displacement Histories at 3 inches from the Source for a Half Space with 5% Damping

harmonic, condition is reached for all cases relatively easily. The amplitudes of motion are almost identical with and without damping for the 0.1 Hz case. The damping decreases only slightly the motion amplitude at 1 Hz. It has, however, a considerable effect on the amplitudes at 10 Hz (they are reduced by a factor of approximately 2). For the 0.1 Hz frequency the wavelength is of the order of 10 ft and the receiver is thus at a very small fraction of a wavelength from the source. For 1 Hz the receiver is approximately at one quarter of the wavelength. The distance from the load to the receiver is, however, 2.5 wavelengths for the 10 Hz case.

The corresponding results for a receiver at 6 inches from the load are shown in Figs. 3.13 and 3.14. The same observations made earlier apply here. In this case the displacement amplitudes are almost the same at 3 and 6 inches for a frequency of 0.1 Hz. They decrease by 25% from the first to the second receiver at 1 Hz and they are reduced by a factor of nearly 3 at 10 Hz.

The results obtained using FEM with steady state load are compared with those obtained from the discrete Green's function and a Fourier expansion in Fig. 3.15. The agreement is still excellent. In this case, however, the displacement amplitudes decrease steadily as the frequency increases since there is no resonance frequency.

In Fig. 3.16, the displacement amplitudes obtained using the FEM with an impact load (durations of 5, 2, and 1 sec), and then a Fast Fourier transform (FFT) are presented by the hollow symbols and compared to those of the harmonic analyses. The displacement amplitudes from these two different methods

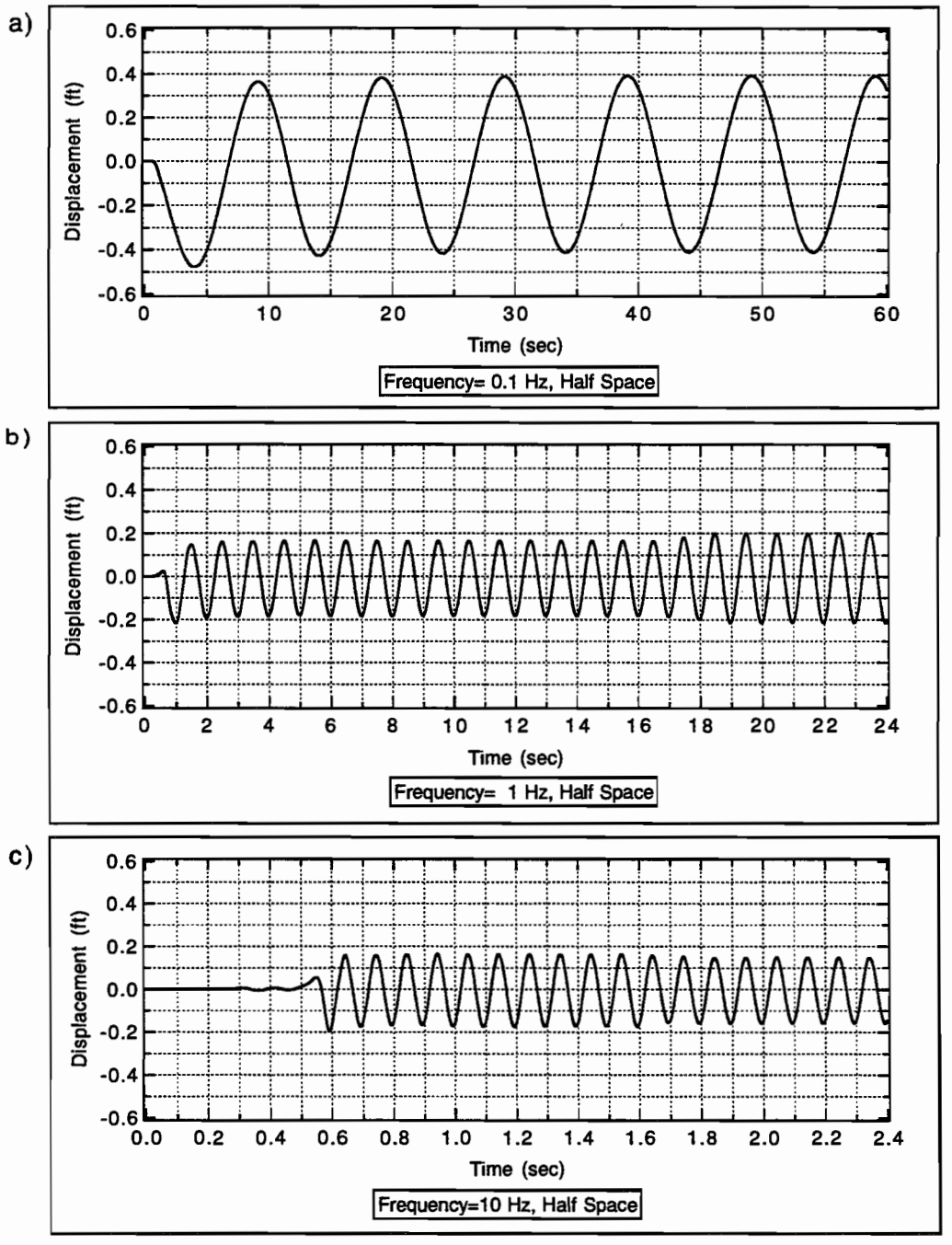


Fig. 3.13 Surface Displacement Histories at 6 inches from the Source for a Half Space without Damping

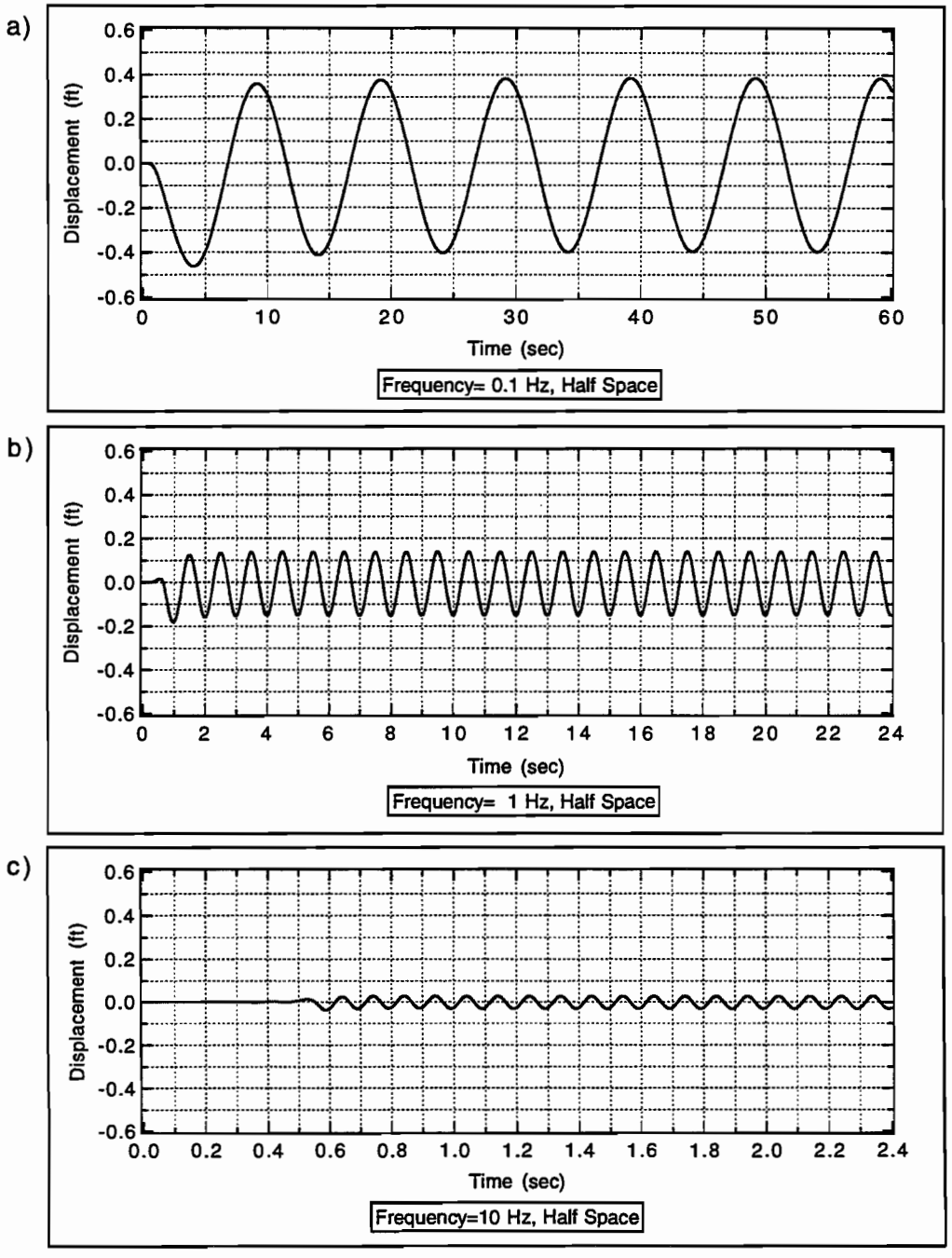


Fig. 3.14 Surface Displacement Histories at 6 inches from the Source for a Half Space with 5% Damping

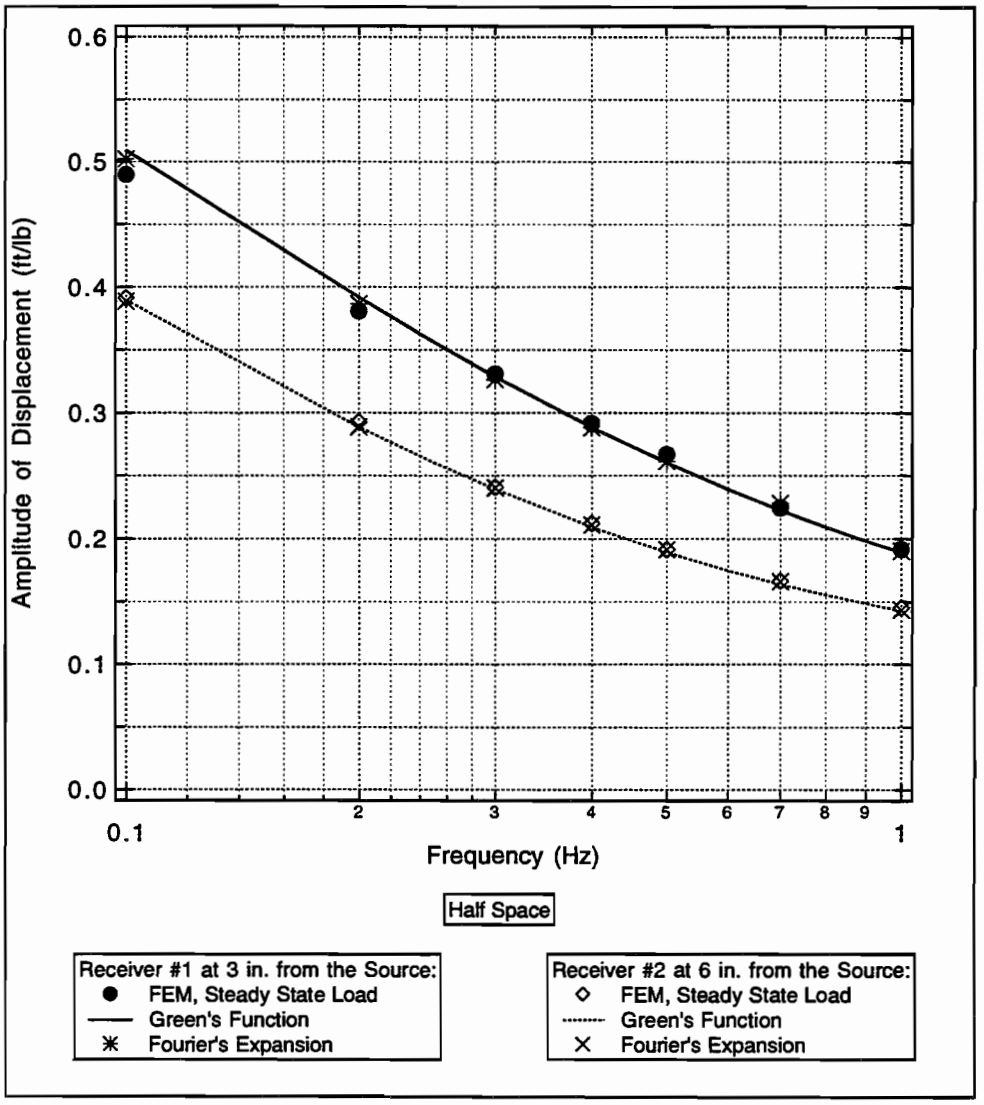


Fig. 3.15 Comparison of the Finite Element Solutions with the other Solutions Using 5 Percent Damping at Various Frequencies in a Half Space

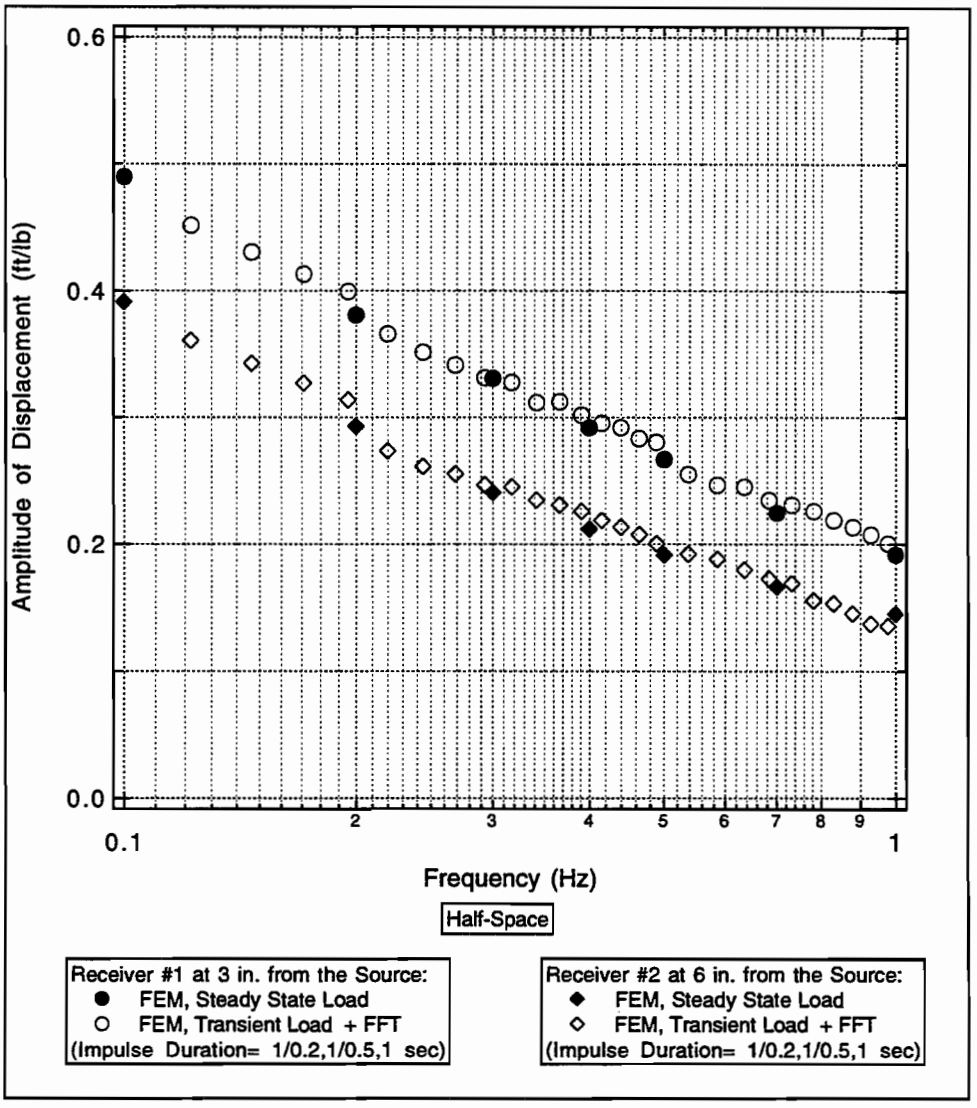


Fig. 3.16 Comparison of the Transient Solutions with the Steady-State Solutions Using 5 Percent Damping at Various Frequencies in a Half Space

generally match very well as long as the duration of the impact is properly selected.

## 3.4 UNIFORM HALF-SPACE WITH A CAVITY

A uniform isotropic and elastic half-space with a shear wave velocity of 1000 ft/sec, a P-wave velocity of 1870 ft/sec, a Poisson's ratio of 0.3, unit weight of 125 lb/ft$^3$ and 5% hysteretic damping was considered next. A cavity with a rectangular cross section, 1.5 ft deep and 2 ft wide was located 1 ft below the free surface as shown in Fig. 3.17. The source was placed on the surface directly over the center of the cavity and the receiver was assumed to be at 3 inches from the source.

With the boundary element method (BEM) in the frequency domain the medium was initially divided into horizontal sublayers with a the thickness equal to 1/20th of the wavelength of S-waves. The same size was used for the boundary elements. For the next run the boundary elements and the sublayers within 5.5 ft from the surface were subdivided into 1/40th of the wavelength of S-waves. Smaller sublayers and boundary elements were used until the results were within 5 percent of those obtained in the previous run. The results for the soil without and with cavity are shown in Fig. 3.18. Without cavity the sizes of the sublayers and the boundary elements make very little difference in the results for the values considered. On the other hand, with cavity the displacement amplitudes increase as the sublayer thickness decreases for frequencies lower than 120 Hz. For frequencies higher than 120 Hz the displacement amplitudes are almost identical

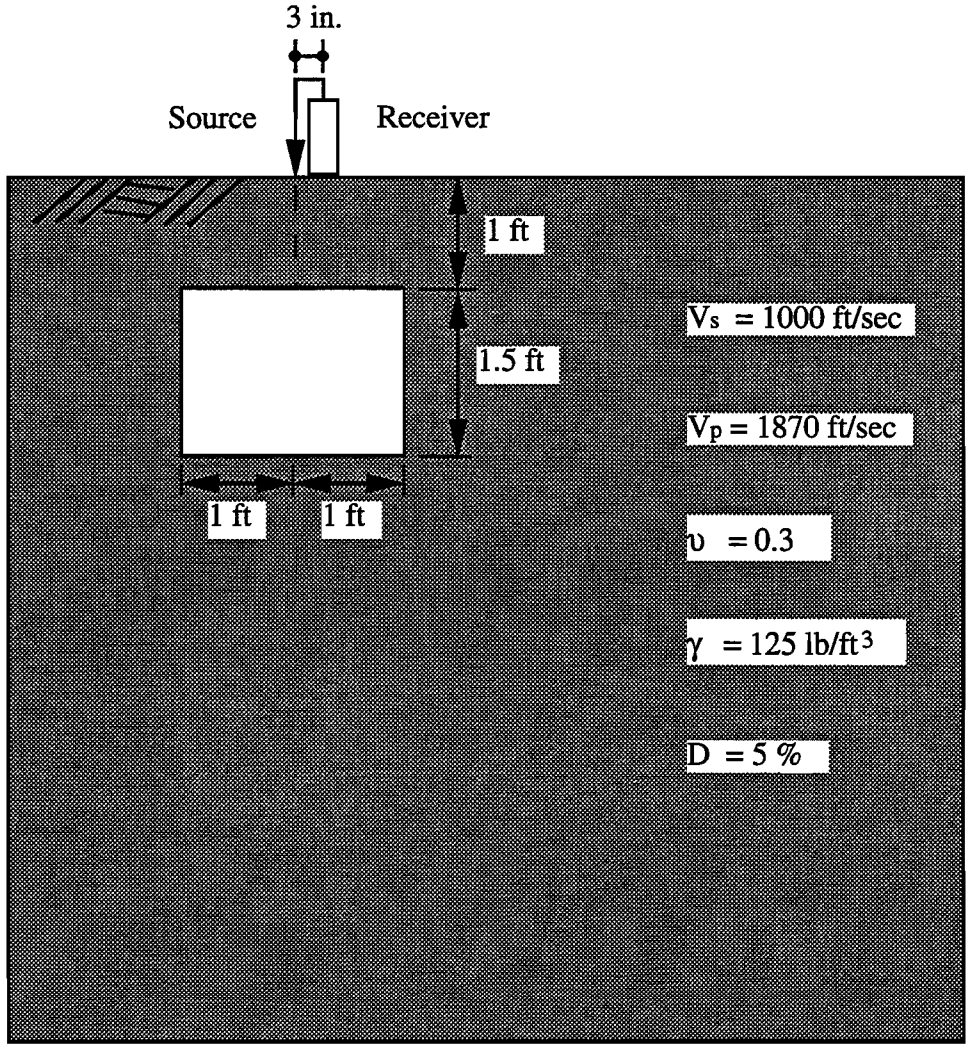


Fig. 3.17 Uniform Half-Space with a Cavity

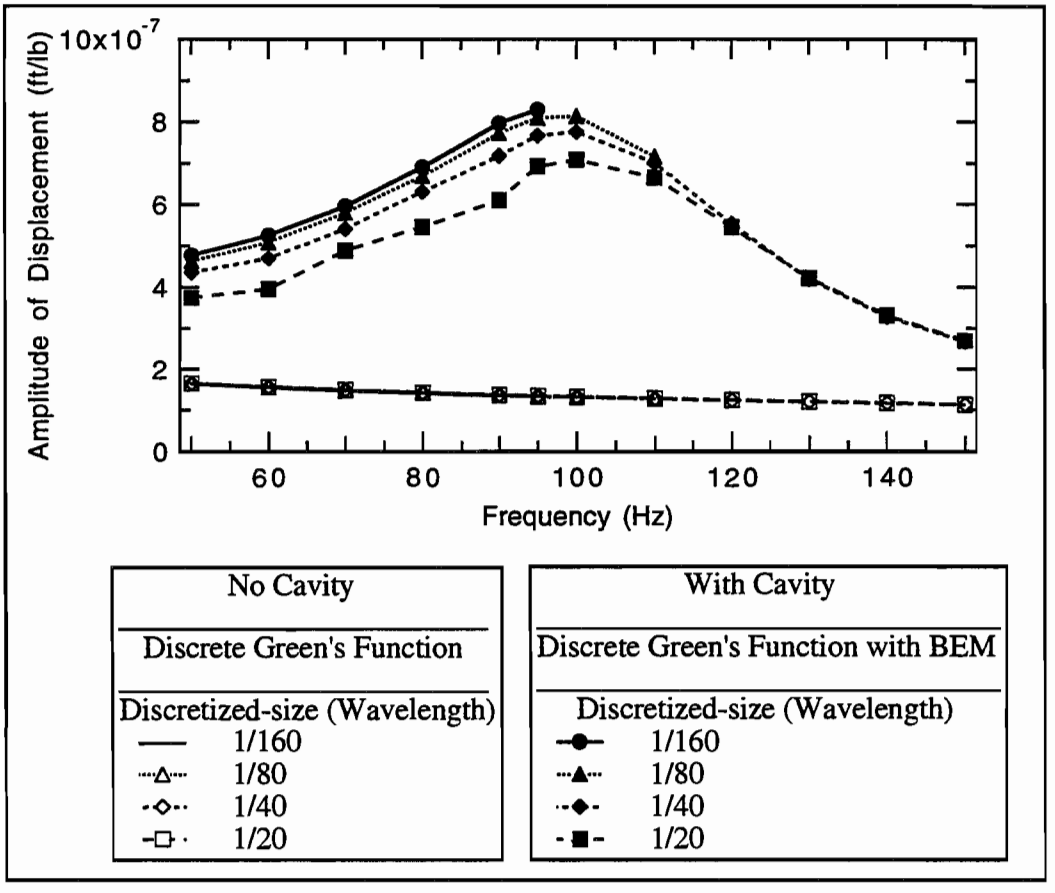


Fig. 3.18 Results with and without Cavity Using Discrete Green's Function and BEM

for all cases. To illustrate better the behavior the results at a frequency of 90 Hz for various sizes of sublayers and boundary elements are shown in Fig. 3.19. For the soil with cavity the analyses require smaller sublayers and boundary elements to obtain reliable results.

Similar behavior was observed in the results with FEM, transient load and the FFT, shown in Fig. 3.20. The solution was obtained in the time domain for a triangular pulse with a duration of 1/95 seconds. The maximum number of finite elements used was 102,400. One way to cut the number of elements and the computer time is to use larger square and rectangular elements beyond the region two diameters around the cavity. The results with 3 in. by 3 in.(1/40th of the wavelength of S-waves), 3 in. by 6 in. and 6 in. by 6 in.(1/20th of the wavelength of S-waves) elements fall on top of the line representing the results with 3 in. by 3 in. square elements in Fig. 3.21. Similarly, the results with 1.5 in. by 1.5 in.(1/80th of the wavelength of S-waves), 1.5 in. by 3 in. and 3 in. by 3 in. elements and the results with 1.5 in. by 1.5 in., 1.5 in. by 6 in. and 6 in. by 6 in. elements fall on top of the line representing the results with 1.5 in. by 1.5 in. square elements in Fig. 3.22. For the purpose of finding the peak in frequency spectrum to study the effects of the cavity, this method works very well.

The comparison of the FEM and the BEM results for various discretization is presented in Figs. 3.23, 3.24, and 3.25 respectively. The agreement between the two solutions for a given mesh size is excellent when using 1/40th or 1/80th of the wavelength. For the larger mesh size (1/20th of the wavelength) and the case of a cavity there are some slight differences but it should be remembered that the results are not very accurate in this case.

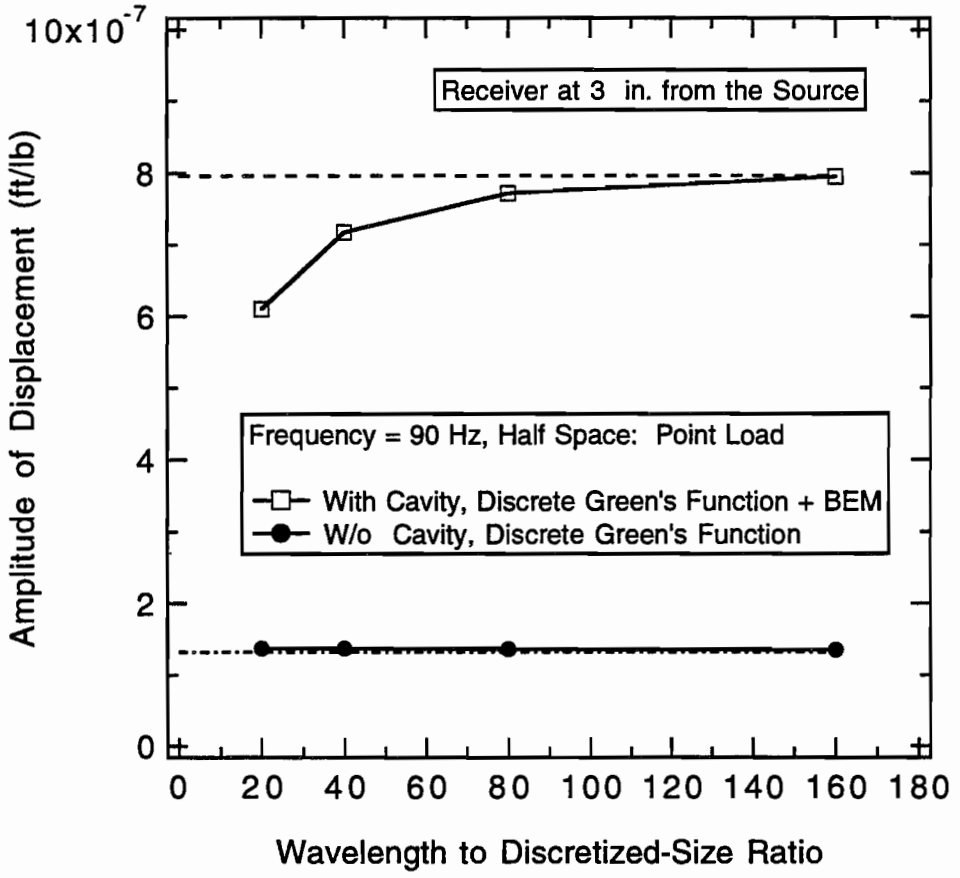


Fig. 3.19 Convergence of Results for a Uniform Half Space with a Cavity

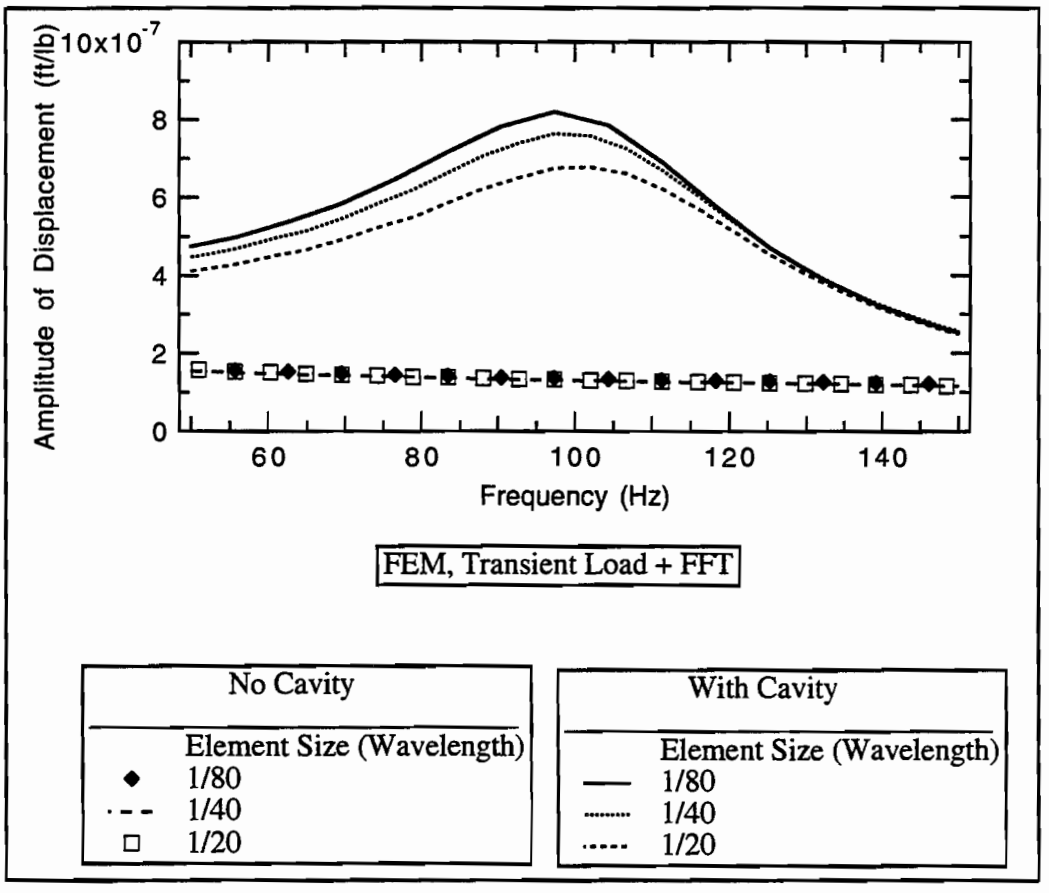


Fig. 3.20 Comparison of Results Using Different Element Size in FEM with Transient Load and FFT

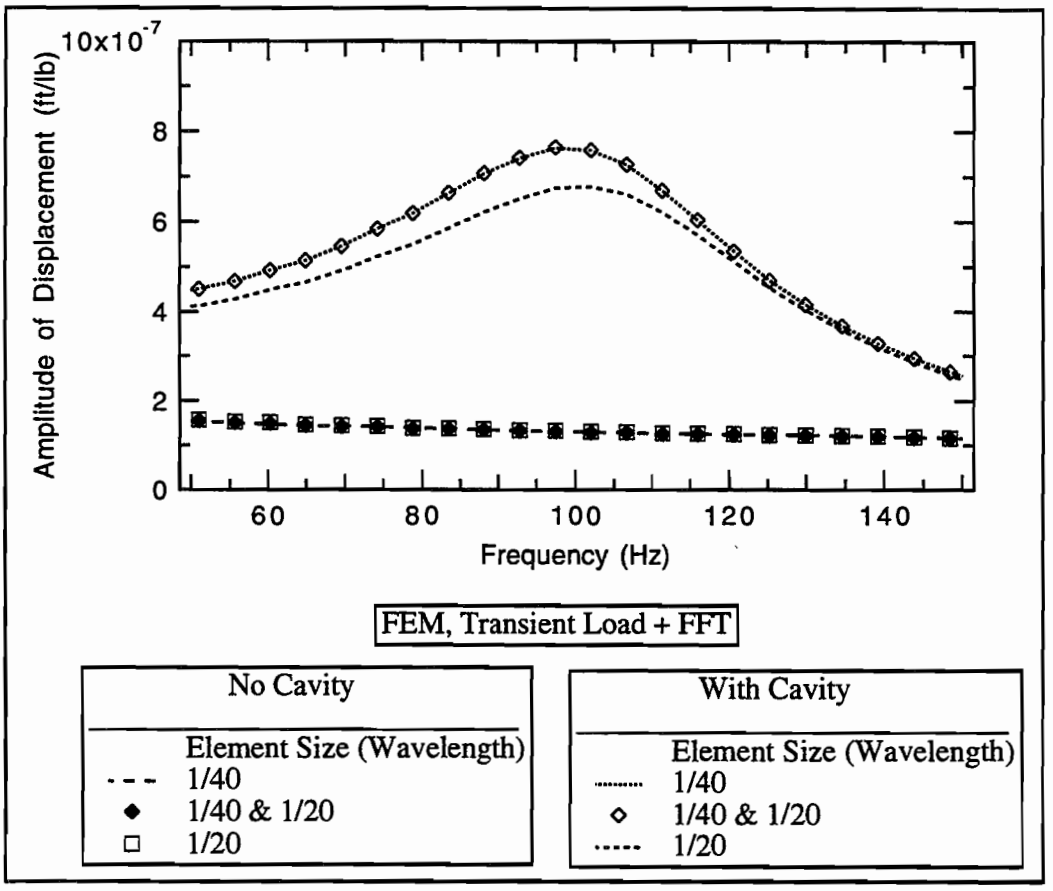


Fig. 3.21 Comparison of Results Using One and Mixed Sizes of Elements in FEM with Transient Load and FFT

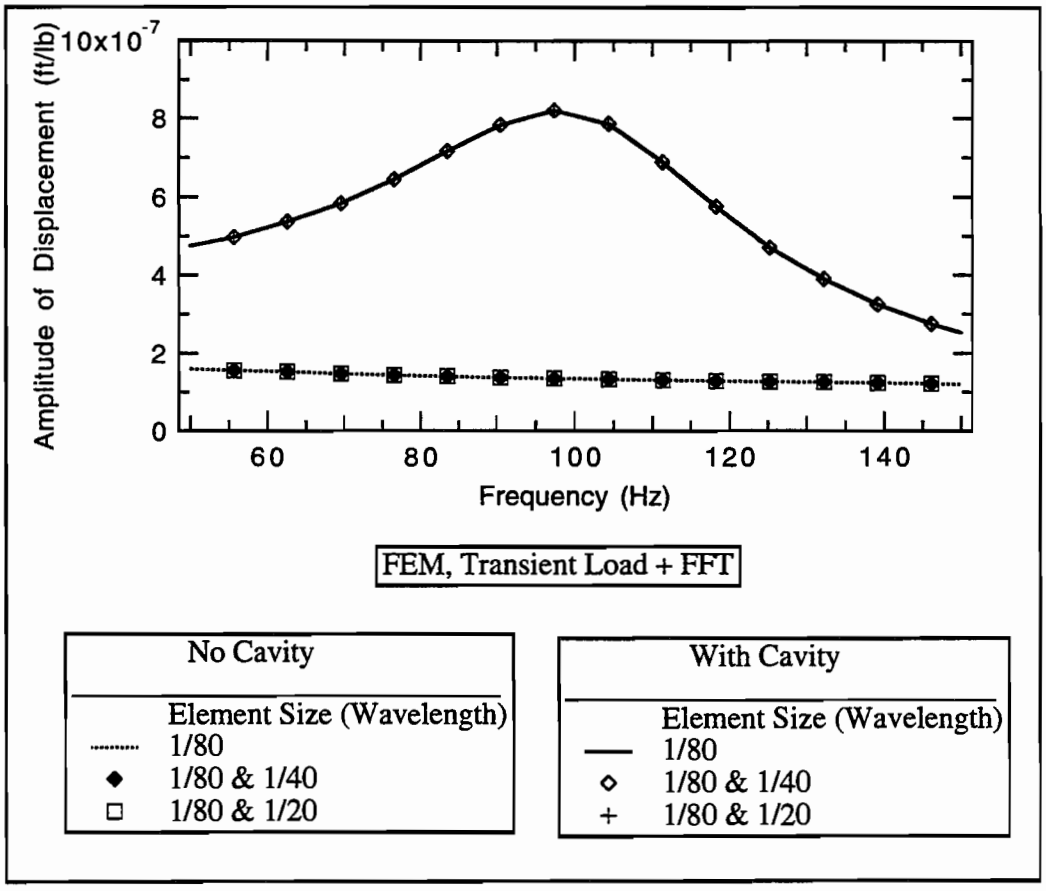


Fig. 3.22 Comparison of Results Using Small Size and Mixed Sizes of Elements in FEM with Transient Load and FFT

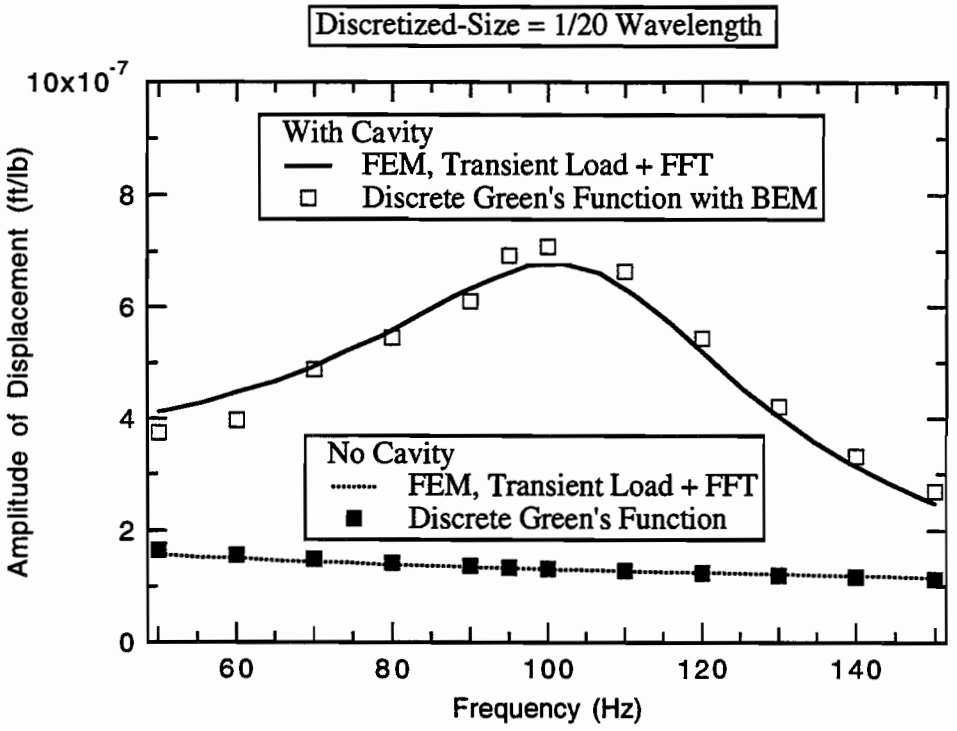


Fig. 3.23 Comparison of FEM and BEM Results Using 1/20th Wavelength of S-waves as Discretized-Size

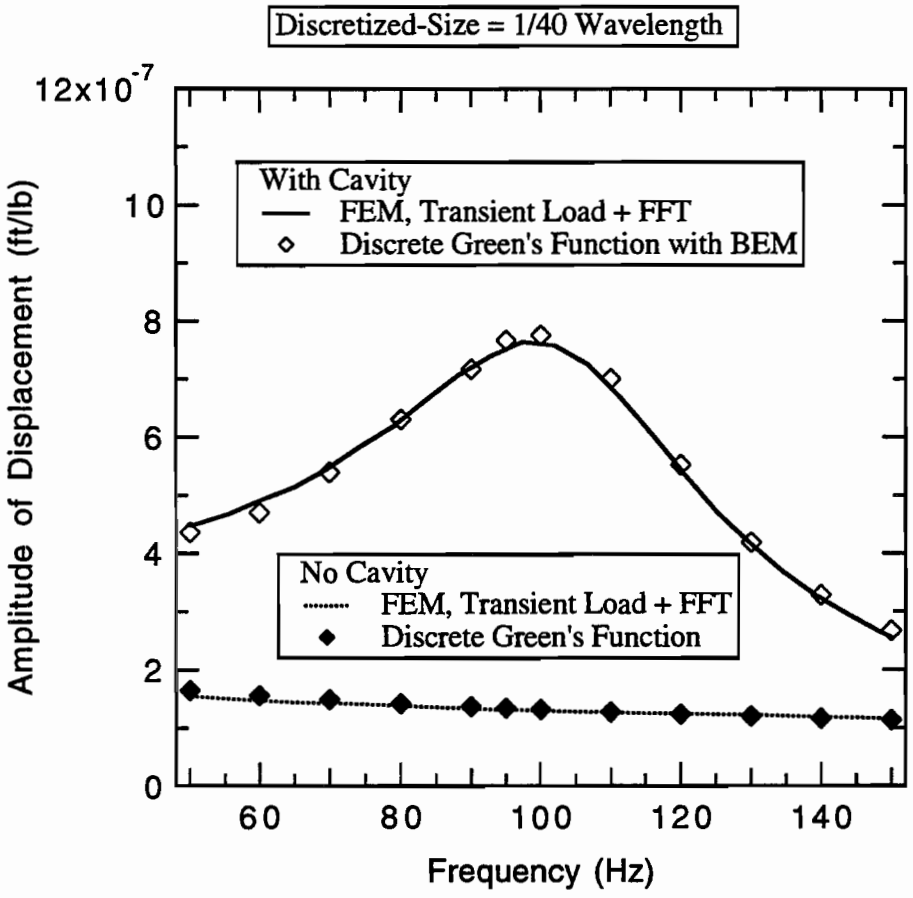


Fig. 3.24 Comparison of FEM and BEM Results Using 1/40th Wavelength of S-waves as Discretized-Size

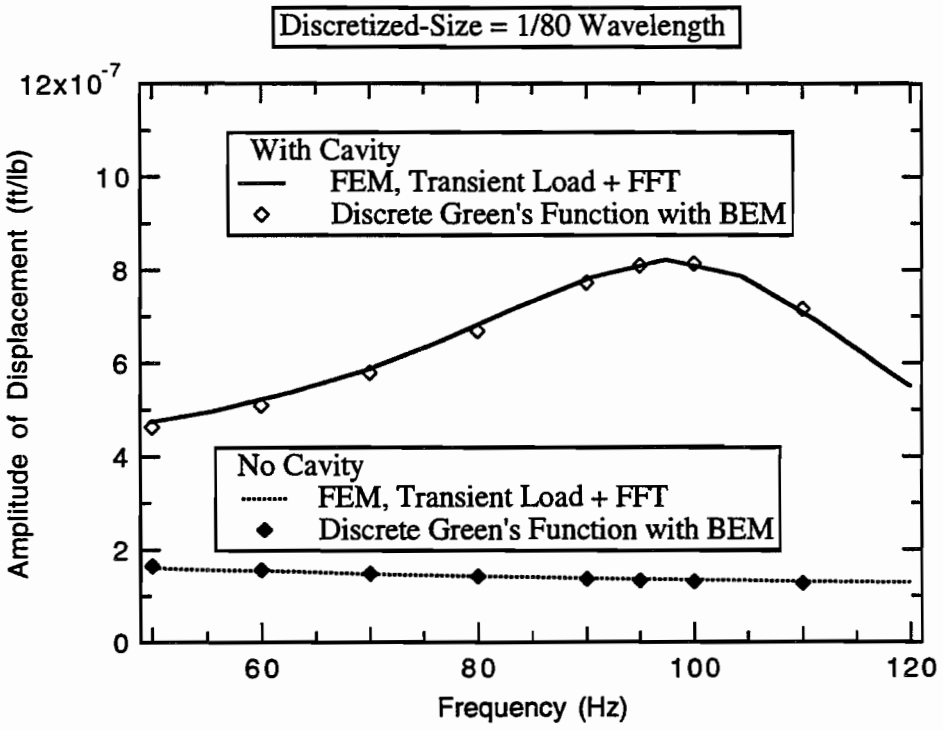


Fig. 3.25 Comparison of FEM and BEM Results Using 1/80th Wavelength of S-waves as Discretized-Size

Studies were also conducted with steady state excitation (time domain solution for steady state loads) of 80, 90, 100, 110, and 120 Hz. The corresponding results are shown in Fig. 3.26, for the soil without cavity and for the soil with cavity. The steady state finite element results fall on top of the line representing the results for the pulse load (after applying the Fourier transform).

## 3.5 LAYERED MEDIUM WITH A VOID

The pavement system shown in Fig. 3.27 was selected for further validation studies. It consists of a surface layer of concrete 10 inches thick over a second layer of asphalt concrete with a thickness of 6 inches. The subbase is 12 inches thick. The shear wave velocities of the materials are from top to bottom 8500, 3000, 1000, and 500 ft/sec. Poisson's ratios were assumed to be 0.2, 0.27, 0.25, and 0.33 respectively and the unit weights are 145, 145, 125, and 110 lb/ft$^3$. A value of hysteretic damping of 2% was considered for all layers.

The pavement was assumed to have first a rectangular void with a thickness of 3 inches and a width of 2 ft placed at the top of the asphalt concrete layer.

The predicted time histories at 3 inches from the source for an impulse duration of 1/8500 seconds is shown in Fig. 3.28. Using the Fast Fourier Transform, displacement amplitudes in the frequency domain were obtained as shown in Fig. 3.29. Based on the previous studies one would expect that the steady state amplitudes obtained this way would be reliable over the range from 4000 to 16000 Hz approximately. The maximum relative difference between the

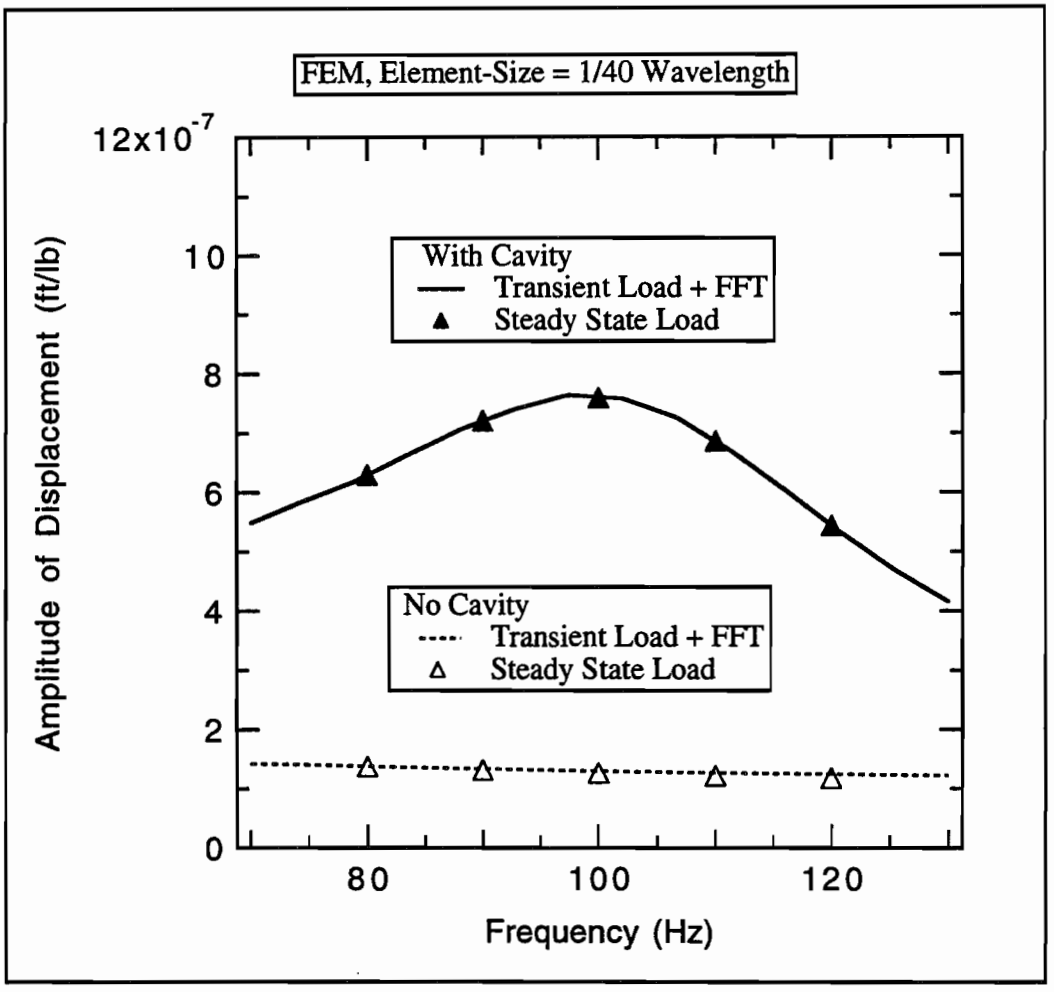


Fig. 3.26 Comparison of Results for Transient and Steady State Load in Finite Element Analysis

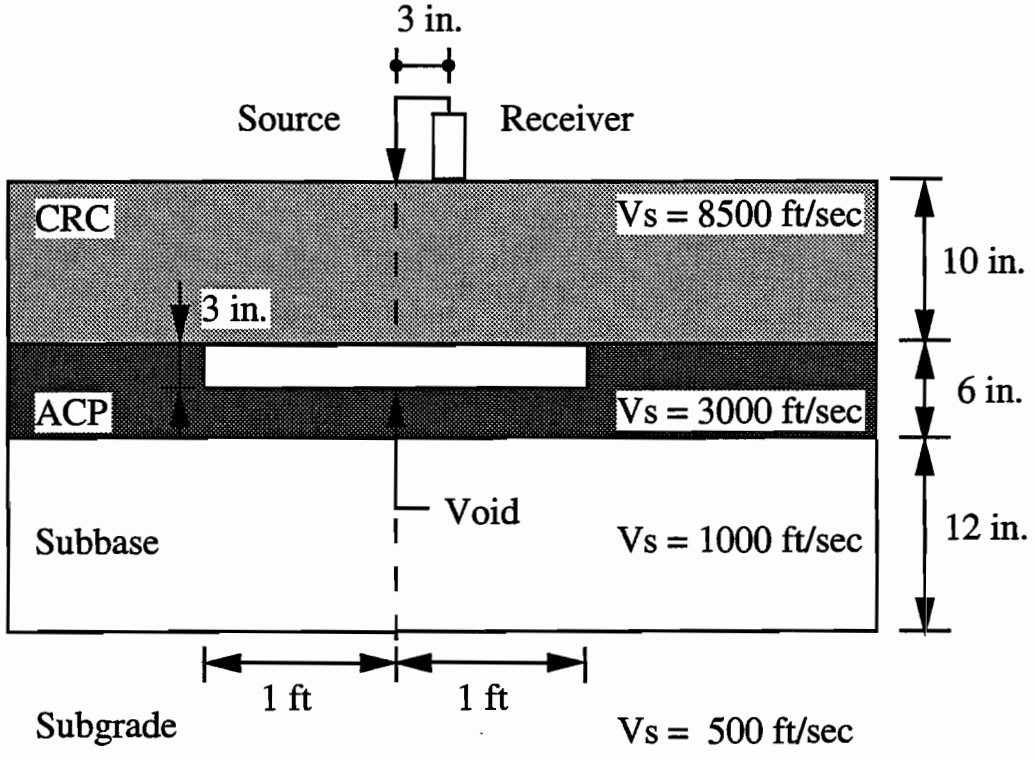


Fig. 3.27 Simulation of Testing on a Pavement System with a Flat Void at the Bottom of the Slab

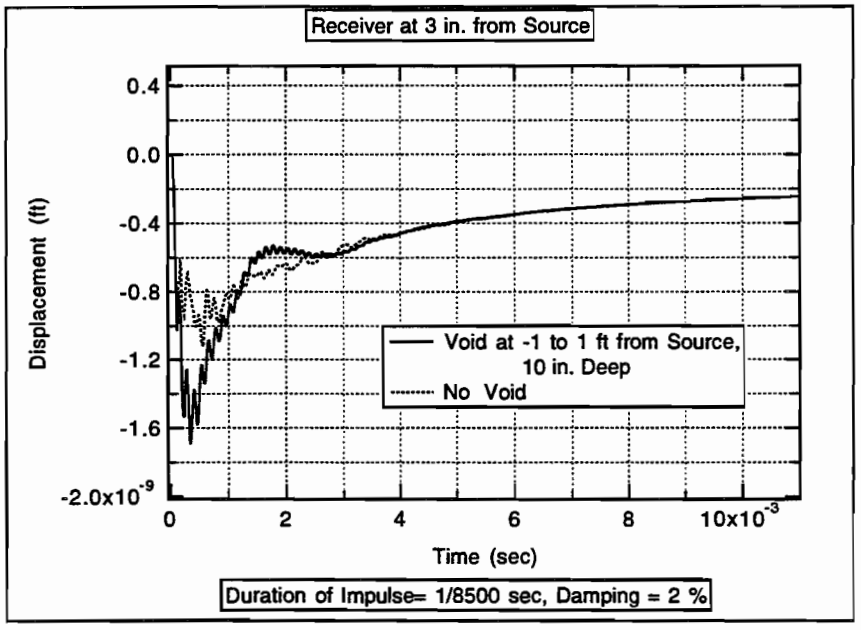


Fig. 3.28 Predicted Displacement Histories at 3 in. from the Source for an Impulse Duration of 1/8500 sec in a Pavement with a Void

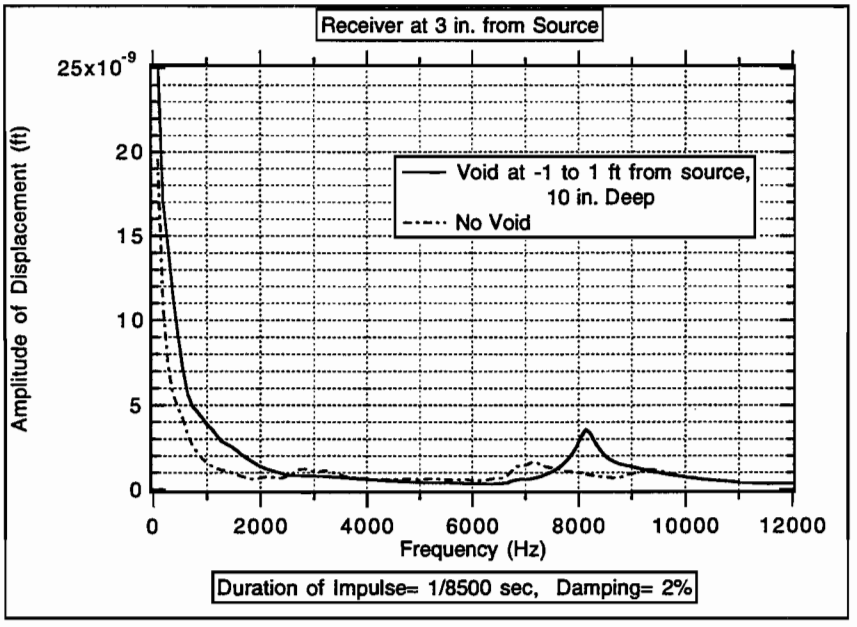


Fig. 3.29 Predicted Displacement Amplitudes at 3 in. from the Source for an Impulse Duration of 1/8500 sec in a Pavement with a Void

results for an intact pavement and one with a flat void occurs at a frequency of about 8000 Hz.

The comparison of the FEM and BEM results for the intact pavement and the pavement with a flat void is presented in Fig. 3.30. The agreement between the two solutions is excellent for frequencies of 3000 Hz or larger.

## 3.6 LAYERED MEDIUM WITH A DELAMINATION

The same pavement system of the previous section but with a horizontal crack (delamination) instead of a void, as shown in Fig. 3.31, was used for additional studies. The horizontal delamination is located at a depth of 3 inches from the surface. The predicted time histories at 3 and 6 inches from the source with an impulse duration of 1/630 seconds are shown in Fig. 3.32. The time histories for the pavement with delamination show very clear oscillations around the response of the intact pavement. The maximum displacement increases considerably due to the delamination. The period of the oscillation is approximately 1/690 seconds.

The displacement amplitudes in the frequency domain obtained using the FFT are shown in Fig. 3.33. A very important amplification of the steady state response is apparent at a frequency of 690 Hz. The steady state results were obtained at a number of frequencies through direct integration in time for a sinusoidal excitation. The agreement with the results from the transient analysis is excellent.

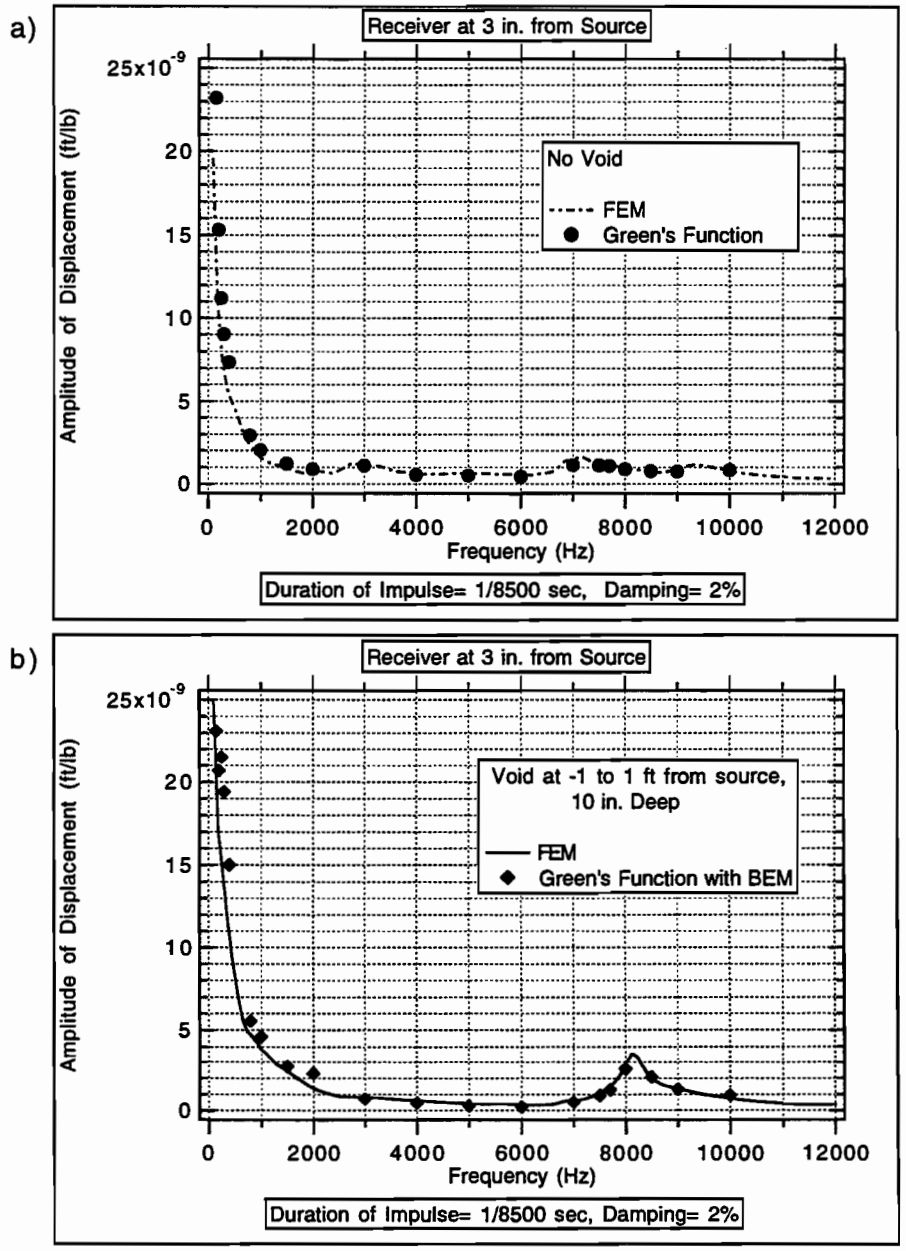


Fig. 3.30 Comparison of FEM and BEM Results for an Intact Pavement and a Pavement with a Void

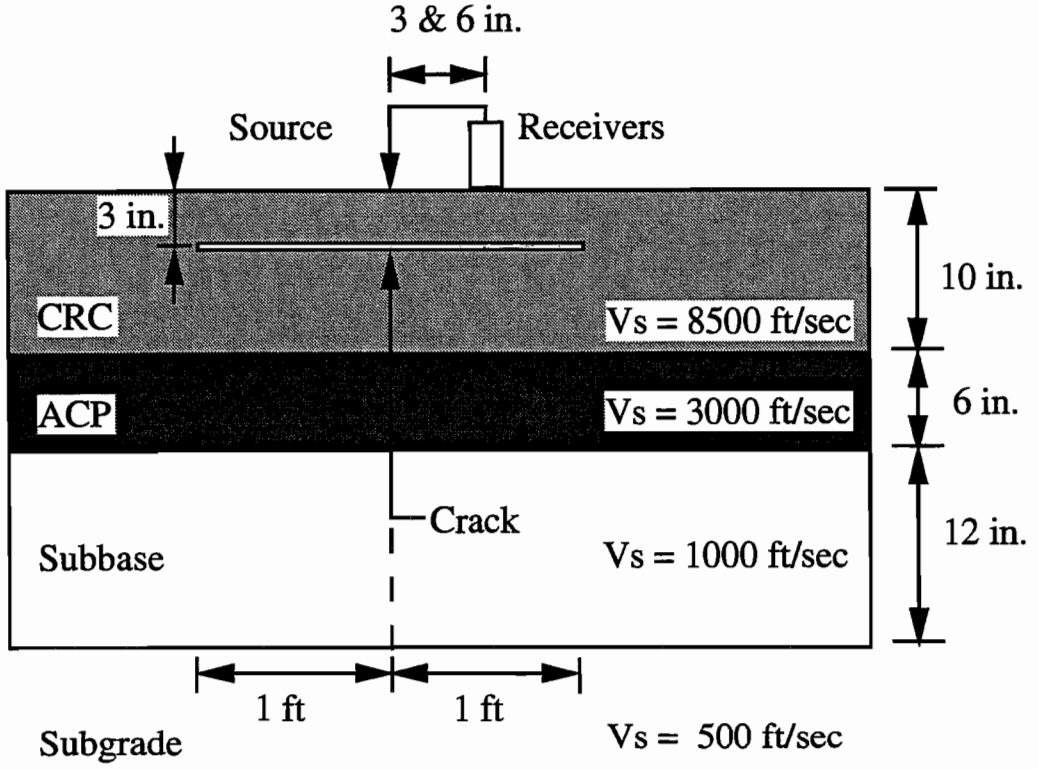


Fig. 3.31 Simulation of Testing on a Pavement System with a Horizontal Crack in the Middle of the Slab

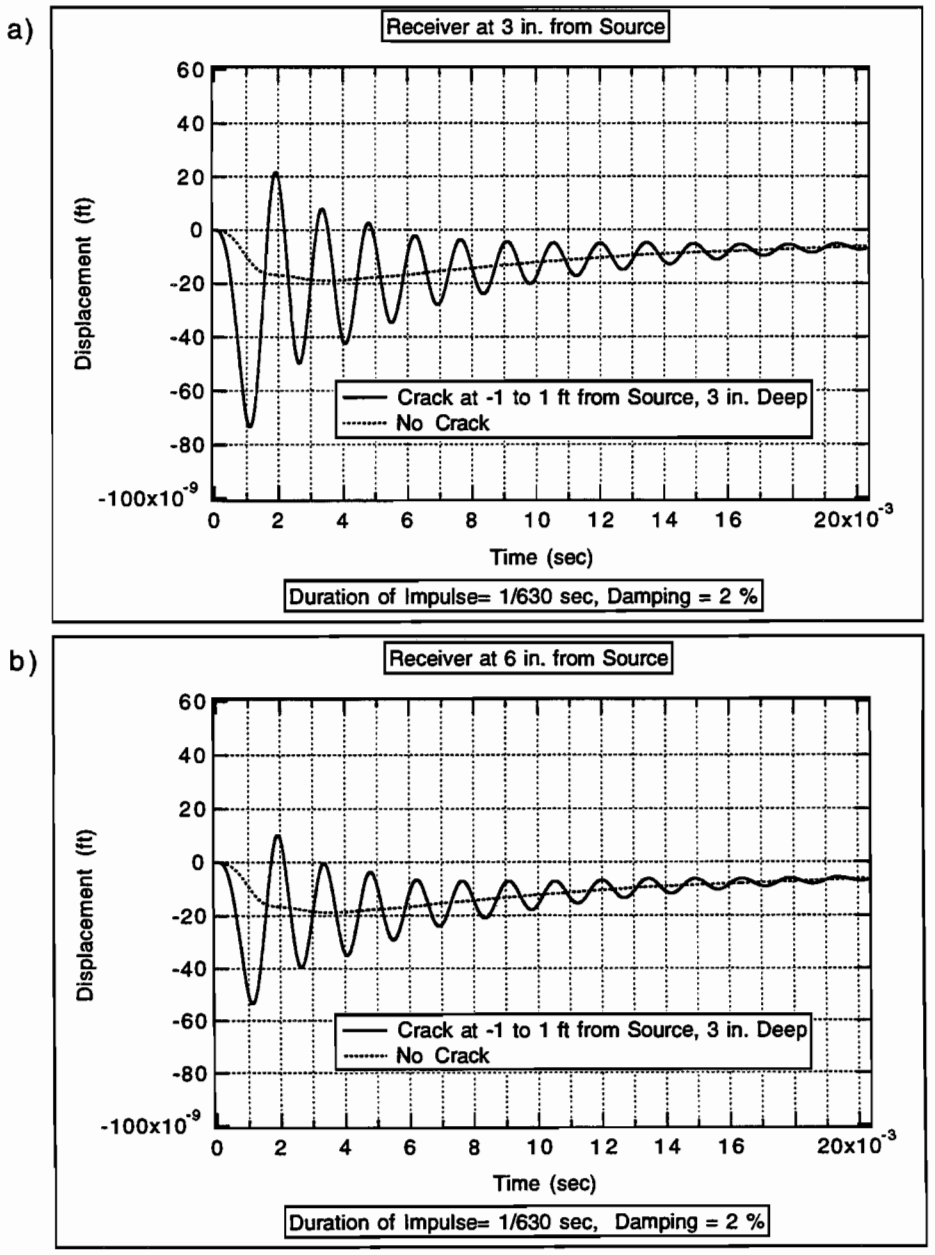


Fig. 3.32 Predicted Displacement Histories at 3 and 6 in. from the Source for an Impulse Duration of 1/630 sec on an Intact Pavement and a Pavement with a Horizontal Crack, All Layers with 2% Damping

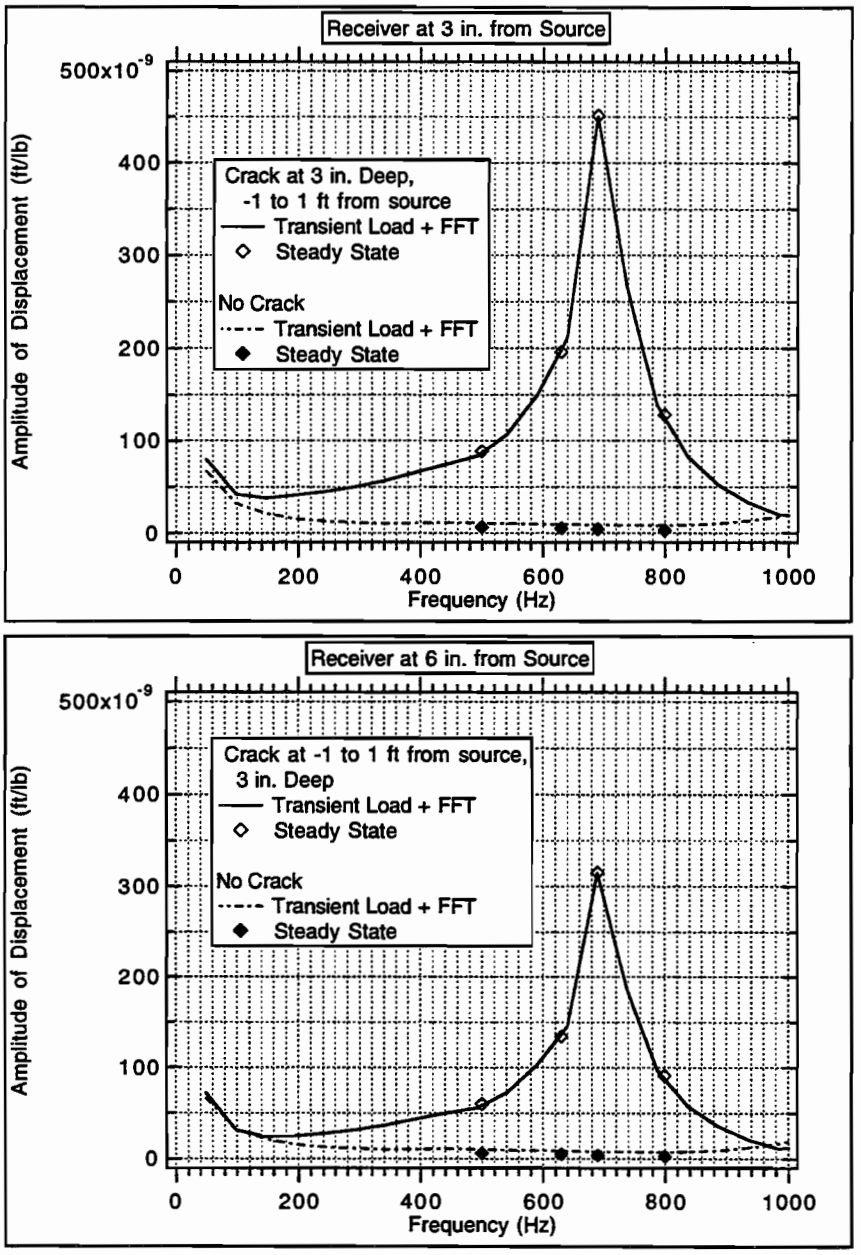


Fig. 3.33 Comparison of the Transient Solutions with the Steady-State Solutions on an Intact Pavement and a Pavement with a Horizontal Crack, All Layers with 2% Damping

## 3.7 SUMMARY

Without internal soil damping it can take a considerable amount of time to reach a steady state condition in time domain solutions using a finite element model subjected to a harmonic load. This is particularly so when there is much stiffer base at a finite depth. It is then advantageous to obtain the solution due to a transient load. The steady state response amplitudes can be computed dividing the Fourier transform of the transient response by that of the excitation. To obtain reliable results with this approach the duration of the transient impulse must be properly selected based on the desired range of frequencies. From the solution for one specific impulse one can select where peaks in the transfer function are located and select then a frequency in the appropriate range to improve the accuracy. A set of pulses with different durations can be used to cover an extended range of frequencies.

To reproduce the behavior of a medium with a void or a crack, the size of the finite elements or boundary elements must be much smaller than that used for intact layers. Once the parameters of the models are properly selected the three approaches considered here will give essentially the same results.

# CHAPTER FOUR

# EFFECTS OF DELAMINATIONS

## 4.1 INTRODUCTION

In the non-destructive testing of pavements considered in this work, the pavements surface would be struck with a hammer or other objects and the waves produced would be examined to identify the existence of a delaminated area. The ultimate objective would be to determine not only the existence but also the depth and size of the delamination. In this chapter, rectangular-shaped and disk-shaped delaminations were simulated. Two spacings between source and receiver, 3 and 6 inches, were considered. The selection of load durations and the corresponding effective frequency range were investigated for various depths of delaminations. The effects of damping ratio, base material and the extent of delamination were also studied. A special case of a delamination which extends to the pavement edge was discussed. Finally, the effects of the position of the source-receiver system with respect to the delamination was investigated to better understand the differences in the responses of intact and delaminated pavements as the source-receiver move along the pavement. Since the receiver may include some noise from the equipment and traffic (if testing is performed on the road), it is desirable to find the largest possible ratios of response of delaminated pavements to those of intact pavements.

## 4.2 PAVEMENT WITH A RECTANGULAR-SHAPED DELAMINATION

The pavement system with a horizontal crack (delamination) of the last chapter shown in Fig. 4.1, was used for the studies presented in this chapter. A value of hysteretic damping of 0.3% was considered for the concrete layer instead of 2% since the latest experimental results of concrete samples indicate that the damping ratios fall between 0.1% and 0.5%. The horizontal delamination was placed at a depth of 3 inches from the surface. In order to study the effect of the moving source-receiver system approaching the delamination, two dimensional plane-strain elements were used to simulate the rectangular-shaped delamination with a long side in the direction perpendicular to the plane which is much larger than the short side. The loading is a line load in the direction of the long side.

### 4.2.1 Load Duration

The length of the crack, L, was assumed to be 2 feet initially. The predicted time histories at 3 and 6 inches from the source for an impulse duration of 1/26000 seconds are shown in Fig. 4.2. The ratios of maximum displacement obtained in the delaminated pavement to that in the intact pavement are approximately 6 for both 3-inch and 6-inch receivers.

The displacement amplitudes in the frequency domain obtained using the FFT are shown in Fig. 4.3. There are two clear peaks in the results for the delaminated pavement at the frequencies of 26300 and 27400 Hz ("P-wave peak-frequency"). At these frequencies, the corresponding ratios of the displacement amplitudes in the defective pavement to those in the intact pavement are

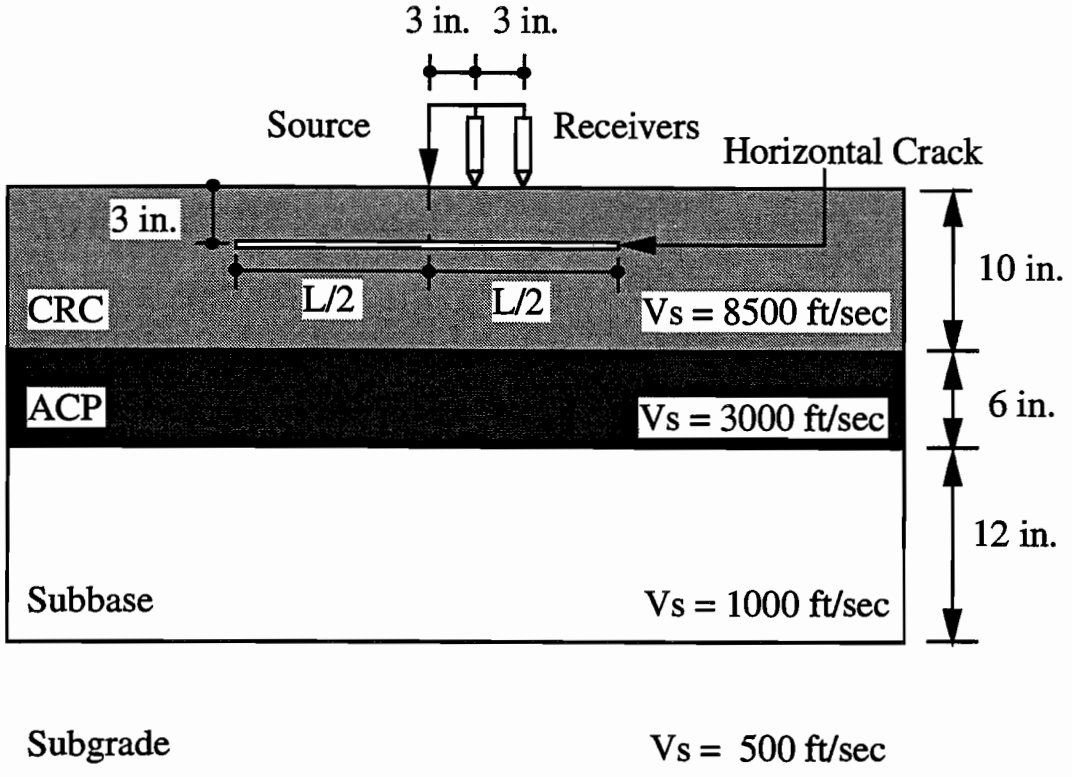


Fig. 4.1 Simulation of Testing on a Pavement System with a Horizontal Crack at a Depth of 3 inches from the Surface

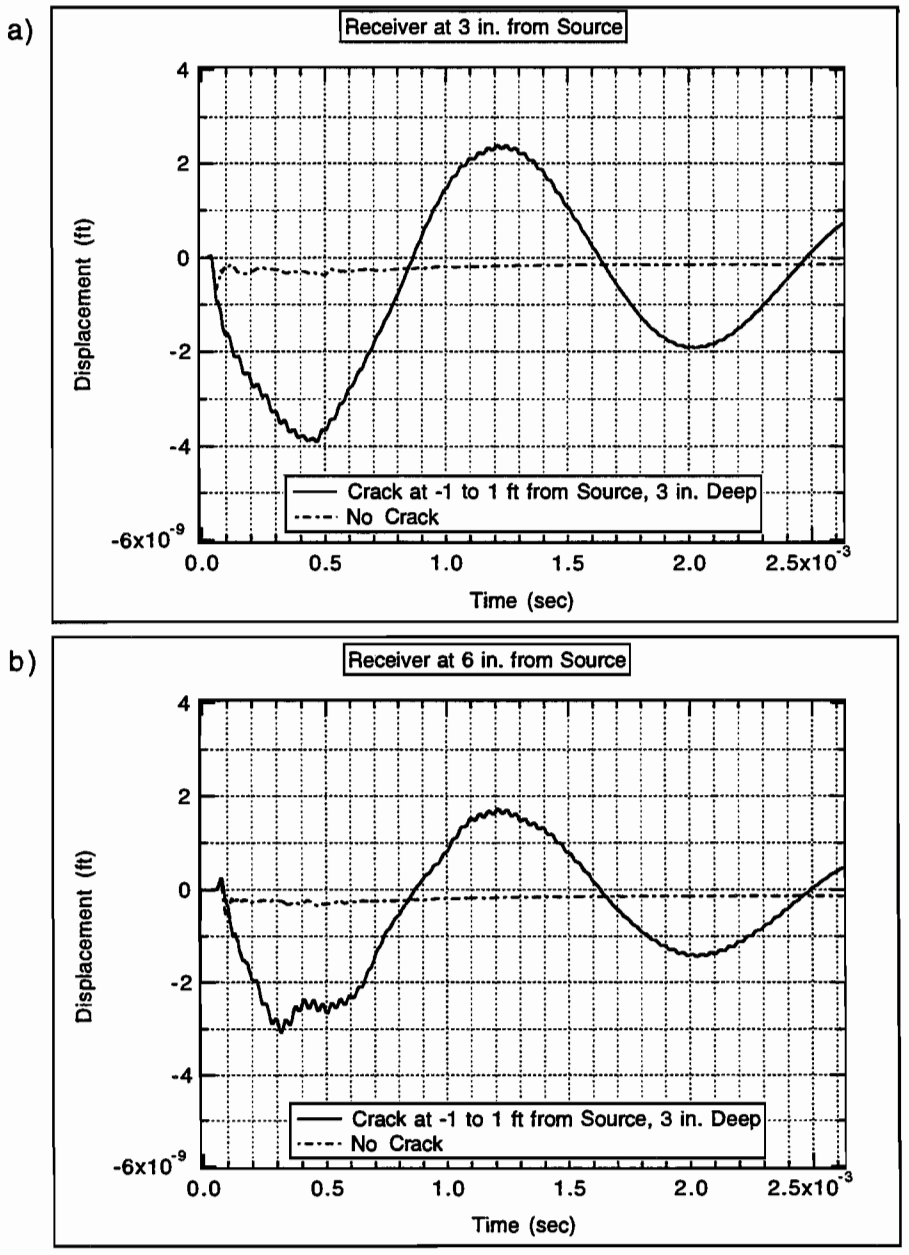


Fig. 4.2 Predicted Displacement Histories at 3 and 6 in. from the Source for an Impulse Duration of 1/26000 sec

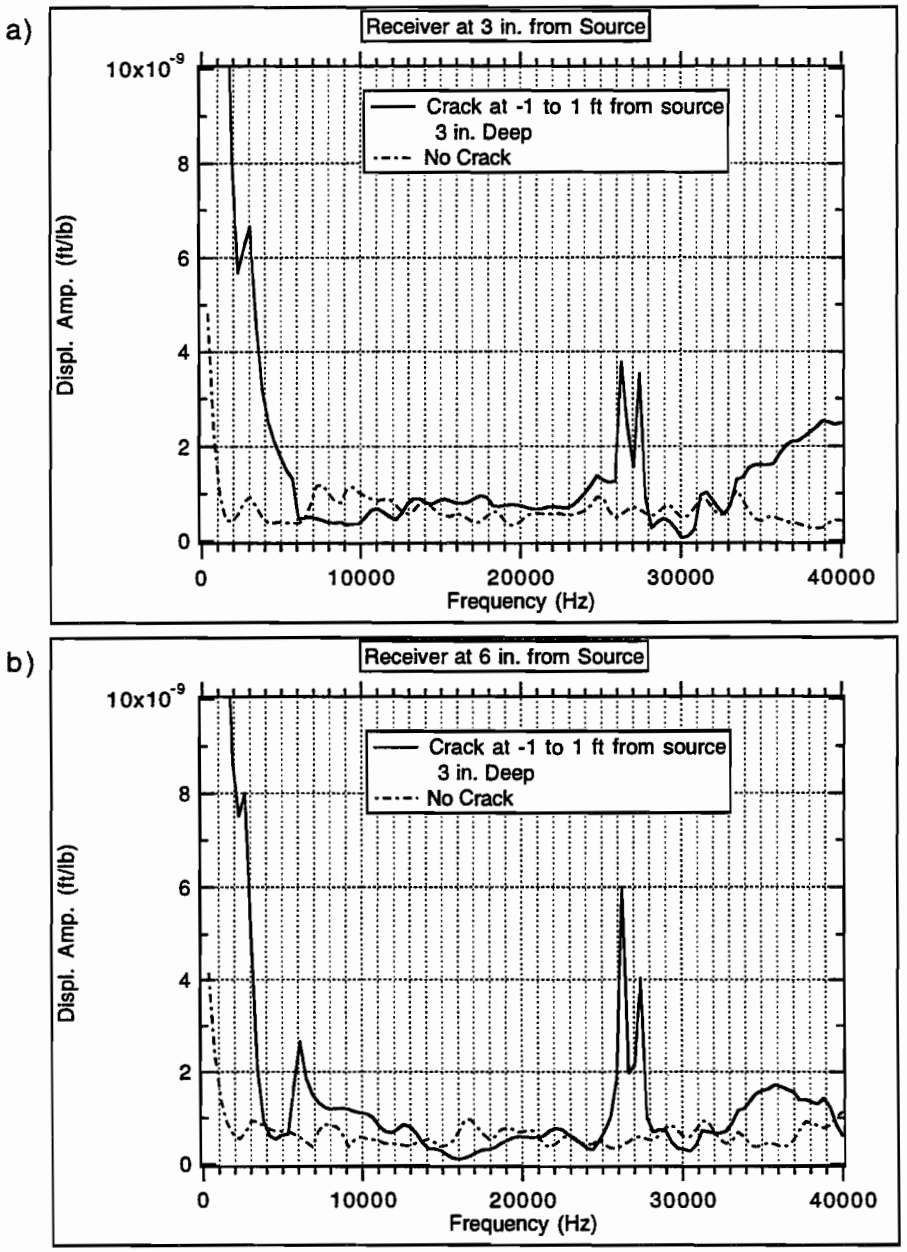


Fig. 4.3 Predicted Displacement Amplitudes at 3 and 6 in. from the Source for an Impulse Duration of 1/26000 sec

approximately 7 and 6 for the 3-inch receiver, and 14 and 8 for the 6-inch receiver, which are larger than the ratios of maximum displacements in the time domain.

In order to obtain a more accurate solution in the lower frequency range, an impulse with a duration of 1/8500 seconds was applied next. The corresponding time histories are shown in Fig. 4.4 and the steady state responses in Fig. 4.5. The time histories for the pavement with delamination oscillate around the response of the intact pavement. The maximum displacement increases considerably due to the delamination. The ratios of maximum displacement obtained in the delaminated pavement to that in the intact pavement are approximately 9 and 8 for the 3-inch and 6-inch receivers respectively. These ratios are a little larger than those obtained for an impulse duration of 1/26000 seconds. The period of the oscillation is approximately 1/700 seconds. A large amplification of the steady state response is also apparent for each receiver in Fig. 4.5 at a frequency of 700 Hz ("flexural peak-frequency"). The corresponding ratios of displacement amplitude in the defective pavement to that in the intact pavement are approximately 120 and 80 for the 3-inch and 6-inch receivers respectively, which are 13 and 10 times larger than the ratios of maximum displacement in the time domain as well as 6 to 20 times larger than the ratios obtained at the "P-wave peaks" for an impulse duration of 1/26000 seconds in the frequency domain.

Finally, and on the basis of these results an impulse with a duration of 1/630 seconds was chosen. The corresponding results are shown in Fig. 4.6 for the time histories and in Fig. 4.7 for the steady state responses. The time histories

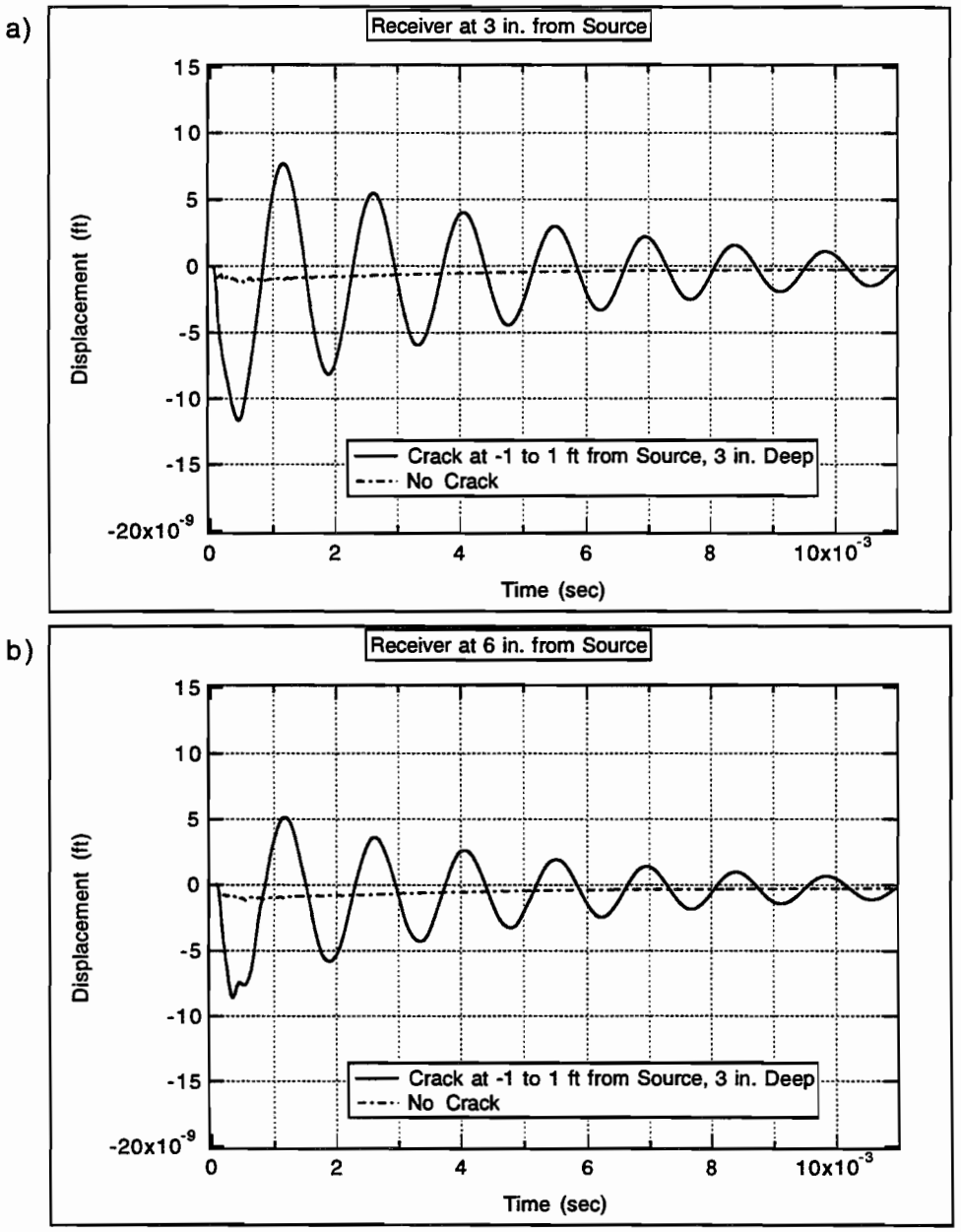


Fig. 4.4 Predicted Displacement Histories at 3 and 6 in. from the Source for an Impulse Duration of 1/8500 sec

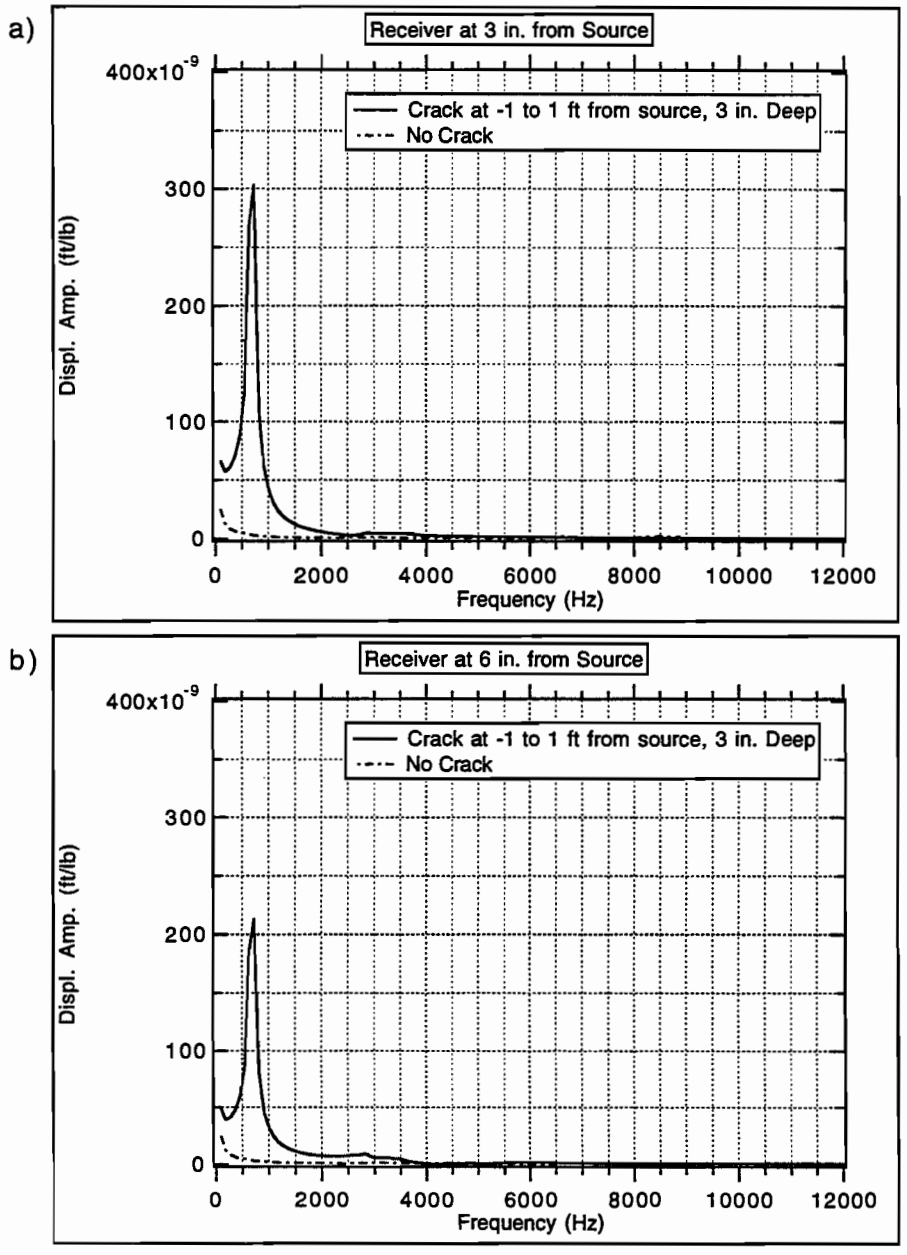


Fig. 4.5 Predicted Displacement Amplitudes at 3 and 6 in. from the Source for an Impulse Duration of 1/8500 sec

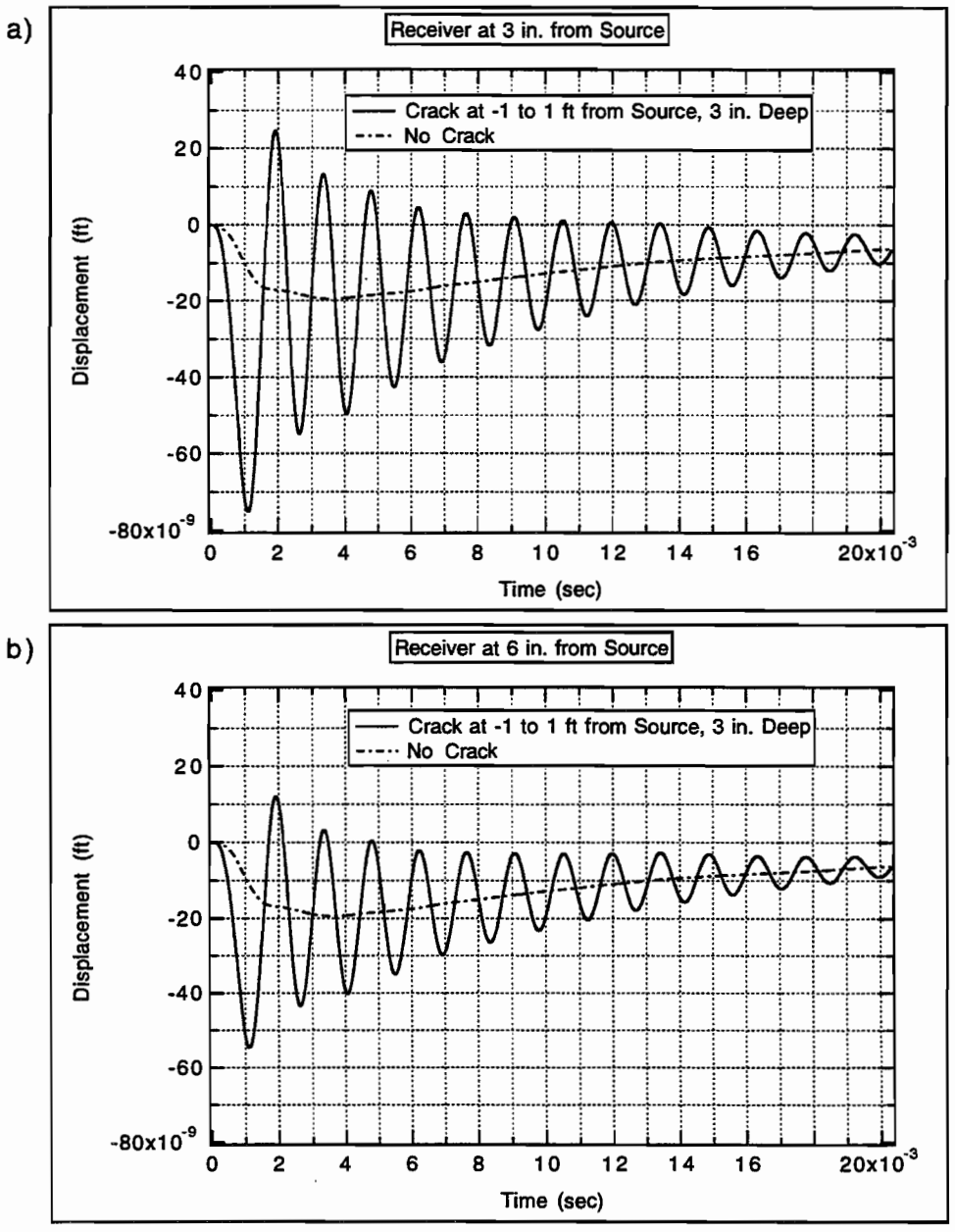


Fig. 4.6 Predicted Displacement Histories at 3 and 6 in. from the Source for an Impulse Duration of 1/630 sec

a) Receiver at 3 in. from Source

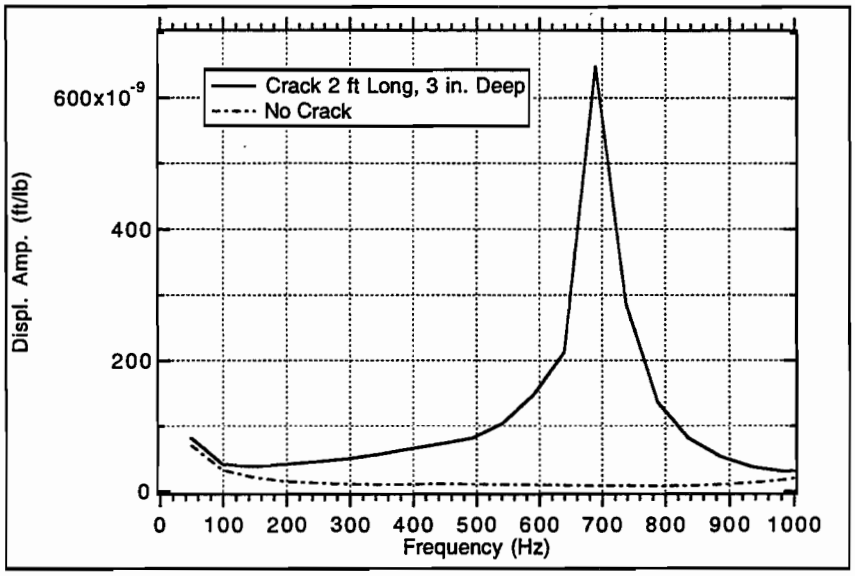


b) Receiver at 6 in. from Source

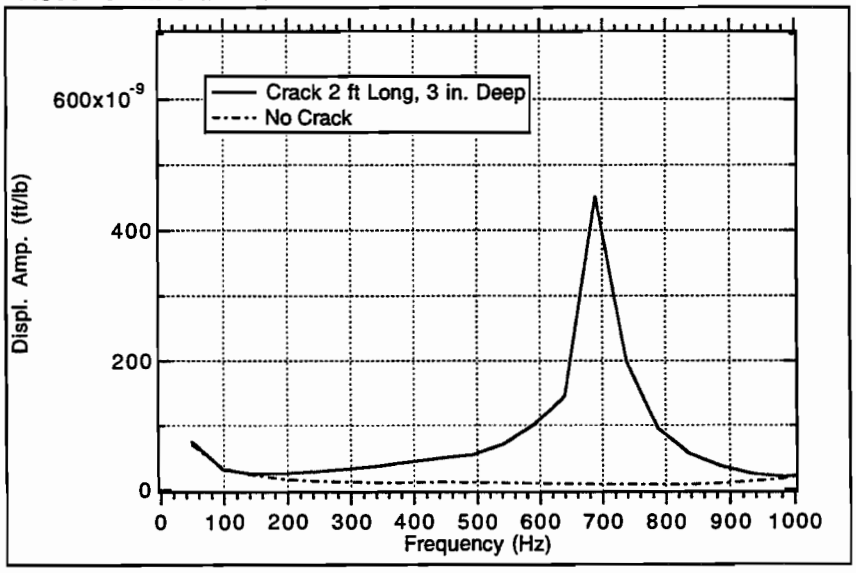


Fig. 4.7 Predicted Displacement Amplitudes at 3 and 6 in. from the Source for an Impulse Duration of 1/630 sec

for the delaminated pavement show very clear oscillations around the response of the intact pavement. The ratios of maximum displacement obtained in the delaminated pavement to that in the intact pavement are approximately 4 and 3 for the 3-inch and 6-inch receivers respectively. It should be noted that these ratios are small compared to those obtained for previous shorter duration of impulses. A very important amplification is, however, apparent in the frequency domain in Fig. 4.7 at a frequency of 690 Hz, which is the same value of the oscillation period in the time domain. The corresponding ratios of displacement amplitude in the defective pavement to that in the intact pavement are approximately 75 and 55 for 3-inch and 6-inch receivers respectively. These ratios are 20 times larger than the ratios of maximum displacement in the time domain. Even though the ratios in the frequency domain are not the largest, they are more reliable than others since the peak-frequency is very close to the predominant frequency, inverse of impulse duration. More importantly these results show that it is not necessary to have an impulse with a duration exactly equal to the inverse of the significant frequency in order to catch adequately the existence of the peak in the frequency domain.

### 4.2.2 Damping Effects

Figure 4.8 illustrates the effect of the damping ratio of the concrete layer on the displacement amplitudes at the "P-wave peaks" for the 3-inch and 6-inch receivers and a delaminated pavement. The peak amplitudes decrease about 40%, 60-70% and 80-85% for a concrete layer with 0.3%, 1% and 2% damping

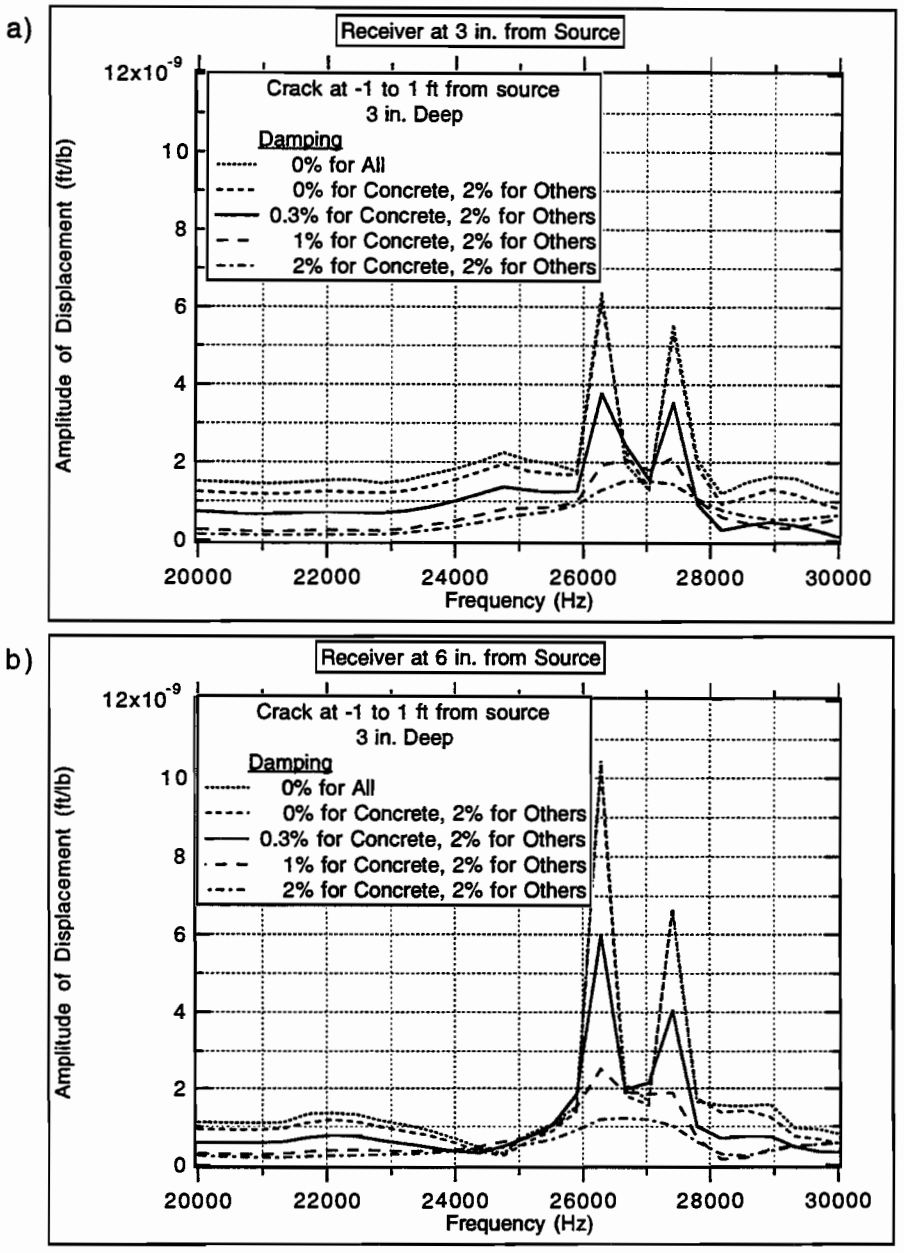


Fig. 4.8 Effect of Damping on the "P-Wave Peaks" for a Pavement with a Horizontal Crack at a depth of 3 in. from the surface

respectively in comparison with an undamped pavement. In addition, the two peaks merge into one as the damping of the concrete reaches 2%. The damping ratios of the other layers beneath the concrete layer have little effect on the displacement amplitude at the "P-wave peaks". The results of an ideal pavement without damping in any layer fall almost on top of the peaks representing the results for a pavement with no damping in the concrete layer and 2 % damping for the other layers over the frequency range from 26000 to 27800 Hz. Comparing the results in Fig. 4.8b to those in Fig. 4.8a, one may find that the displacement amplitudes at the "P-wave peaks" for the 6-inch receiver are larger than those at the 3-inch receiver. This is probably due to the reflections of the line load.

The results for an intact pavement are shown in Fig. 4.9. Although a number of waves can be seen in Fig. 4.9a, the difference in the displacement amplitudes for the 3-inch receiver at frequencies of 25000, 27000, and 29300 Hz is relatively small, as the damping ratio of the concrete varies from 0% to 2% with the damping ratios of the other layers equal to 2%. The small dot lines, representing the ideal case of a pavement system without any damping, show increases at the frequencies of 22450, 25150 and 27750 Hz. The results for the 6-inch receiver, shown in Fig. 4.9b, exhibit similar trends with smaller variations for the different values of damping. The damping of the other layers, beneath the concrete pavement, have larger effect on the displacement amplitudes for an intact pavement as shown in Fig. 4.9. This difference probably indicates that most waves generated were prevented from traveling down by the delamination and reflected up. However, the displacement amplitudes in Fig. 4.9 are so small,

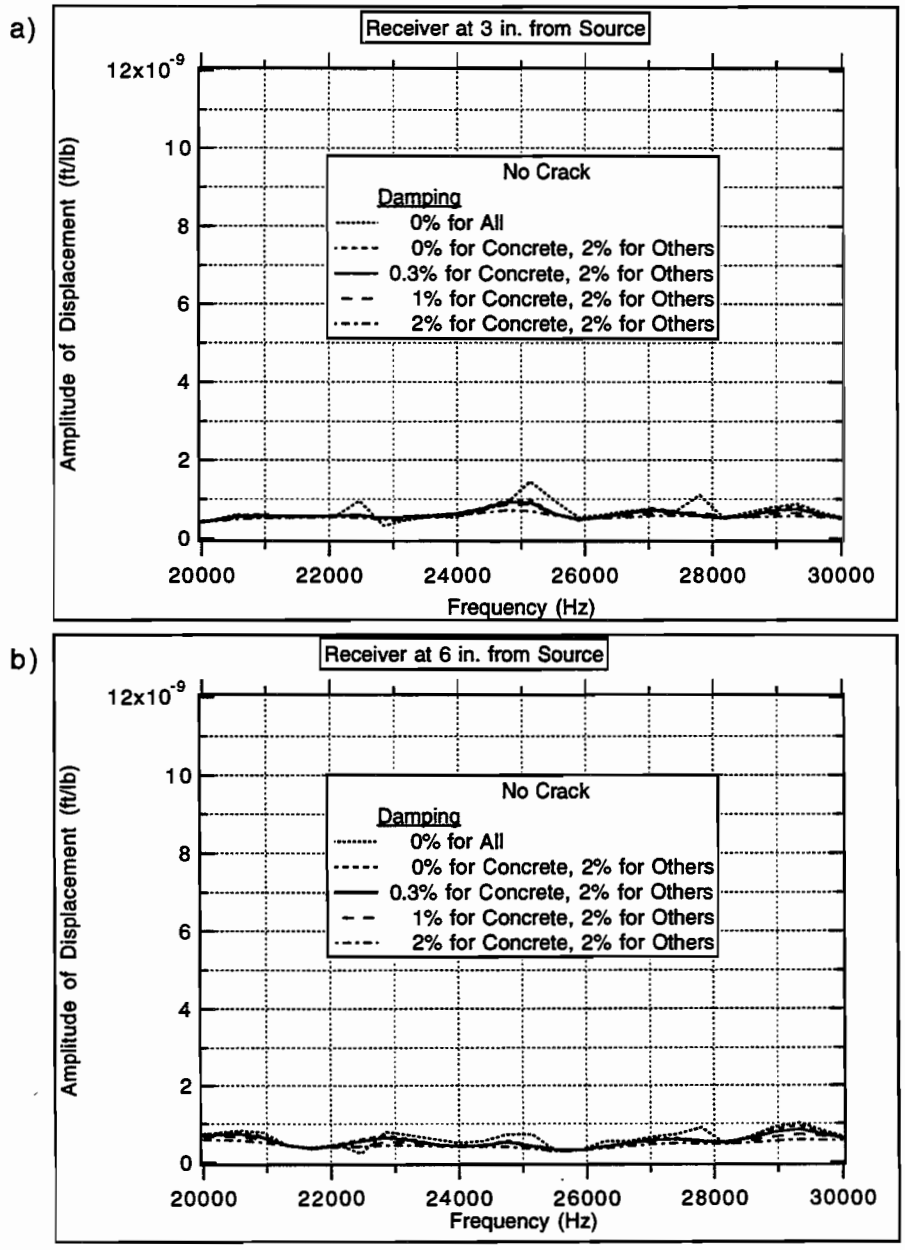


Fig. 4.9 Effect of Damping on the Displacement Amplitudes in the High frequency Range for an Intact Pavement

compared to the peak amplitudes for the delaminated pavement of Fig. 4.8, that the response of the delaminated pavement can be easily distinguished.

The damping ratio of the concrete layer has less effect on the displacement amplitude at the "flexural peak" than at the "P-wave peaks" for the 3-inch and 6-inch receivers and a delaminated pavement, as shown in Fig. 4.10. The explanation could be that the longer wavelengths attenuate less over these fixed distances. The peak amplitudes decrease about 7%, 21% and 35% as the damping ratio of the concrete layer varies from 0% to 0.3%, 1% and 2% respectively. The damping ratios of the other layers beneath the concrete pavement have, however, similar effects on the displacement amplitude at the "flexural peak" and those at the "P-wave peaks". The peak amplitudes decrease about 4% as the damping ratios of the lower layers beneath the concrete layer change from 0% to 2% for both receivers. The displacement amplitudes around the "flexural peak" for the 6-inch receiver, shown in Fig. 4.10b, are 30% lower than the amplitudes at 3-inch receiver in Fig. 4.10a.

The results for an intact pavement are shown in Fig. 4.11. The damping ratios of the concrete layer have almost no effect on the displacement amplitudes over the frequency range from 100 to 1000 Hz. The damping ratios of the lower layers have a stronger effect again on the displacement amplitude of intact pavements than for delaminated pavements. Again, this difference is due to the facts that the waves in an intact pavement can travel deeper without being trapped above the delamination in the concrete layer. The peak amplitudes decrease from 0% to 45% over the frequency range from 130 to 1000 Hz as the damping ratios of the lower layers change from 0% to 2%. It should be noted that the

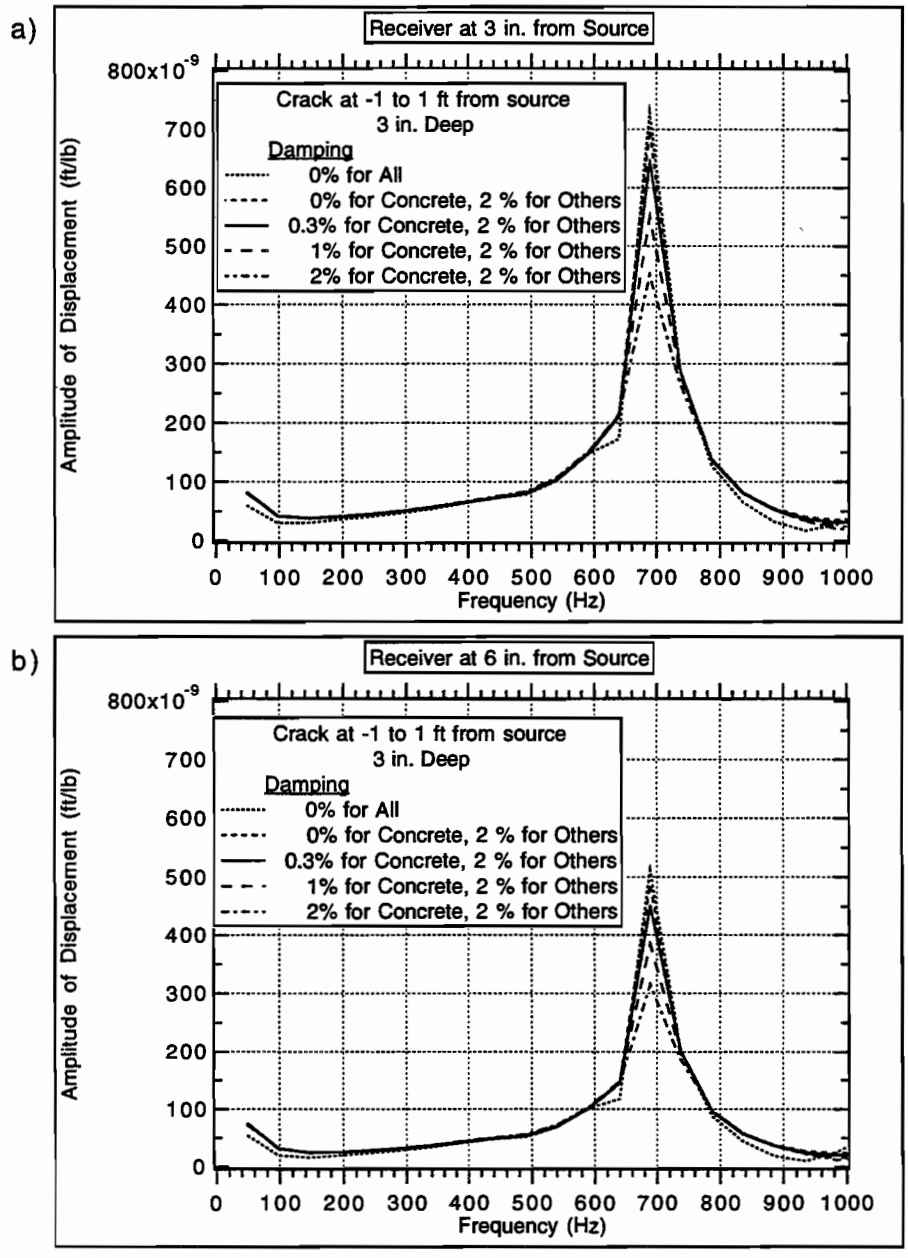


Fig. 4.10 Effect of Damping on the "Flexural Peaks" for a Pavement with a Horizontal Crack at a depth of 3 in. from the surface

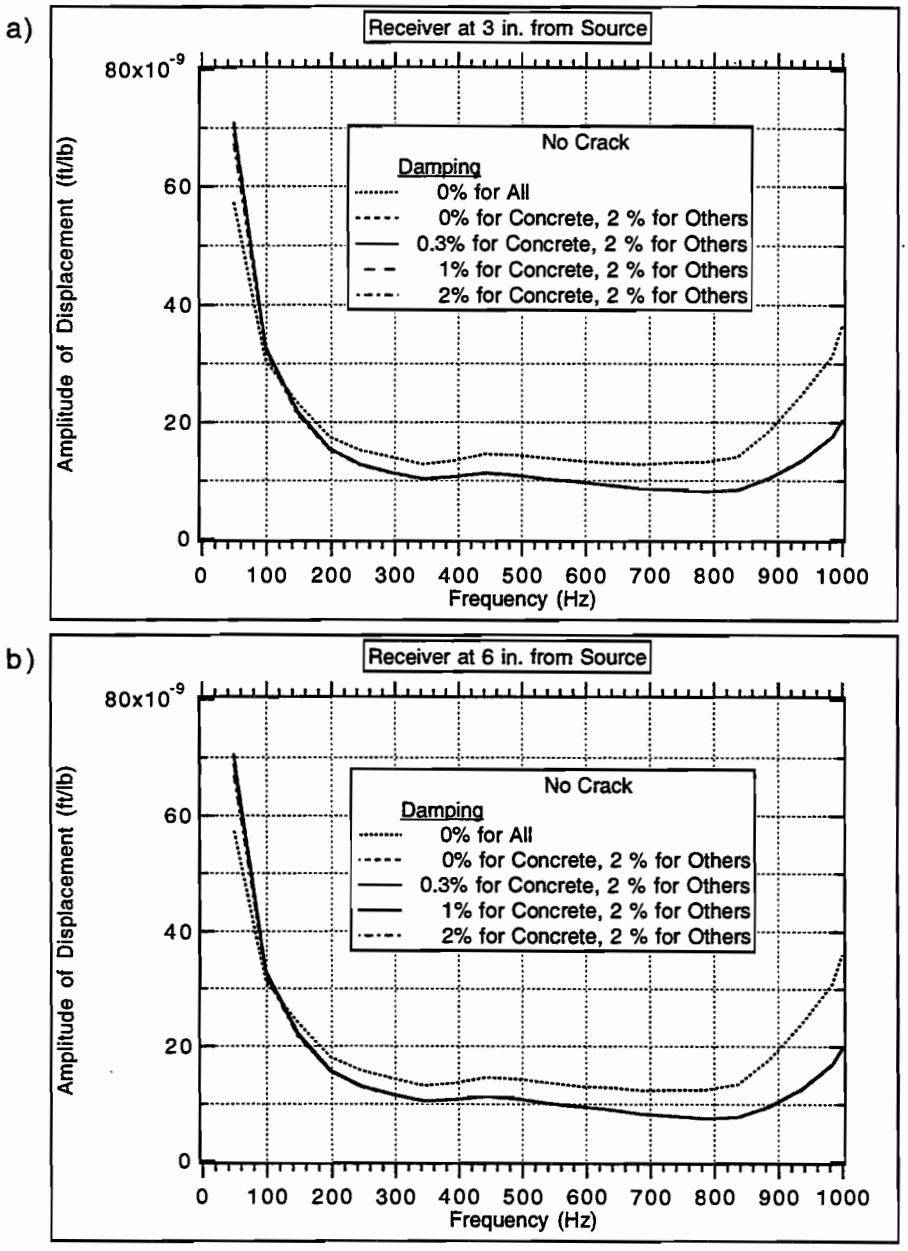


Fig. 4.11 Effect of Damping on the Displacement Amplitudes in the Low Frequency Range for an Intact Pavement

displacement amplitudes for the 6-inch receiver are almost identical to those at the 3-inch receiver due to the line load.

### 4.2.3 Effects of Delamination Length

Three lengths of the horizontal crack (delamination), 1, 2, and 3 feet, were considered. The predicted displacement histories at 3 and 6 inches from the source with an impulse duration of 1/26000 seconds are shown in Figs. 4.12 and 4.13. The ratios of maximum displacement obtained in the delaminated pavement to that in the intact pavement are 3, 5.8 and 8.2 for crack lengths of 1, 2 and 3 feet respectively at the 3-inch receiver. These ratios are 1.6, 5.7 and 8.6 at the 6-inch receiver. These ratios indicate little difference between the measurements at the 3-inch and 6-inch receivers for the crack lengths of 2 and 3 feet, but the ratio decreases almost in half for the 1-foot crack as the receiver is moved from 3 to 6 inches. The oscillations in the displacement histories for the 1-foot crack is quite significant at the 3-inch receiver but almost vanish at the 6-inch receiver. The period of this oscillation is approximately 1/1800 seconds.

The steady state responses in the frequency domain for the two receivers are shown in Figs. 4.14 and 4.15. The "P-wave peak-frequencies" for the 3-inch receiver appear to be 27400 Hz for the 1-foot crack, 26300 and 27400 Hz for the 2-foot crack, and 26300 Hz for the 3-foot crack. The "P-wave peak" at the 6-inch receiver nearly vanishes for the 1-foot crack. The largest ratio of displacement amplitude obtained in the delaminated pavement to that in the intact pavement is 2.8 at a frequency of 26700 Hz (Fig. 4.15). The length of the delamination has

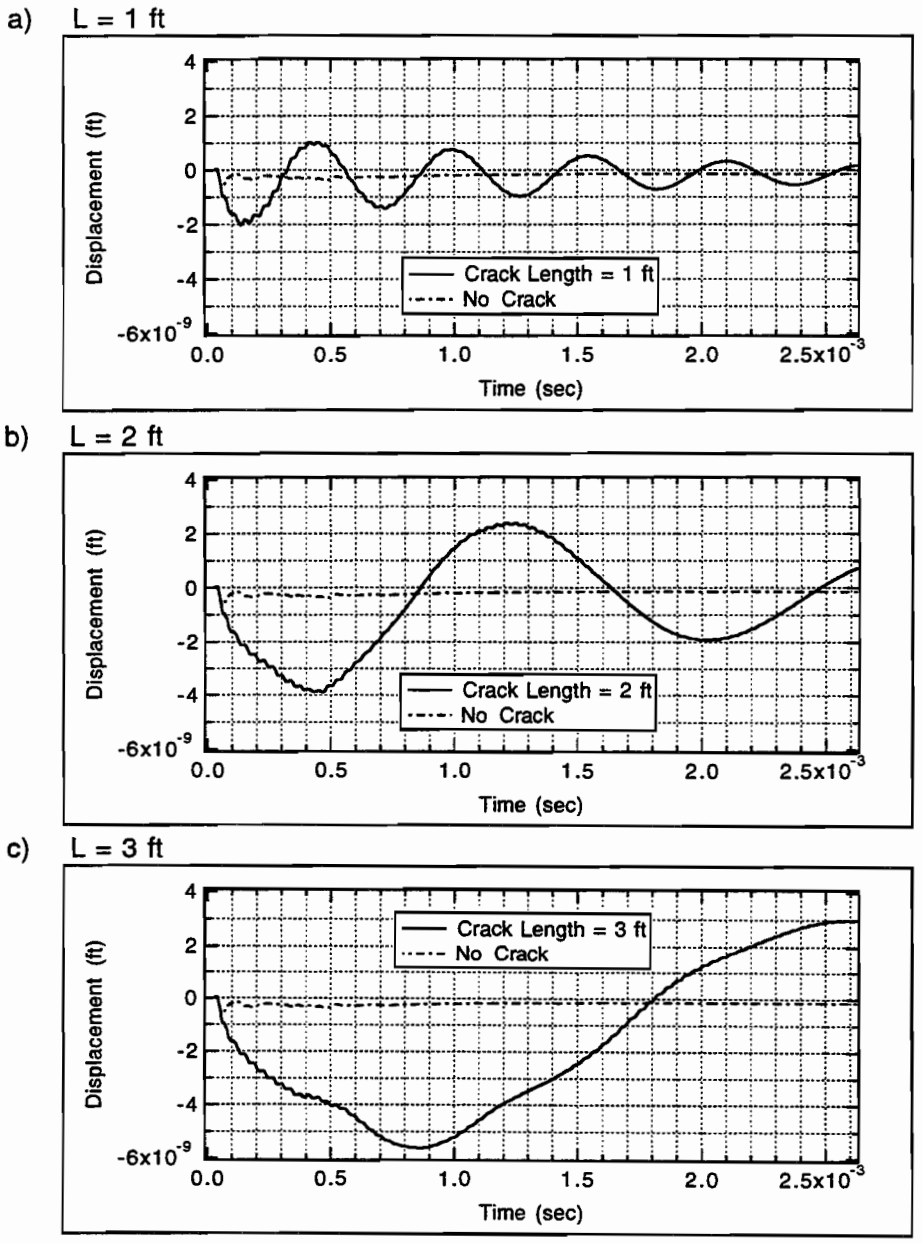


Fig. 4.12 Effect of Crack Length on the Predicted Time Histories at 3 in. from Source for an Impulse Duration of 1/26000 sec

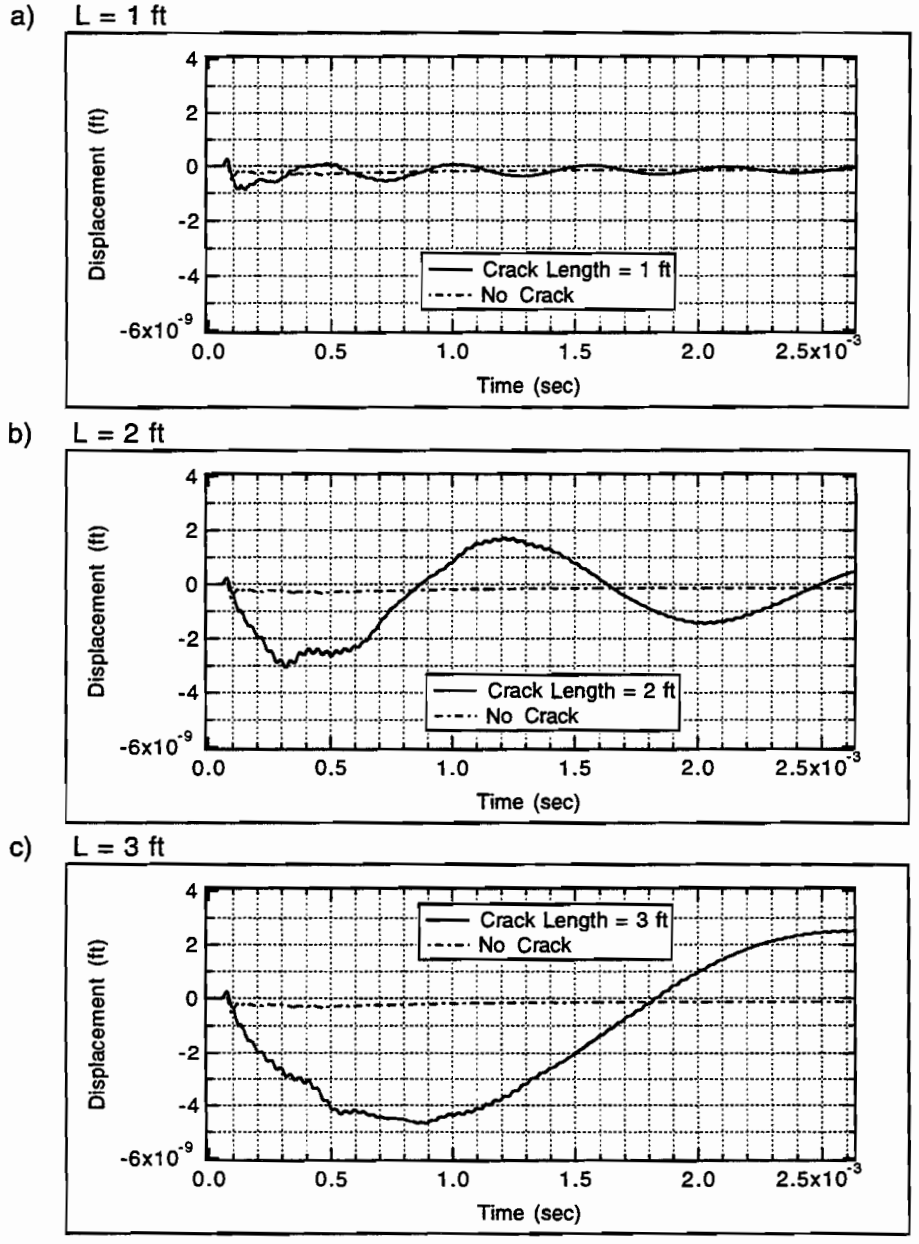


Fig. 4.13 Effect of Crack Length on the Predicted Time Histories at 6 in. from Source for an Impulse Duration of 1/26000 sec

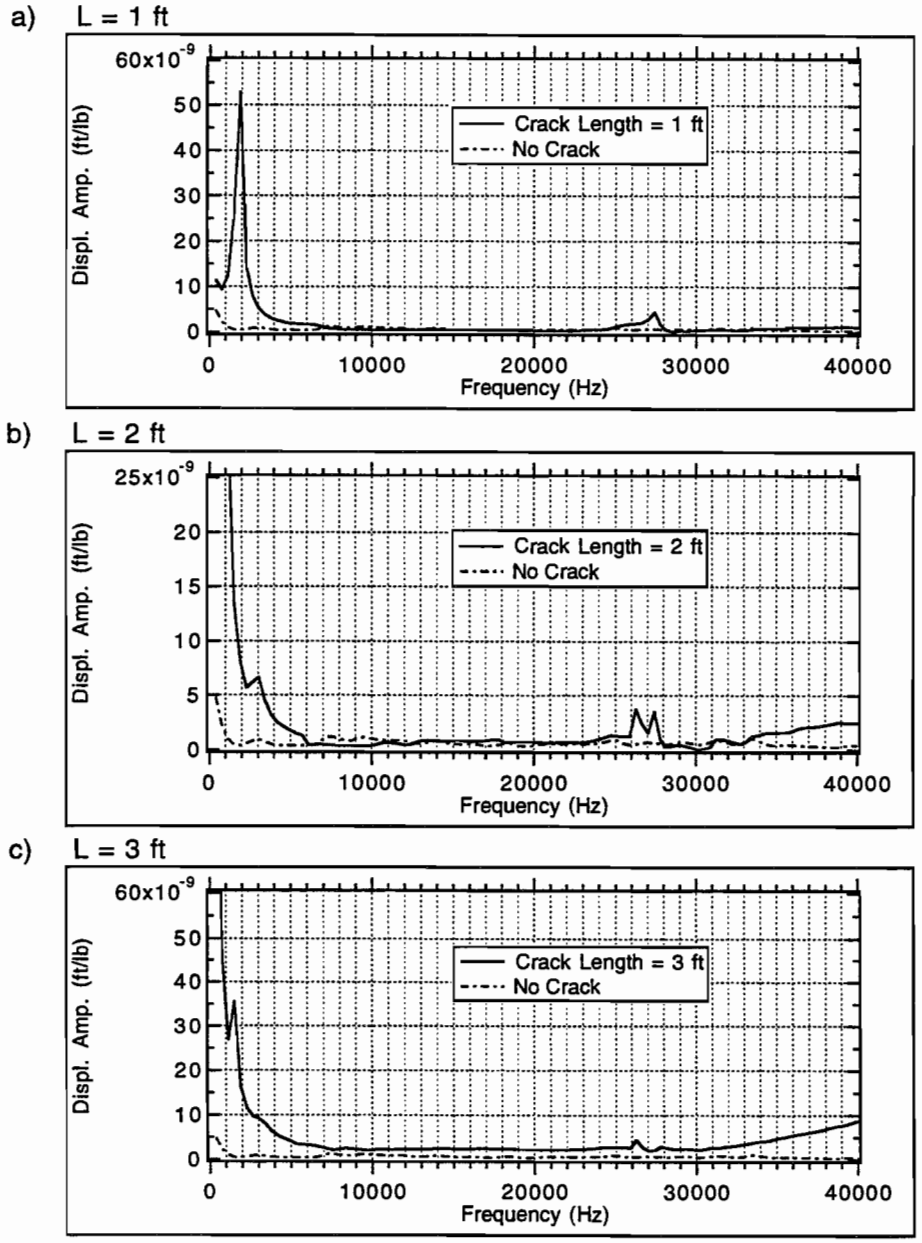


Fig. 4.14 Effect of Crack Length on the Predicted Displacement Amplitude at 3 in. from the Source for an Impulse Duration of 1/26000 sec

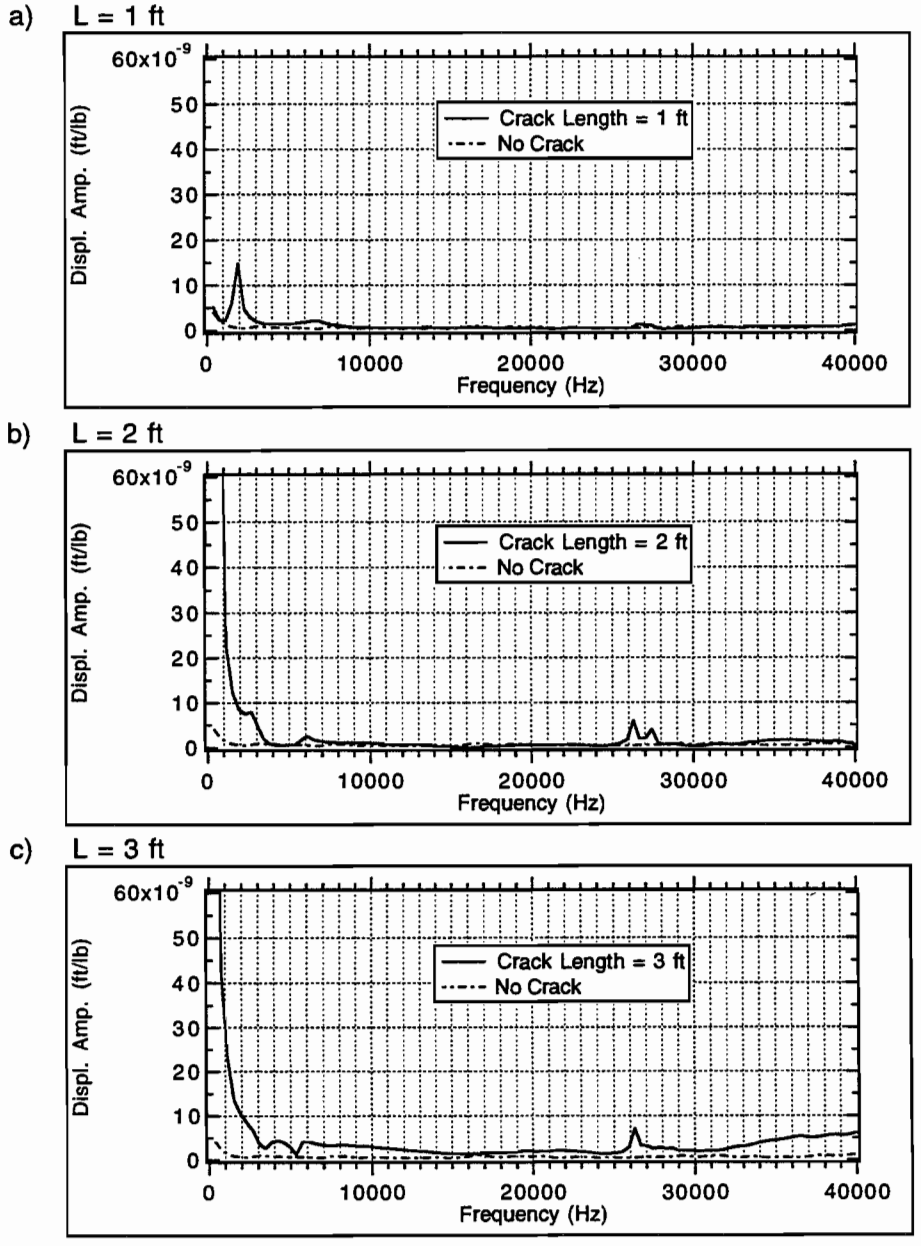


Fig. 4.15 Effect of Crack Length on the Predicted Displacement Amplitude at 6 in. from the Source for an Impulse Duration of 1/26000 sec

thus very little effect on the "P-wave peak-frequency". This "P-wave peak-frequency" is related to P-wave reflections.

An impulse with a duration of 1/8500 seconds was then applied to obtain a more accurate solution in the lower frequency range. The corresponding results are shown in Figs. 4.16 and 4.17 for the time histories and in Figs. 4.18 and 4.19 for the steady state responses. The ratios of maximum displacement in the delaminated and the intact pavements are 4, 9 and 14 for crack lengths of 1, 2 and 3 feet respectively at the 3-inch receiver. These ratios are 2, 8 and 13 respectively at the 6-inch receiver. These ratios are larger than those obtained using an impulse duration of 1/26000 seconds. The periods of the oscillation are approximately 1/2000, 1/700, and 1/350 seconds. The "flexural peak-frequencies" in the steady state response appear to be 1900, 700 and 350 Hz for the 1-foot, 2-foot and 3-foot cracks respectively in Figs. 4.18 and 4.19. The larger the delamination the smaller the "flexural peak-frequency" at which the peak amplification occurs. The "flexural peak-frequency" is associated with flexural vibration of the layer above the delamination.

An impulse with a duration of 1/630 seconds was next used. The corresponding results are shown in Figs. 4.20 and 4.21 for the time histories and in Figs. 4.22 and 4.23 for the steady state responses. No oscillation appears in the time histories for the 1-foot crack, whereas very clear oscillations can be seen around the response of the intact pavement in the time histories for the 2-foot and 3-foot cracks. The ratios of maximum displacement in the delaminated and the intact pavements are 1, 4 and 10 for crack lengths of 1, 2 and 3 feet respectively at the 3-inch receiver. These ratios are 1, 3 and 9 respectively at the 6-inch receiver.

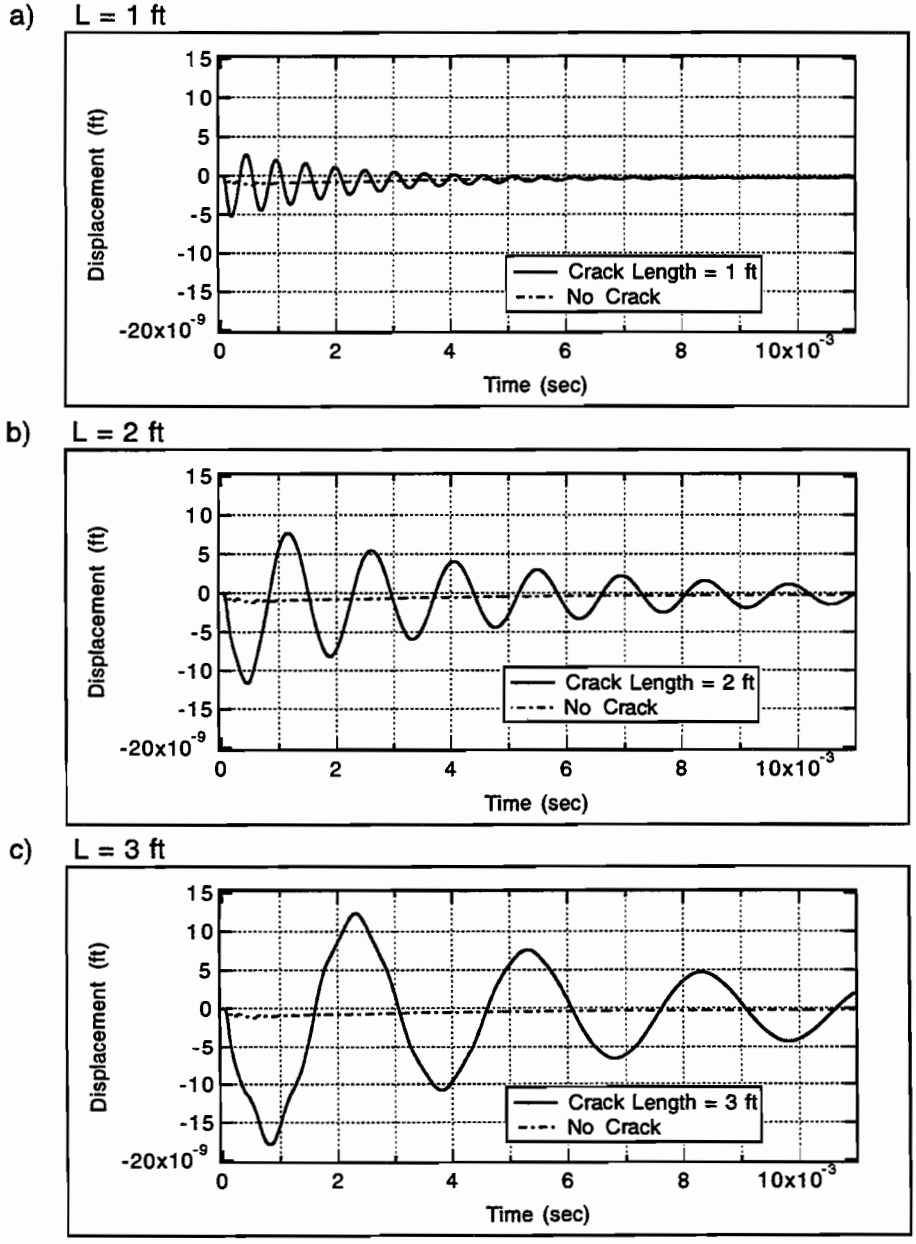


Fig. 4.16 Effect of Crack Length on the Predicted Time Histories at 3 in. from Source for an Impulse Duration of 1/8500 sec

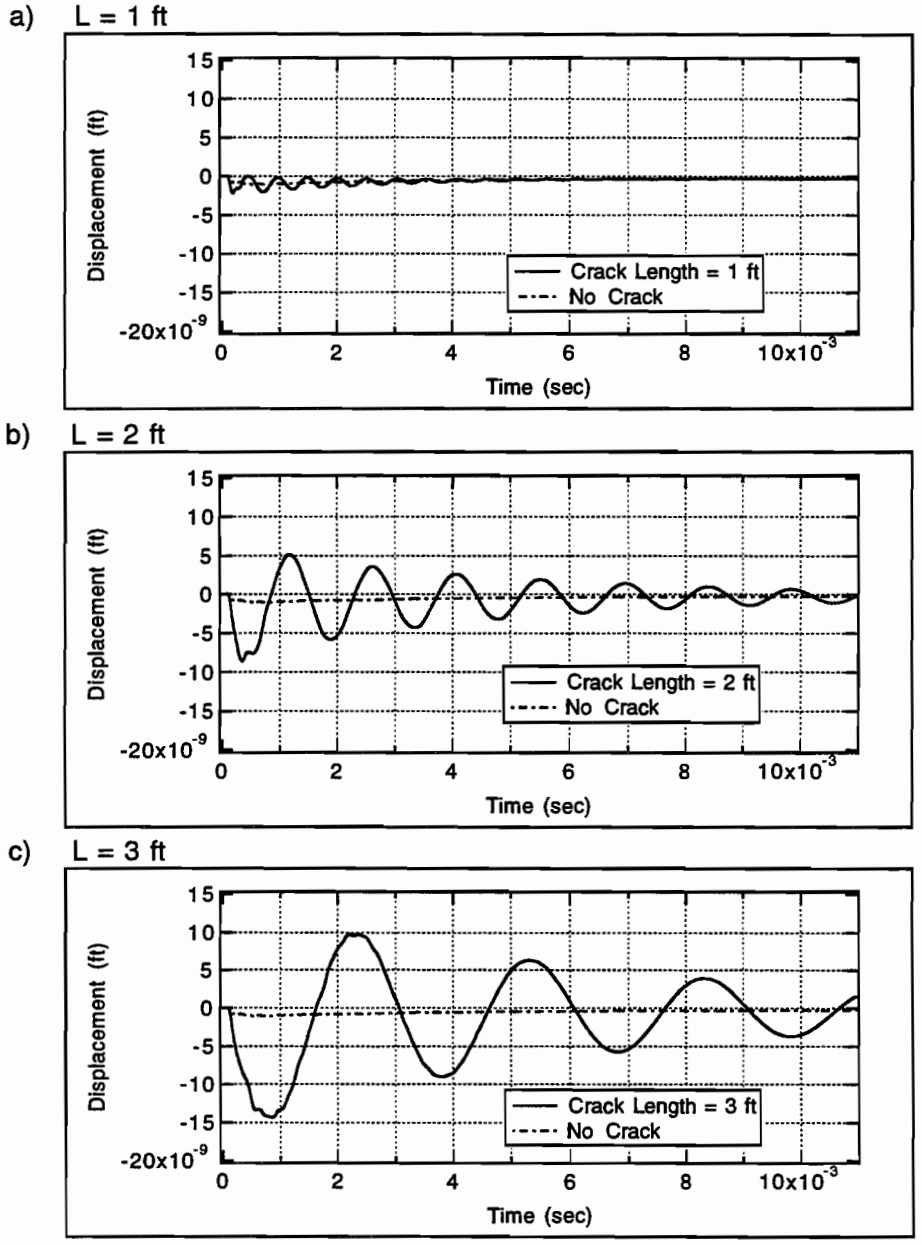


Fig. 4.17 Effect of Crack Length on the Predicted Time Histories at 6 in. from Source for an Impulse Duration of 1/8500 sec

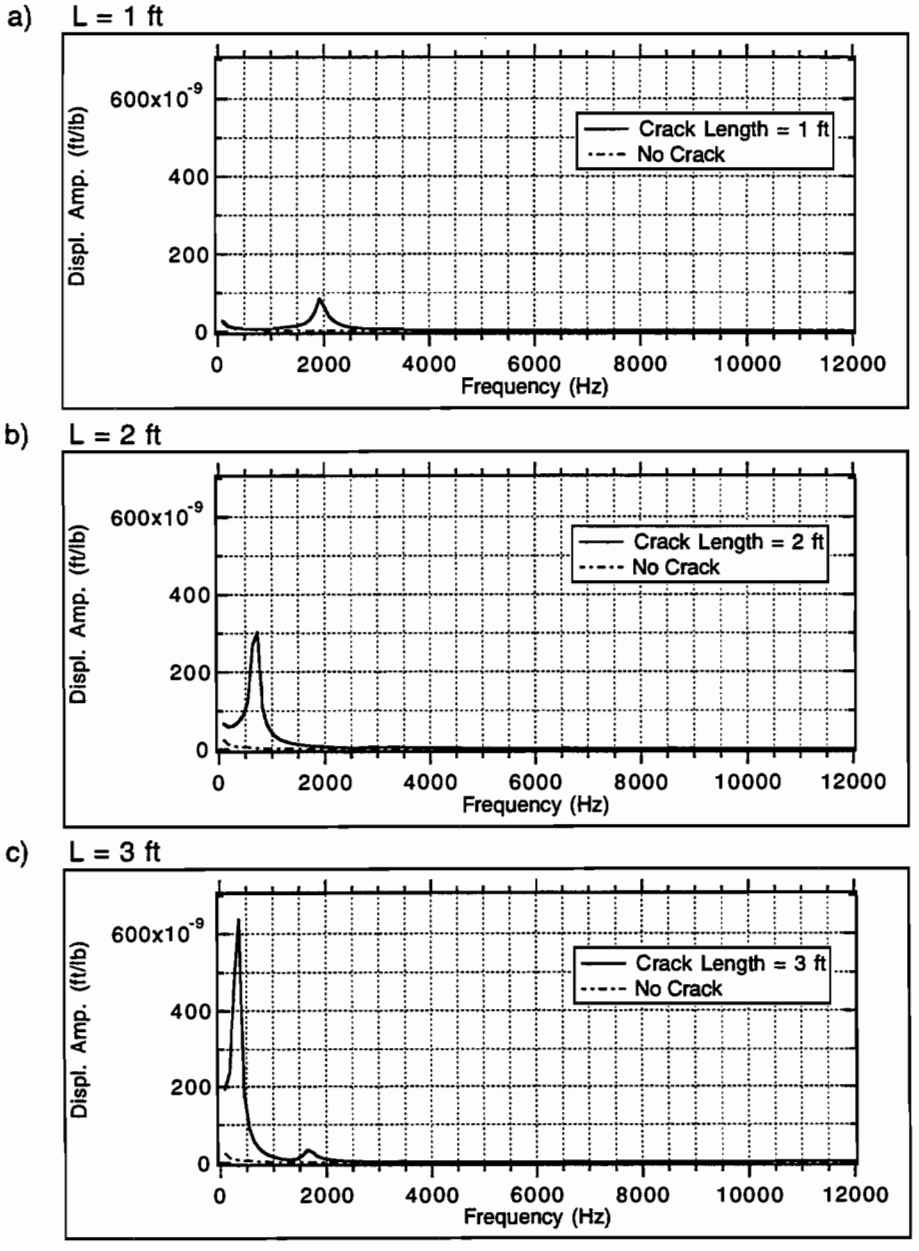


Fig. 4.18 Effect of Crack Length on the Predicted Displacement Amplitude at 3 in. from the Source for an Impulse Duration of 1/8500 sec

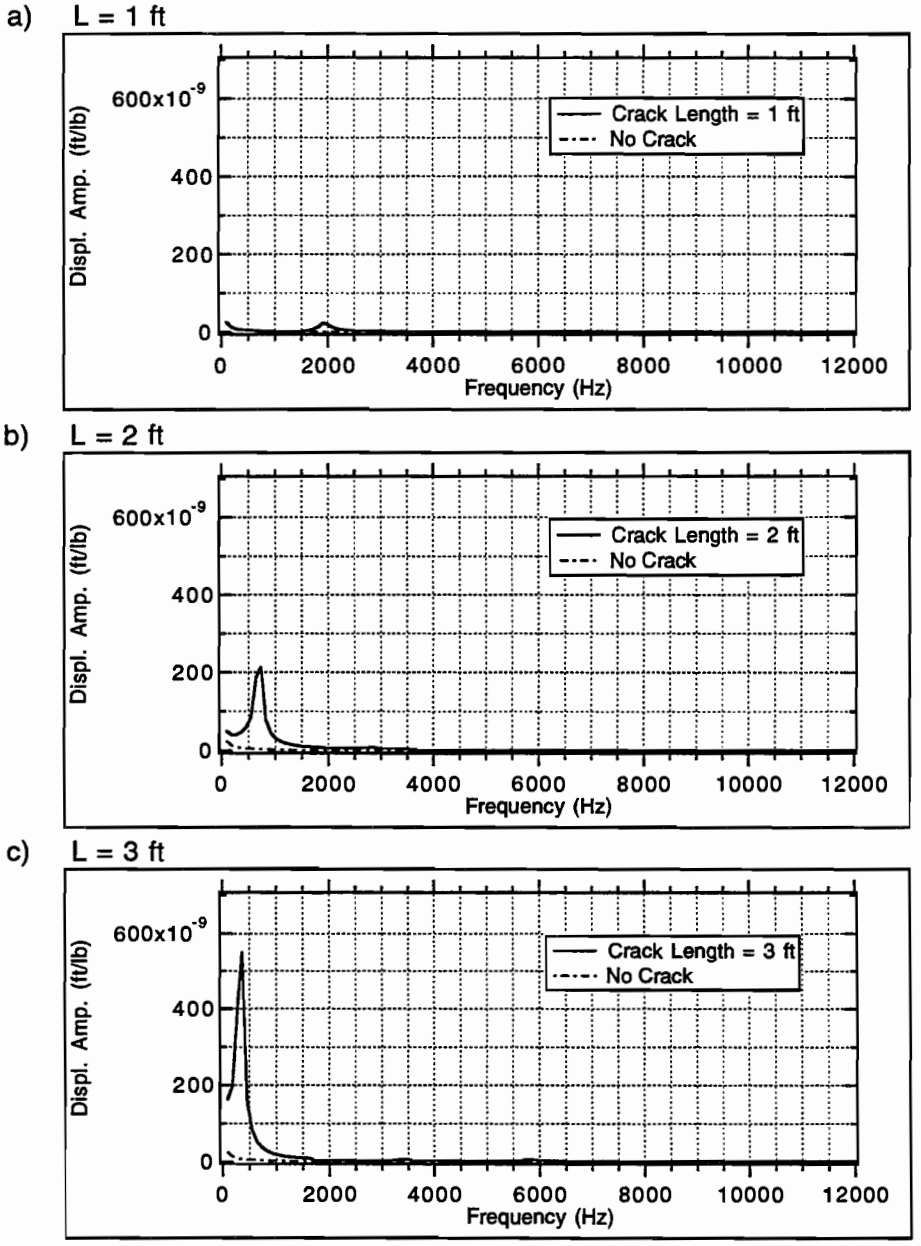


Fig. 4.19 Effect of Crack Length on the Predicted Displacement Amplitude at 6 in. from the Source for an Impulse Duration of 1/8500 sec

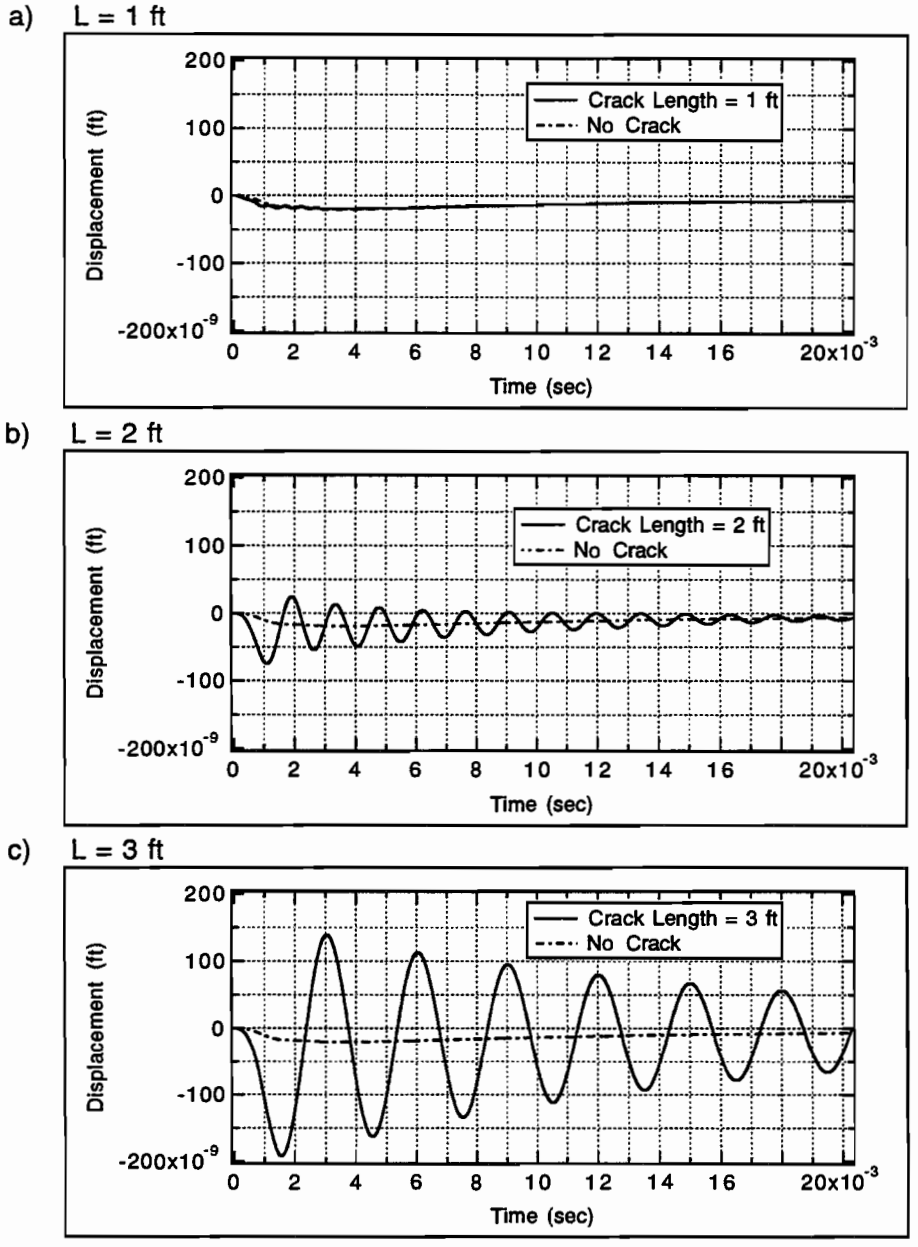


Fig. 4.20 Effect of Crack Length on the Predicted Time Histories at 3 in. from Source for an Impulse Duration of 1/630 sec

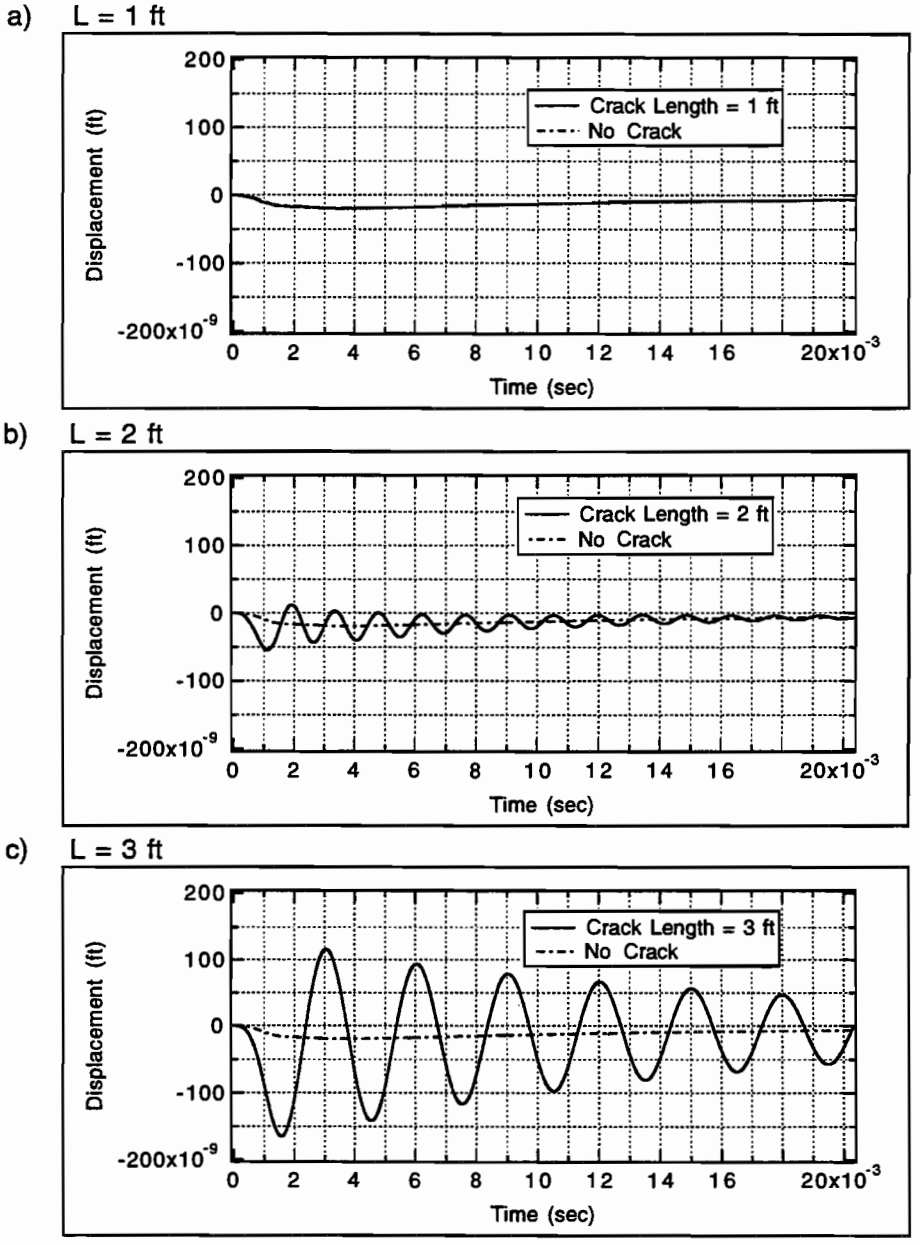


Fig. 4.21 Effect of Crack Length on the Predicted Time Histories at 6 in. from Source for an Impulse Duration of 1/630 sec

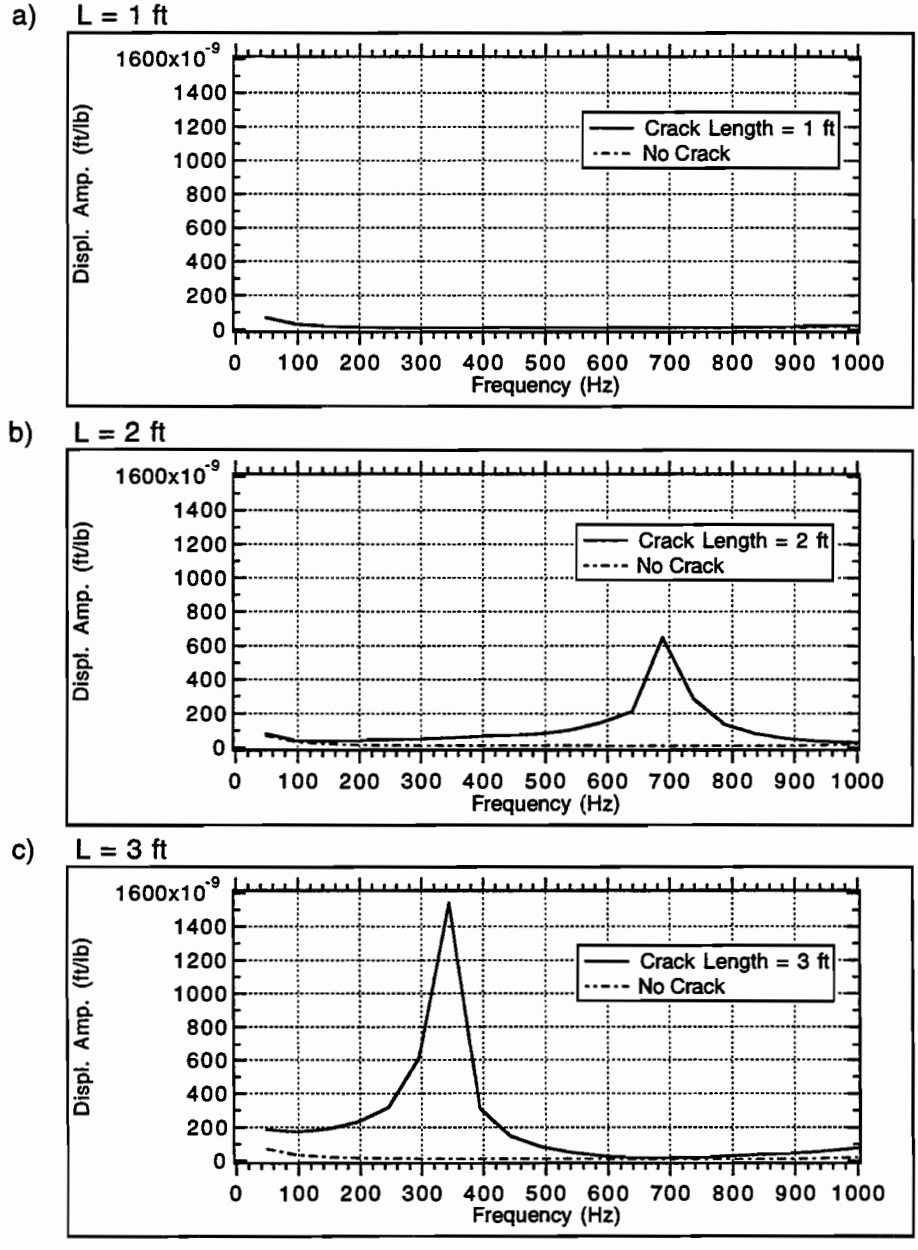


Fig. 4.22 Effect of Crack Length on the Predicted Displacement Amplitude at 3 in. from the Source for an Impulse Duration of 1/630 sec

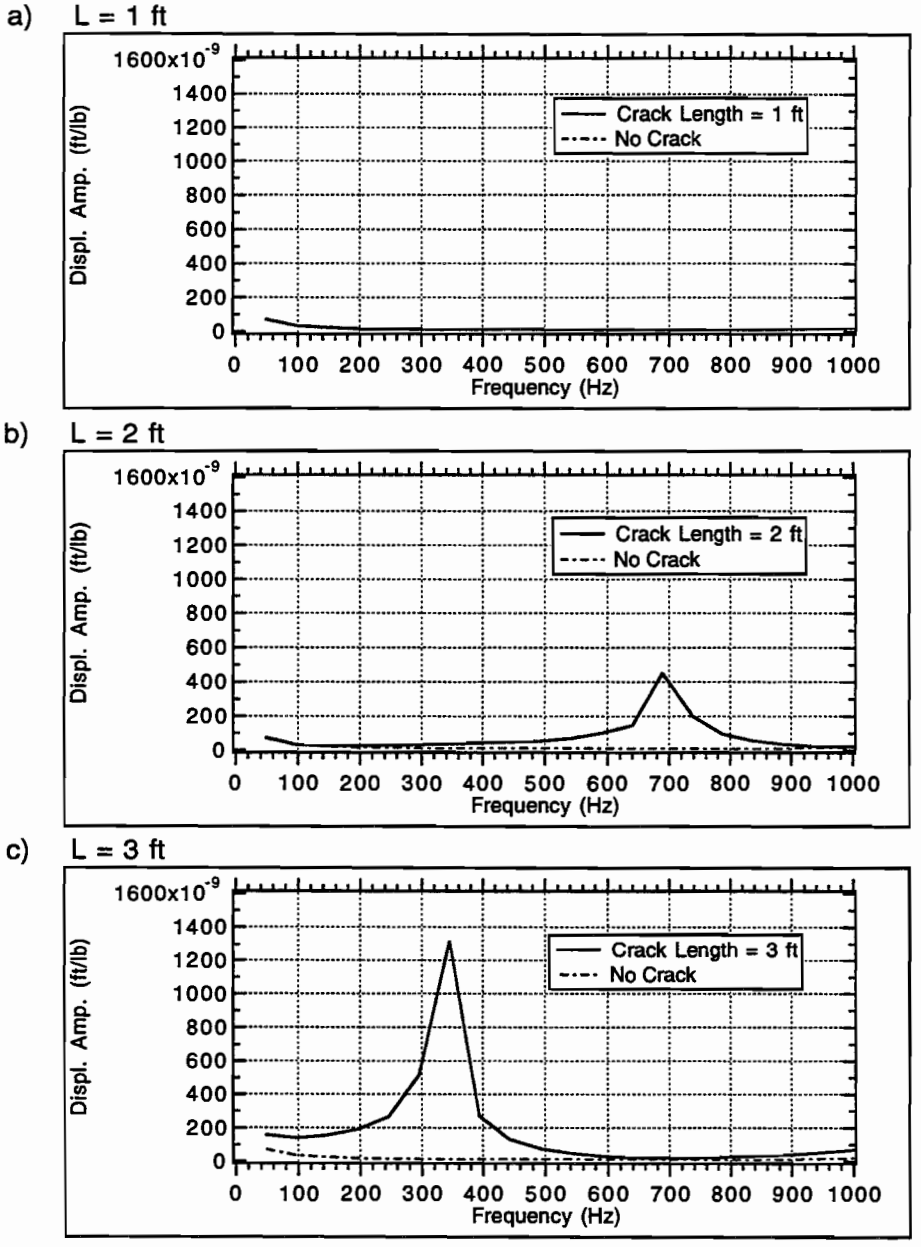


Fig. 4.23 Effect of Crack Length on the Predicted Displacement Amplitude at 6 in. from the Source for an Impulse Duration of 1/630 sec

Most of these ratios are smaller than those obtained using impulse durations of 1/26000 and 1/8500 seconds. On the other hand, the ratios of steady state response at the 3-inch and 6-inch receivers at the "flexural peak" are approximately 75 and 55 for the 2- foot crack, and 180 and 160 for the 3- foot crack. The periods of the oscillation are approximately 1/700 and 1/350 seconds for the 2-foot and 3-foot cracks. The "flexural peak-frequencies" in the steady state response appear to be again at 690 and 340 Hz for the 2-foot and 3-foot cracks respectively (Figs. 4.22 and 4.23).

### 4.2.4 Effects of Position of the Moving Source-Receiver System

The aforementioned results were obtained with the load applied at the center of the delamination, which is the case where the largest contrast between the results of delaminated and intact pavements will occur. This was done in order to see first the best ratios that can be expected. In this section, the responses of delaminated pavements are presented as the source-receiver move along the pavement. The numbers 1 through 13 indicate the locations of the receiver as shown in Fig. 4.24. The source is always 3 inches to the left of the receiver. The displacement histories, above the intact and delaminated pavements, are shown in Figs. 4.25 and 4.26. At locations 1, 2 and 3, the displacements for delaminated pavements are hard to distinguish from those of intact pavements. At location 4, the displacement history starts to display some oscillations. Clear oscillations can be seen at location 5, whereas larger and smoother oscillations are found at location 6. It is interesting to notice that the displacement history at location 7 is

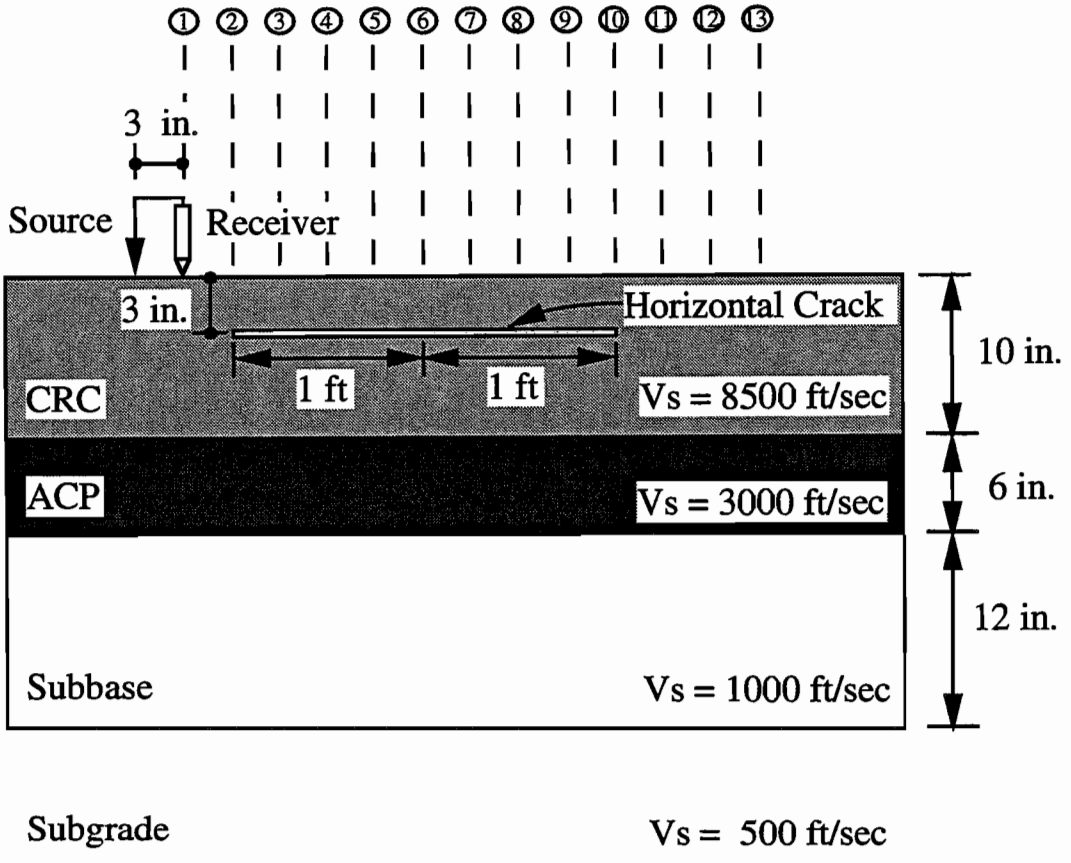


Fig. 4.24 Simulation of the Moving Source-Receiver Testing on a Pavement with a Horizontal Crack at a Depth of 3 inches from the Surface

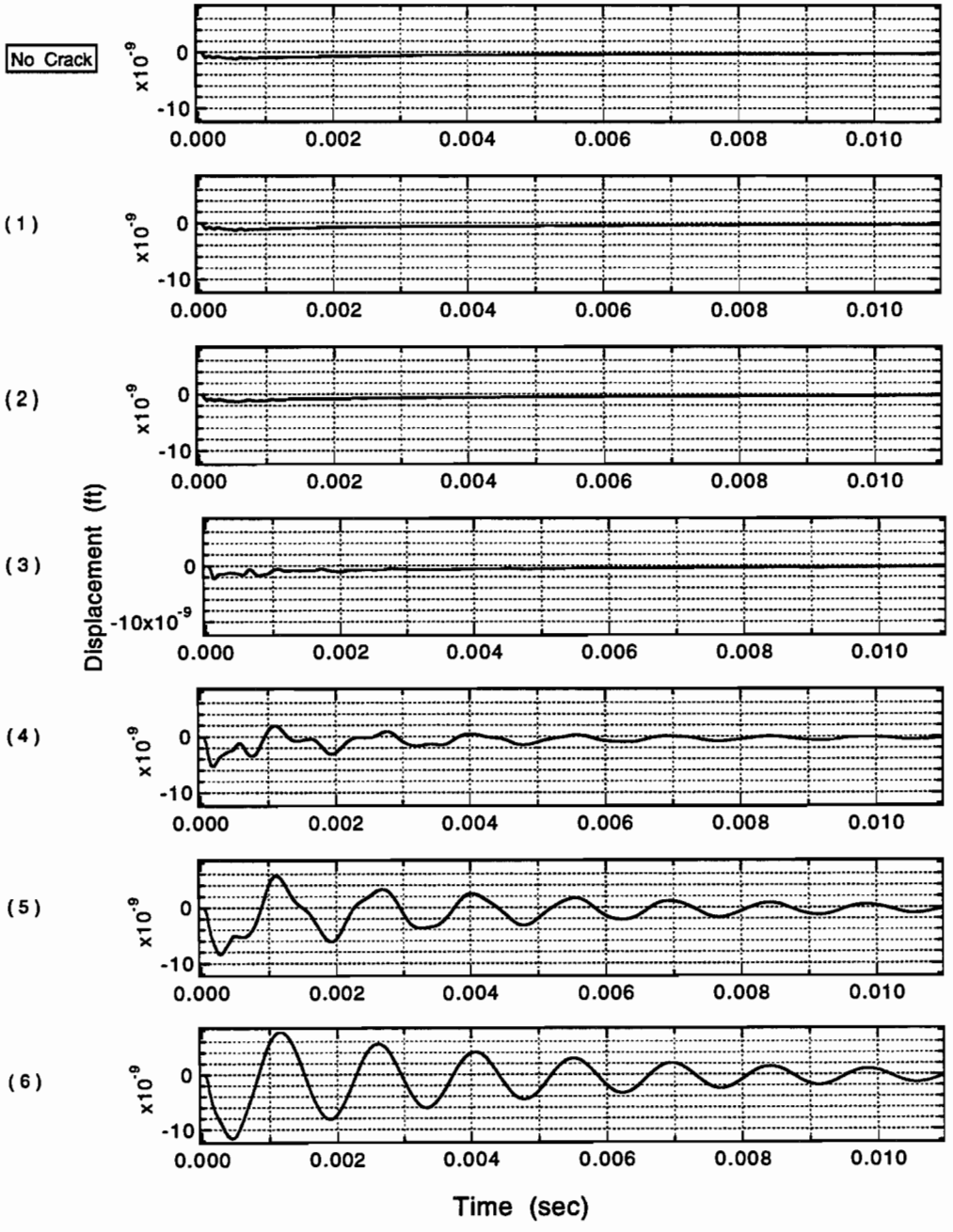


Fig. 4.25 Displacement Histories at 3 inches from the Source As the Receiver is on the Intact Pavement and Moves from Positions 1 to 6 on the Delaminated Pavement

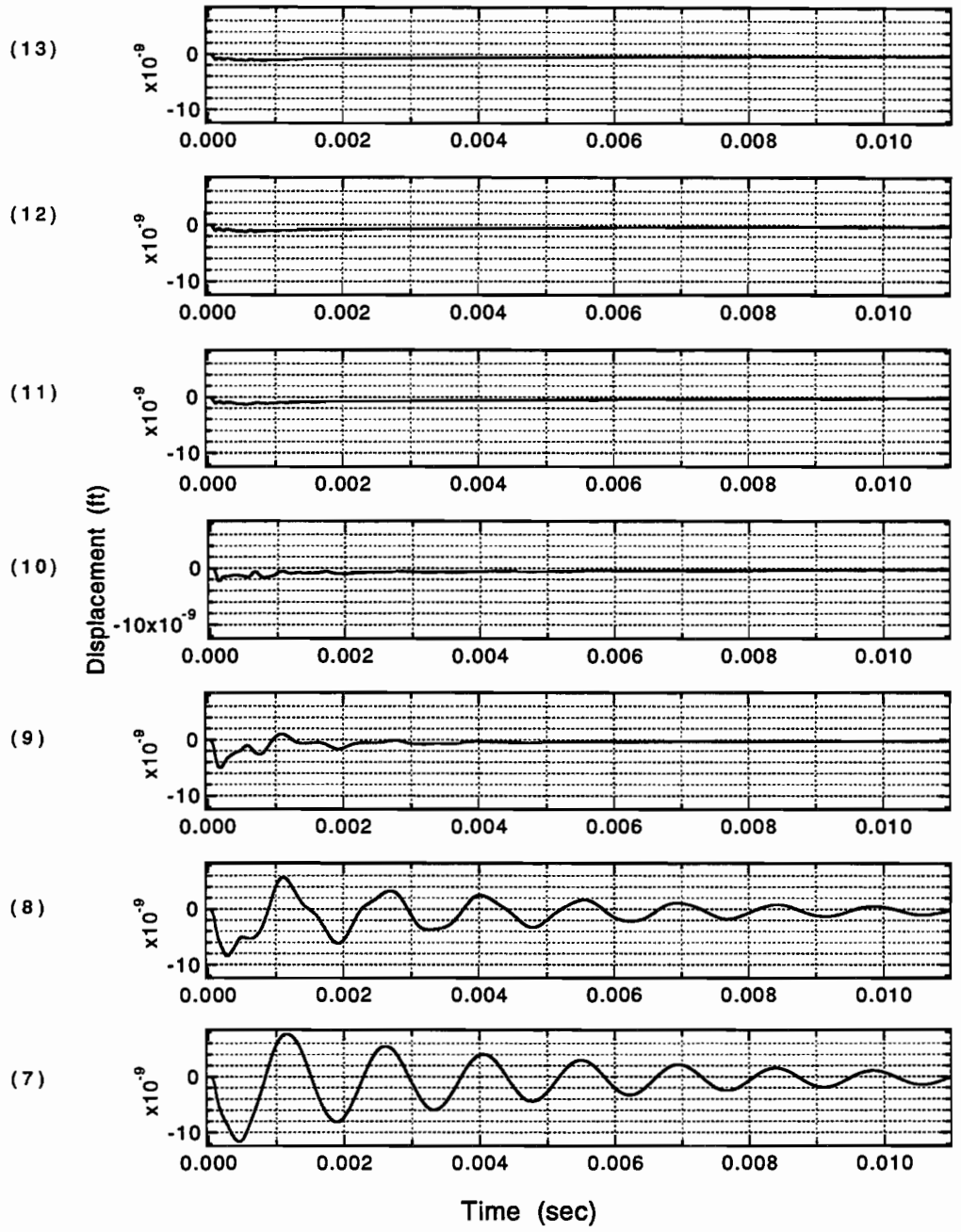


Fig. 4.26 Displacement Histories at 3 inches from the Source As the Receiver Moves from Positions 7 to 13 on the Delaminated Pavement

similar to that at location 6, and the results at location 8 are similar to those at location 5. The shape of the results at location 9 are similar to that at location 4, but the peak displacements at location 9 are smaller. As the receiver moves to location 10, above the edge of the delamination, the results are similar to those at location 3. At locations 11, 12 and 13, the results are almost indistinguishable from those of intact pavements.

The displacement amplitudes in the steady state response for intact and delaminated pavements are shown in Figs. 4.27 and 4.28. The results of delaminated pavements appear similar until the receiver approaches location 4. At location 4, two flexural peaks were found at the frequencies of 700 and 1750 Hz. As the receiver moves another 3 inches toward the center of delamination, two peaks are still present at the same frequencies. However, both peak amplitudes increase and the amplitude of the first peak increases more. When the receiver or the source is right above the center of the delamination, locations 6 or 7, only one peak appears at a frequency of 700 Hz in the frequency spectrum. The peak amplitudes at location 8 are similar to those at location 5. The shape of the amplitudes at location 9 is similar to that at location 4, but the peak amplitudes at location 9 are smaller. As the receiver moves to locations 10, 11, 12 and 13, the amplitudes are very small and can not be distinguished from those of the intact pavements.

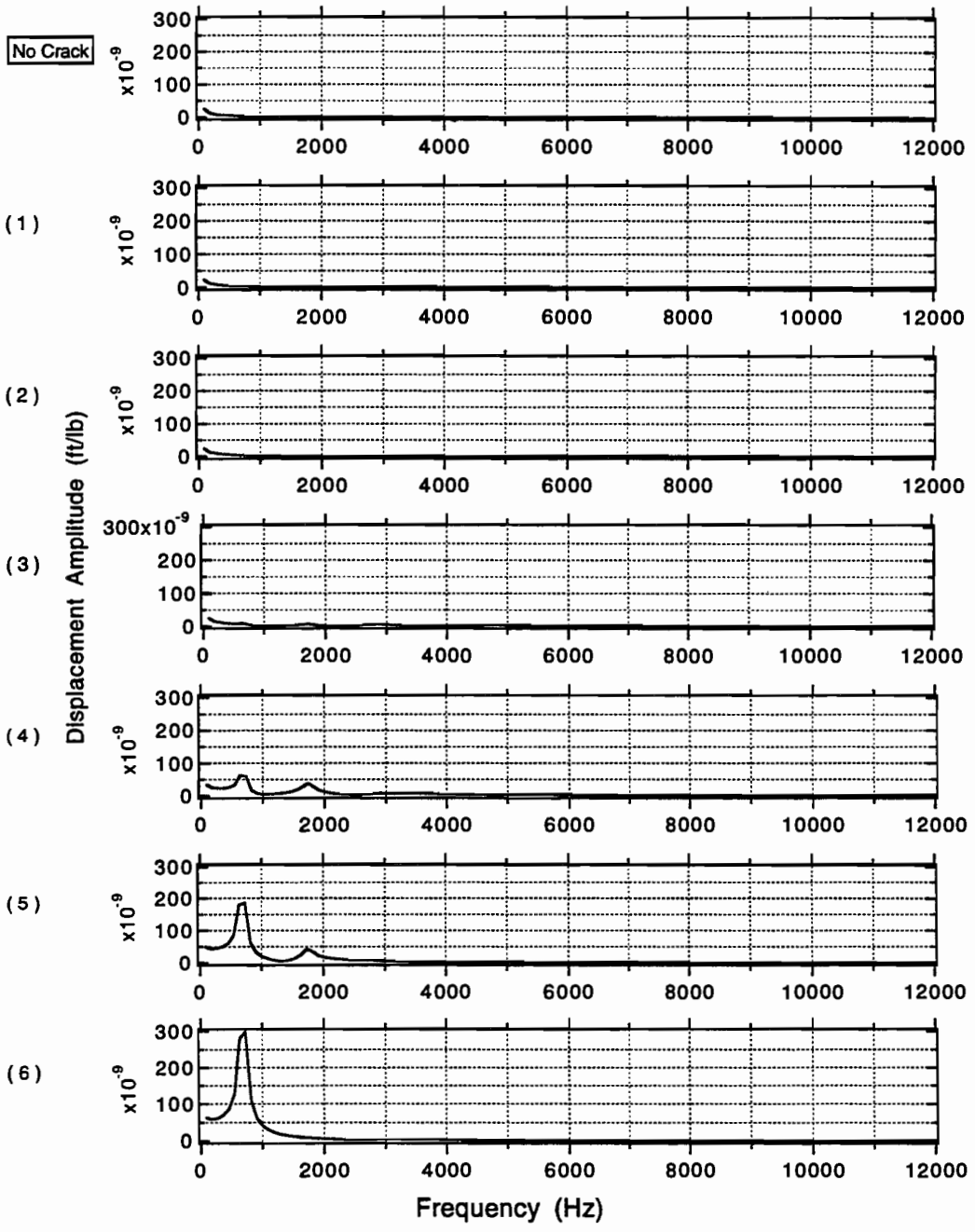


Fig. 4.27 Displacement Amplitudes at 3 inches from the Source As the Receiver is on the Intact Pavement and Moves from Positions 1 to 6 on the Delaminated Pavement

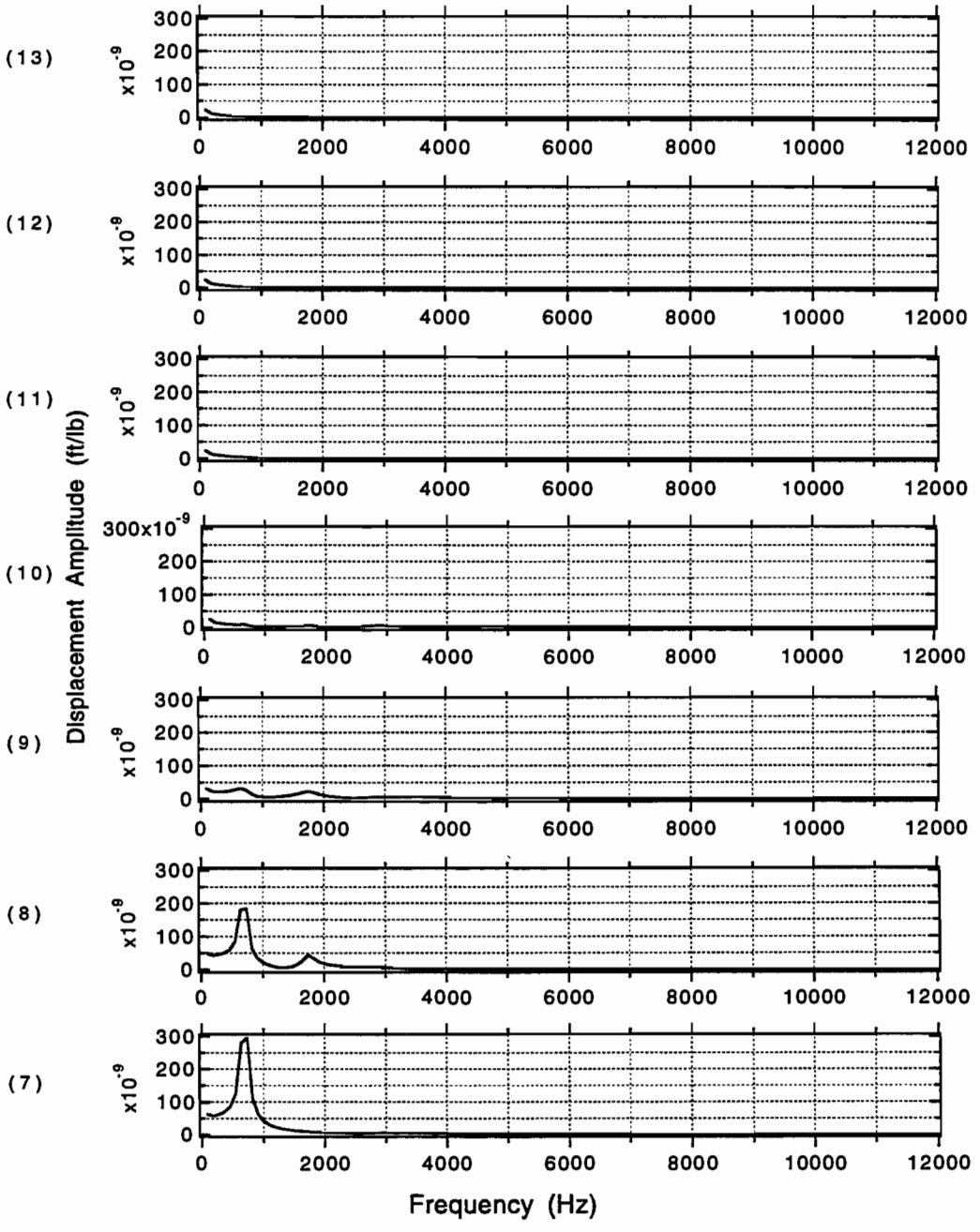


Fig. 4.28 Displacement Amplitudes at 3 inches from the Source As the Receiver Moves from Positions 7 to 13 on the Delaminated Pavement

### 4.2.5 Effects of Delamination Depth

As the depth of the delamination increases from 3 to 6 and then to 10 inches, the corresponding "P-wave peak-frequencies" decrease from the 26300-27400 range to 13700 and 8100 Hz in Fig. 4.29. The deeper the delamination, the lower the "P-wave peak-frequency", as could be expected. Moreover there is an almost linear relation between the depth and the inverse of the frequency. For the 3-inch receiver, the displacement amplitude at the peak increases as the delamination goes deeper. Unlike the results for the 3-inch deep delamination, the peak amplitudes for the 6-inch receiver are smaller than those of 3-inch receiver for both cases of 6-inch and 10-inch deep delaminations.

The "flexural peak-frequency" increases, on the other hand, from 690 to 830 Hz as the depth of the delamination increases from 3 to 6 inches in Fig. 4.30. The deeper the delamination, the higher the "flexural peak-frequency". In addition, the peak amplitudes decrease by about 90% for both the 3-inch and 6-inch receivers. The "flexural peak" can not be found in Fig. 4.31 or at higher frequencies when the delamination is located at 10 inches deep. The largest ratio of the displacement amplitude of delaminated pavement to that of intact pavement is only about 2, which is too small to be distinguished in practice, at a frequency of 380 Hz.

### 4.2.6 Effects of Delamination Extending to Pavement Edge

More often than not, some delaminations extend to the pavement edge as shown in Fig. 4.32. The frequency spectrum of the displacement amplitudes in

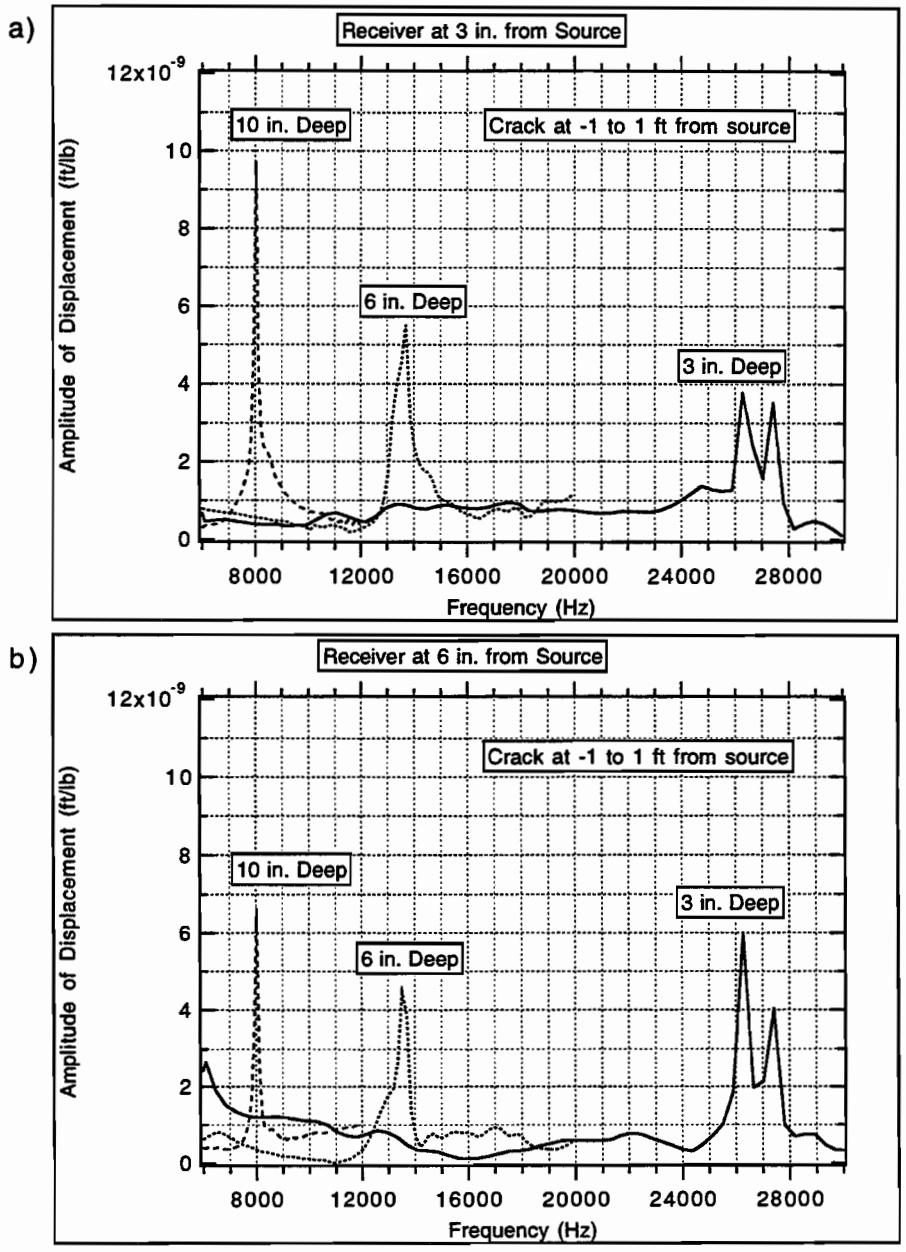


Fig. 4.29 Effect of the Depth of the Crack on the "P-wave Peaks"

a) Receiver at 3 in. from Source

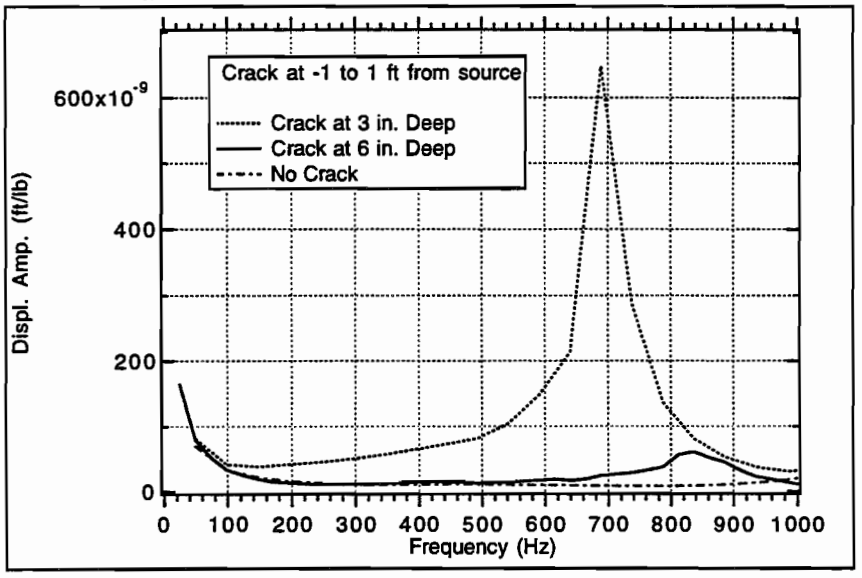


b) Receiver at 6 in. from Source

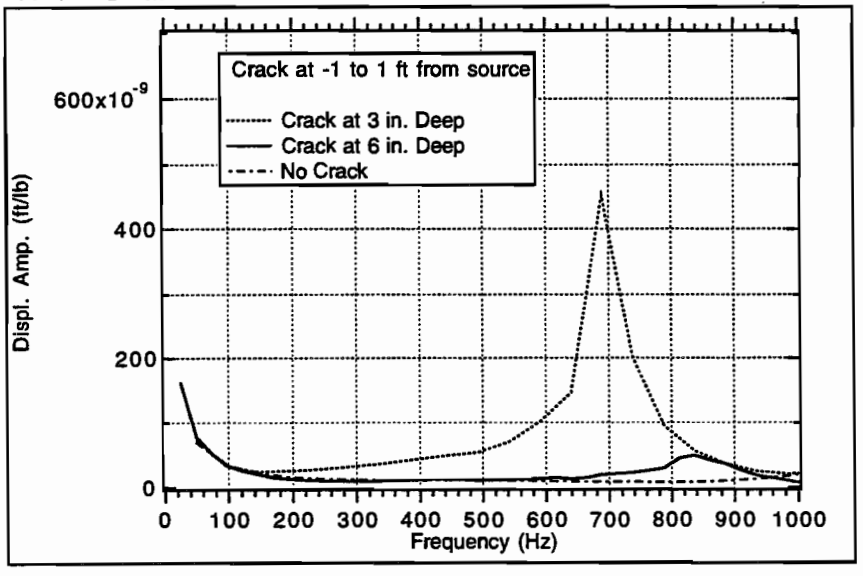


Fig. 4.30 Effect of the Depth of the Crack, 3 and 6 in., on the "Flexural Peaks"

a) Receiver at 3 in. from Source

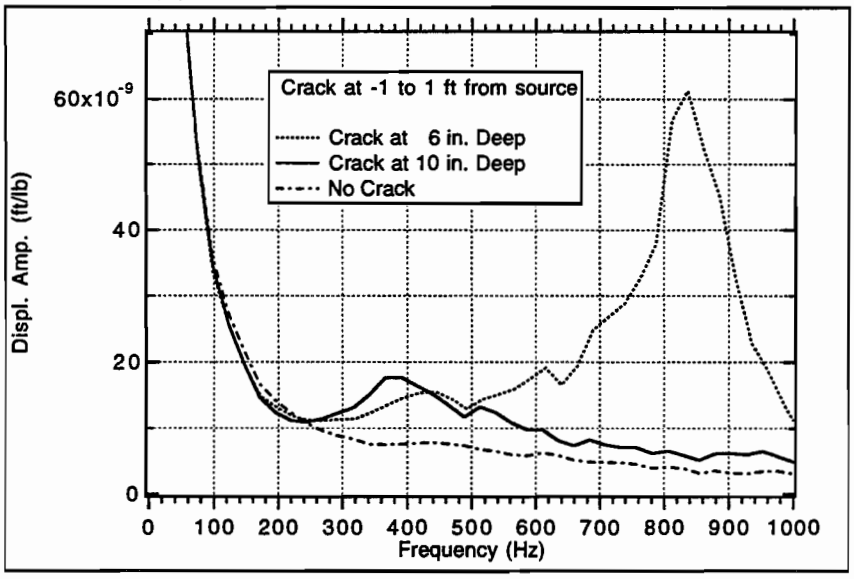


b) Receiver at 6 in. from Source

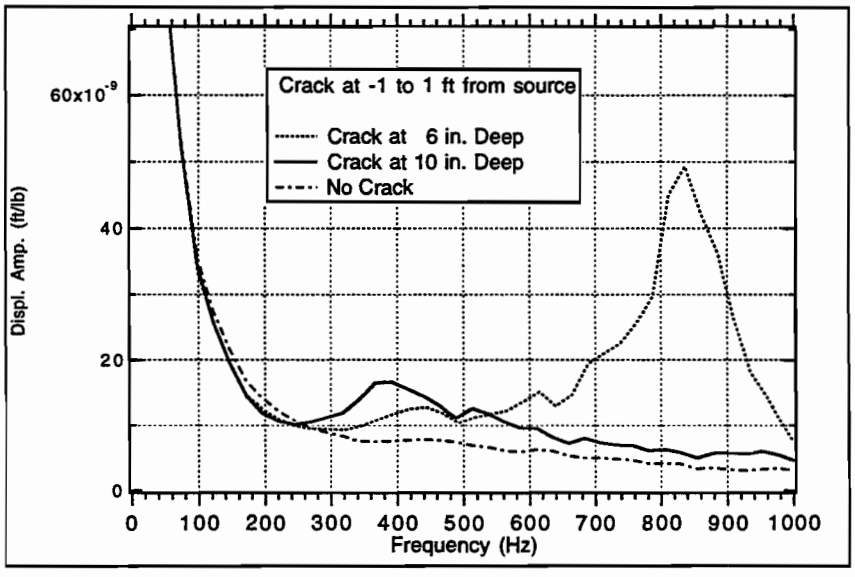


Fig. 4.31 Effect of the Depth of the Crack, 6 and 10 in., on the "Flexural Peaks"

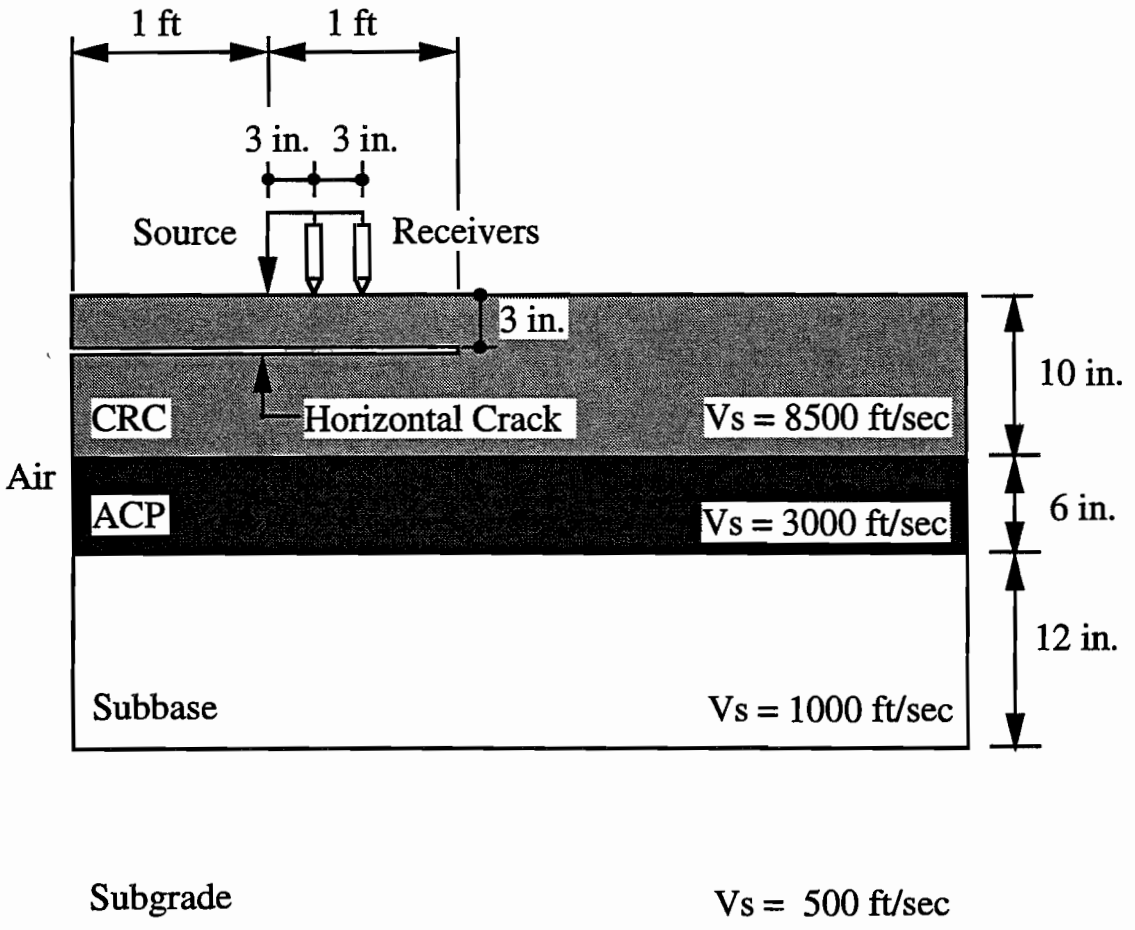


Fig. 4.32 Simulation of Testing near the Pavement Edge with a Horizontal Crack Extending to the Pavement Edge

this case are presented in Fig. 4.33. Around the "P-wave peaks", a number of small peaks due to the reflections from the edge make the "P-wave peaks" less pronounced. The two major peaks merge into one for the 3-inch receiver, while for the 6-inch receiver they change somewhat their relative amplitudes but tend to remain at the same location.

The results in the low frequency range are shown in Fig. 4.34. The "flexural peak-frequency" shifts from 690 to 720 Hz and the amplitude at this frequency decreases by about half as the delamination is extended to the pavement edge. In addition, another much larger peak appears at a frequency of 120 Hz, probably due to the reflections from the pavement edge. It should be noticed however that these effects are likely to be much smaller in actual practice since one would not have air over the complete depth of the pavement system.

## 4.3 PAVEMENT WITH A DISK-SHAPED DELAMINATION

In reality most tests will use a point load or a load distributed over a circular area instead of a line load, and the shape of the delamination will usually be irregular. In order to better understand the effects of a point load and the shape of the delamination, an axisymmetric model was used to simulate a circular delamination with a point load applied at the axis. The material properties of the pavement used in this section are the same as those of the system in Section 4.2.

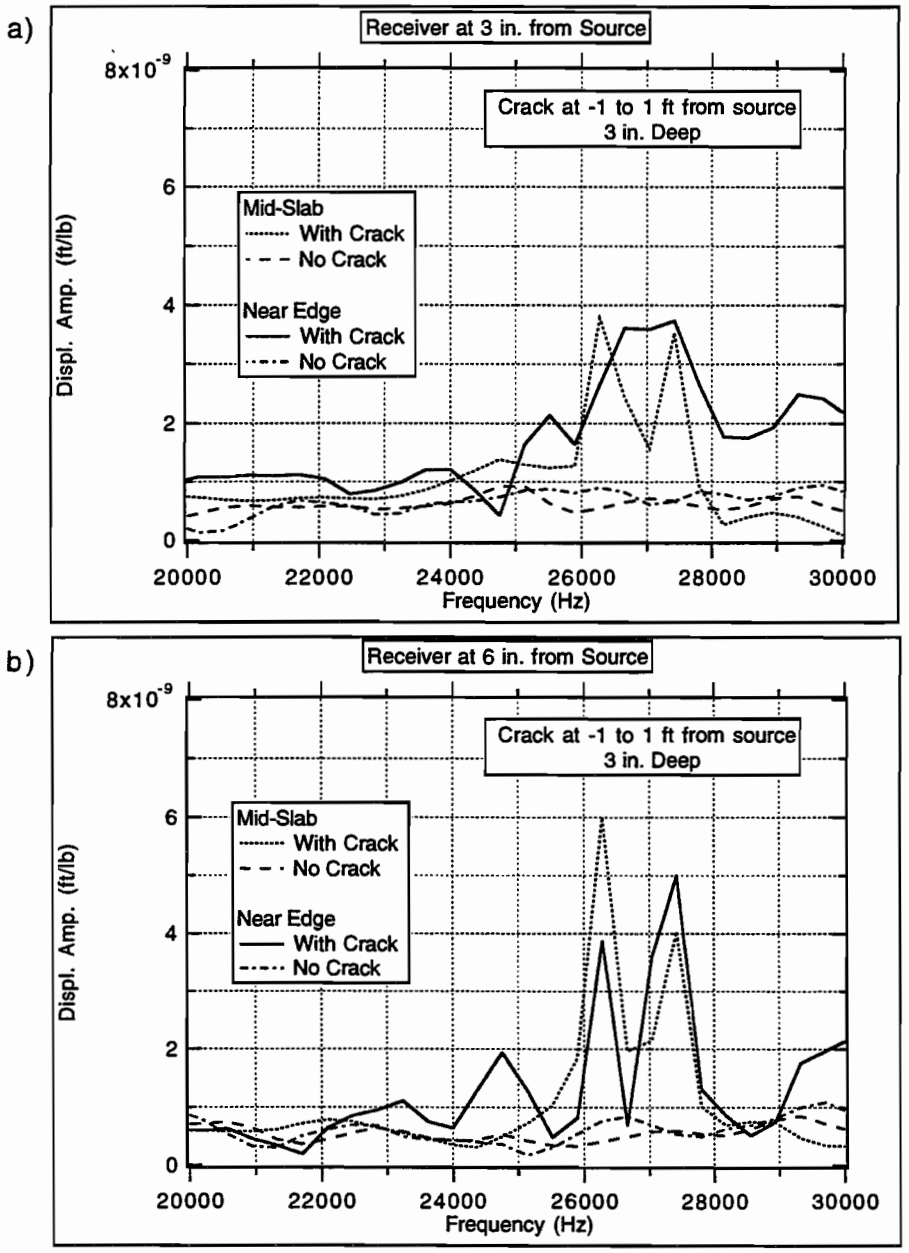


Fig. 4.33 Edge Effect of the Delaminations on the "P-Wave Peaks"

a) Receiver at 3 in. from Source

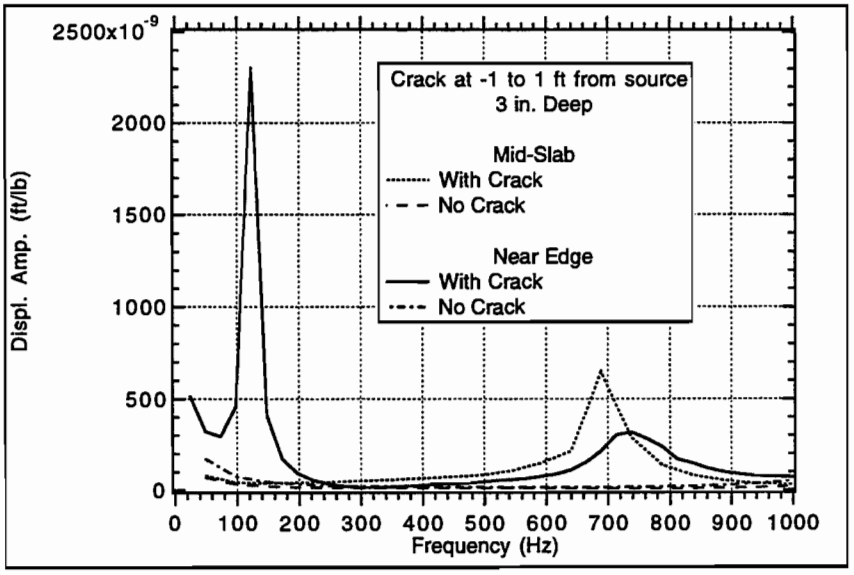


b) Receiver at 6 in. from Source

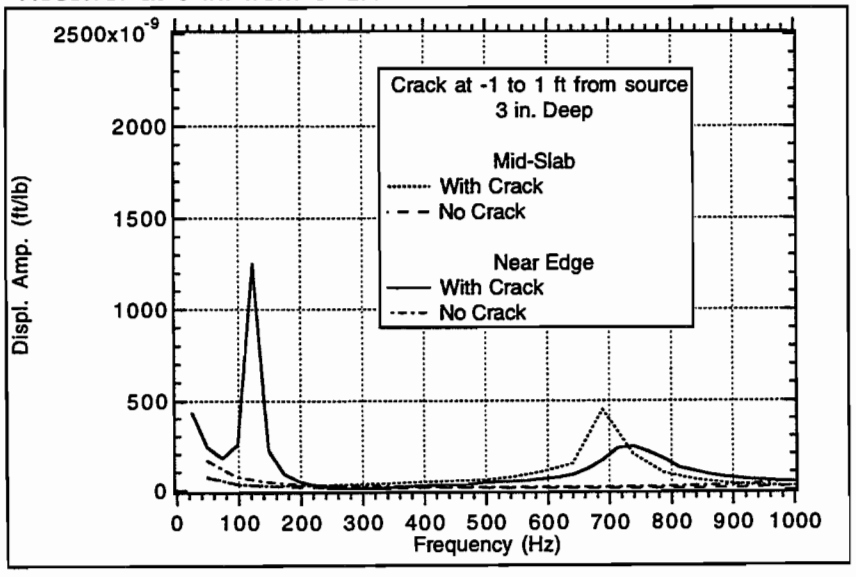


Fig. 4.34 Edge Effect of the Delaminations on the "Flexural Peaks"

### 4.3.1 Damping Effects

In Fig. 4.35, there is only one "P-wave peak" at 25500 Hz for the 3-inch receiver, while two peaks appear at 25500 and 27000 Hz for the 6-inch receiver. The damping ratio of the concrete layer has an important effect on the displacement amplitude at the "P-wave peak" for both the 3-inch and the 6-inch receivers and a delaminated pavement. The peak amplitudes decrease about 52% and 85% when the concrete layer has 0.3% and 1% damping respectively. The damping ratios of the lower layers, on the other hand, have little effect on the displacement amplitude at the "P-wave peak". The results for an ideal pavement without damping in any layer are similar to the results for a pavement with no damping in the concrete layer and with 2 % damping for the other layers. The displacement amplitudes at the "P-wave peak" for the 6-inch receiver are only 11-27% of those of the 3-inch receiver.

The results for an intact pavement are shown in Fig. 4.36. The displacement amplitudes for the 3-inch and the 6-inch receivers are relatively small, as the damping ratio of concrete varies from 0% to 1% and the damping ratios of the other layers are all 2%. The small dot lines, representing the ideal case of a pavement without any damping, show two peaks at the frequencies of 31600 and 32300 Hz. The damping of the lower layers has more effect on the displacement amplitude for an intact pavement than for a delaminated one. However, the displacement amplitudes in Fig. 4.36 are so small, compared to the peak amplitudes of the delaminated pavement in Fig. 4.35, that the response of

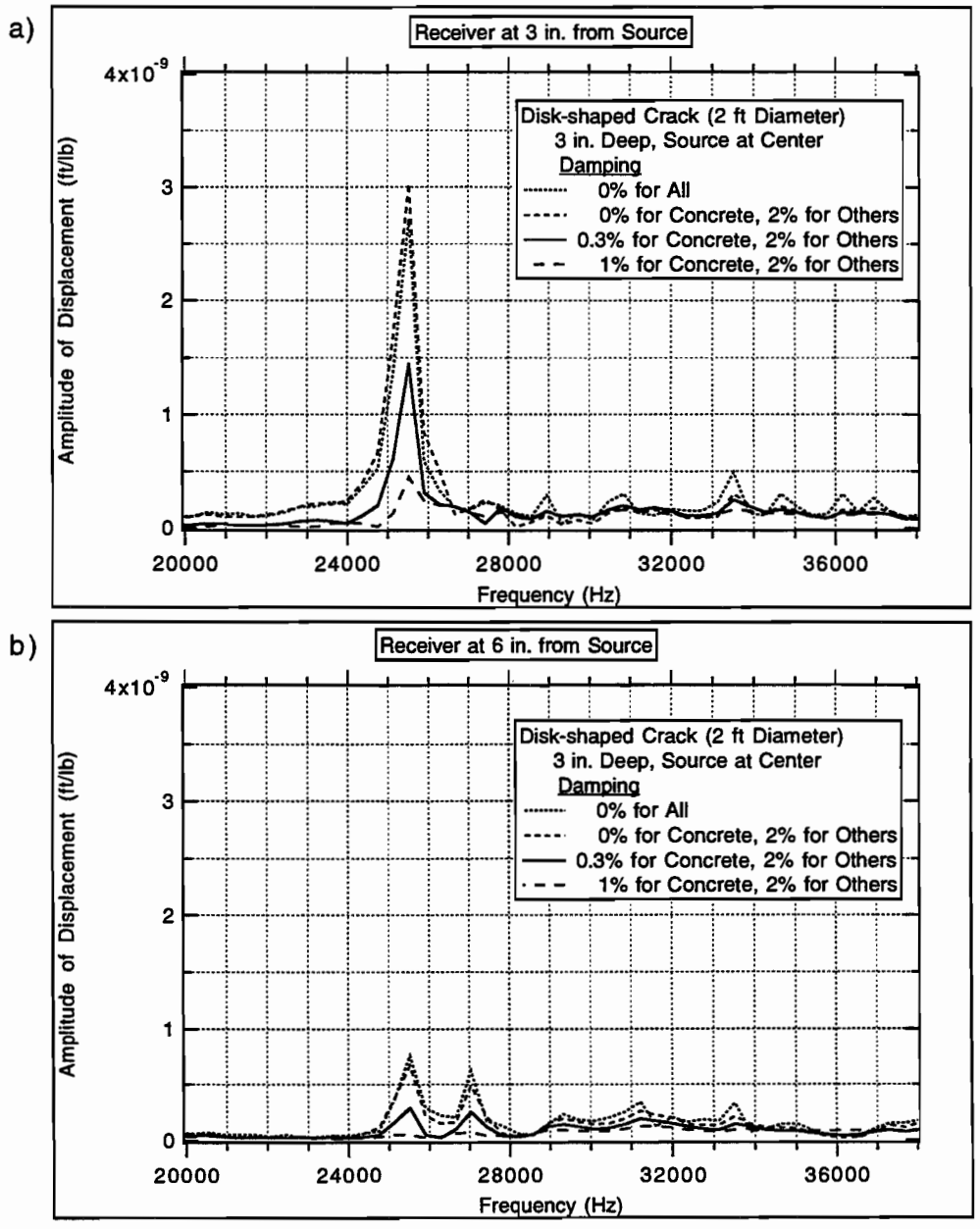


Fig. 4.35 Effect of Damping on the "P-Wave Peaks" for a Pavement with a Disk-Shaped Crack at a Depth of 3 in. from the surface

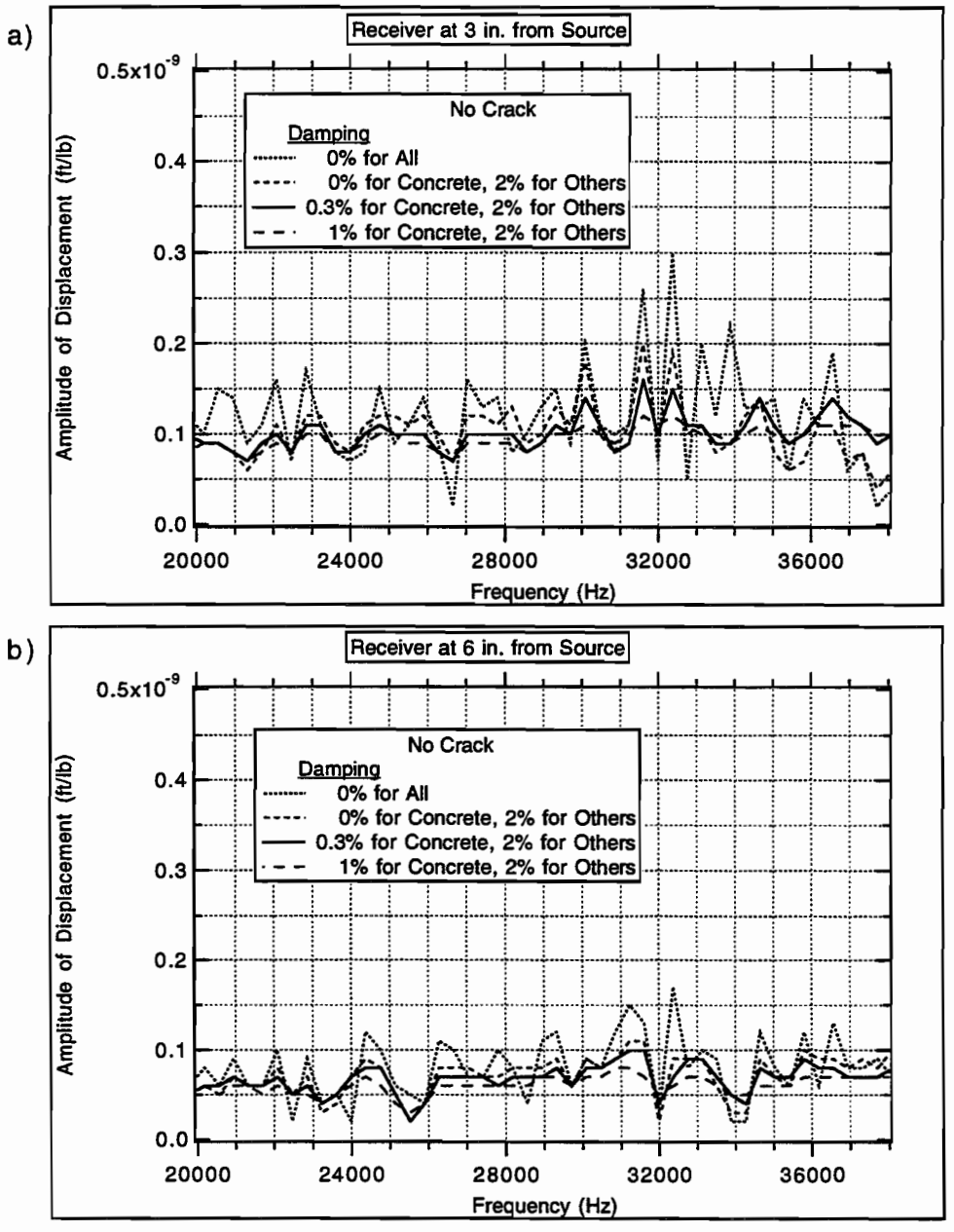


Fig. 4.36 Effect of Damping on the Displacement Amplitudes in the High Frequency Range for an Intact Pavement in Axisymmetric Case

delaminated pavement can be easily distinguished. Similar trends can be seen in Figs. 4.8 and 4.9.

The damping ratio of the concrete layer has less effect on the displacement amplitude at the "flexural peak" than at the "P-wave peak" for a delaminated pavement, as shown in Fig. 4.37. The peak amplitudes decrease about 19% and 34% as the damping ratio of the concrete layer varies from 0% to 0.3% and 1% respectively. The displacement amplitudes around the "flexural peak" for the 6-inch receiver, shown in Fig. 4.37b, is 40% smaller than the amplitudes at the 3-inch receiver in Fig. 4.37a.

The results for an intact pavement are shown in Fig. 4.38. Unlike the results in Fig. 4.11 for the line load, the existence of some damping ratios (compared to no damping) for the concrete layer seems to have an effect on the displacement amplitudes. However, both cases with higher damping ratios than 0.3% for the concrete layer yield the same displacement amplitudes for the 3-inch and the 6-inch receivers.

### 4.3.2 Effects of Delamination Size

Three diameters of disk-shaped crack (delamination), 1, 2, and 3 feet, were considered. The predicted displacement histories at 3 and 6 inches from the source with an impulse duration of 1/26000 seconds for different crack diameters are shown in Figs. 4.39 and 4.40. The ratios of the maximum displacement in the delaminated pavement to that in the intact pavement are 1.6, 2.2 and 2.7 for crack diameters of 1, 2 and 3 feet respectively at the 3-inch receiver. These ratios are

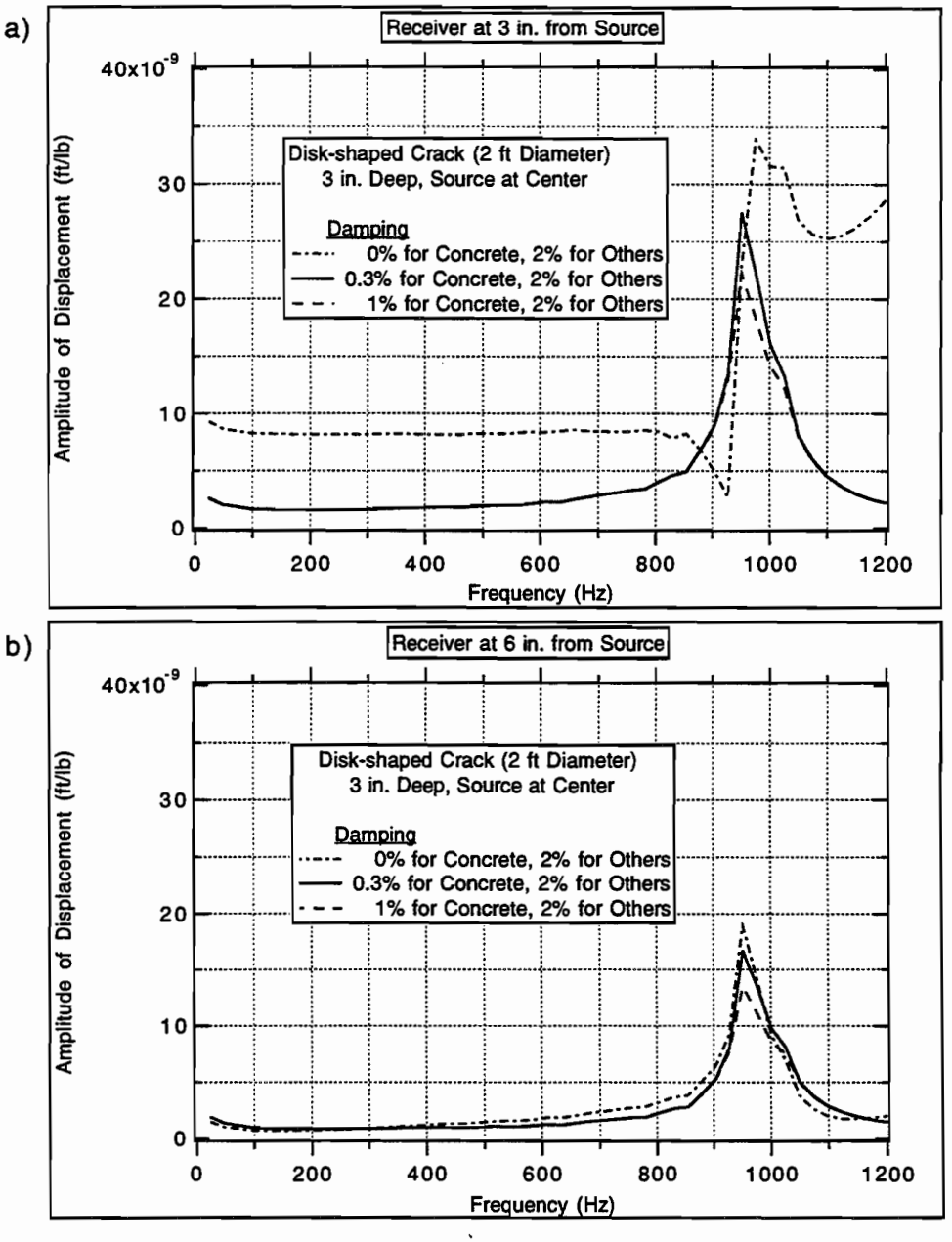


Fig. 4.37 Effect of Damping on the "Flexural Peaks" for a Pavement with a Disk-Shaped Crack at a Depth of 3 in. from the surface

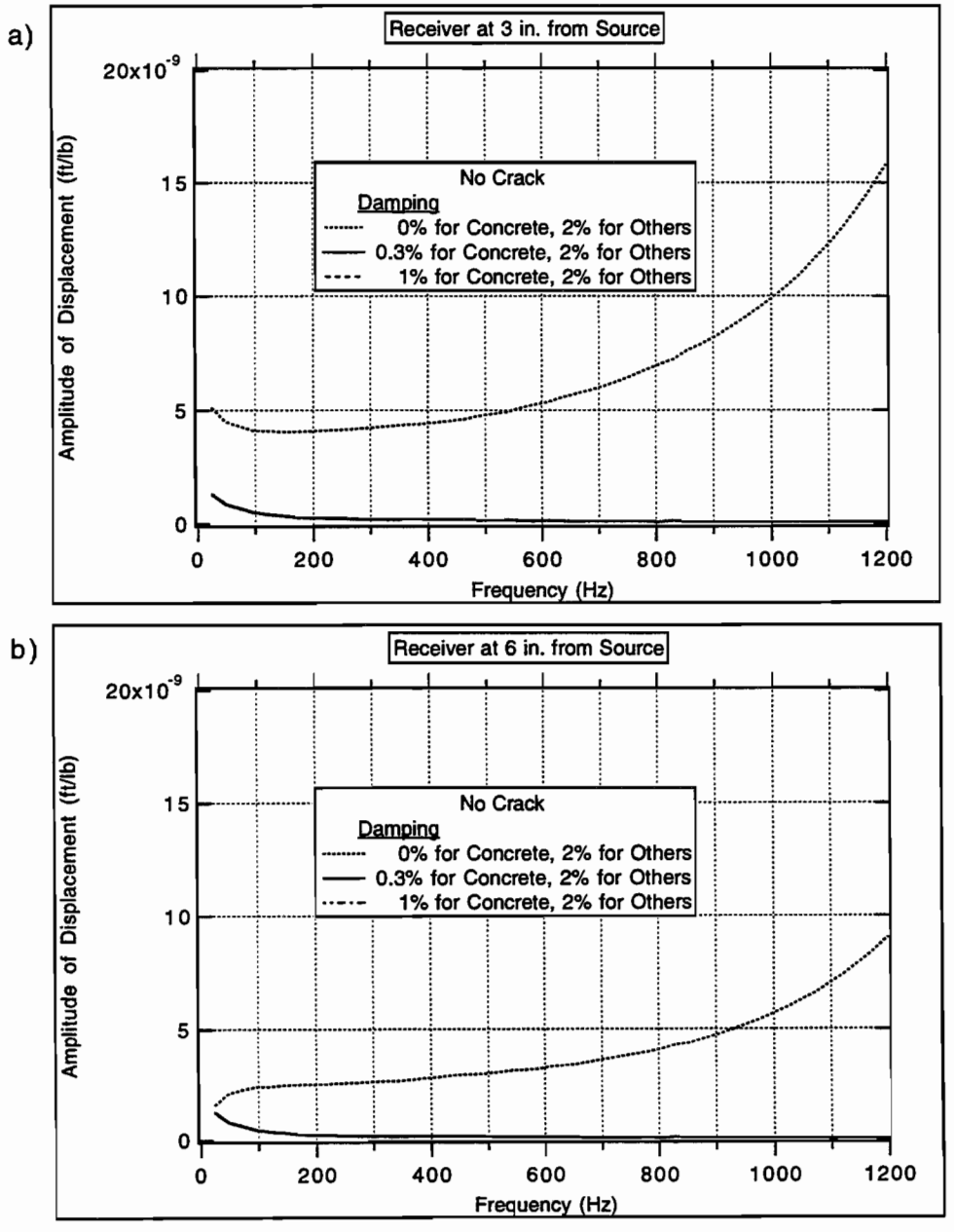


Fig. 4.38 Effect of Damping on the Displacement Amplitudes in the Low Frequency Range for an Intact Pavement in Axisymmetric Case

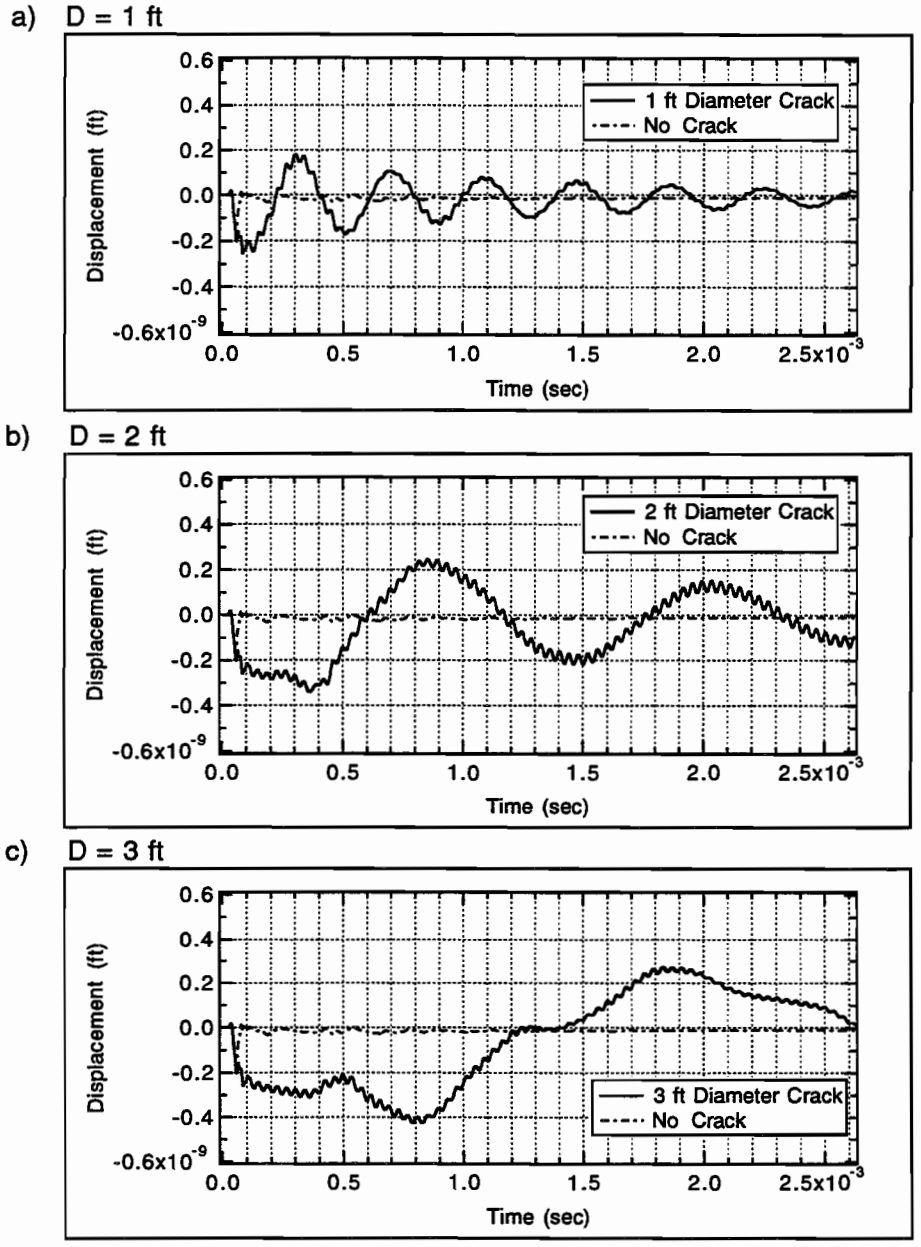


Fig. 4.39 Effect of the Size of Disk-Shaped Crack on the Predicted Time Histories at 3 in. from Source for an Impulse Duration of 1/26000 sec

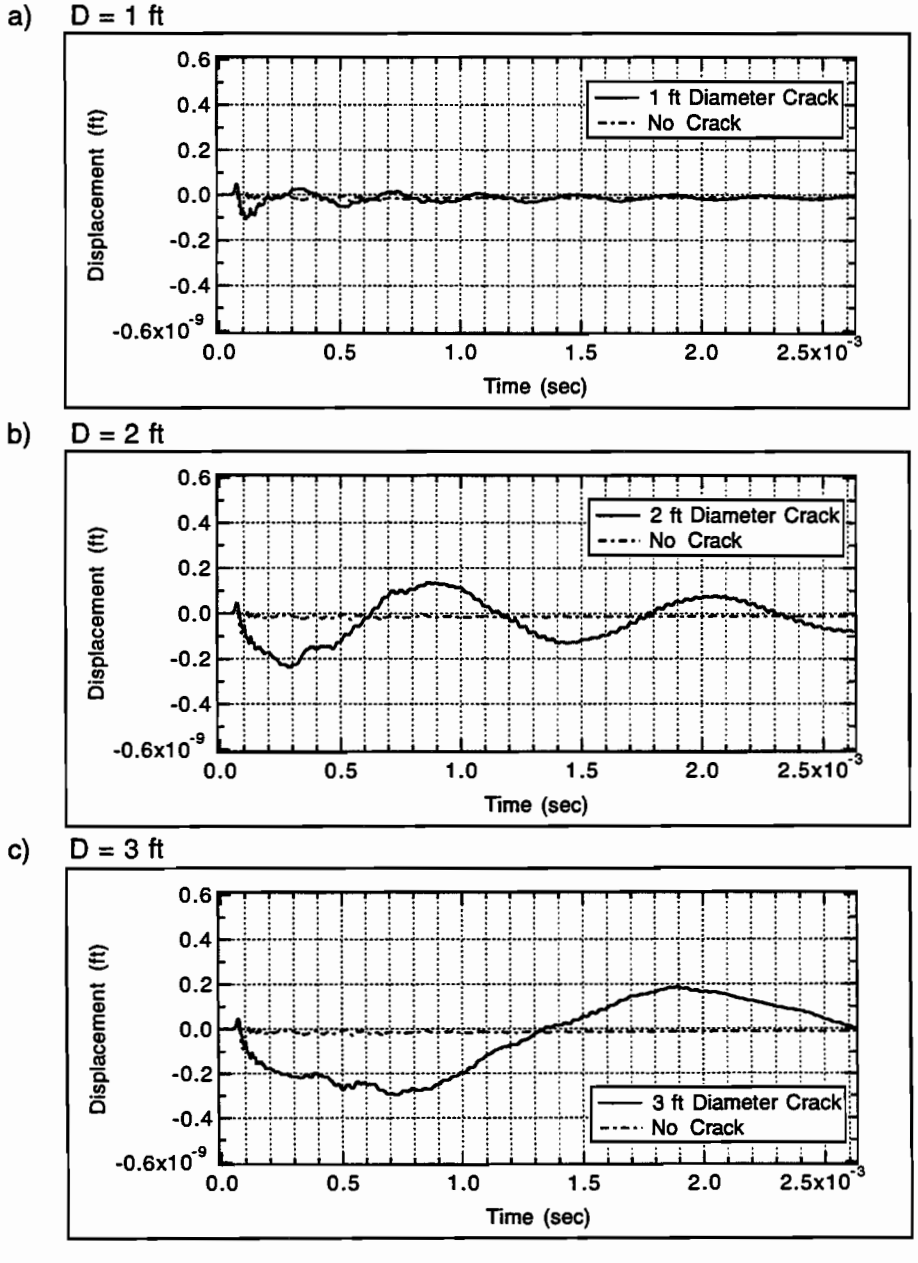


Fig. 4.40 Effect of the Size of Disk-Shaped Crack on the Predicted Time Histories at 6 in. from Source for an Impulse Duration of 1/26000 sec

1.2, 2.7 and 3.4 respectively at the 6-inch receiver. These ratios are smaller than those for a long rectangular-shaped crack under a line load in Figs. 4.12 and 4.13, especially for the 2-foot and 3-foot cracks. The oscillations in the displacement histories at the 3-inch receiver are more pronounced than those at the 6-inch receiver.

The steady state responses at the 3-inch and 6-inch receivers in the frequency domain are shown in Figs. 4.41 and 4.42. The "P-wave peak-frequencies" at the 3-inch receiver appear to be 25500, 27000 Hz for the 1-foot diameter crack, 25500 Hz for the 2-foot crack, and 25500, 27400 Hz for the 3-foot crack. At the 6-inch receiver, the "P-wave peaks" occur at 25500 Hz for the 1-foot crack, 25500, 27000 Hz for the 2-foot crack and 25500 Hz for the 3-foot crack. These frequencies are just a little lower than the 26300 and 27400 Hz, obtained for a long rectangular-shaped crack under a line load. The ratios of displacement amplitudes in the delaminated pavement and the intact pavement are 4.7, 4.3 (1-foot diameter crack), 14.5 (2-foot diameter crack), 8.8 and 2.5 (3-foot diameter crack) respectively at the 3-inch receiver. These ratios for the 6-inch receiver are 9 (1-foot diameter crack), 14.5, 3.6 (2-foot diameter crack) and 6 (3-foot diameter crack) respectively. Again, the length of the delamination has no effect on the "P-wave peak-frequency" which is related to P-wave reflections.

An impulse with a duration of 1/630 seconds was then applied to obtain a more accurate solution in the lower frequency range. The corresponding results are shown in Figs. 4.43 and 4.44 for the time histories and in Figs. 4.45 and 4.46 for the steady state responses. No oscillation is apparent in the time histories for the 1-foot diameter crack, whereas very clear oscillations can be observed in the

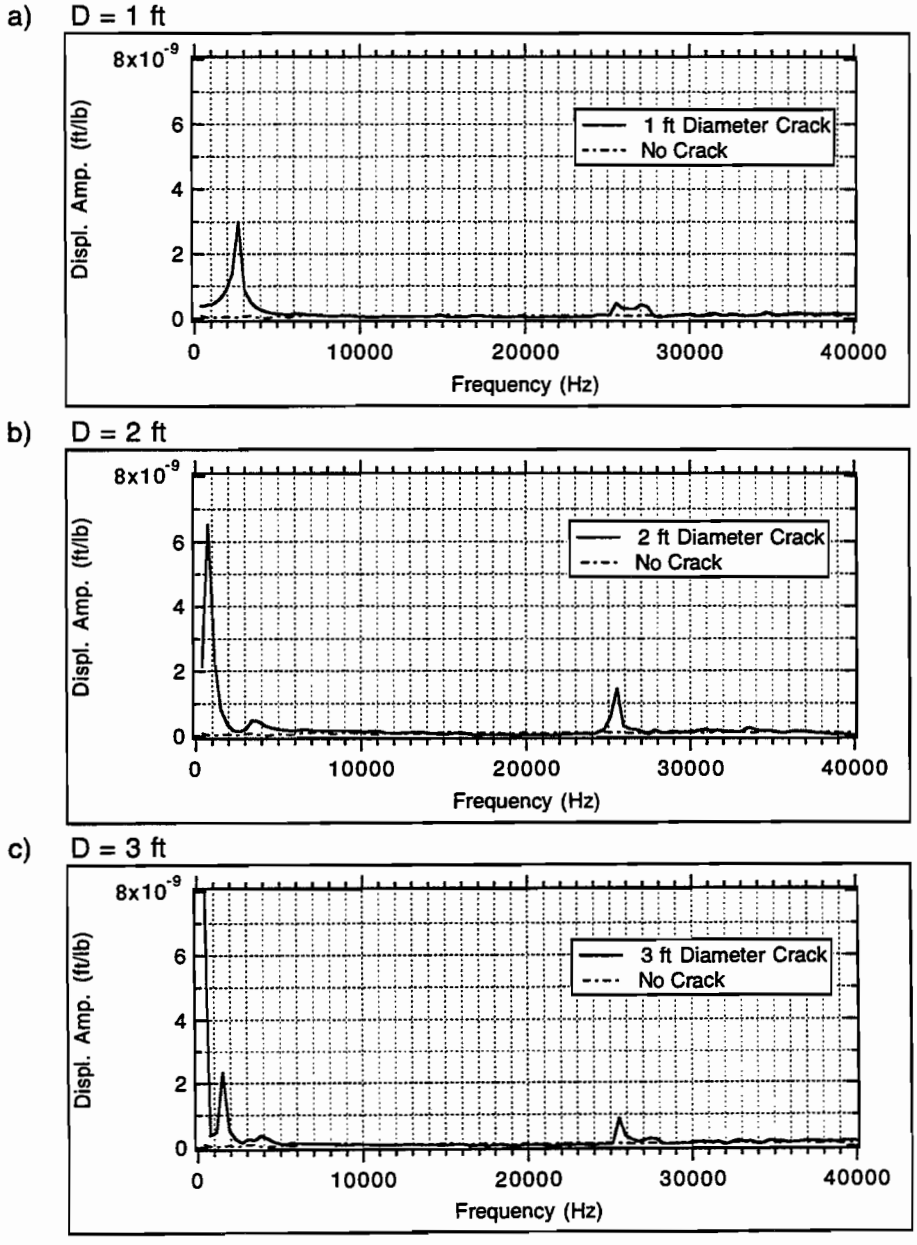


Fig. 4.41 Effect of the Size of Disk-Shaped Crack at 3 in. from the Surface on the Predicted Displacement Amplitude at 3 in. from Source for an Impulse Duration of 1/26000 sec

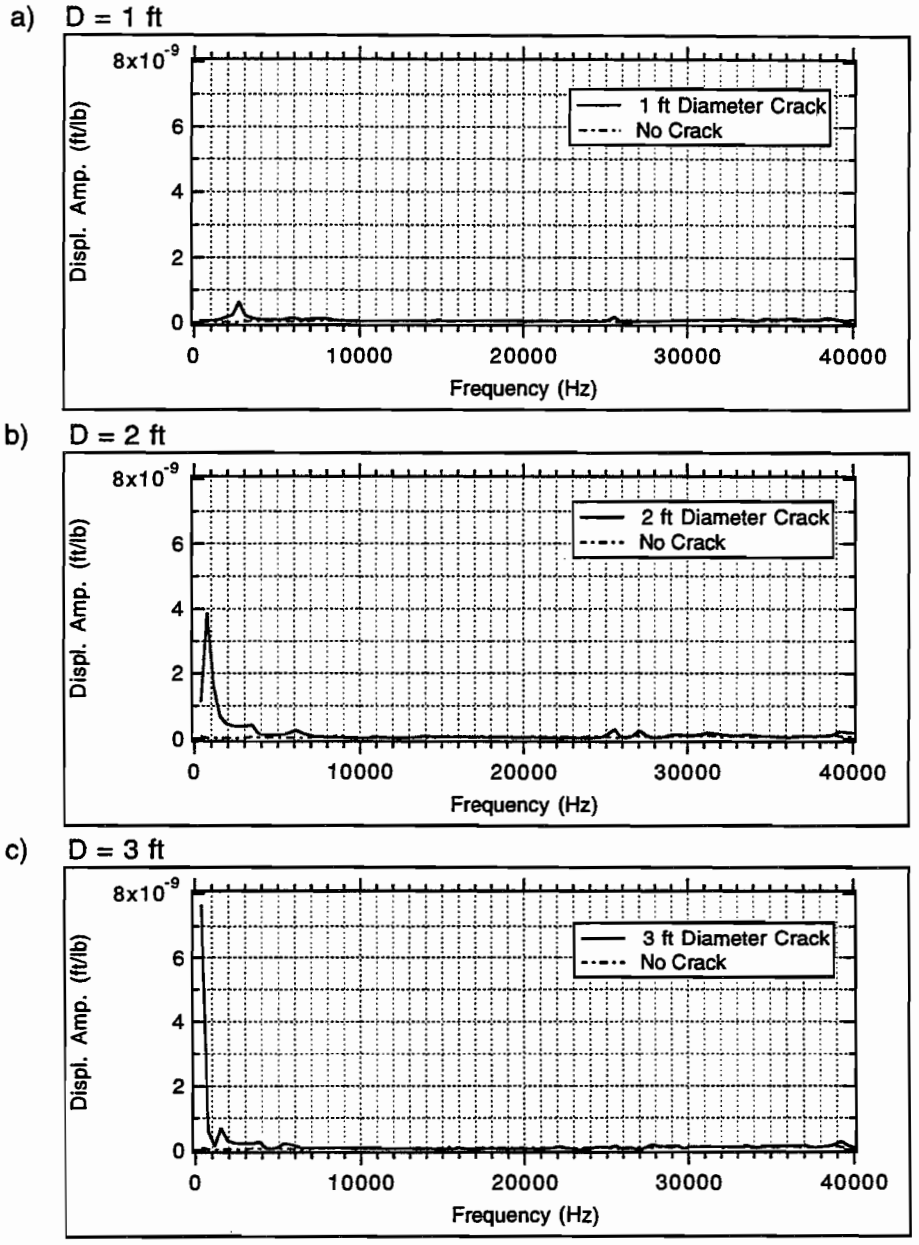


Fig. 4.42 Effect of the Size of Disk-Shaped Crack at 3 in. from the Surface on the Predicted Displacement Amplitude at 6 in. from Source for an Impulse Duration of 1/26000 sec

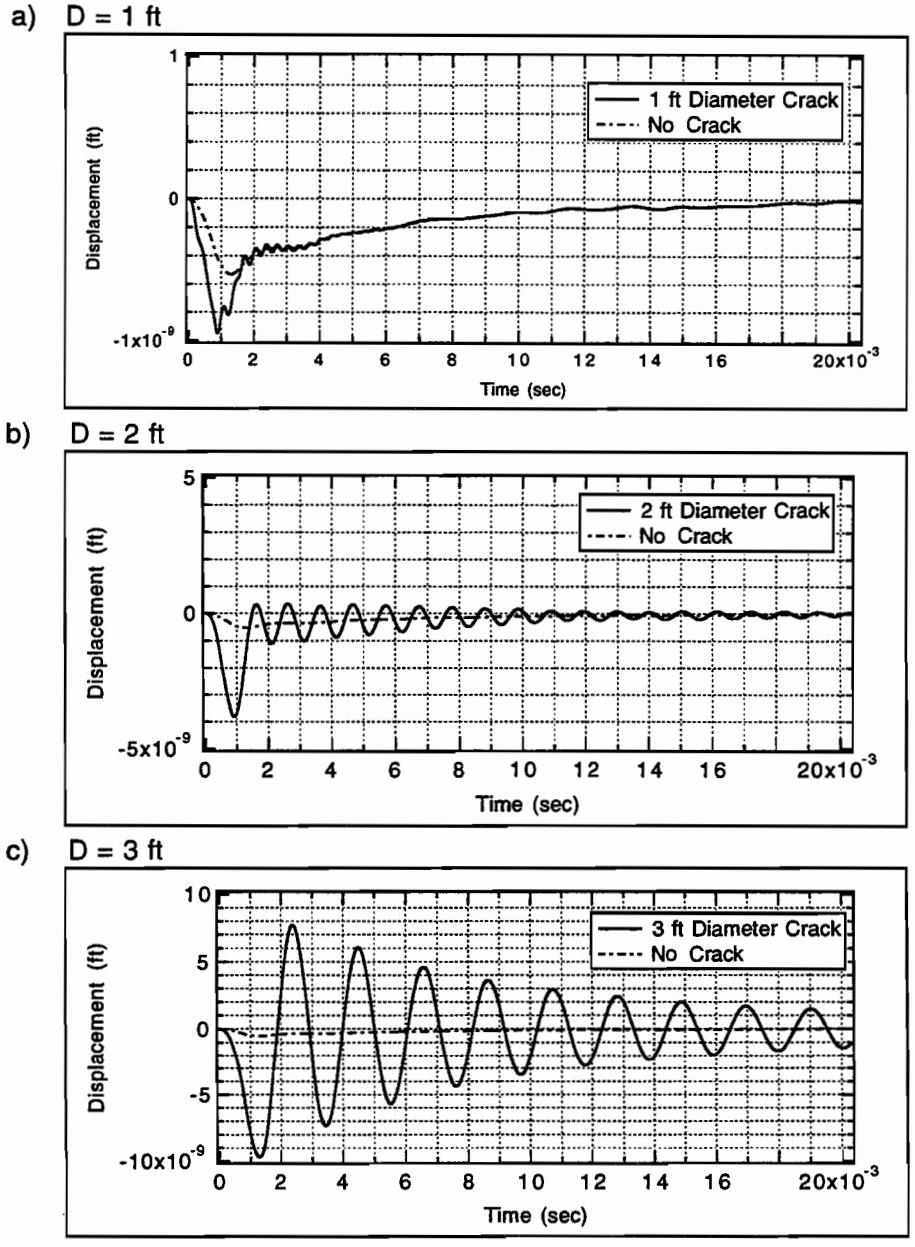


Fig. 4.43 Effect of the Size of Disk-Shaped Crack on the Predicted Time Histories at 3 in. from Source for an Impulse Duration of 1/630 sec

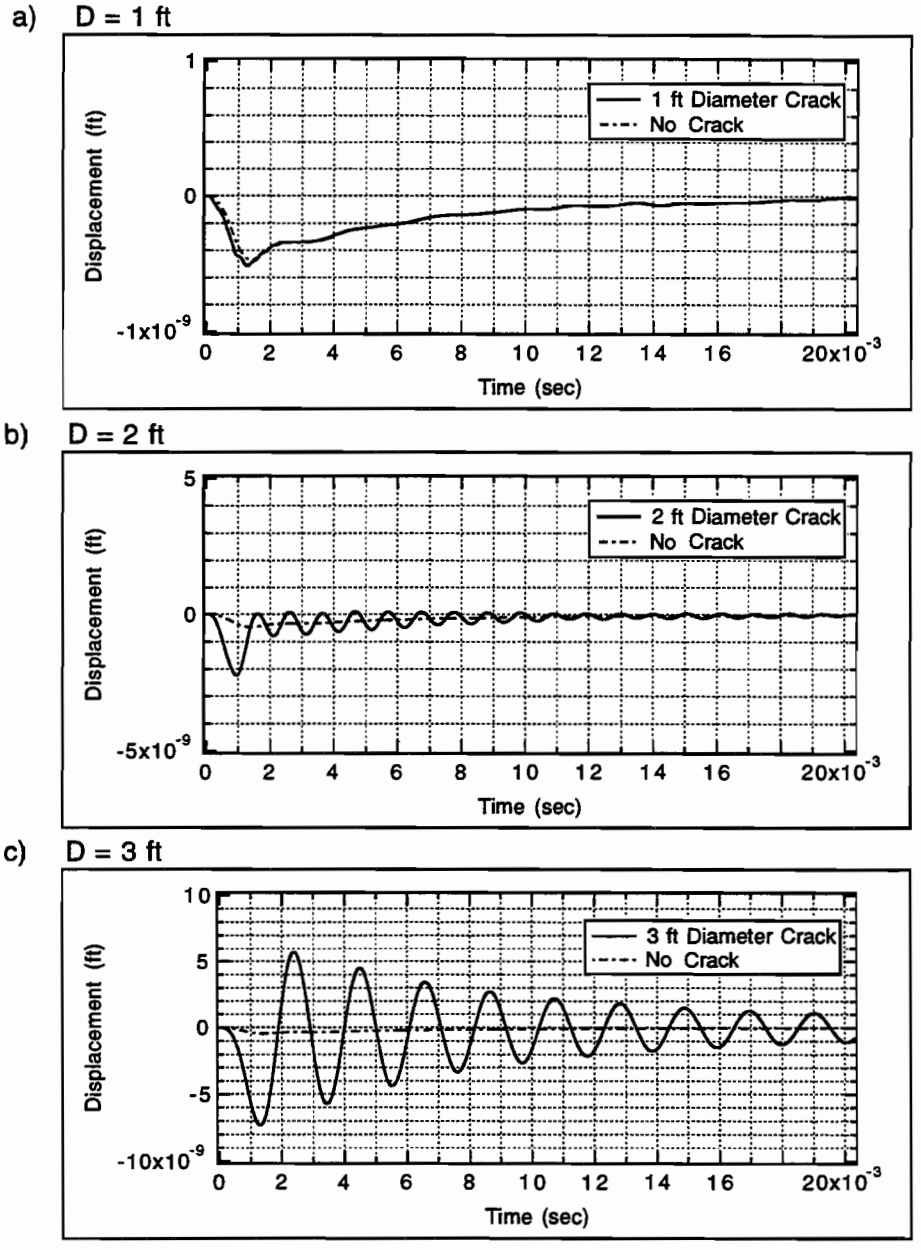


Fig. 4.44 Effect of the Size of Disk-Shaped Crack on the Predicted Time Histories at 6 in. from Source for an Impulse Duration of 1/630 sec

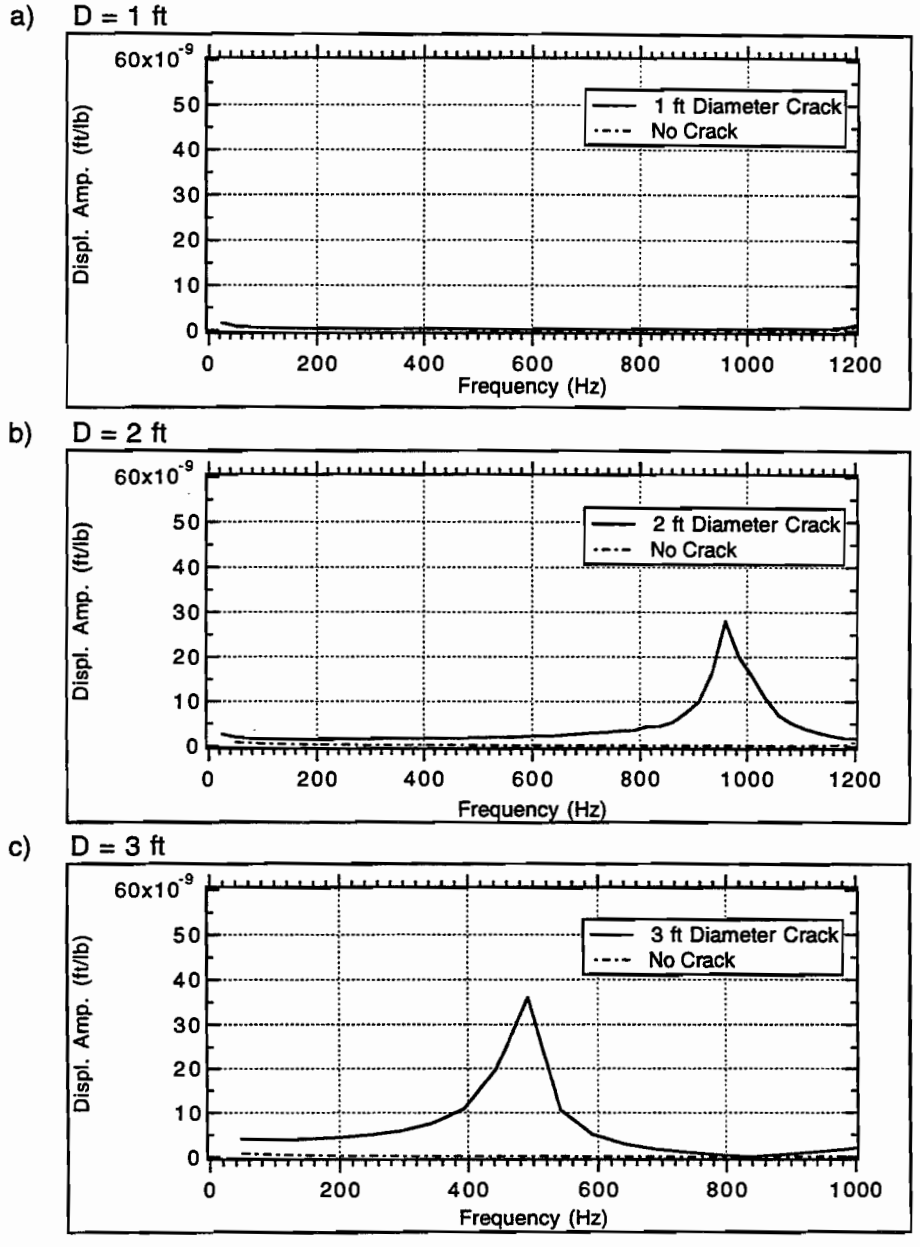


Fig. 4.45 Effect of the Size of Disk-Shaped Crack at 3 in. from the Surface on the Predicted Displacement Amplitude at 3 in. from Source for an Impulse Duration of 1/630 sec

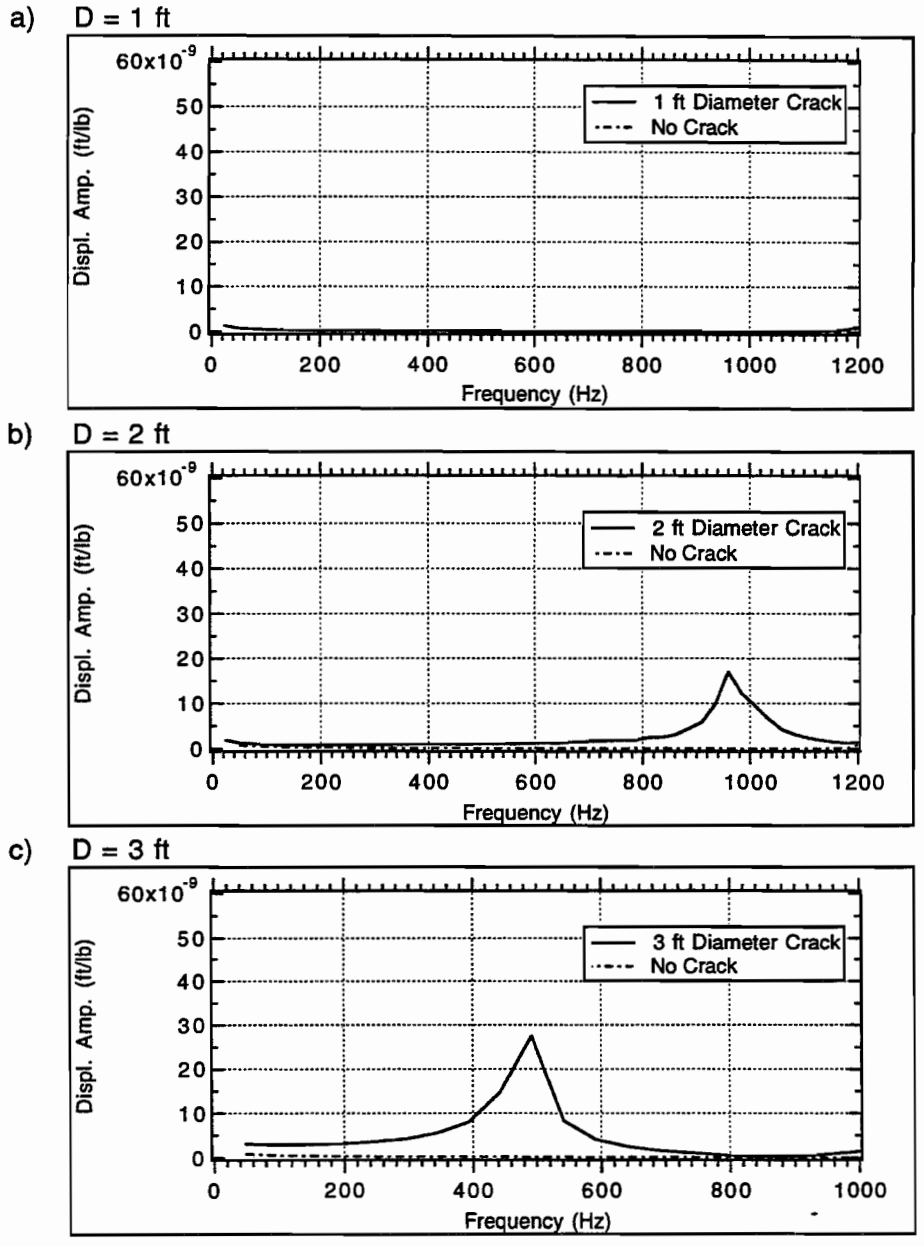


Fig. 4.46 Effect of the Size of Disk-Shaped Crack at 3 in. from the Surface on the Predicted Displacement Amplitude at 6 in. from Source for an Impulse Duration of 1/630 sec

time histories for the 2-foot and 3-foot cracks. The ratios of maximum displacement in the delaminated pavement and the intact pavement are 1.8, 7 and 18 for the 1-foot, 2-foot and 3-foot crack respectively at the 3-inch receiver. These ratios are 1.1, 4.7 and 15.5 respectively at the 6-inch receiver. The ratios for the 2-foot and 3-foot crack are larger than those obtained using an impulse duration of 1/26000 seconds.

The ratios of steady state response at the 3-inch and 6-inch receivers at the "flexural peak" are approximately 350 and 340 for the 2- foot crack, and 240 and 210 for the 3- foot crack. The periods of the oscillation are approximately 1/1000 and 1/500 seconds for the 2-foot and 3-foot cracks. As shown in Figs. 4.45 and 4.46, the "flexural peak-frequencies" in the steady state response appear to be 960 and 490 Hz for the 2-foot and 3-foot cracks respectively for both receivers. These frequencies are higher than the 690 and 340 Hz, which were obtained for a long rectangular-shaped crack under a line load. A result would be consistent with the consideration of a circular plate instead of a one-way slab.

### 4.3.3 Effects of Delamination Depth

As the depth of the delamination increases from 3 to 6 and then 10 inches, the corresponding "P-wave peak-frequencies" decrease from 25500 (and 27000 for the 6-inch receiver) to 12700 and 7700 Hz in Fig. 4.47. The deeper the delamination, the lower the "P-wave peak-frequency". The peak amplitudes at the 6-inch receiver are much smaller than those at the 3-inch receiver for the various depth of the delamination.

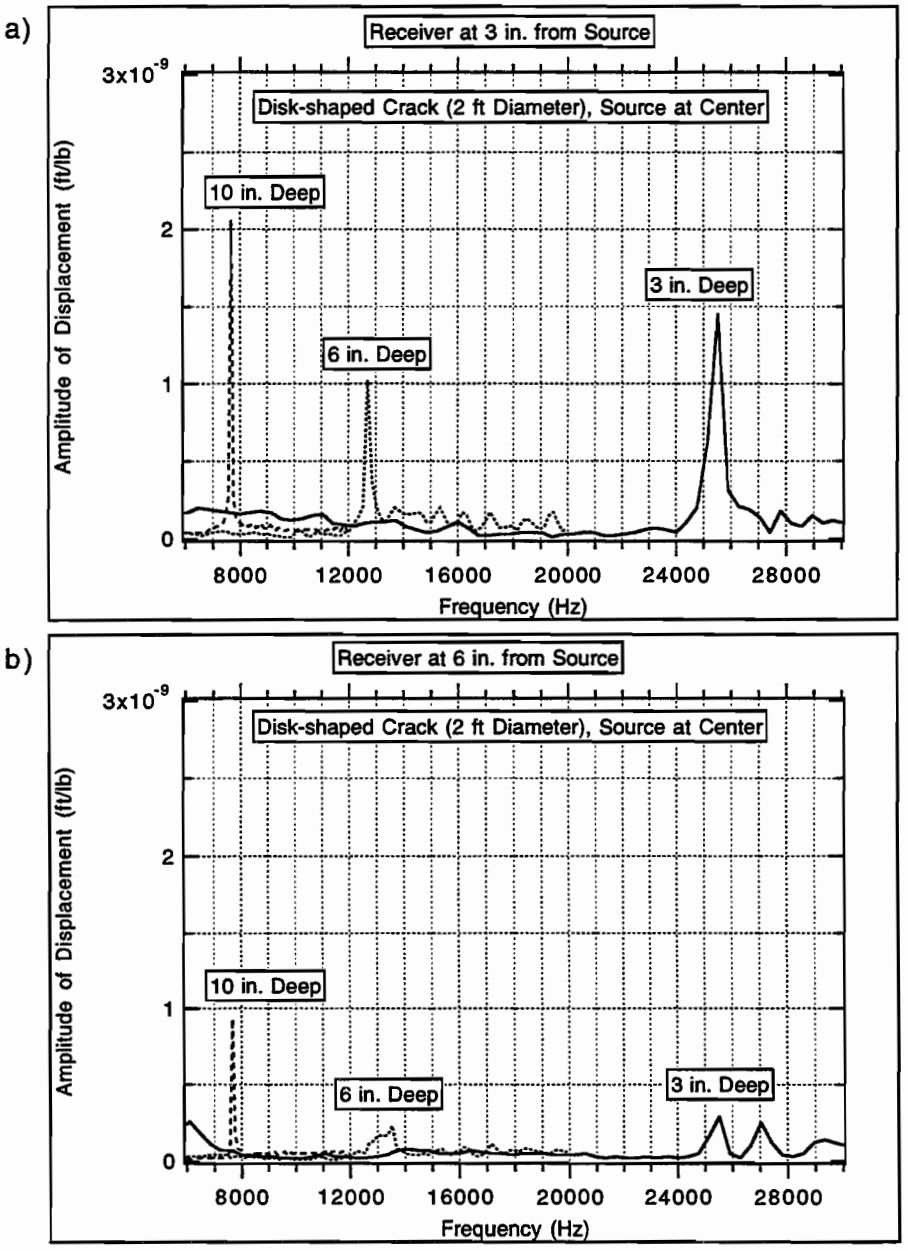


Fig. 4.47 Effect of the Depth of the Disk-Shaped Crack on the "P-wave Peaks"

The "flexural peak-frequency" increases from 960 to 1100 and 1560 Hz as the depth of delamination increases from 3 to 6 and then 10 inches in Figs. 4.48 and 4.49. The deeper the delamination, the higher the "flexural peak-frequency". In addition, the peak amplitudes decrease about 95% and 99% as the depth of the delamination increases from 3 to 6 and 10 inches for both the 3-inch and the 6-inch receivers. Compared to the results of a long rectangular-shaped crack under a line load in Fig. 4.30, the loss of peak amplitude between the 3-inch and the 6-inch cracks is similar. It is interesting to notice that the "flexural peak" of the 10-inch disk-shaped crack seems to appear at a frequency of 1550 Hz, which is the frequency expected, but the peak can not be observed in the case of a long rectangular-shaped crack under a line load.

### 4.3.4 Effects of Base Material

All the results shown so far in this chapter are based on the same pavement configuration and material properties. In this section the effects of the base material on the "P-wave peak" and the "flexural peak" are investigated. A second layer of asphalt concrete with a shear wave velocity of 3000 ft/sec, a Poisson's ratio of 0.27 and a mass density of 145 $lb/ft^3$, is referred to as a "medium base" here. Two other extreme cases are considered. The "hard base" has a shear wave velocity of 8500 ft/sec, a Poisson's ratio of 0.2 and a unit weight of 145 $lb/ft^3$, while the "soft base" has a shear wave velocity of 1000 ft/sec, a Poisson's ratio of 0.25 and a unit weight of 125 $lb/ft^3$.

a) Receiver at 3 in. from Source

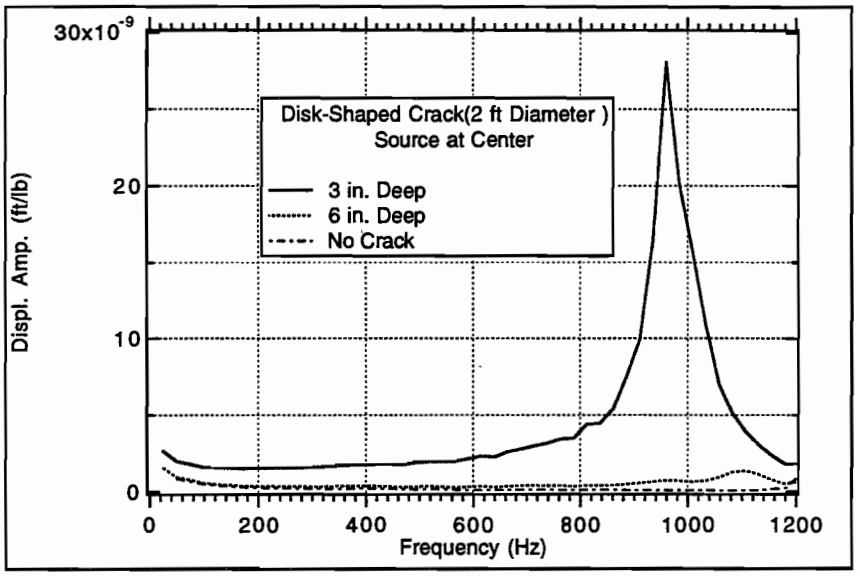


b) Receiver at 6 in. from Source

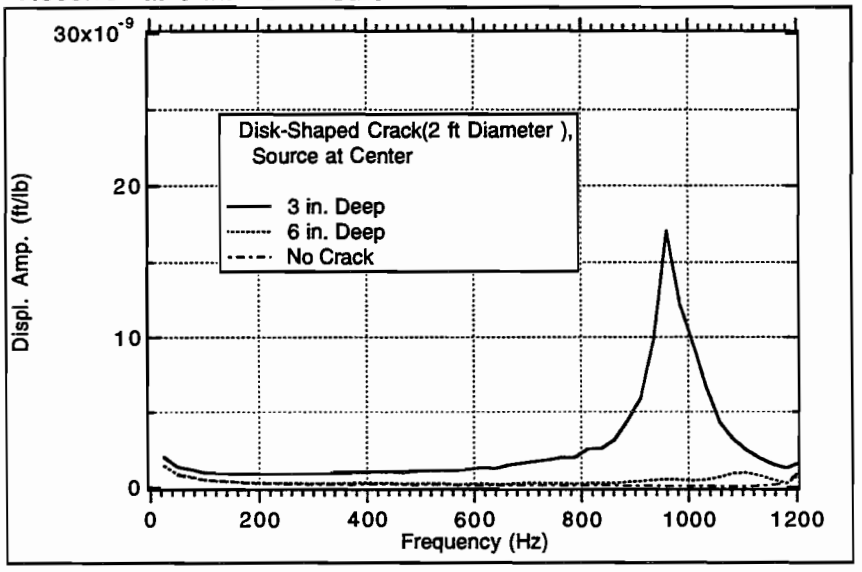


Fig. 4.48 Effect of the Depth of the Disk-Shaped Crack, 3 and 6 in., on the "Flexural Peaks"

a) Receiver at 3 in. from Source

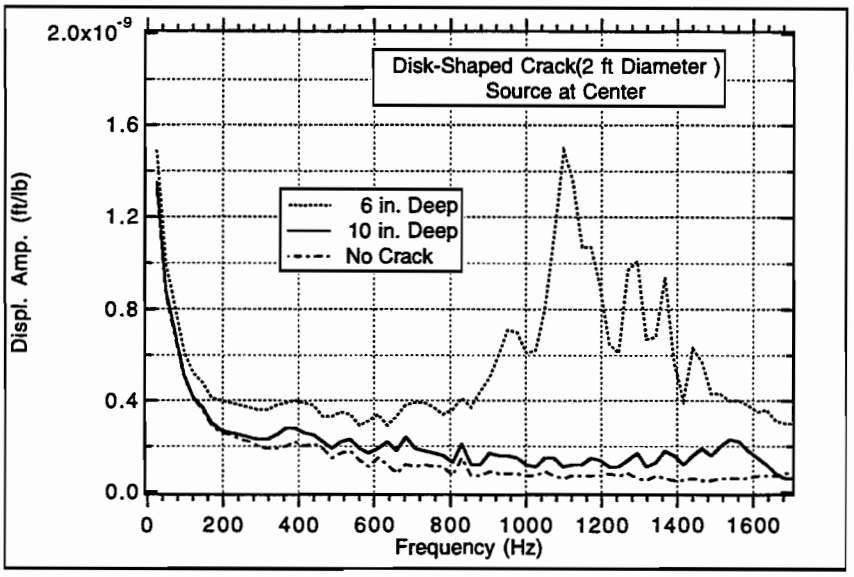


b) Receiver at 6 in. from Source

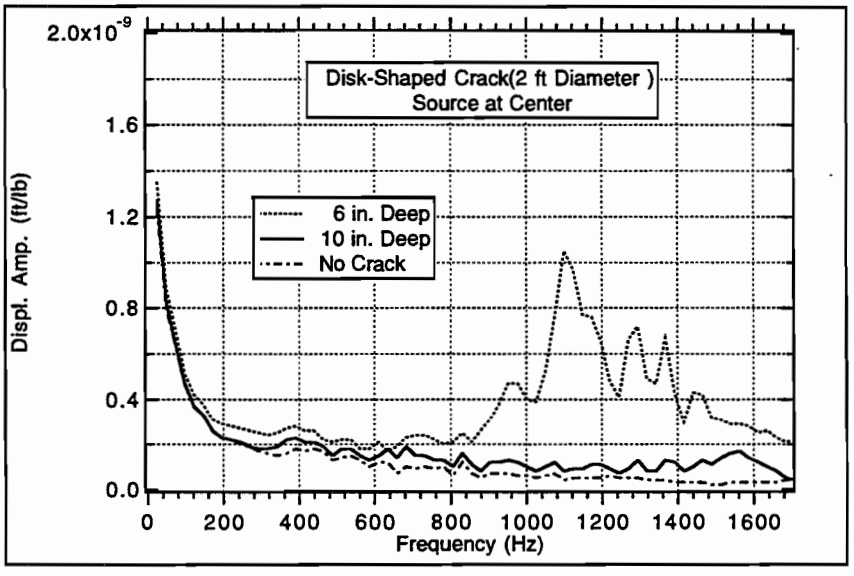


Fig. 4.49 Effect of the Depth of the Disk-Shaped Crack, 6 and 10 in., on the "Flexural Peaks"

The results in the high frequency range for the pavement with "hard base" are shown in Fig. 4.50. The ratio of the displacement amplitude in the delaminated pavement to that in the intact pavement at the "P-wave peak" is 19 for the 3-inch receiver, while it is of the order of 5 at the 6-inch receiver (over the frequency range from 20 to 38 kHz the values of the ratios are smaller than 6). It seems therefore that for the pavement with "hard base" the receiver should be placed near the source to measure the larger displacement ratio at the "P-wave peak". The ratios for the pavement with "medium base" have the same value, 14.5, at the 3-inch and the 6-inch receivers, as shown in Fig. 4.51. For the pavement with "soft base", the ratios are 16 and 19 for the 3-inch and the 6-inch receivers respectively as shown in Fig. 4.52.

The responses around the "flexural peak" for the pavement with "hard base", "medium base" and "soft base" are shown in Figs. 4.53, 4.54 and 4.55 respectively. In all cases, the ratios of the displacement amplitude at the "flexural peak" show little difference between the 3-inch and the 6-inch receivers.

## 4.4 SUMMARY

There are two significant frequency ranges for a pavement with a horizontal delamination, a "P-wave peak-frequency" usually associated with high frequencies, and a "flexural peak-frequency" usually in the lower frequency range. The deeper the delamination, the lower the "P-wave peak-frequency" and the higher the "flexural peak-frequency". The length of the delamination has no effect on the "P-wave peak-frequency", but as it increases the "flexural peak-

a) Receiver at 3 in. from Source

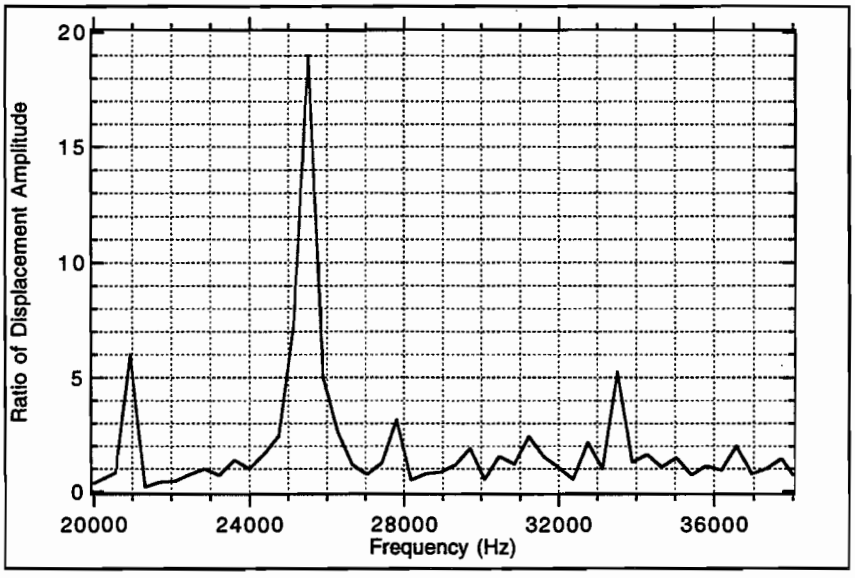


b) Receiver at 6 in. from Source

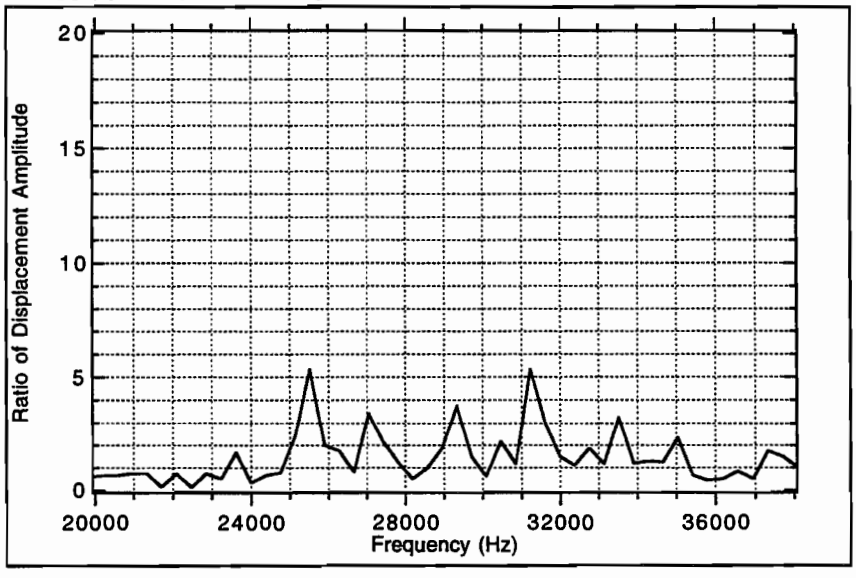


Fig. 4.50 Effect of the Hard Base on the Ratio of Displacement Amplitude in the Delaminated and the Intact Pavements at the "P-Wave Peaks" (2 ft Diameter Crack at 3 inches from surface)

a) Receiver at 3 in. from Source

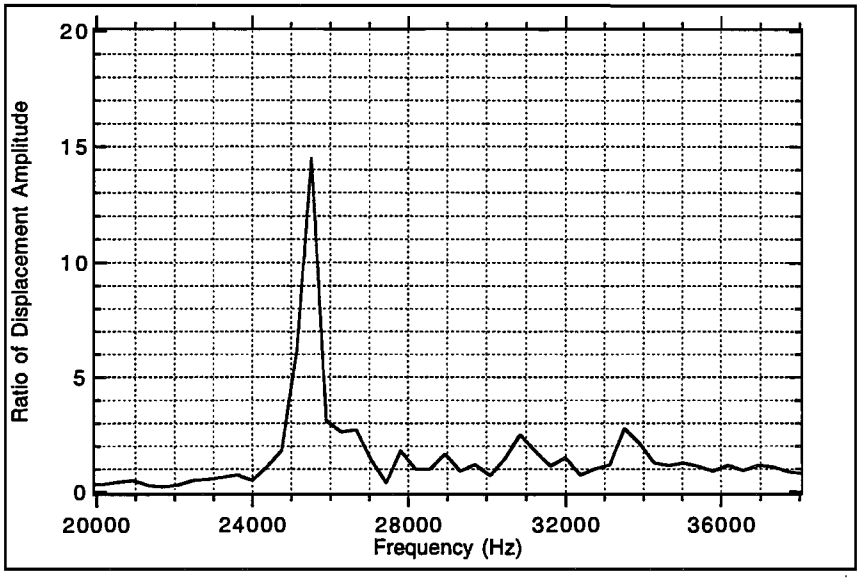


b) Receiver at 6 in. from Source

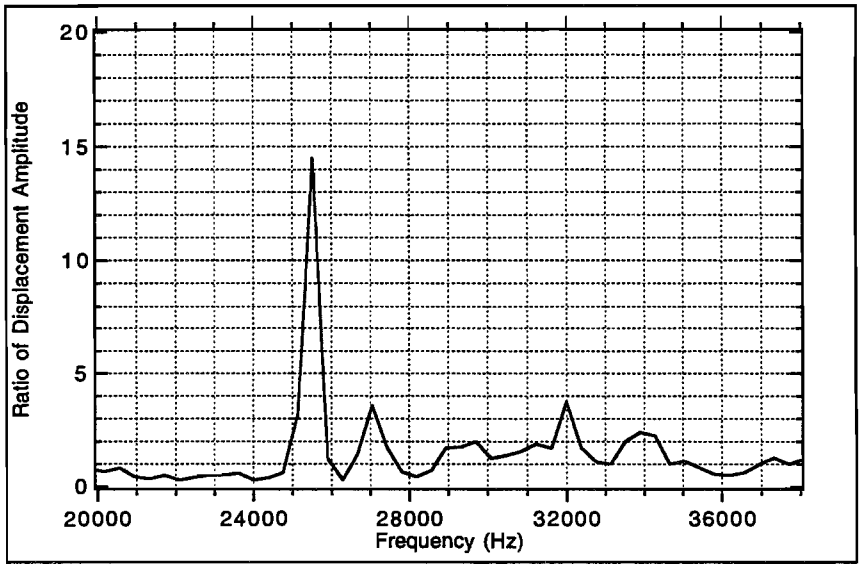


Fig. 4.51 Effect of the Medium Base on the Ratio of Displacement Amplitude in the Delaminated and the Intact Pavements at the "P-Wave Peaks" (2 ft Diameter Crack at 3 inches from surface)

a) Receiver at 3 in. from Source

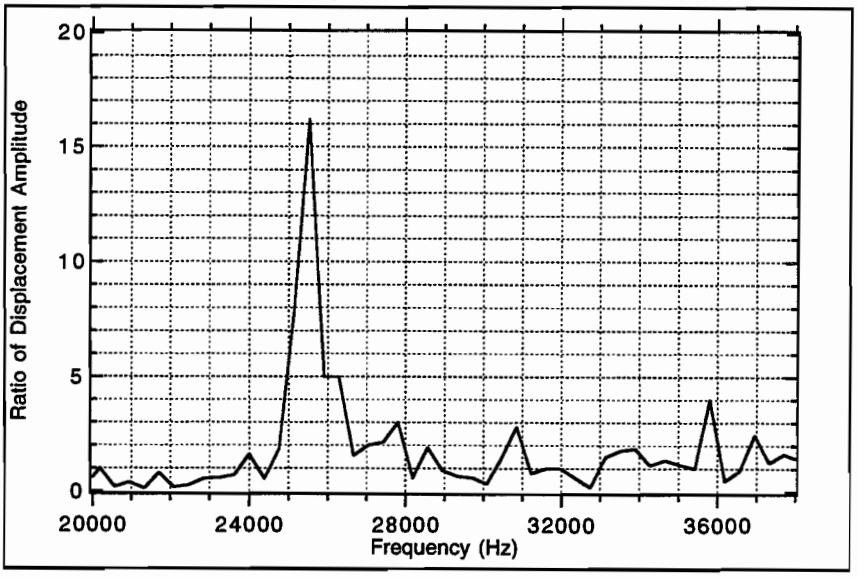


b) Receiver at 6 in. from Source

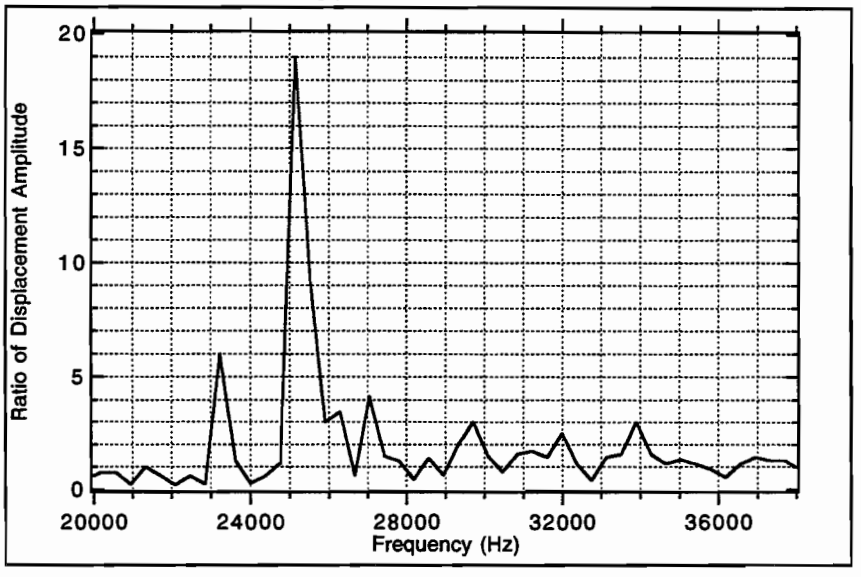


Fig. 4.52 Effect of the Soft Base on the Ratio of Displacement Amplitude in the Delaminated and the Intact Pavements at the "P-Wave Peaks" (2 ft Diameter Crack at 3 inches from surface)

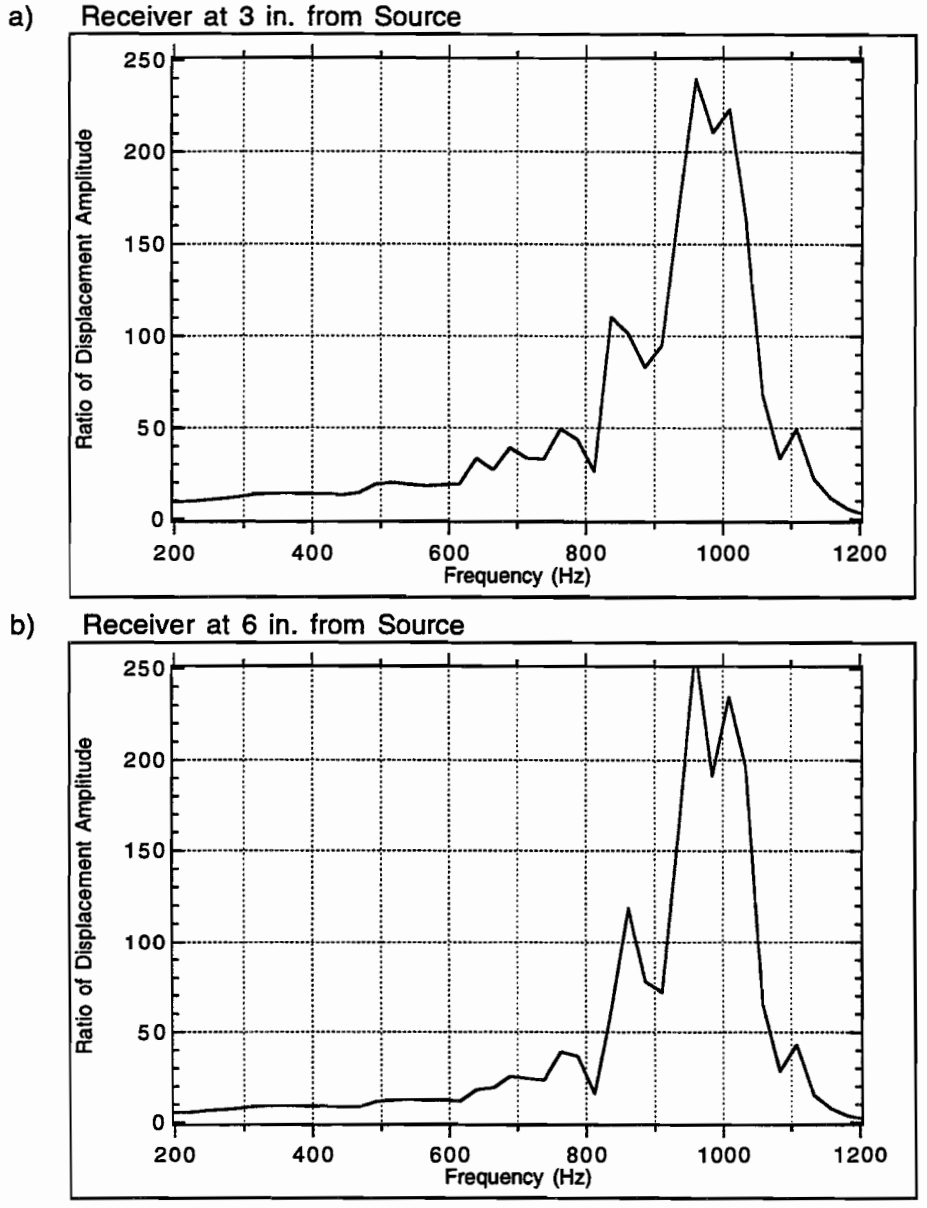


Fig. 4.53 Effect of the Hard Base on the Ratio of Displacement Amplitude in the Delaminated and the Intact Pavements at the "Flexural Peaks" (2 ft Diameter Crack at 3 inches from surface)

a) Receiver at 3 in. from Source

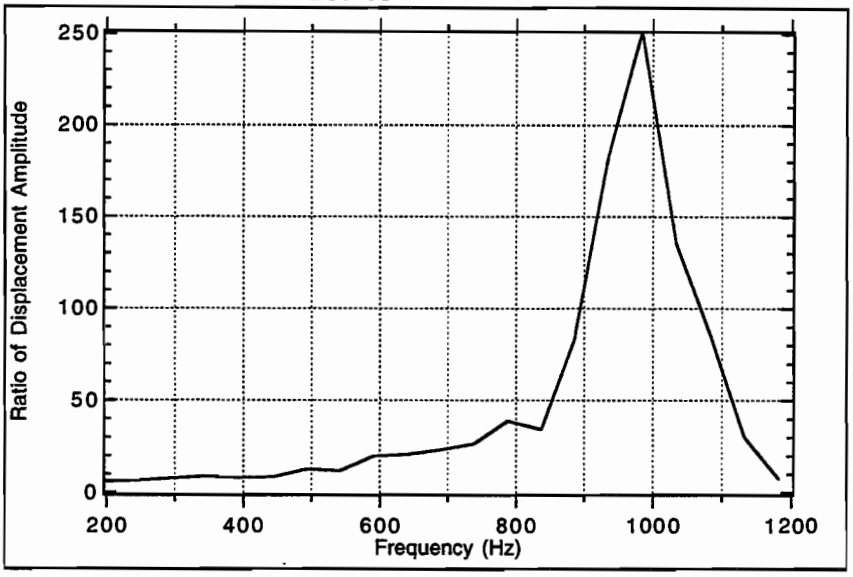


b) Receiver at 6 in. from Source

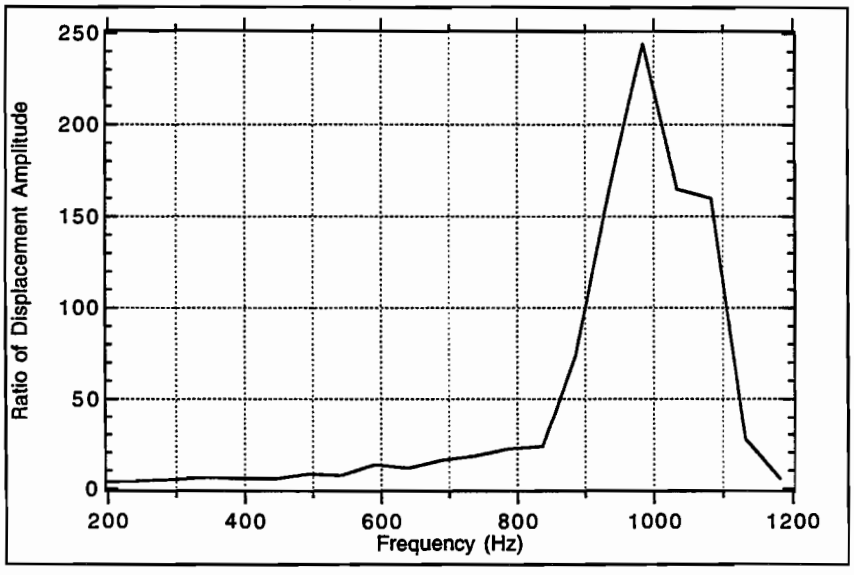


Fig. 4.54 Effect of the Medium Base on the Ratio of Displacement Amplitude in the Delaminated and the Intact Pavements at the "Flexural Peaks" (2 ft Diameter Crack at 3 inches from surface)

a) Receiver at 3 in. from Source

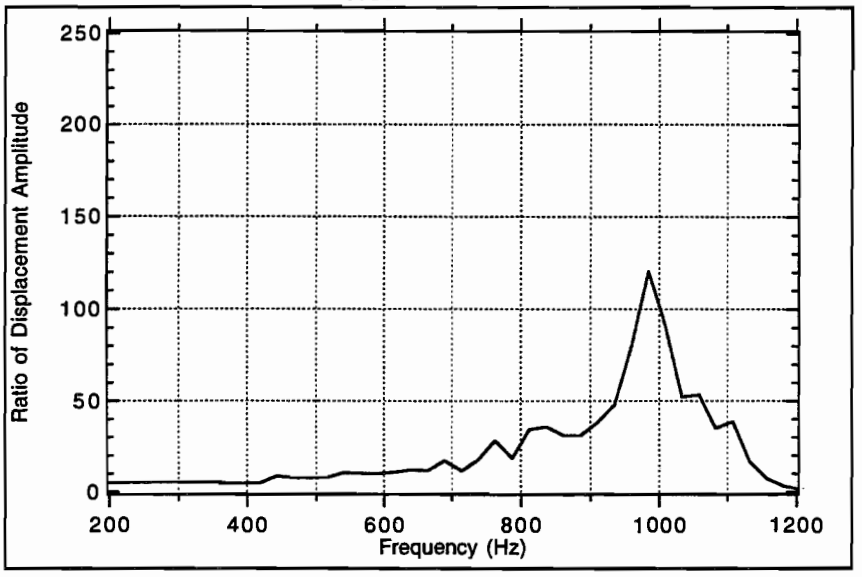


b) Receiver at 6 in. from Source

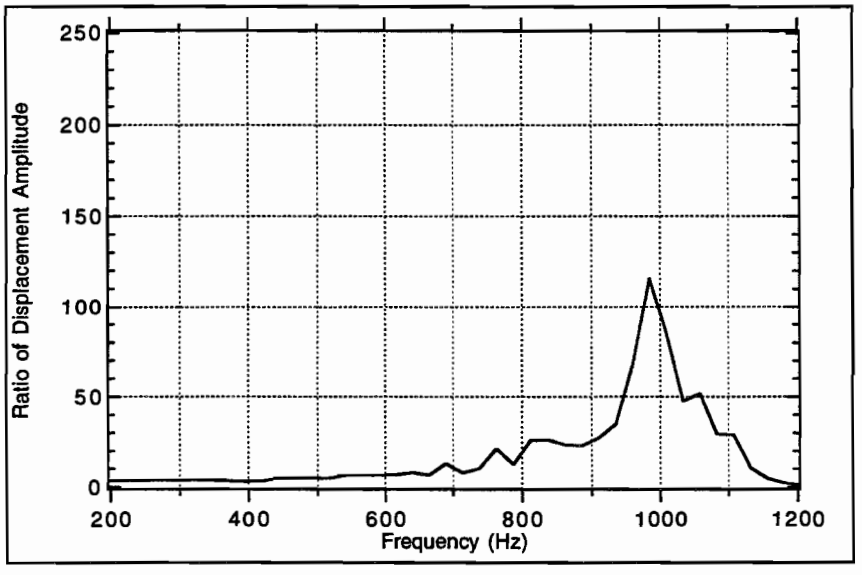


Fig. 4.55 Effect of the Soft Base on the Ratio of Displacement Amplitude in the Delaminated and the Intact Pavements at the "Flexural Peaks" (2 ft Diameter Crack at 3 inches from surface)

frequency" decreases. The "P-wave peak-frequency" is related to P-wave reflections, which can be estimated from $V_p$ / 2d, where $V_p$ is the velocity of propagation of P-waves in the material considered and d is the depth of the delamination from the surface. The "flexural peak-frequency" is associated with flexural vibrations of the layer above the defect. Basically this peak-frequency is a function of the depth but mostly the size of the delamination. If one obtains both the "P-wave peak-frequency" and the "flexural peak-frequency", one could estimate the depth of the delamination from the "P-wave peak-frequency" and assess the size of the delamination from the "flexural peak-frequency".

Selecting an appropriate load duration $t_d$ will ensure that the results will be valid over a range of frequencies centered at the predominant frequency, $f = 1 / t_d$ (in Hz).

The displacement amplitudes associated with a point or disk load are smaller than those associated with a line load for either intact or delaminated pavements. In addition, the displacement amplitudes at the 3-inch receiver are always larger than those at the 6-inch receiver for the 3D case. In both cases the "P-wave peak-frequencies" are similar, while the "flexural peak-frequencies" are higher for the 3D case applied above a disk-shaped crack . In the latter case the amplitude of "P-wave peak" attenuates much faster than that of "flexural peak" from the 3-inch receiver to the 6-inch receiver.

The damping ratio of the concrete layer has more effect on the displacement amplitude at the "P-wave peak" than that at the "flexural peak" for the 3-inch and 6-inch receivers and a delaminated pavement. On the other hand,

the stiffness of the base has more effect on the displacement amplitudes at the "flexural peak" than those at the "P-wave peak".

The largest contrast between the results for delaminated and intact pavements will occur when the load is placed over the center of the delamination.

# CHAPTER FIVE

# EFFECTS OF VOIDS

## 5.1 INTRODUCTION

Delaminations are frequently formed above the top reinforcement and vertical cracks exist within the concrete layer, while voids usually occur beneath the concrete layer at the edge or near a joint. Voids can result in widespread cracks which can then cause delaminations. In this chapter voids of finite thickness are considered instead of delaminations which are assumed to have no thickness in the finite element analysis. The results of displacement histories and displacement amplitudes are almost identical for voids and delaminations with the same length as long as the depth from the surface to the top face of the void equals the depth to the delamination. Thus, only the results showing the effects of the position of the moving source-receiver system on a pavement with a void at a depth of 10 inches are presented. The analytical results are compared to experimental data to evaluate the ability of existing techniques for detection of voids in pavements. In addition to the motion amplitudes, the phase differences and phase velocity are investigated. The experimental tests were conducted by graduate research assistants, James Bay and Brent Rosenblad (1994), using the impact-echo, the impulse-response and the spectral-analysis-of-surface-wave (SASW) techniques.

## 5.2 EFFECTS OF POSITION OF THE MOVING SOURCE-RECEIVER SYSTEM

The response of the pavement with a void, 2 ft long and 1.5 inches thick, is studied as the source and receiver move along the pavement. The pavement has the same material properties used in the last chapter for each layer. Numbers 1 through 13 indicate the locations of the receiver as shown in Fig. 5.1. The source is always 3 inches to the left of the receiver. The displacement histories, above the intact and defective pavements, are shown in Figs. 5.2 and 5.3. As the receiver moves from location 1 to location 6, above the center of the void, the peak displacements increase. Then as the receiver moves away from the center line of the void, the peak displacements decrease in a nearly symmetric way (the displacement history at location 7 is similar to that at location 6, the results at location 8 are similar to those at location 5, the results at location 9 are similar to those at location 4, etc.). The peak displacements reach their maximum value at locations 6 and 7, but is less than two times the peak displacement on the intact pavement, an increase which may be hard to distinguish in practice.

Similar symmetry can be seen on the displacement amplitudes in the frequency domain shown in Figs. 5.4 and 5.5. The displacement spectrum of the intact pavement exhibit two small peaks at 6.6 and 8.5 kHz, which are due to the reflections from the layer interfaces. These peaks are amplified a little as the receiver moves to location 1, while they decrease as the receiver moves to location 2. A clear peak occurs at 8 kHz when the receiver is at location 3 and the magnitude of this peak increases as the receiver moves from location 4 to location 6. At this frequency, 8 kHz, the ratio of the displacement amplitude on

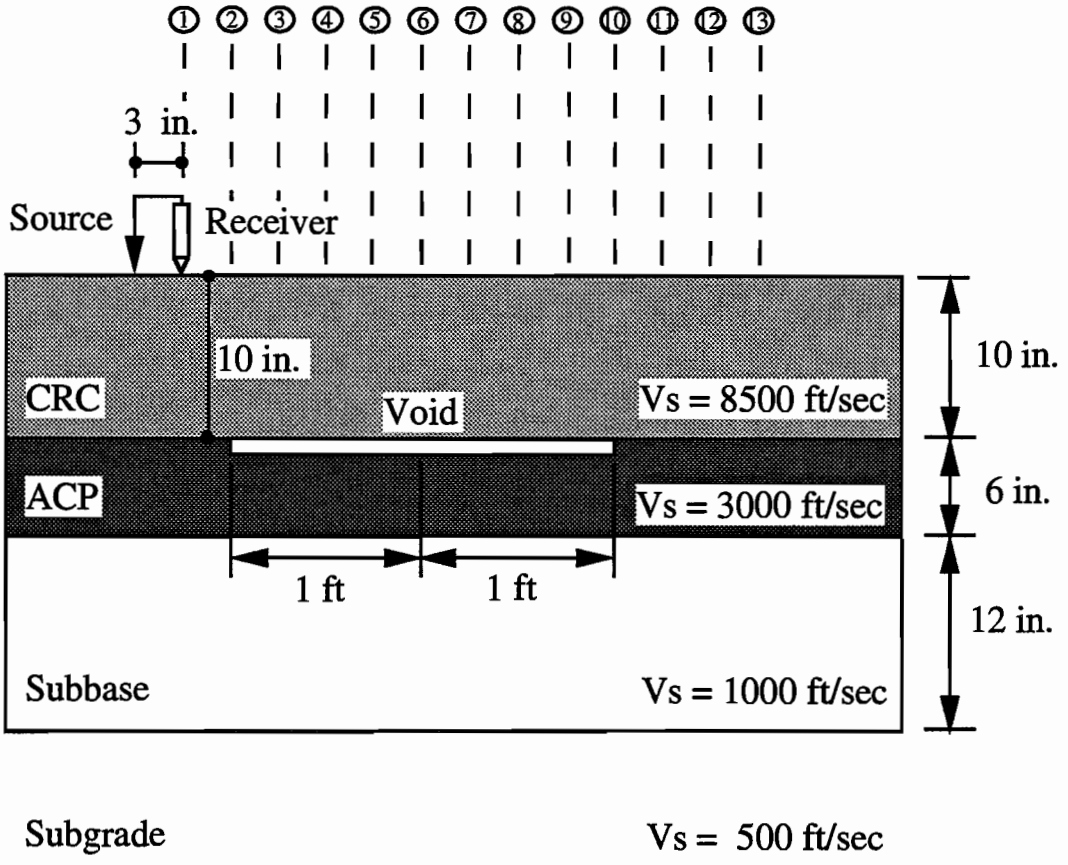


Fig. 5.1 Simulation of the Moving Source-Receiver Testing at a Pavement with a Void at a Depth of 10 inches from the Surface

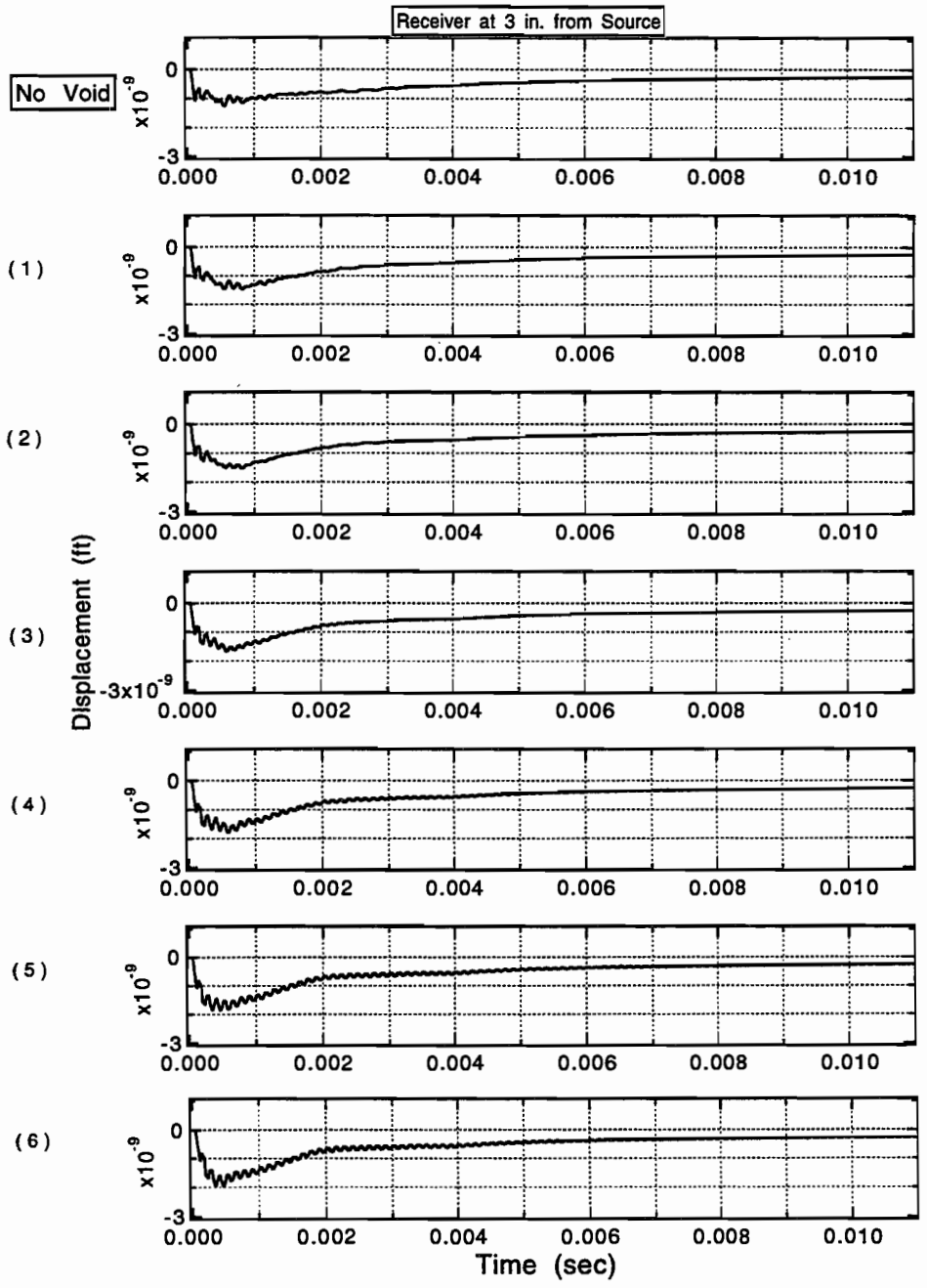


Fig. 5.2 Displacement Histories at 3 inches from the Source as the Receiver is on the Intact Pavement and Moves from Position 1 to 6 on the Pavement with a Void at 10 inches from the Surface

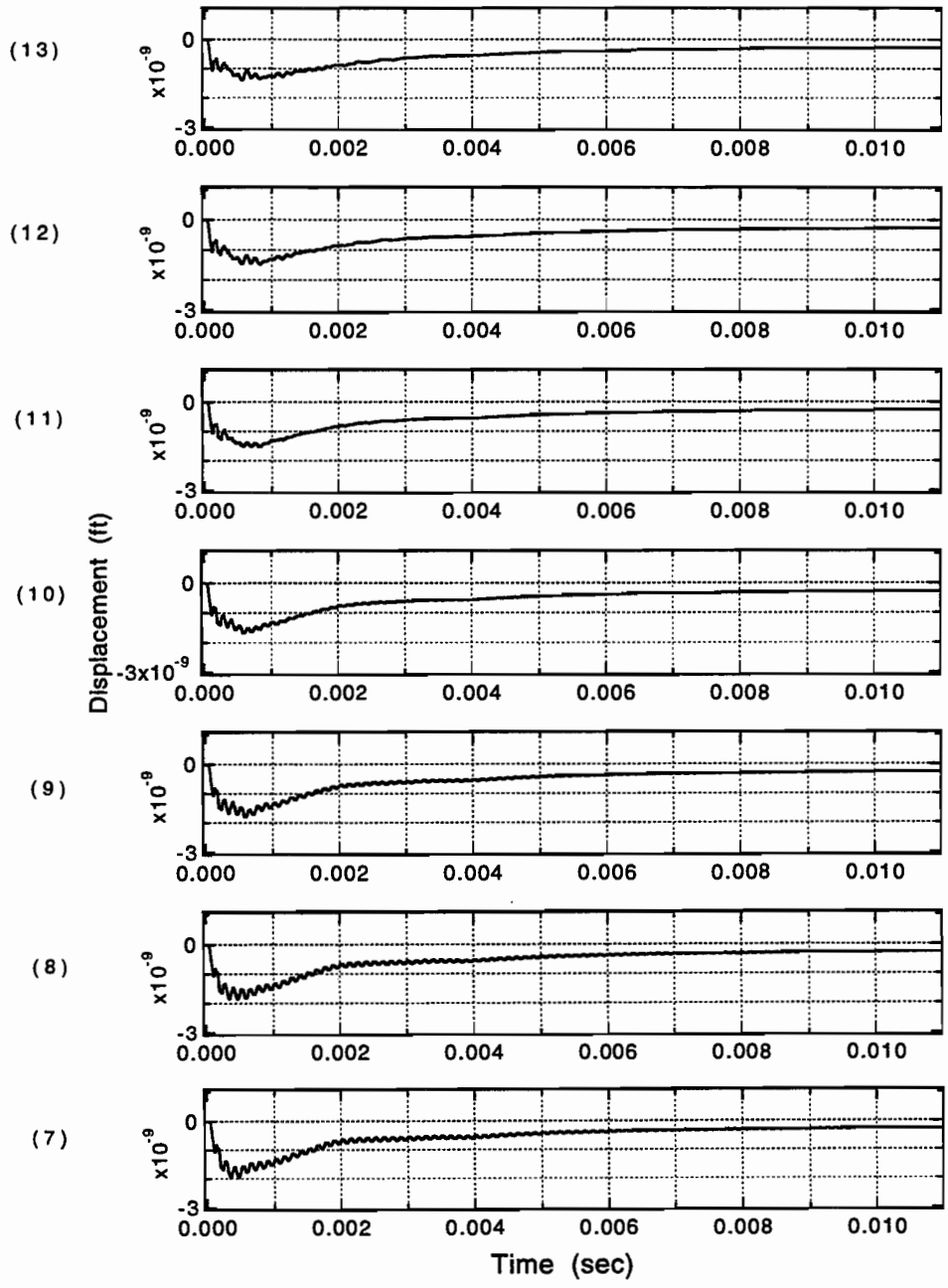


Fig. 5.3 Displacement Histories at 3 inches from the Source as the Receiver Moves from Position 7 to 13 on the Pavement with a Void at 10 inches from the Surface

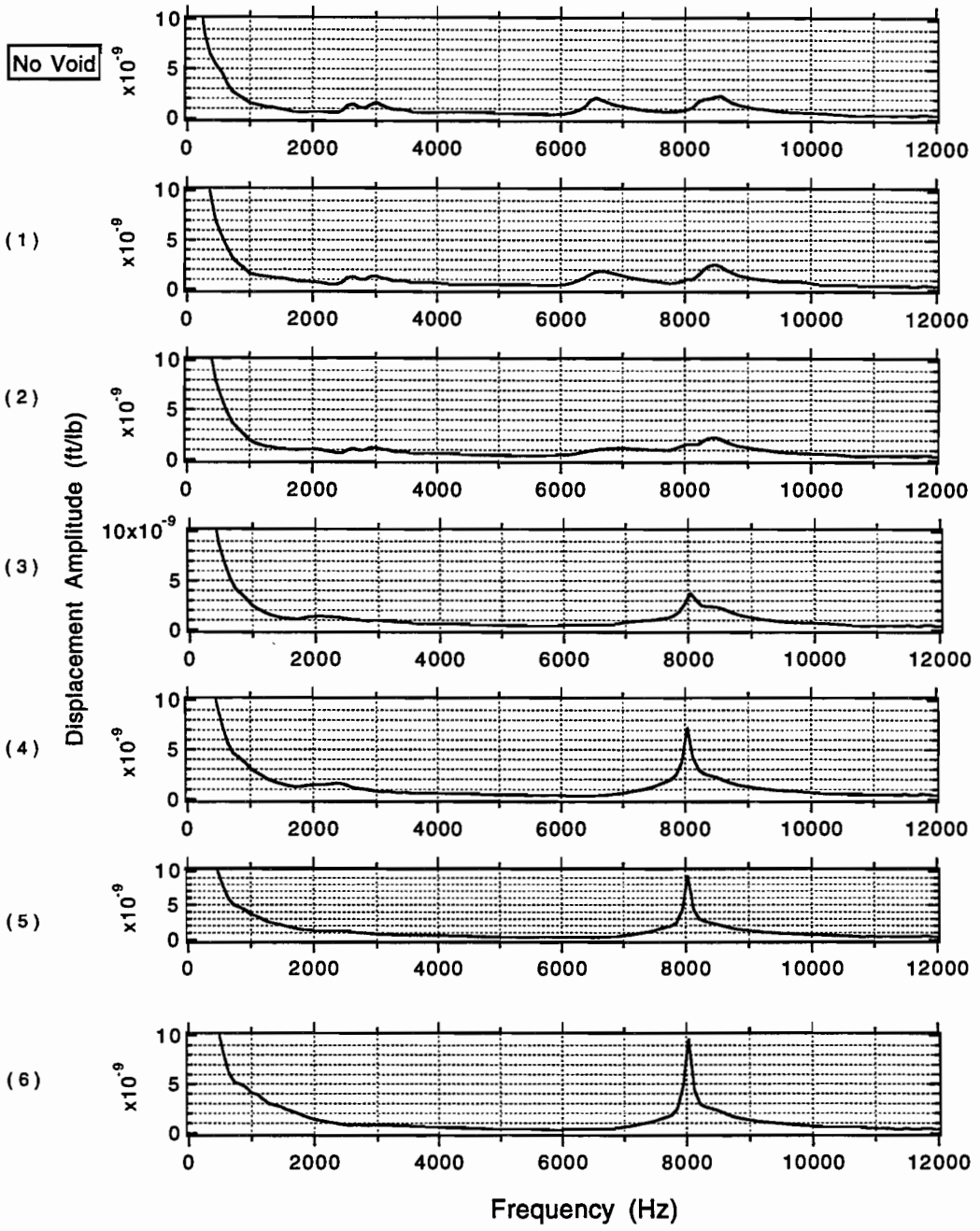


Fig. 5.4 Displacement Amplitudes at 3 inches from the Source As the Receiver is on the Intact Pavement and Moves from Positions 1 to 6 on the Pavement with a Void at 10 inches from the Surface

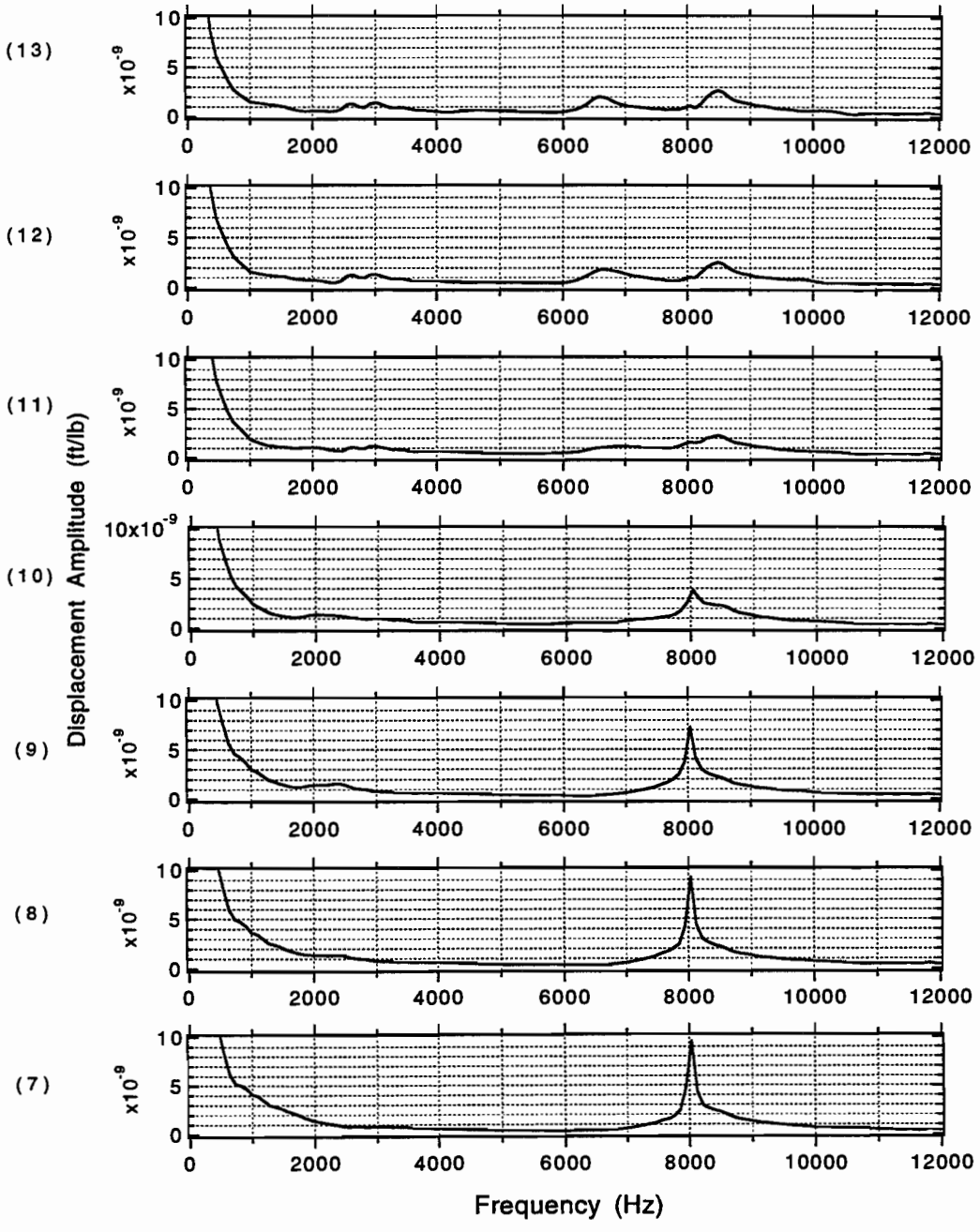


Fig. 5.5 Displacement Amplitudes at 3 inches from the Source As the Receiver Moves from Positions 7 to 13 on the Pavement with a Void at 10 inches from the Surface

the defective pavement to that on the intact pavement is much larger than the ratio of peak displacements in the time domain, so the defective pavement should be easier to identify using the results in the frequency domain..

## 5.3 COMPARISON WITH EXPERIMENTAL WORK

### 5.3.1 Texas A&M Pavements

The test pavement at Texas A&M University, shown in Fig. 5.6, consists of a surface layer of concrete 7 inches thick over a second layer of cement treated base with a thickness of 4 inches. The pavement has a 3-foot square void with a thickness of 1 inch placed at the pavement edge and the bottom of the concrete layer. An instrumented hammer was used to apply an impact at the location E3 above the void and at the location A7 above a debonded area as shown in Fig. 5.6. An accelerometer used as a receiver was placed around 0.5 inches from the loading point. The acceleration histories were converted into frequency domain using the Fast Fourier Transform (FFT) and divided by $\Omega^2$ (circular frequency) to obtain the displacement amplitudes shown in Fig. 5.7a. Two dimensional, plane stain, finite element analyses were performed in the time domain. From the computed displacement histories the steady state amplitudes shown in Fig. 5.7b were obtained using the FFT.

The experimental results for the test above the void show a large peak at a frequency of 13.8 kHz accompanied by two other peaks at 14.8 and 16.3 kHz. The key parameter affecting these "P-wave peaks" is the P-wave velocity of the

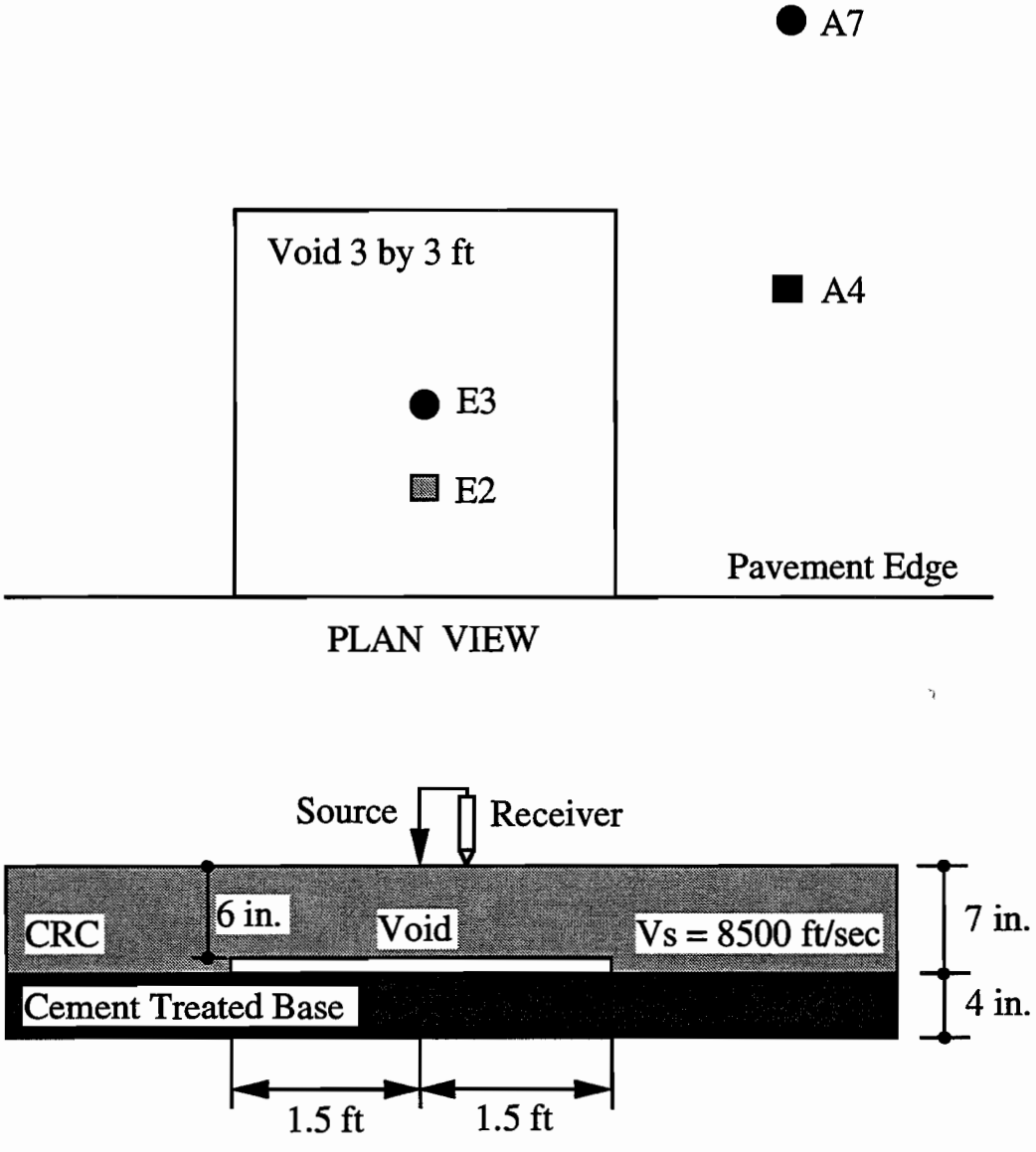


Fig. 5.6 Simulation of the Testing at Texas A&M Pavement with a Void at a Depth of 6 inches from the Surface

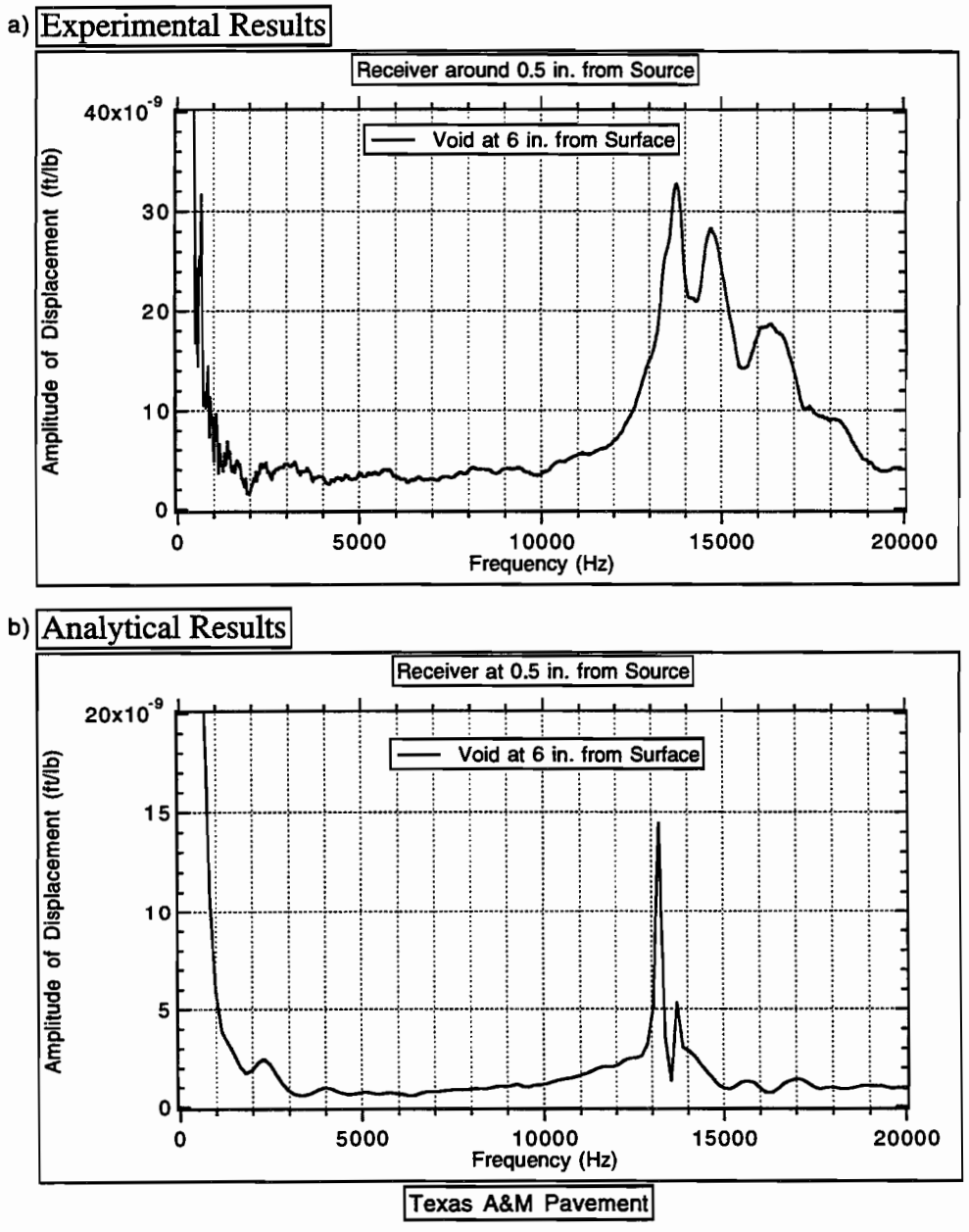


Fig. 5.7 Comparison of Experimental and Analytical Results Using Impact-Echo Technique

concrete layer. Since the material properties were unknown, the shear-wave velocity of the concrete layer was assumed to be 8500 ft/sec, Poisson's ratio was assumed to be 0.2 and the unit weight 145 lb/ft$^3$. A value of hysteretic damping of 0.3% was considered for the concrete layer. For the cement treated base, the shear-wave velocity, Poisson's ratio, unit weight and damping ratio were assumed to be 6000 ft/sec, 0.27, 145 and 2% respectively. With these assumptions the analytical results contain a large peak at a frequency of 13.2 kHz and a smaller peak at 13.6 kHz as shown in Fig. 5.7b. The differences in the peak frequencies, though small, indicate that the shear-wave velocity of the concrete layer could be higher than 8500 ft/sec. The trends of the responses are similar for the experimental and the analytical results although the actual shapes and values are not in good agreement.

For the test conducted above the debonded area, a wide spread peak at 11.7 kHz was obtained experimentally (Fig. 5.8a), while two peaks appear at the frequencies of 11.4 and 11.7 kHz in the analytical results,. The analytical results (Fig. 5.8b) were based on the assumption that the concrete layer and the cement treated base were totally separated in the debonded area. Without debonding at the interface and with a shear-wave velocity of the cement treated base of 6000 ft/sec, the results would be much flatter as shown also in Fig. 5.8b.

The results without debonding but with a deterioration of the properties of the base (a reduction of the shear wave velocity to 3000, 2000 and 1000 ft/sec) are shown in Fig. 5.9. Finally the effect of the distance from the source to the receiver on the results for both cases (void and debonding) are shown in Fig. 5.10. It can be seen that as the distance increase to 6 inches, the two peaks that were

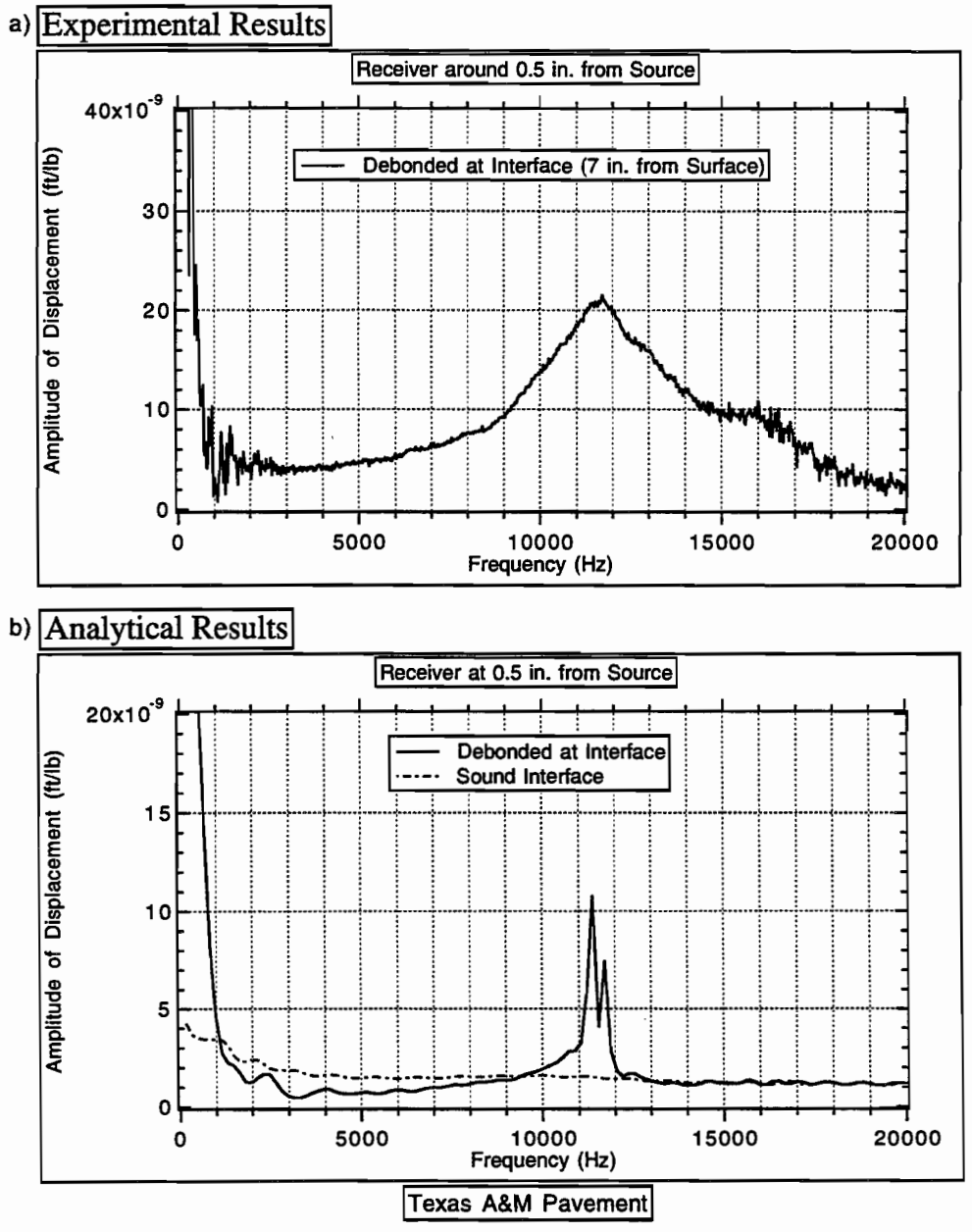


Fig. 5.8 Effect of the Debonded Interface on the "P-Wave Peak"

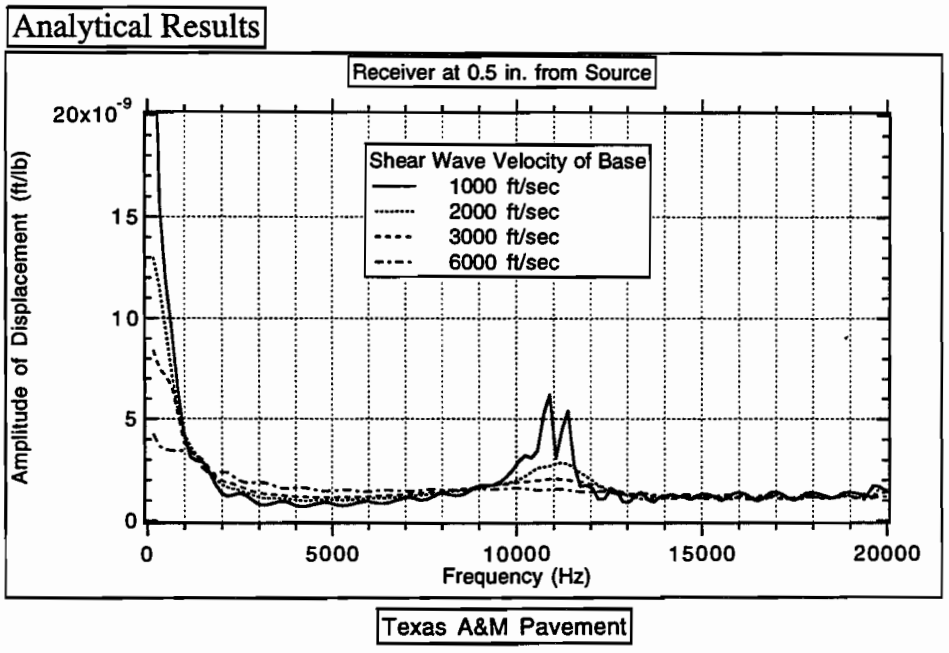


Fig. 5.9 Effect of the Base Material on the "P-Wave Peak"

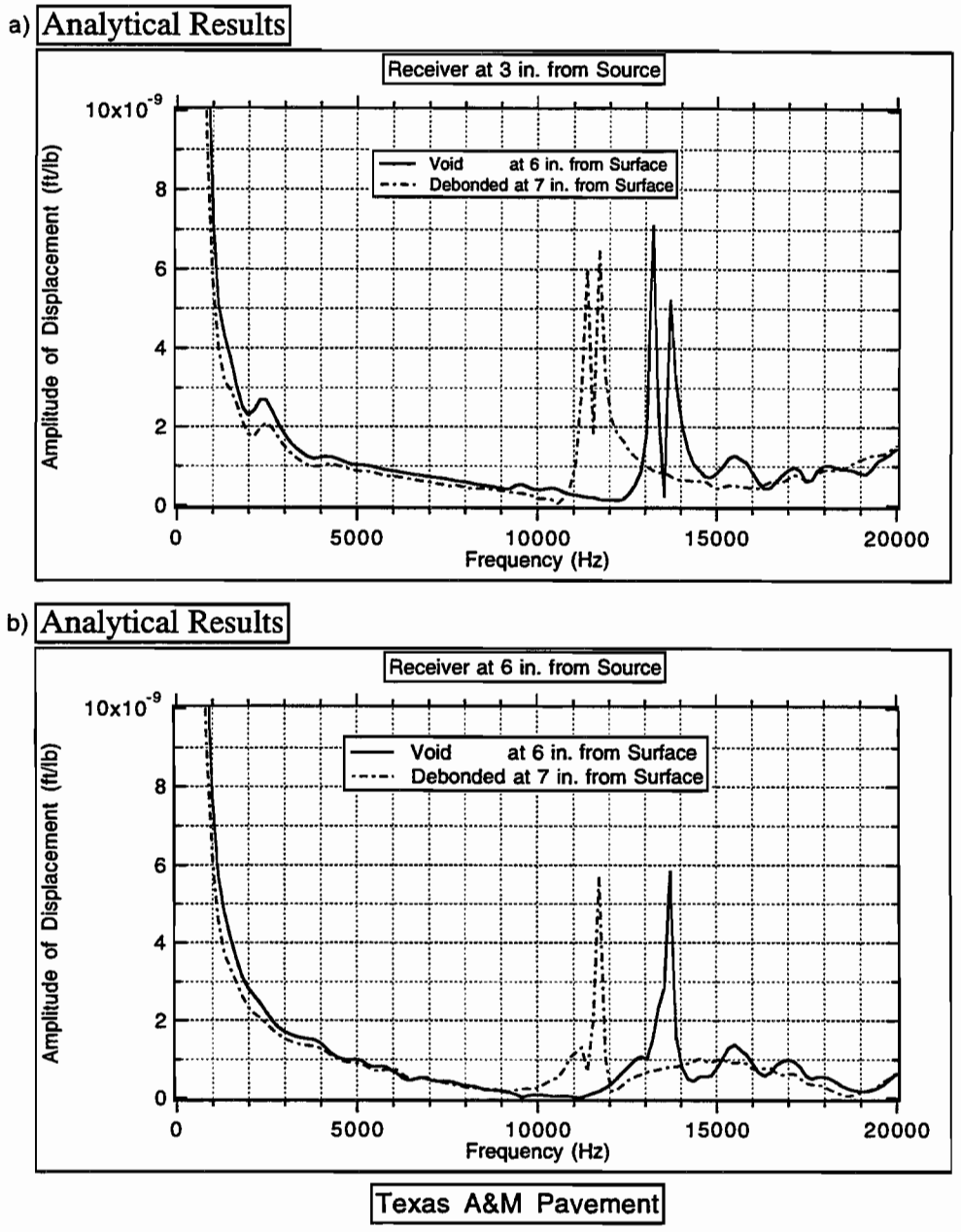


Fig. 5.10 Effect of the Source-Receiver Spacing on the "P-Wave Peaks"

obtained for 0.5 and 3 inches reduce to one. The peaks are still, however, much sharper than those obtained experimentally and their amplitudes are smaller.

From these results it appears that the two dimensional plane strain analytical solution (where there is a line load and a cavity or irregularity of infinite length in the out of plane direction) cannot reproduce well the experimental data obtained for a three dimensional condition. It predicts however with a relatively good degree of accuracy (considering the uncertainties in the material properties) the occurrence of clear amplifications at the "P-wave frequencies".

A bigger hammer was used to generate lower range frequencies at the location E2 above the void and at the location A4 above the debonded area shown in Fig. 5.6. A geophone placed around 3 inches from the loading point was used as a receiver to obtain the velocity histories. From the velocity histories the displacement amplitudes in the frequency domain shown in Fig. 5.11a were obtained using the FFT and dividing by circular frequency, $\Omega$. A "flexural peak" occurs experimentally at a frequency of 155 Hz, while the analytical results display a somewhat broader peak at 200 Hz in Fig. 5.11b. Since the waves generated are within the low frequency range and have therefore long wavelengths relative to the size of void, the results may be affected by the location of the void with respect to the edge which is not taken into consideration in the analytical results shown in Fig. 5.11b. To investigate the potential importance of this effect an extreme case with a void at the pavement edge was considered. The results are shown in Fig. 5.12b. Because of the two dimensional nature of the model when the void is located at an edge without lateral support the

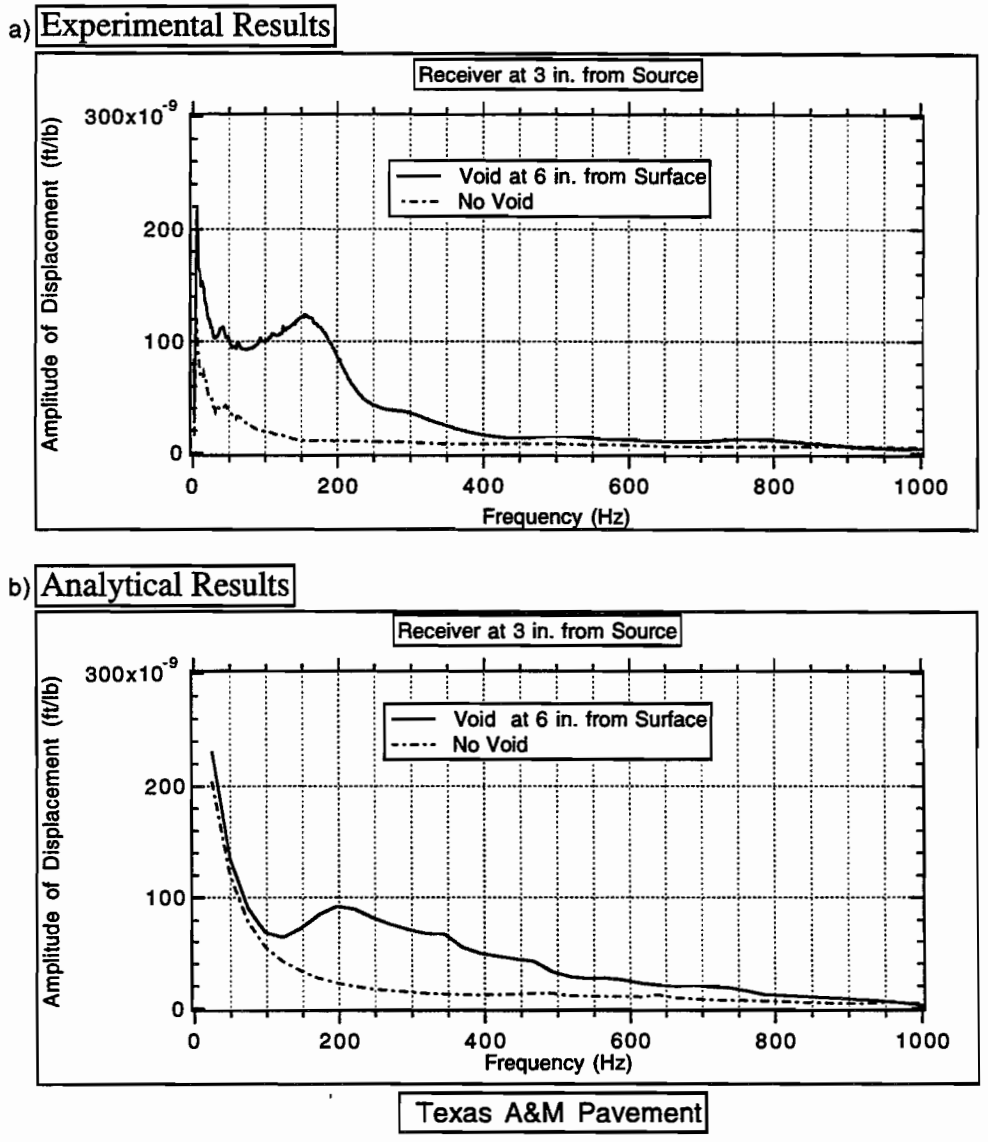


Fig. 5.11 Comparison of Experimental and Analytical Results Using Impulse-Response Technique

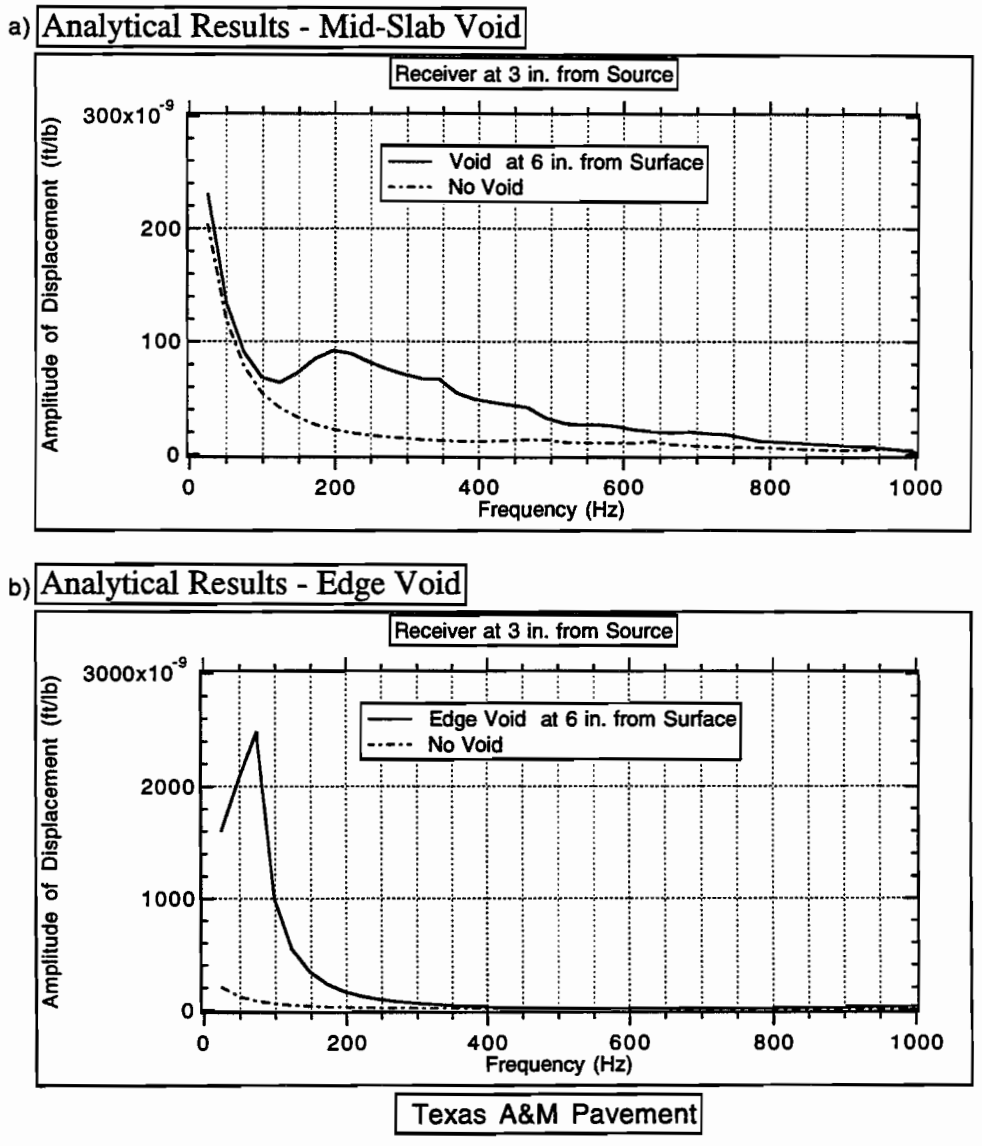


Fig. 5.12 Effect of the Edge Void on the "Flexural Peak"

displacement amplitudes increase considerably. The important feature of these results is, however, the shift in the frequency at which the peak occurs. The peak frequency which was originally 200 Hz, with the void in the middle of the slab, becomes of the order of 70 Hz with the void at the edge. This helps to explain the difference between the analytical and experimental results although it is not possible with the 2D model to produce exactly the conditions of the experiment.

### 5.3.2 ECJ Concrete Slab

The spectral-analysis-of-surface-wave (SASW) method utilizes the dispersive nature of Rayleigh waves to measure the shear stiffness of a medium. The dispersion of Rayleigh waves implies that surface waves with different frequencies or wavelengths propagate with different velocities in a layered medium. For a homogeneous medium, the phase velocity should be nearly constant with wavelength. The concrete slab of Fig. 5.13 with a 2-inch square void was tested in the ECJ building of the University of Texas at Austin.

An instrumented hammer and two accelerometers were used in the experiment. The acceleration histories from the two receivers were transformed into frequency domain using the FFT and the phase differences were calculated. The phase differences after applying an exponential window function to eliminate noise were shown in Fig. 5.14. The phase velocity shows an average value of 7200 ft/sec over the depth (or wavelength of surface wave) for the intact concrete.

In the analytical work the shear wave and P-wave velocities of the concrete slab were assumed to be 8500 and 13880 ft/sec respectively. Poisson's

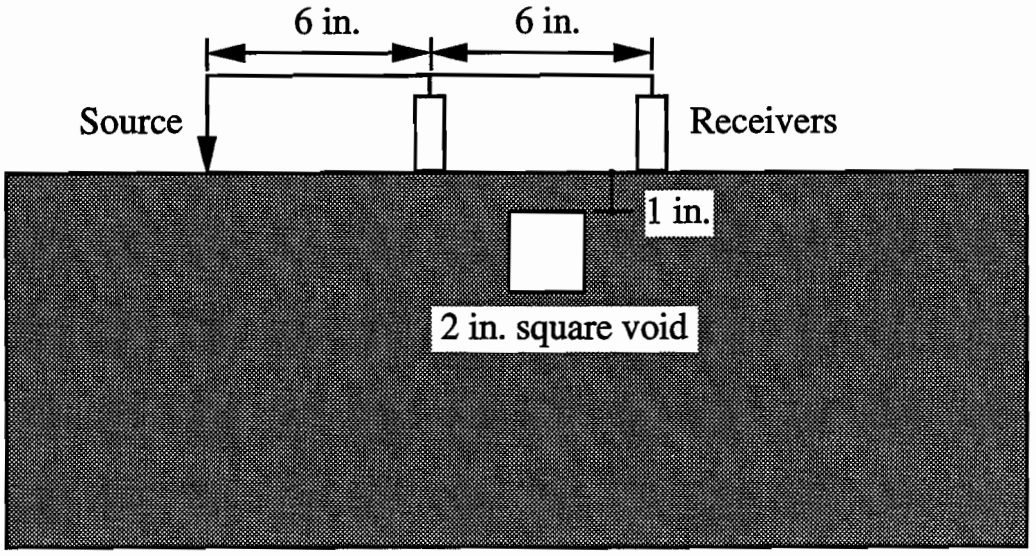


$V_s$ = 8500 ft/sec

$V_p$ = 13880 ft/sec

$\upsilon$ = 0.2

$\gamma$ = 145 lb/ft$^3$

D = 0.3 %

Fig. 5.13 Typical SASW Testing for Detection of Void in the ECJ Concrete Slab

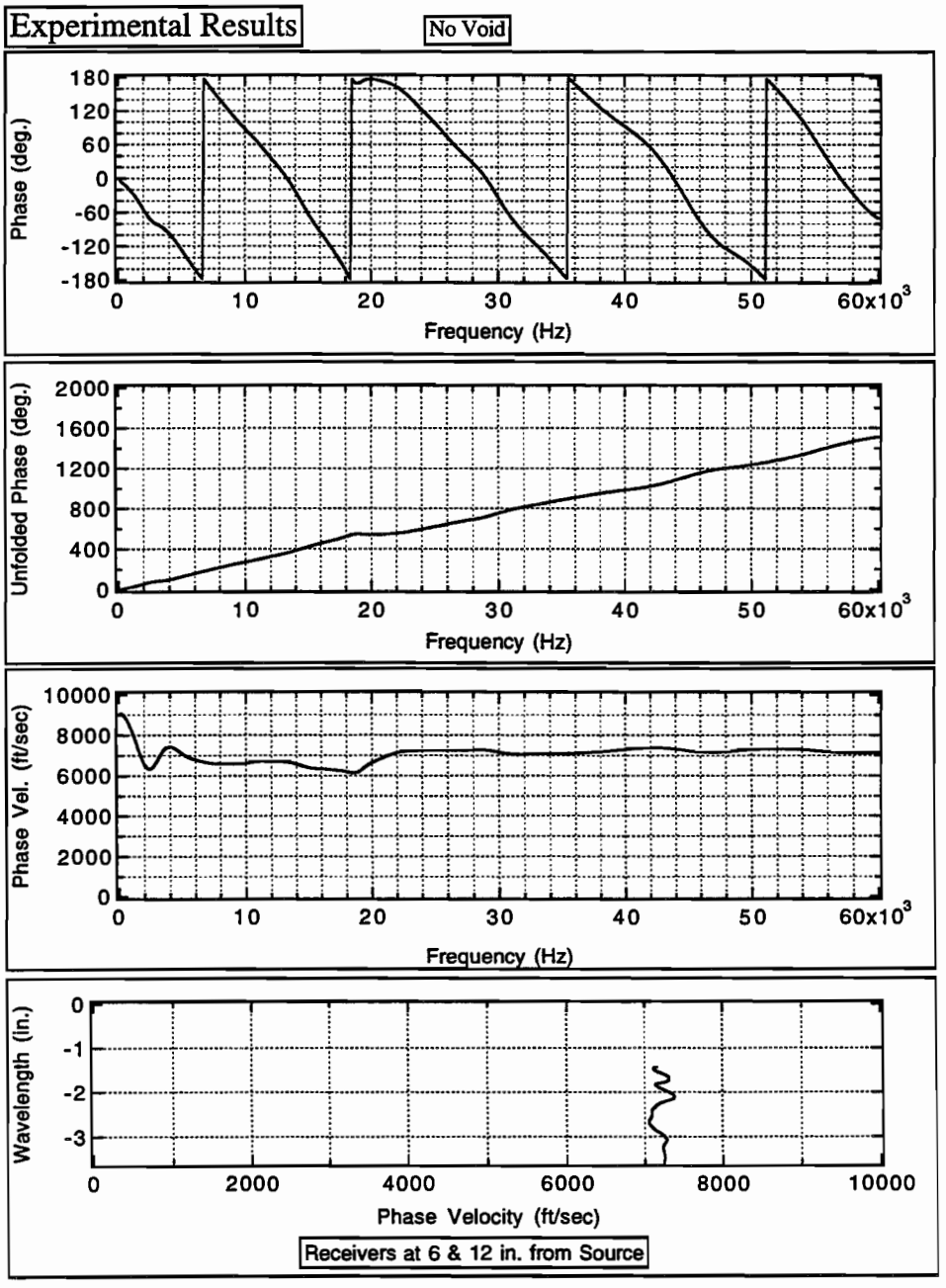


Fig. 5.14 Phase and Phase Velocity of Intact Concrete Slab in the Experimental Results

ratio was assumed to be 0.2 and the unit weight 145 lb/ft$^3$. Damping was assumed to be 0.3%. A receiver spacing of 6 inches and a duration of 1/40000 sec for the impulse load were selected. For the intact concrete the average computed phase velocity is around 7700 ft/sec as shown in Fig. 5.15. This suggests that the shear-wave velocity of the concrete layer is actually lower than 8500 ft/sec.

The first case studied had the void located right below the second receiver. A sharp peak appears at a frequency of 20.3 kHz in the phase diagram of the experimental results. The phase velocity decreases from 7000 to 6600 ft/sec with depth as shown in Fig. 5.16. Similar trends (decreasing phase velocity with depth and smaller phase velocities than those of intact concrete) were obtained in the analytical results shown in Fig. 5.17. The analytical phase velocities decrease from 7400 to 6700 ft/sec with depth.

The second case studied had the void located between the two receivers. The phase velocity of the experimental results, shown in Fig. 5.18, are lower and decrease more with depth than the phase velocities of the first case. The analytical results show a similar trend (Fig. 5.19).

The third case had the void located between the source and the first receiver. A small peak appears at a frequency of 36.4 kHz in the phase diagram of the experimental results. The experimental phase velocities are generally higher than the phase velocity of the intact concrete but still decrease with depth as shown in Fig. 5.20. On the other hand, the analytical results shown in Fig. 5.21 using the same material properties as in the other cases indicate the average value of the phase velocity almost identical to the phase velocity of the intact concrete, 7700 ft/sec.

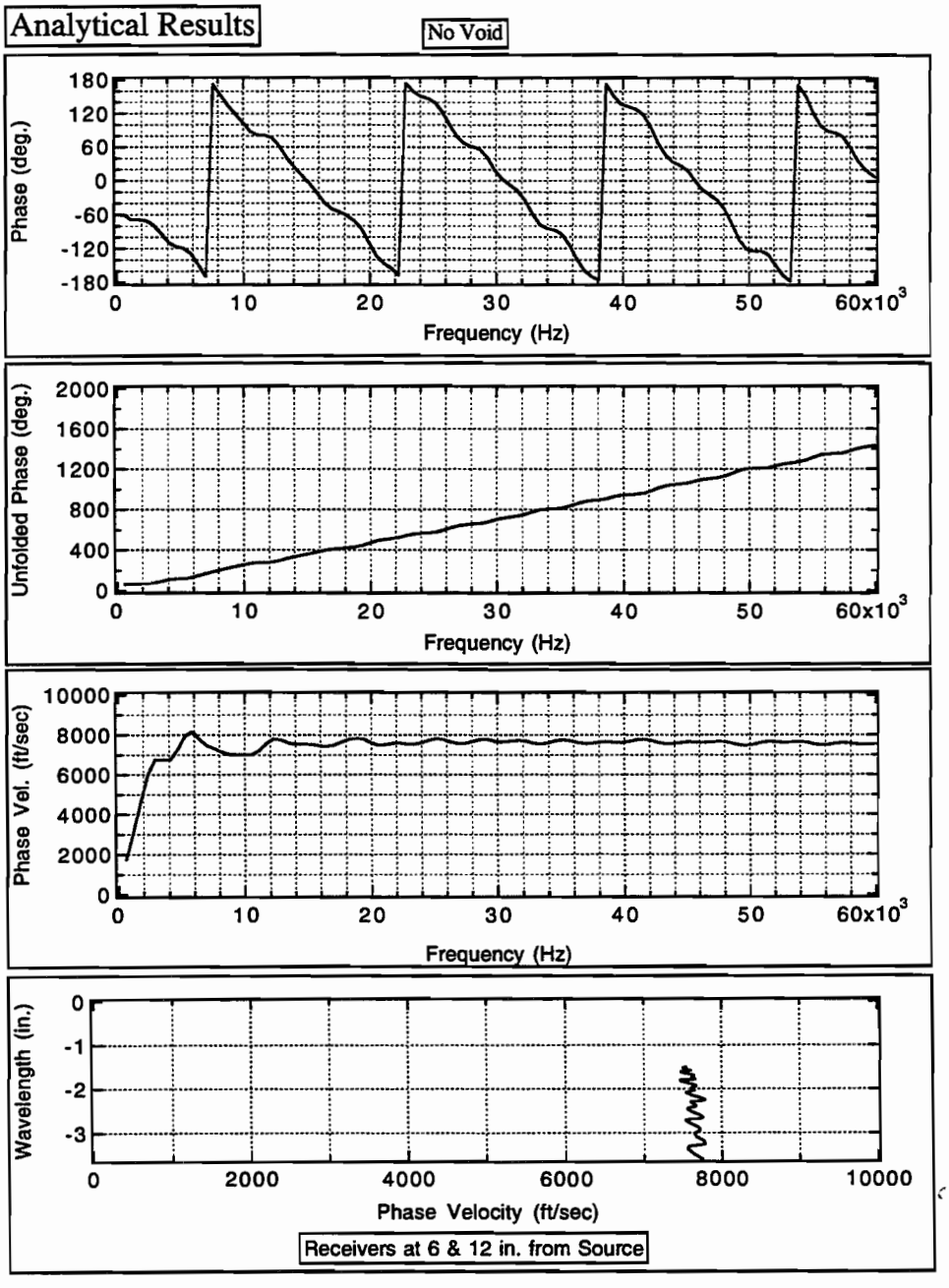


Fig. 5.15 Phase and Phase Velocity of Intact Concrete Slab in the Analytical Results

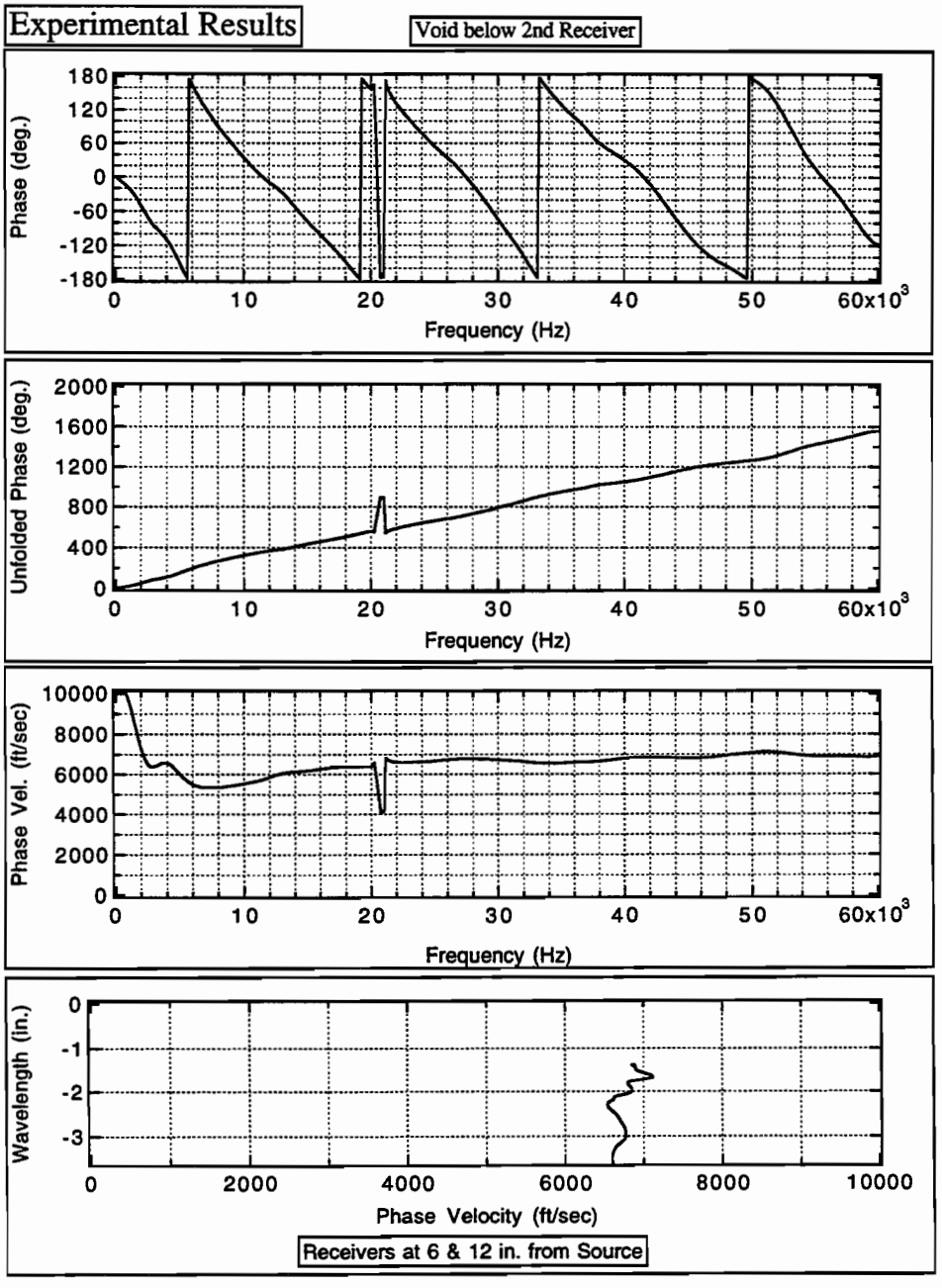


Fig. 5.16 Experimental Results of ECJ Concrete Slab with a Void below Second Receiver

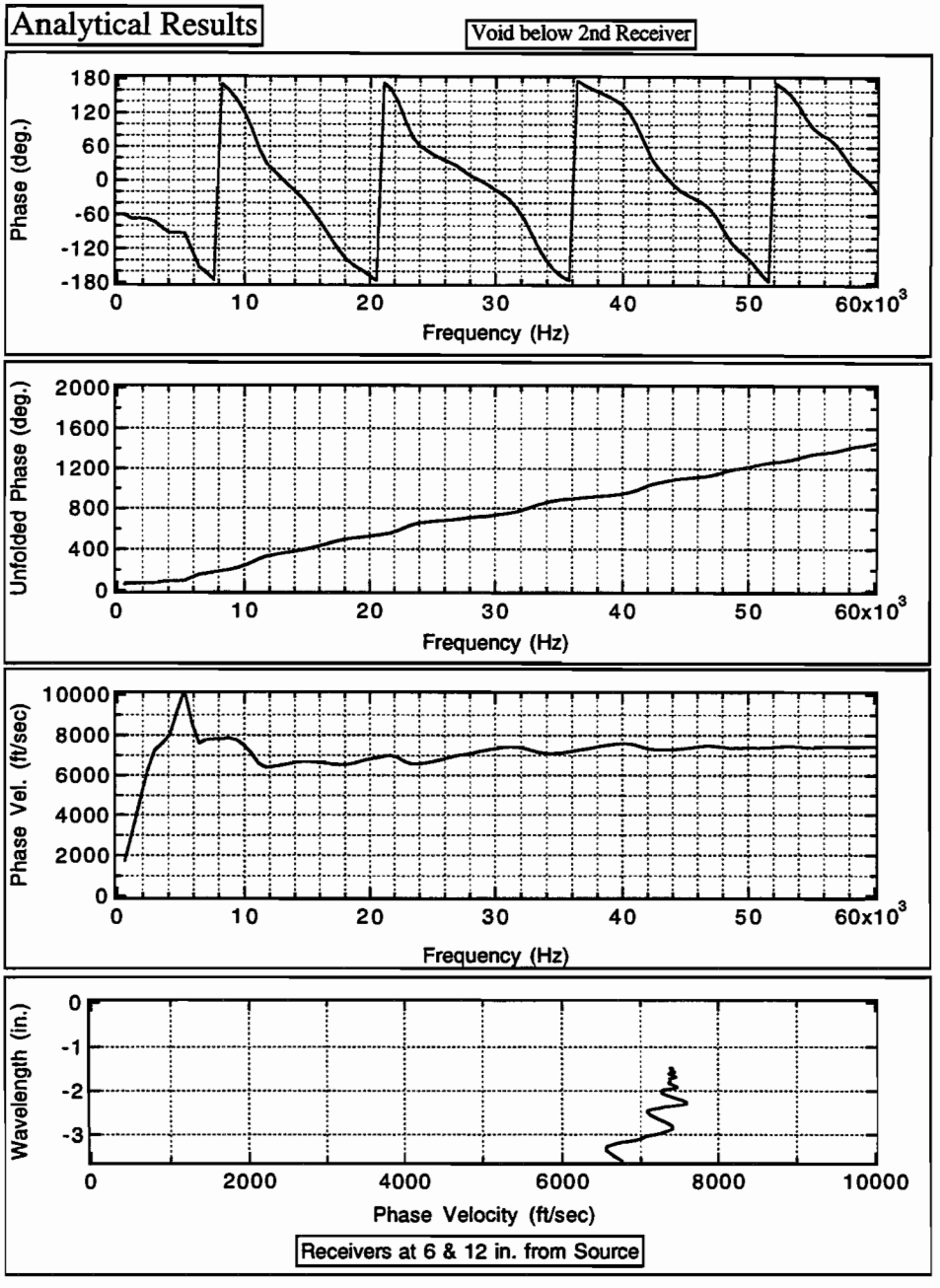


Fig. 5.17 Analytical Results of ECJ Concrete Slab with a Void below Second Receiver

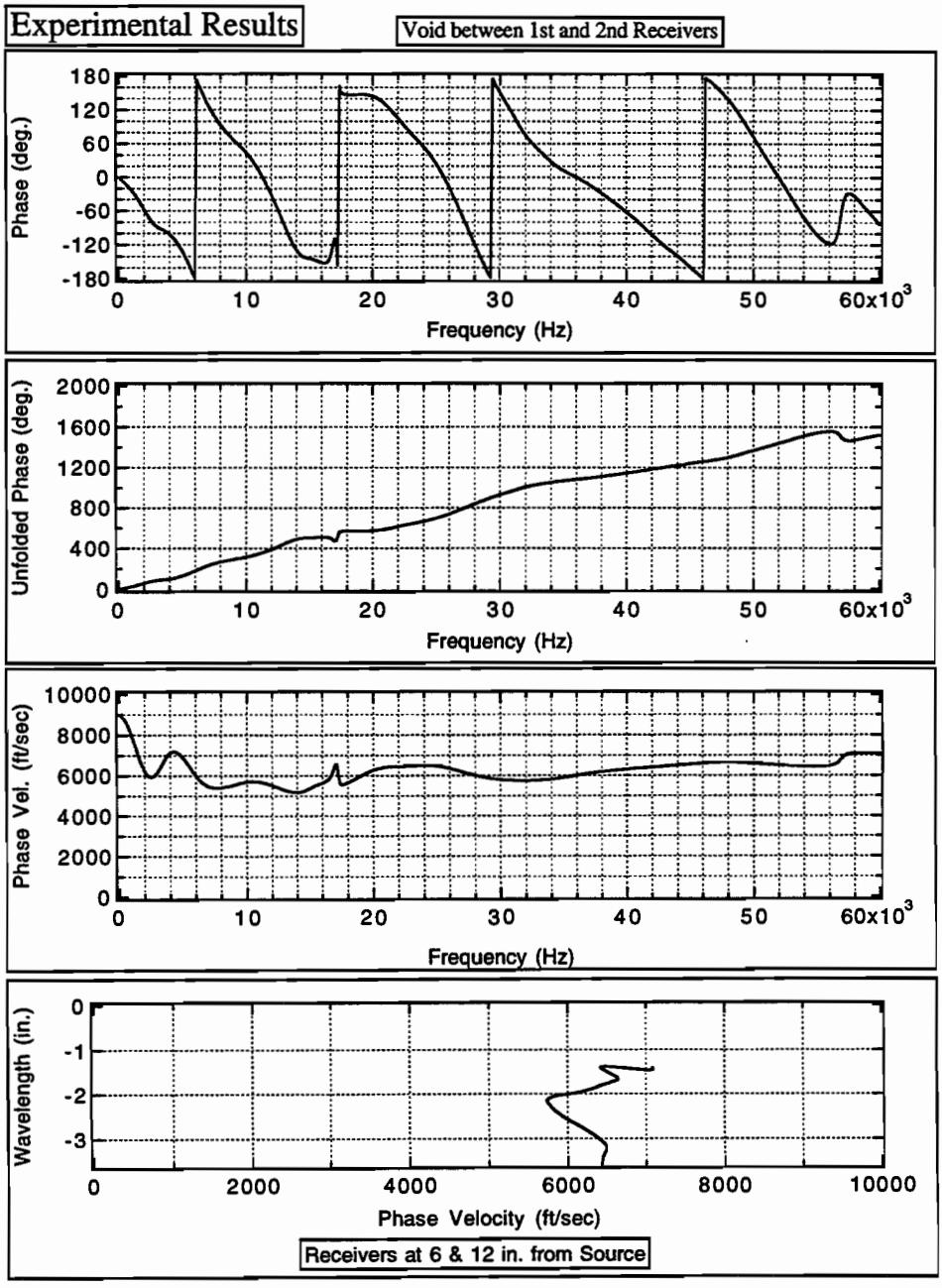


Fig. 5.18 Experimental Results of ECJ Concrete Slab with a Void between the Two Receivers

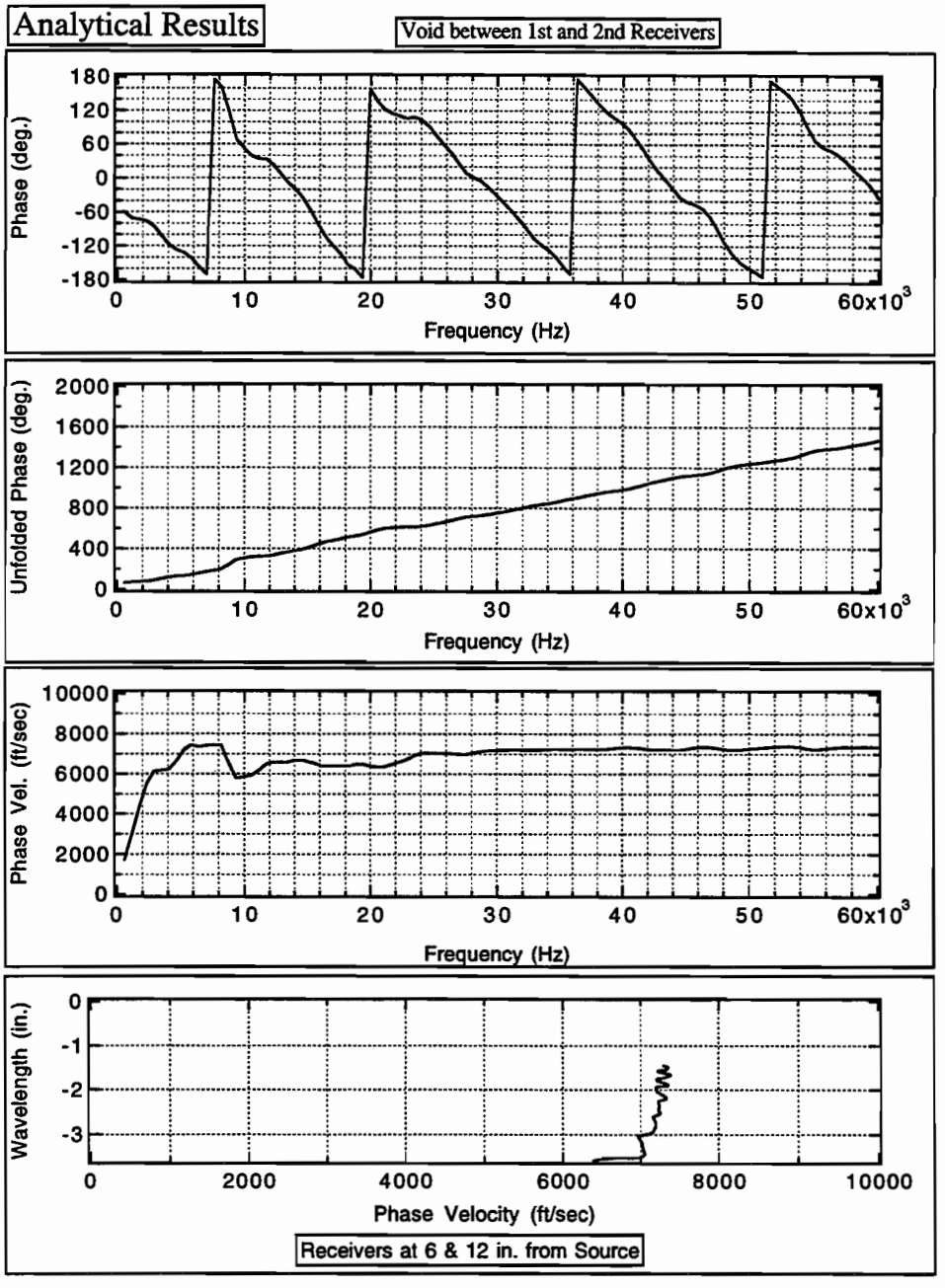


Fig. 5.19 Analytical Results of ECJ Concrete Slab with a Void between the Two Receivers

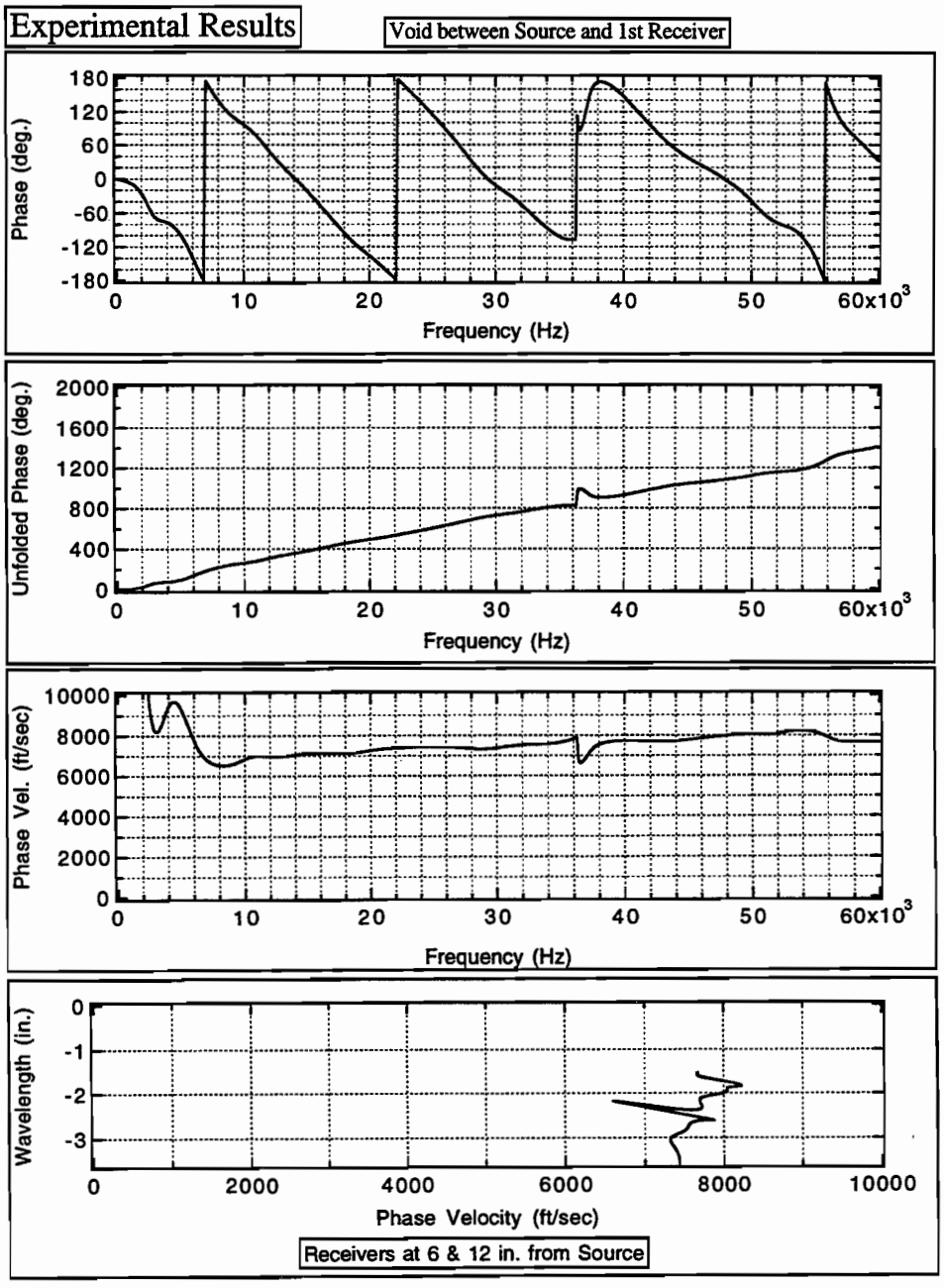


Fig. 5.20 Experimental Results of ECJ Concrete Slab with a Void between the Source and the First Receiver

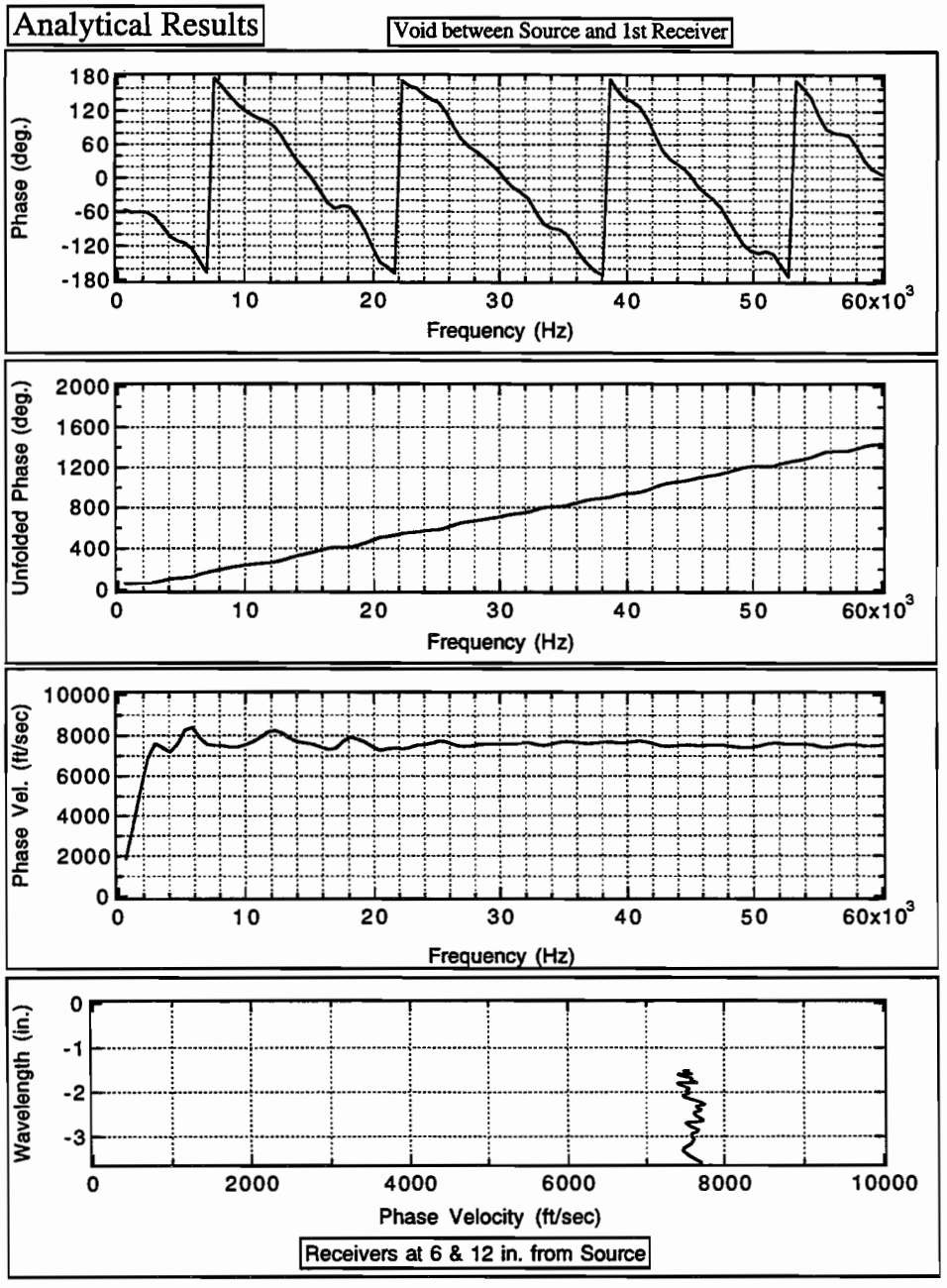


Fig. 5.21 Analytical Results of ECJ Concrete Slab with a Void between the Source and the First Receiver

The largest effect of the void takes place when the void is in-between the two receivers. The reduction of the average velocity indicates that the void lowers the average stiffness of the material between the two receivers.

## 5.4 SUMMARY

The results of displacement histories and displacement amplitudes are almost identical for voids and delaminations with the same length when the depth from the surface to the top face of the void or the delamination is the same. The thickness of the void has little effect on the "P-wave peak-frequency" and the "flexural peak-frequency".

Agreement between the experimental and analytical results is relatively good in predicting the "P-wave peak" and the "flexural peak" frequencies but the 2D model cannot reproduce exactly the results of 3D experiments.

Both the experimental and analytical results show similar trends (reduction of the phase velocity with depth due to the existence of the void) using the spectral-analysis-of-surface-wave technique. There is a potential to identify the thickness of the voids by using this method.

# CHAPTER SIX

# EFFECTS OF VERTICAL CRACKS

## 6.1 INTRODUCTION

Vertical cracks are the most common defects in pavement systems. Some cracks are surface-piercing, visible on the surface. Other are below the surface and can not be seen from the surface. It would be very useful to find a possible way to determine their existence and the depth at which they are located so that a remedy can be applied before the subsurface crack extends to the surface. To investigate the possibility of achieving this goal, a source and two receivers were used to study the phase difference between the two receivers, the absolute phase and the displacement amplitude at each receiver. Three cases were considered for the crack location: crack outside the source-receiver system, crack between the two receivers, and crack between the source and the first receiver. The crack depths were 3, 4.5, and 6 inches (some cases extended to 8 and 10 inches) for surface-piercing cracks, and from 2 to 10 and 4 to 10 inches below the surface for subsurface cracks.

The displacement amplitudes of the receiver responses in the frequency domain were next analyzed as a source with one receiver moves across a vertical subsurface crack in order to estimate its depth and location.

## 6.2 SOURCE WITH TWO RECEIVERS

The pavement system shown in Fig. 6.1, was used for the studies of vertical cracks presented in this chapter. It consists of a surface layer of 10-inch thick concrete over a second layer of asphalt concrete with a thickness of 6 inches. The subbase is 12 inches thick. The shear wave velocities of the materials are 8500, 3000, 1000, and 500 ft/sec from top to bottom. Poisson's ratios were assumed to be 0.2, 0.27, 0.25, and 0.33 respectively and the unit weights are 145, 145, 125, and 110 lb/ft$^3$. A value of hysteretic damping of 0.3% was considered for the concrete layer and 2% for the other layers. Since two dimensional plane-strain elements were used, the vertical crack was a plane perpendicular to the plane analyzed. The plane of line loading is parallel to the plane of the vertical crack.

The source is 6 inches to the left of the first receiver and the spacing between receivers is also 6 inches as shown in Fig. 6.1. A triangular load with an impulse duration of 1/40000 seconds was used in the time domain FEM analyses. The phases and steady state amplitudes of displacement were obtained after the FFT was applied to the displacement histories.

### 6.2.1 Crack Outside Source-Receiver System

When the source-receiver system is on one side of the crack in the pavement shown in Fig. 6.1, the phase cycles and the phase velocities are very similar for pavements with various depths of crack and for intact pavements. For some cases, there are a few jumps or fluctuations caused by wave reflections

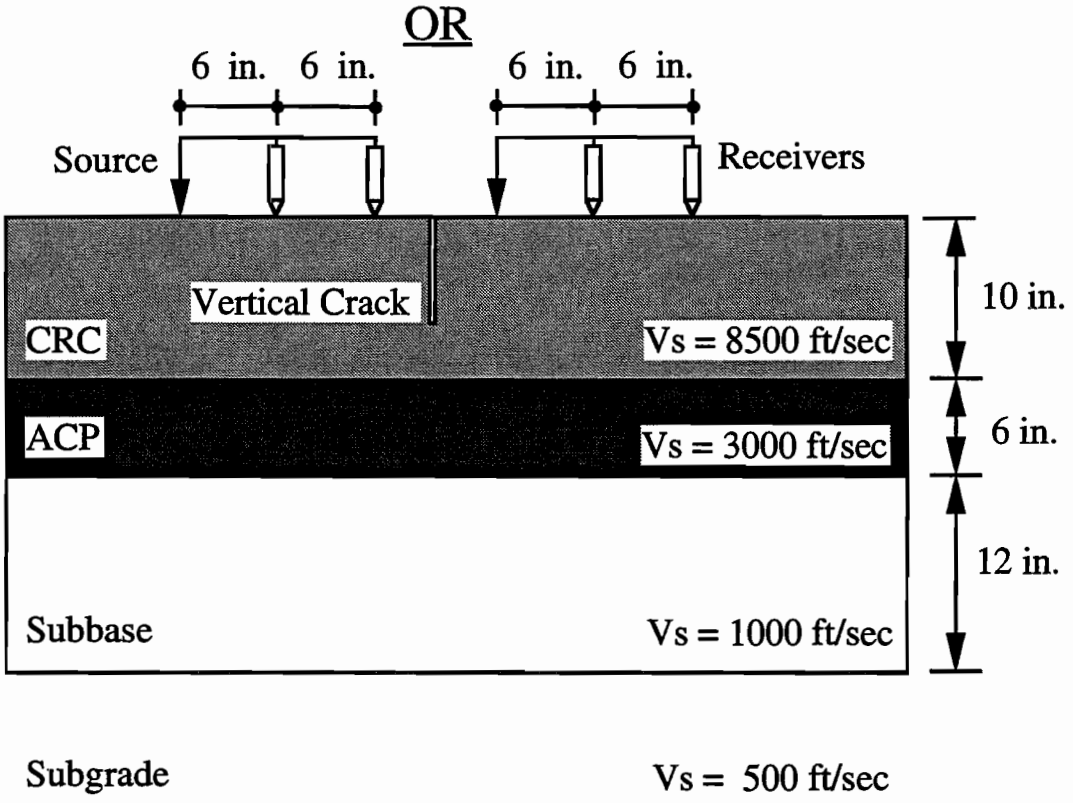


Fig. 6.1 Simulation of SASW Testing with Two Receivers on a Pavement with a Vertical Crack outside the Source-Receiver System

generated by the vertical crack. One example presented here is when the crack is located at 6 inches left of the source. The phase difference between the two receivers for pavements with 3-inch, 4.5-inch, and 6-inch deep crack, are shown in Fig. 6.2. There is a spike around 6.5 kHz for each case which is probably due to a wave reflection.

### 6.2.2 Crack Between Two Receivers

A pavement with a vertical crack located between the two receivers, as shown in Fig. 6.3, was investigated next. One example is when the crack is located in the middle of two receivers. The phase diagrams for pavements with 3-inch, 4.5-inch, 6-inch, 8-inch and 10-inch deep cracks are shown in Fig. 6.4 initially. It is very hard to interpret the phase cycles to obtain the phase velocities. It is interesting however to notice that there is a change in the slope of the phase, which has been observed in the field tests, in the results for a pavement with 10-inch deep crack. In order to better understand this phenomenon the absolute phase of each receiver and the phase difference between these two receivers are shown in Fig. 6.5. Since the first receiver and the source are on the same side of the crack, the phase of the first receiver is only slightly affected by the reflection of waves from the vertical crack. On the other hand, most of the waves propagating from the source are blocked by the 10-inch vertical crack from the second receiver so that the phase angle at the second receiver does not exhibit clear cycles and stays within a small range of values for the various frequencies. The effects of a 10-inch vertical crack on the displacement amplitudes as a

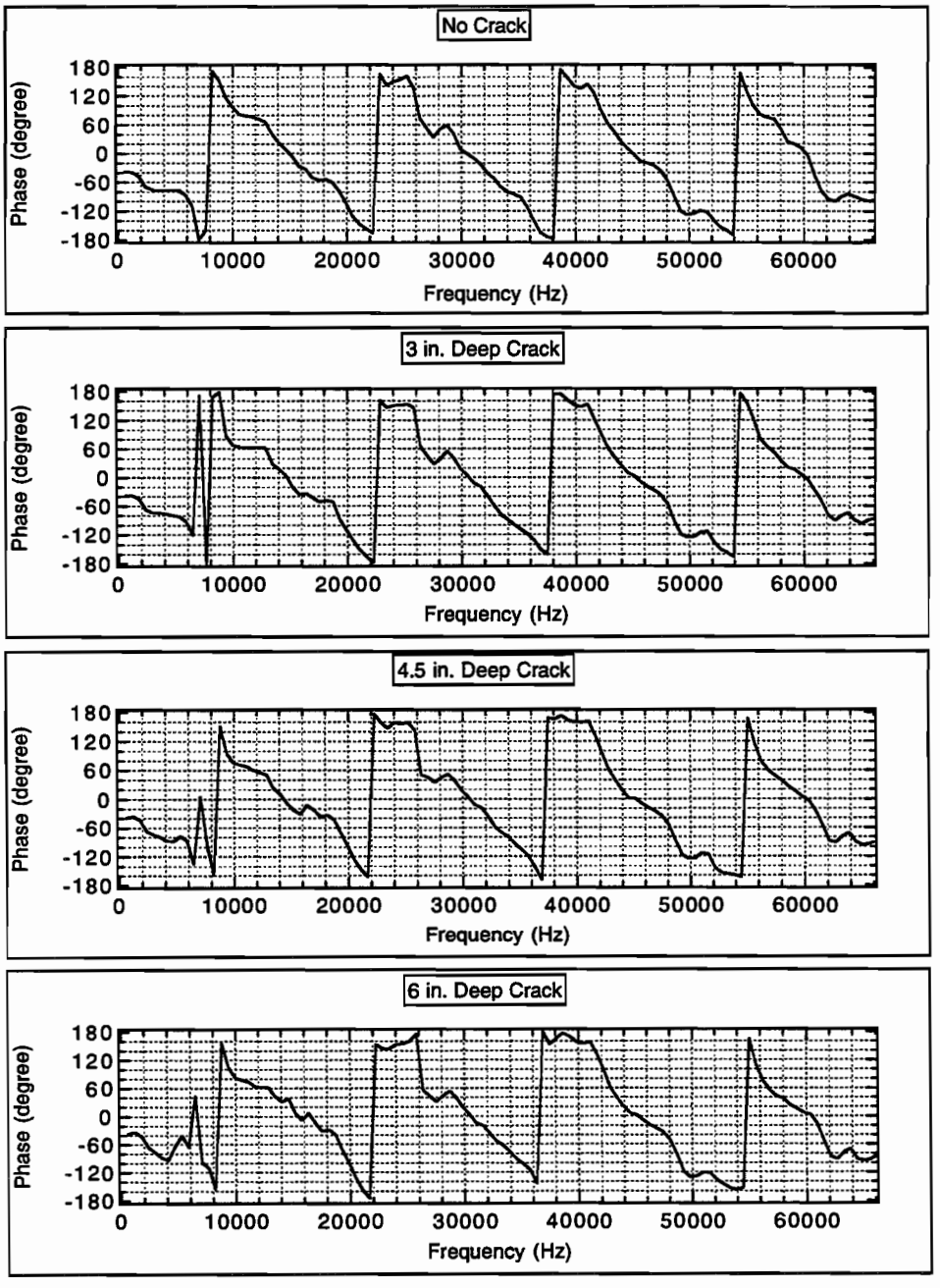


Fig. 6.2 Effect of the Depth of Vertical Cracks, at 6 inches to the Left of Source, on the Phases

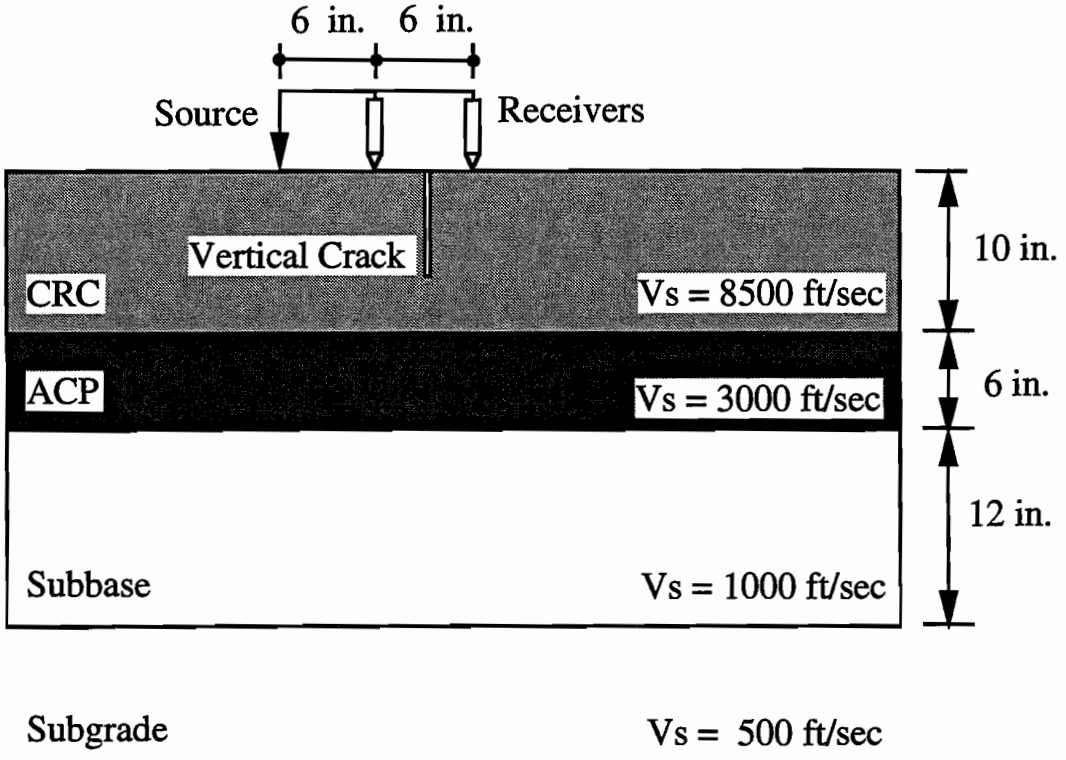


Fig. 6.3 Simulation of SASW Testing with Two Receivers on a Pavement with a Vertical Crack Located between the Two Receivers

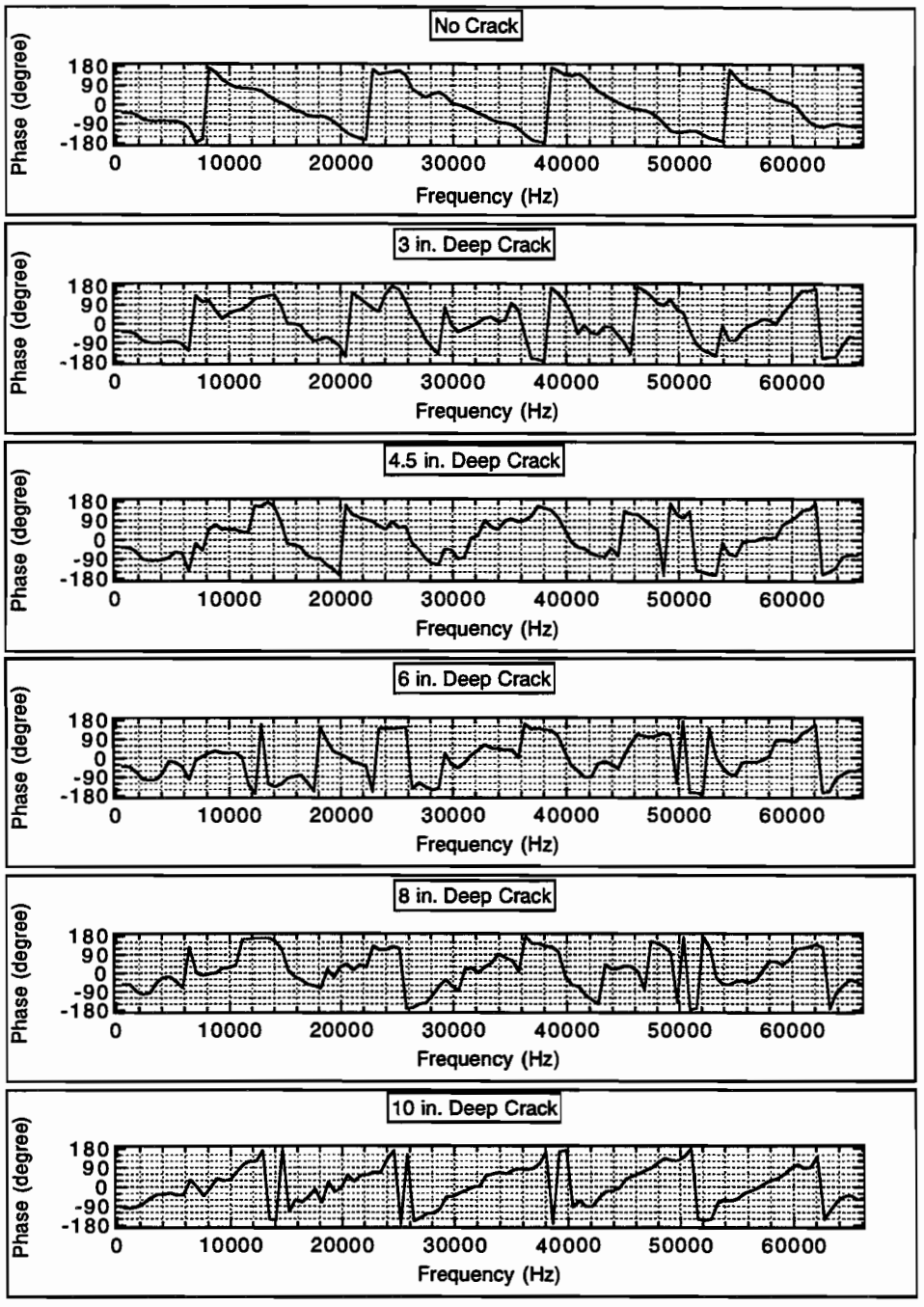


Fig. 6.4 Effect of the Depth of Vertical Cracks, in the Middle of the First and Second Receivers, on the Phases

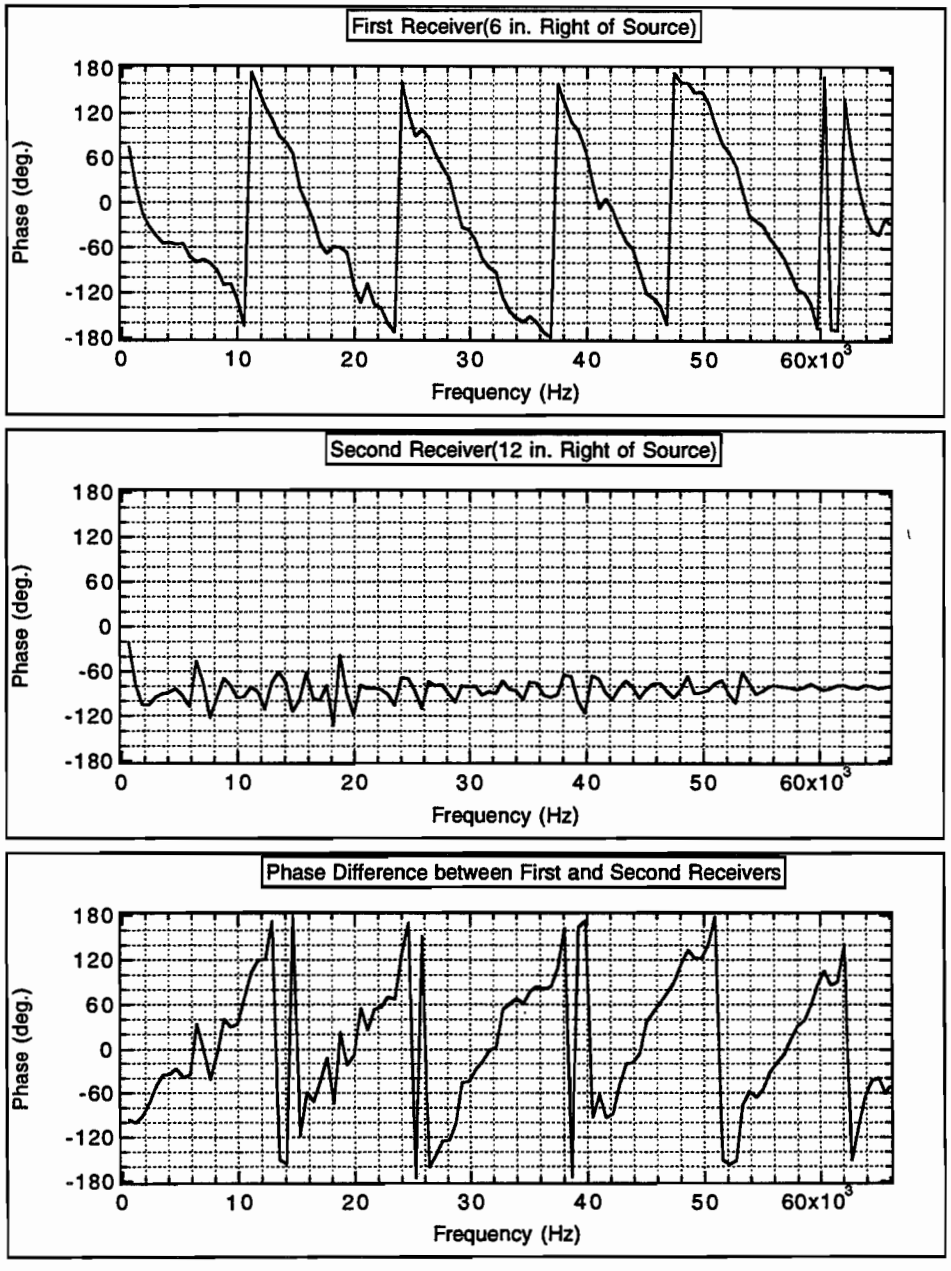


Fig. 6.5 Phase of Each Receiver and Phase Difference between the Two Receivers As 10-inch Vertical Cracks is in the Middle of the Two Receivers

function of frequency are shown in Fig. 6.6. The displacement amplitudes at the second receiver above 8 kHz are greatly reduced by the 10-inch crack. In the case of a 3-inch crack the amplitudes at the second receiver above 8.5 kHz (Fig. 6.7) are not reduced as much as in the case of a 10-inch crack, but they are still much smaller than the response of the intact pavement and the effect is clearly observed.

If the crack moves to the right so that the second receiver is just past the crack, the phase diagrams (shown in Fig. 6.8) exhibit more cycles than those of intact pavements. The number of cycles over the frequency range considered seems to increase as the depth of the crack increase from 3 to 6 inches. For the 10-inch crack, however, one sees still a phase diagram with reverse slope as in the case where the crack was at the midpoint between receivers. The phase velocities calculated from the phase diagrams for the crack depths from 3 to 6 inches are shown in Fig. 6.9. There is a clear decrease in velocity above 10 kHz between an intact pavement and a pavement with a vertical crack, but the effect of crack depth is small. For the 8-inch and 10-inch cracks it is very hard to identify the cycles, and obtain phase velocities as was the case previously.

### 6.2.3 Crack Between Source And First Receiver

When the vertical crack is between the source and the first receiver (Fig. 6.10), the phase diagrams for pavements with various crack depths are shown in Fig. 6.11. The phase cycles for a 3-inch crack are irregular particular for high frequencies. As the crack depth increases the waves are again blocked from the two receivers. In this example the phase diagrams obtained in a pavement with a

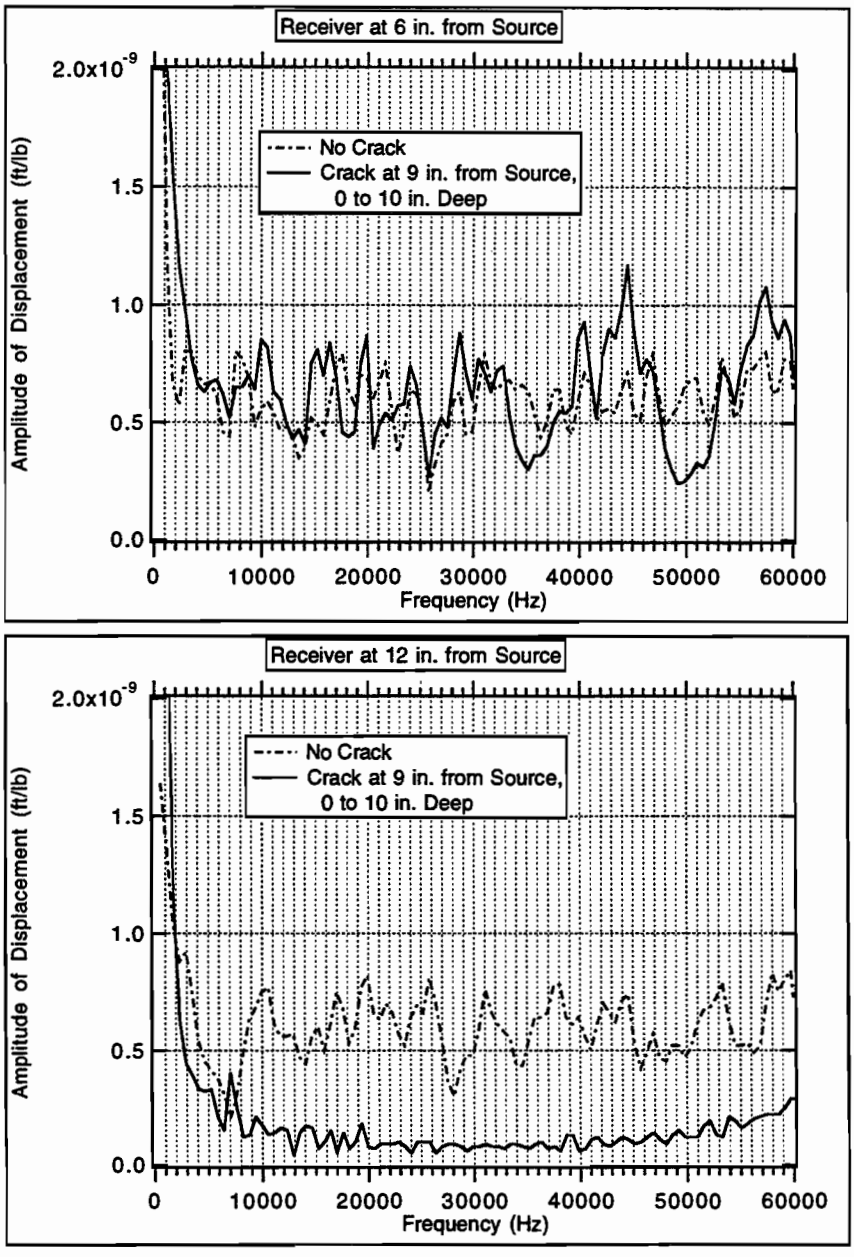


Fig. 6.6 Effect of 10-inch Vertical Cracks, in the Middle of the First and Second Receivers, on the Displacement Amplitudes

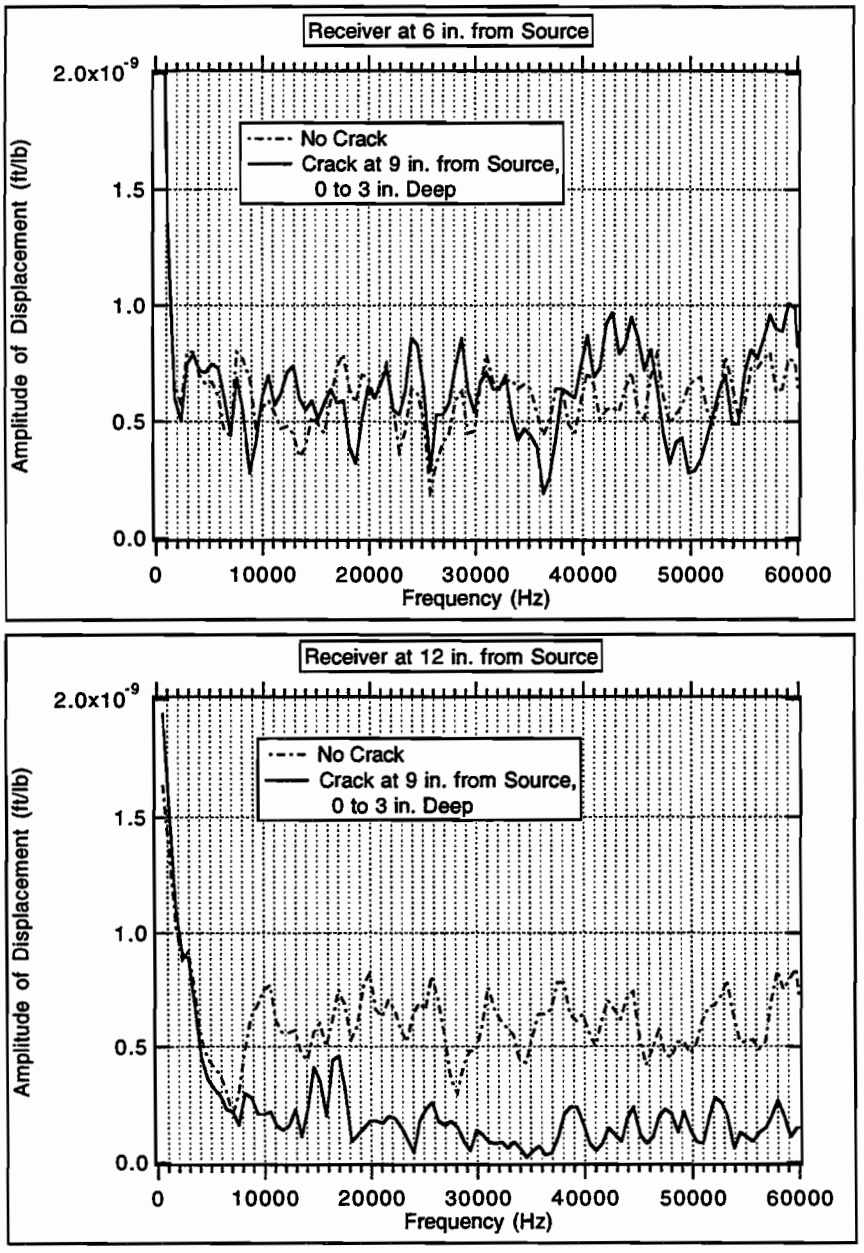


Fig. 6.7 Effect of 3-inch Vertical Cracks, in the Middle of the First and Second Receivers, on the Displacement Amplitudes

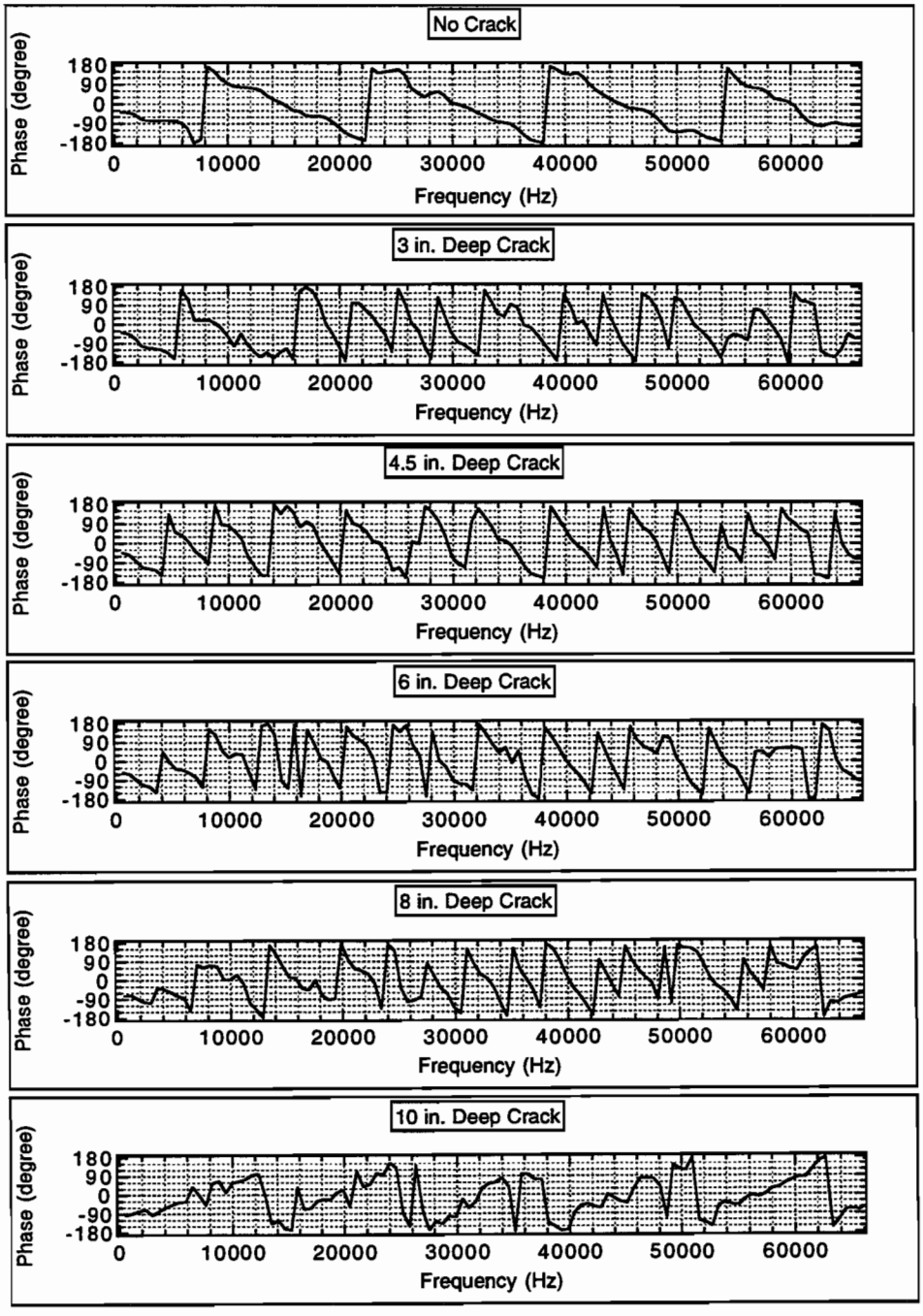


Fig. 6.8 Effect of the Depth of Vertical Cracks, just to the left of the Second Receiver, on the Phases

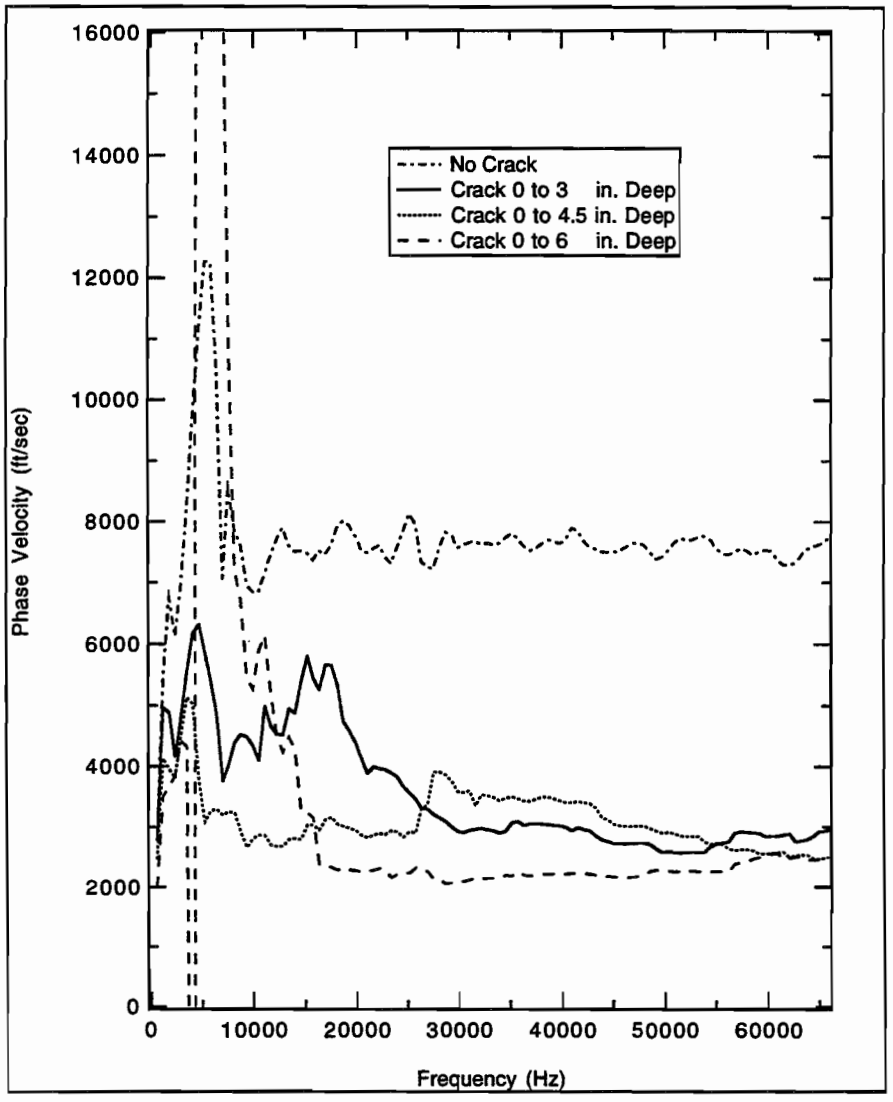


Fig. 6.9 Effect of the Depth of Vertical Cracks, just to the left of the Second Receiver, on the Phase Velocities

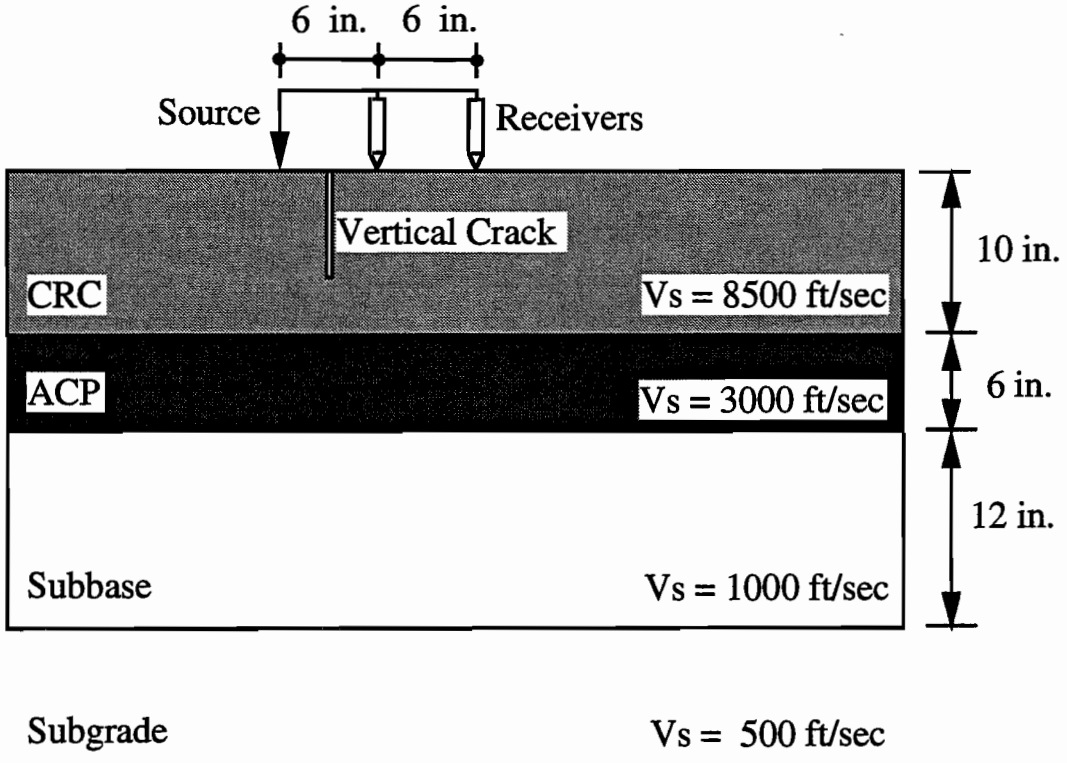


Fig. 6.10 Simulation of SASW Testing with Two Receivers on a Pavement with a Vertical Crack Located between the Source and the First Receiver

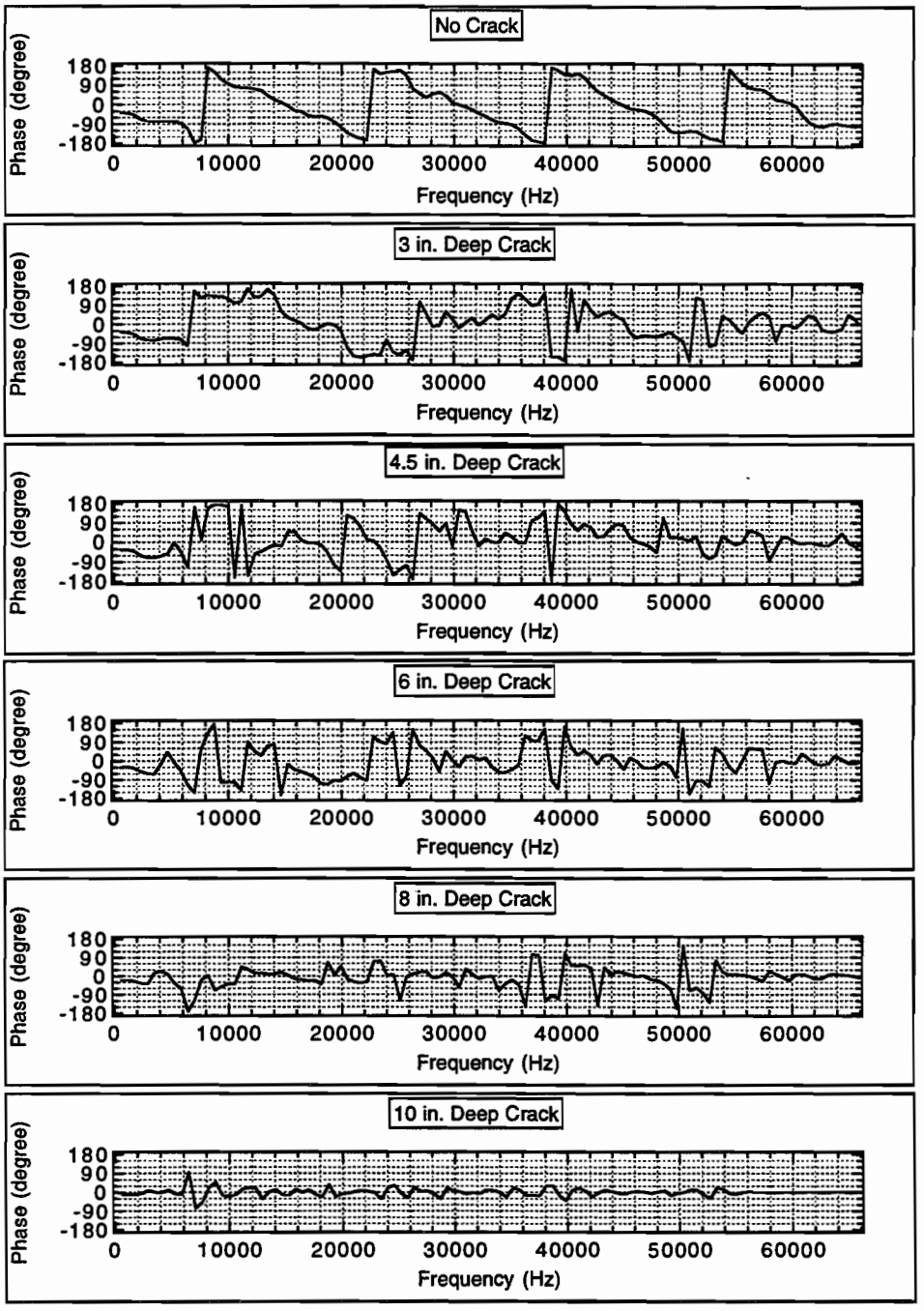


Fig. 6.11 Effect of the Depth of Vertical Cracks, in the Middle of the Source and the First Receiver, on the Phases

10-inch crack lose almost entirely the response over the complete frequency range. The absolute phases of both receivers, shown in Fig. 6.12, are similar to the phase difference between these two receivers. The effects of 10-inch vertical crack on the displacement amplitudes for the different frequencies are shown in Fig. 6.13. The displacement amplitudes of both receivers above 8.5 kHz are greatly reduced by the 10-inch crack. The amplitudes above 8.5 kHz for the 3-inch crack are shown in Fig. 6.14. Although the reduction is not as large as for the 10-inch crack, it is still quite pronounced.

### 6.2.4 Subsurface Cracks

Since subsurface cracks can not be seen from the surface, it is particularly useful to find a method to locate them from surface observations. To investigate the possibility of detecting subsurface cracks their effect on the phases of the motions at the two receivers were studied.

Vertical cracks starting 10 inches below the surface of the pavement and extending upwards for 6 and 8 inches were considered. The case where the cracks are located at the midpoint between the two receivers, as indicated in Fig. 6.15 was studied first. Figure 6.16 shows the phase diagrams, representing the phase difference between the motions at the two receivers, for an intact pavement, the pavement with the 6-inch crack, which extends up to a depth of 4 inches, and the pavement with the 8-inch crack (extending up to a depth of 2 inches). The three diagrams are very similar. The results for the 8-inch crack shows a very marked oscillation at a frequency of approximately 26 kHz. It should be noticed,

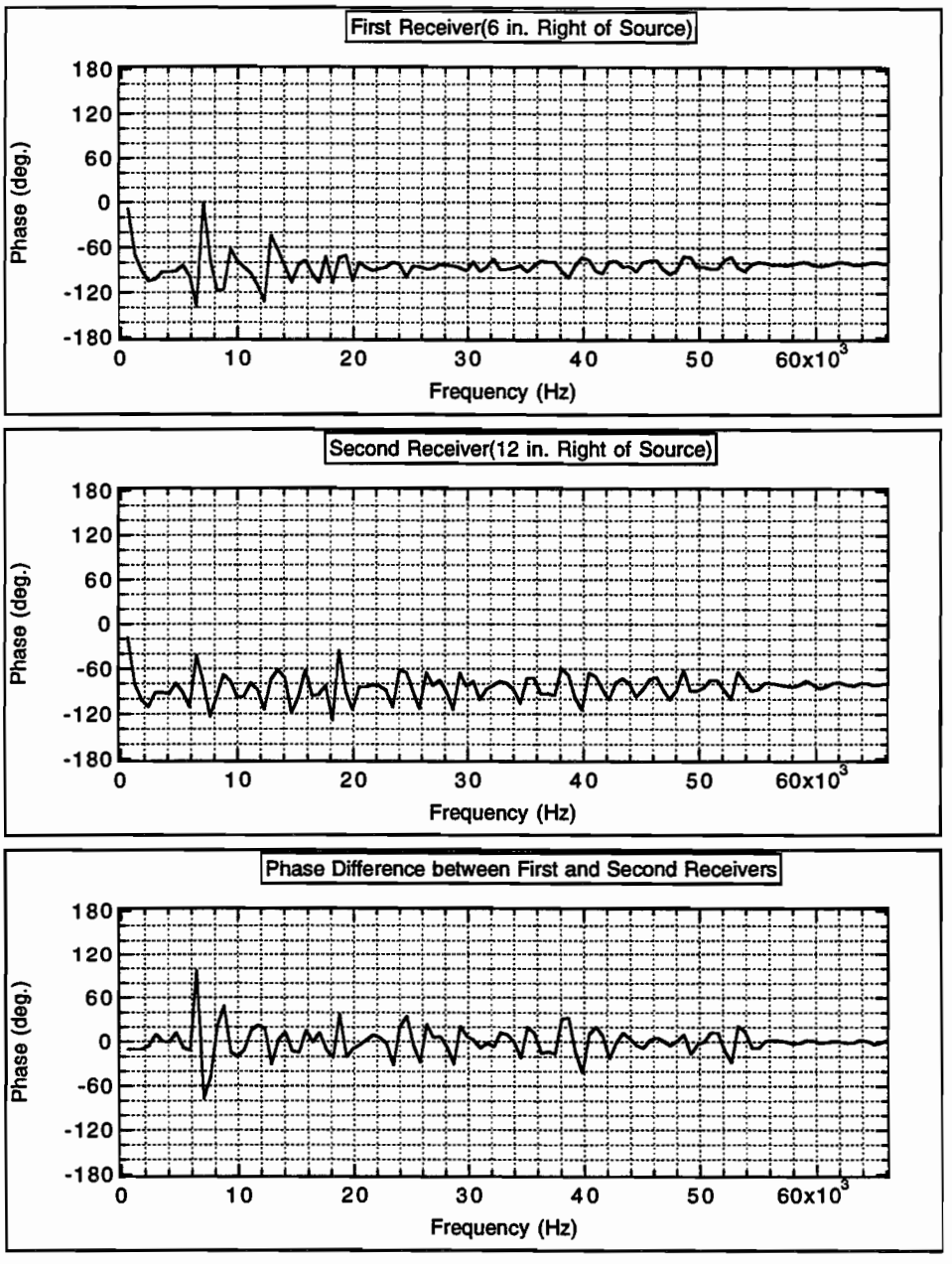


Fig. 6.12 Phase of Each Receiver and Phase Difference between the Two Receivers As 10-inch Vertical Cracks is in the Middle of the Source and the First Receiver

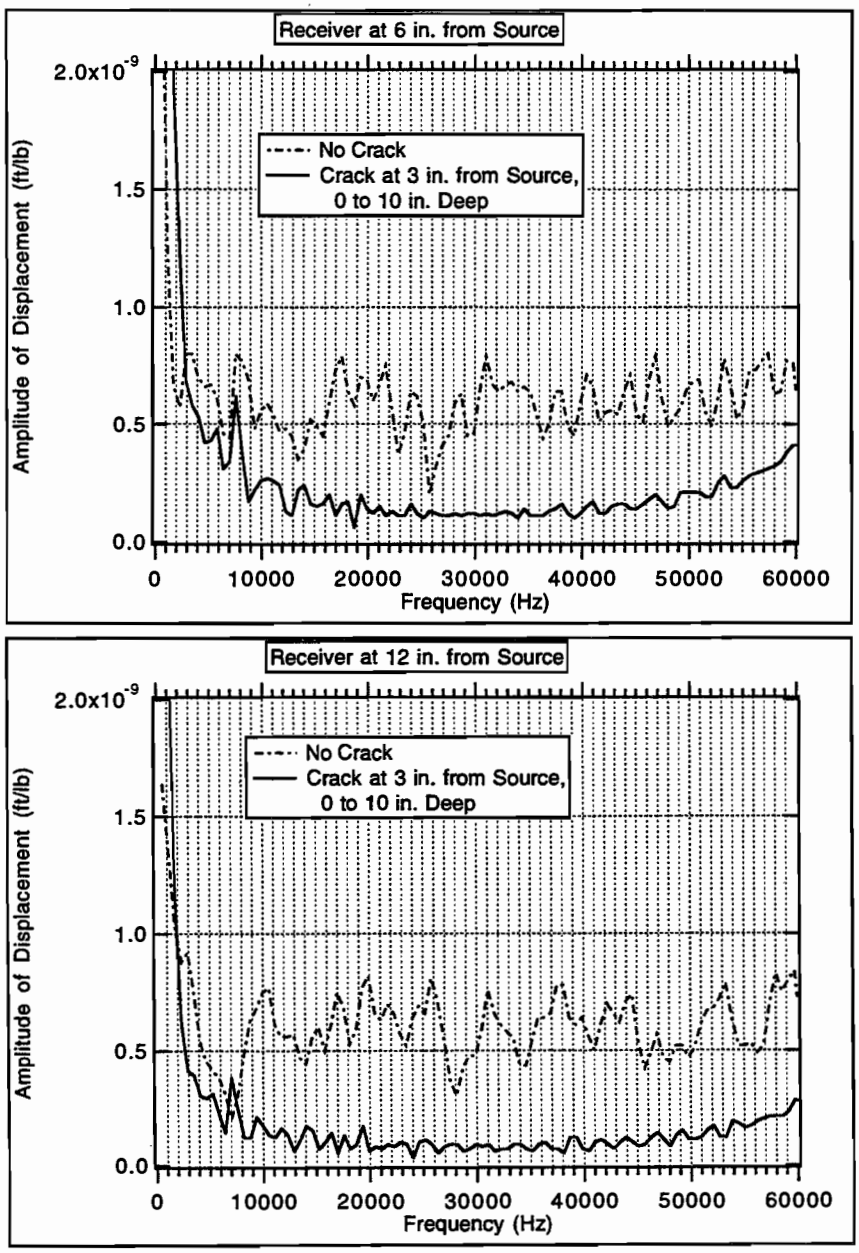


Fig. 6.13 Effect of 10-inch Vertical Cracks, in the Middle of the Source and the First Receiver, on the Displacement Amplitudes

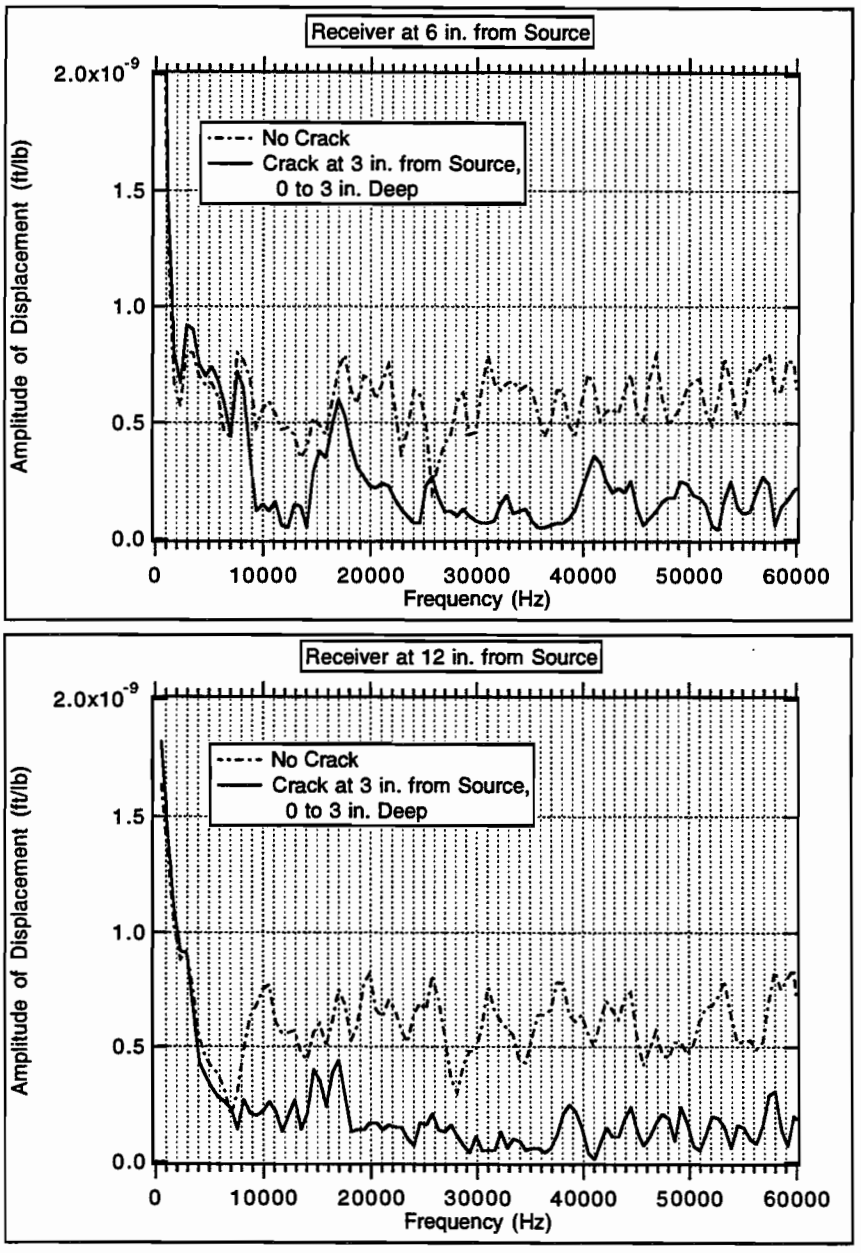


Fig. 6.14 Effect of 3-inch Vertical Cracks, in the Middle of the Source and the First Receiver, on the Displacement Amplitudes

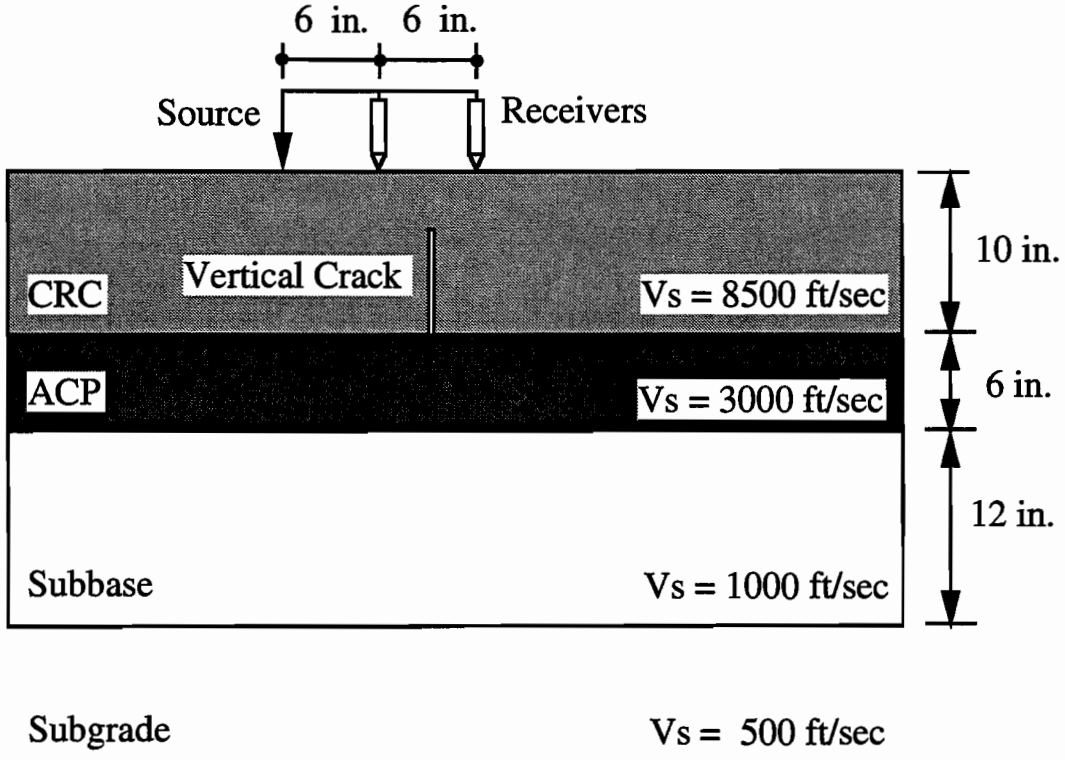


Fig. 6.15 Simulation of SASW Testing with Two Receivers on a Pavement with a Vertical Crack below the Surface and between the Two Receivers

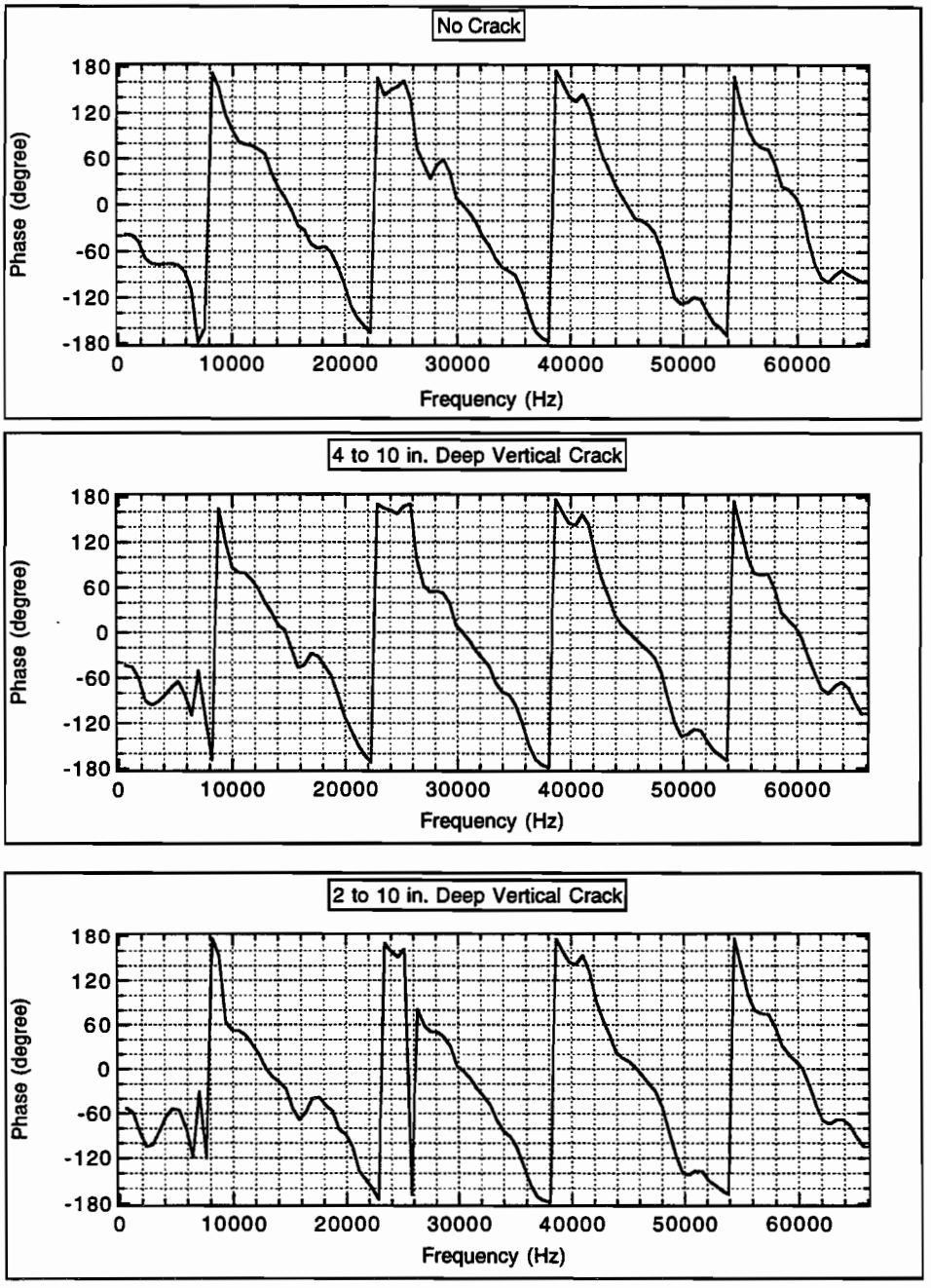


Fig. 6.16 Effect of the Depth of Subsurface Cracks, in the Middle of the First and Second Receivers, on the Phase Difference

however, that because the phase difference at a frequency slightly under 26 kHz is close to 180 degrees and that at around 26 kHz is -180 degrees what appears to be a significant change would be in fact very small (a phase difference of 181 degrees would be represented in this type of diagram with a value of -179 degrees). This further illustrated by considering the absolute phases at the two receivers (phase difference between the motions at each of the receivers and the applied load) as shown in Figs. 6.17, 6.18 and 6.19. The main effect of the cracks seems to be a peak at a frequency of about 7 kHz which is not present in the intact pavement.

Figures 6.21 through 6.23 show the corresponding results when the cracks are located at the midpoint between the source and the first receiver, as illustrated in Fig. 6.20. The phase diagrams corresponding to the phase differences between the records obtained at the two receivers, shown in Fig. 6.21, are again very similar for the intact pavement and the pavements with 6-inch and 8-inch cracks. The main differences, which are very small, occur in the range of frequencies below 10 kHz. These difference are more apparent in the phase diagram for the absolute phase at the first receiver (phase difference between the motion recorded at the first receiver and the applied load). A peak is clearly visible at around 7 kHz in the results for the 6-inch crack (Fig. 6.22) and for the 8-inch crack (Fig. 6.23). This peak exists in the results for the intact pavement (Fig. 6.17) but it is much smaller.

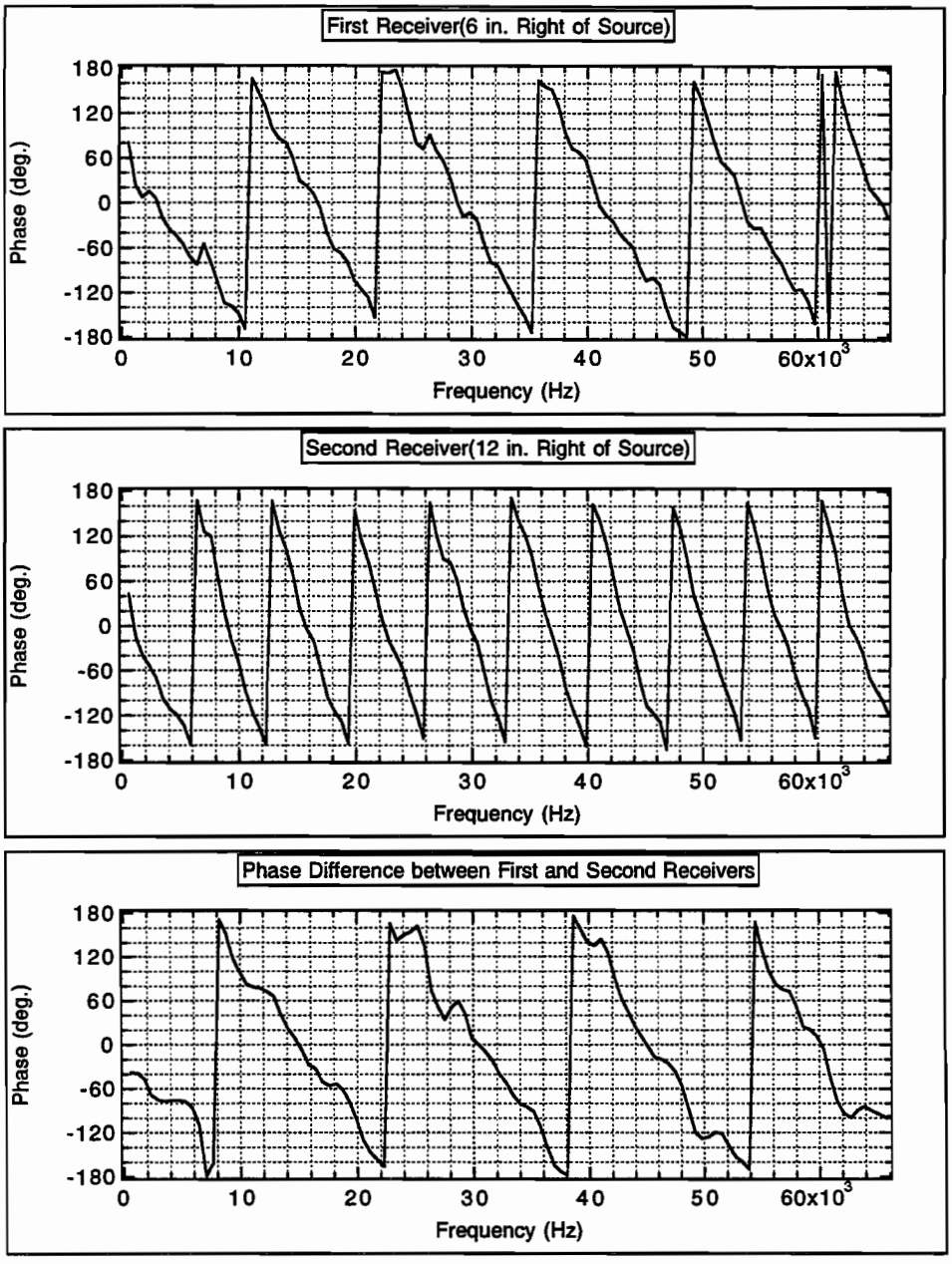


Fig. 6.17 Absolute Phases of the First and Second Receivers, as well as Phase Difference between the Two Receivers for an Intact Pavement

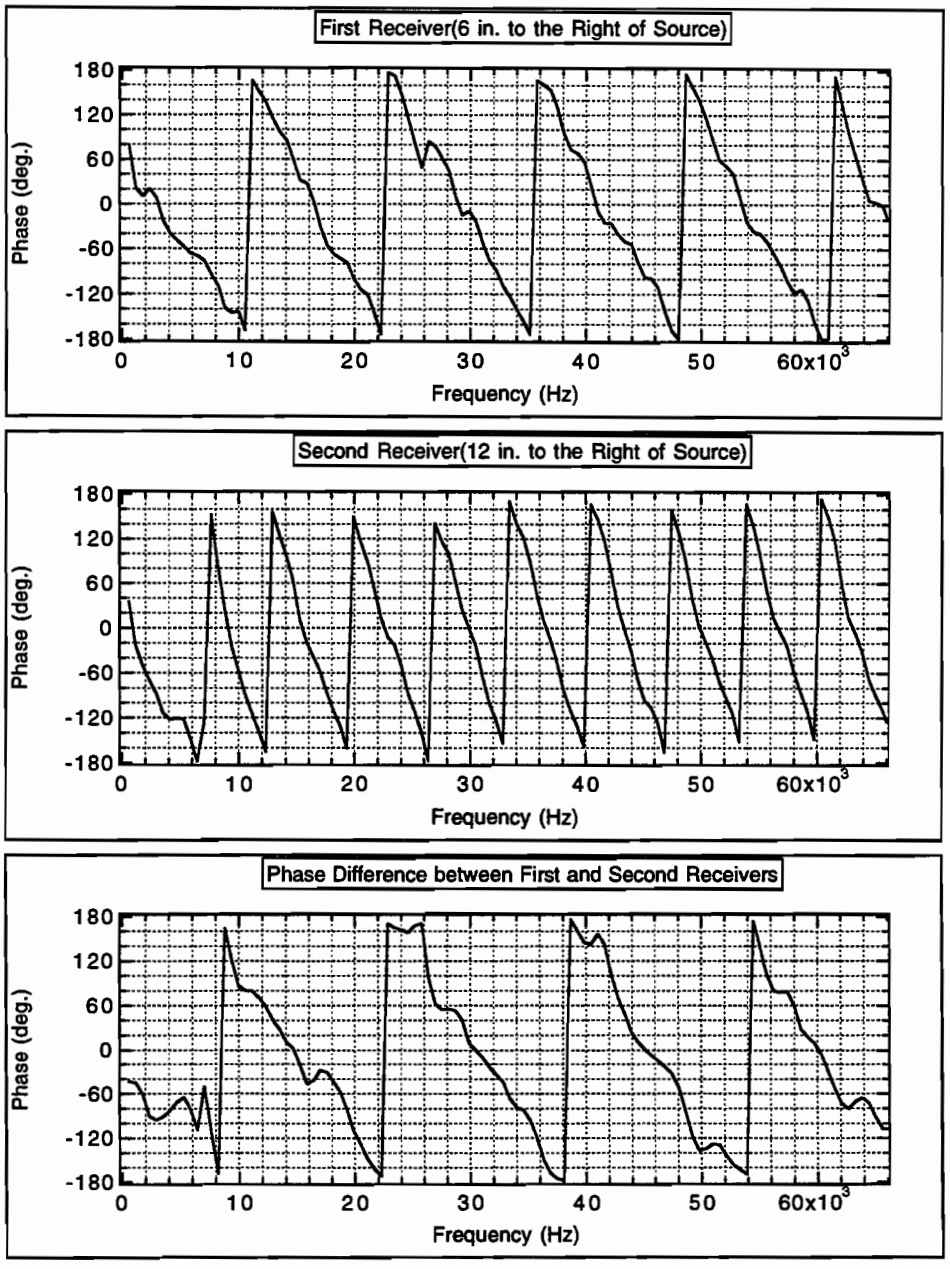


Fig. 6.18 Effect of the Subsurface Crack (4 to 10 in.), in the Middle of the First and Second Receivers, on the Absolute Phases and Phase Difference

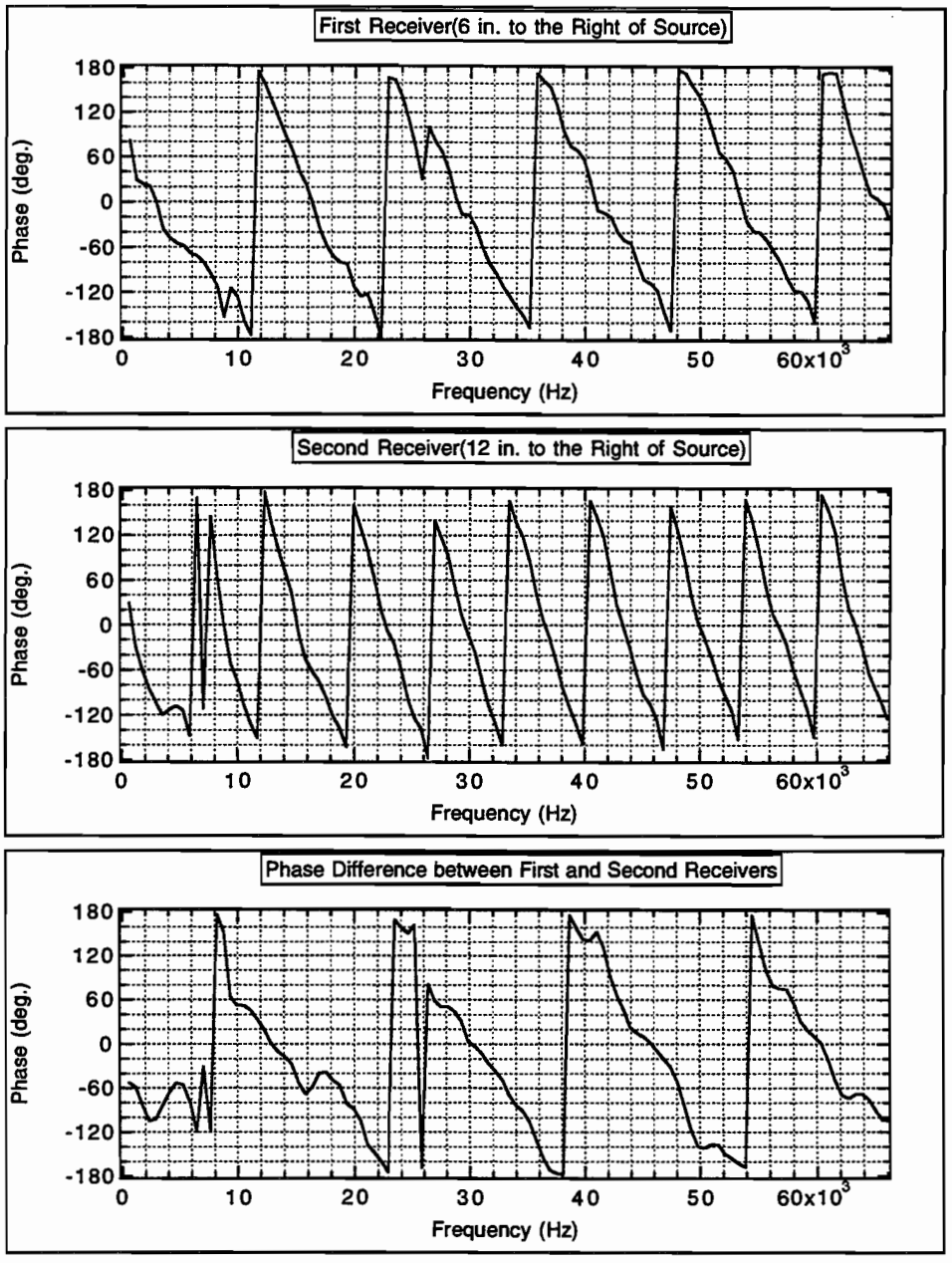


Fig. 6.19 Effect of the Subsurface Crack (2 to 10 in.), in the Middle of the First and Second Receivers, on the Absolute Phases and Phase Difference

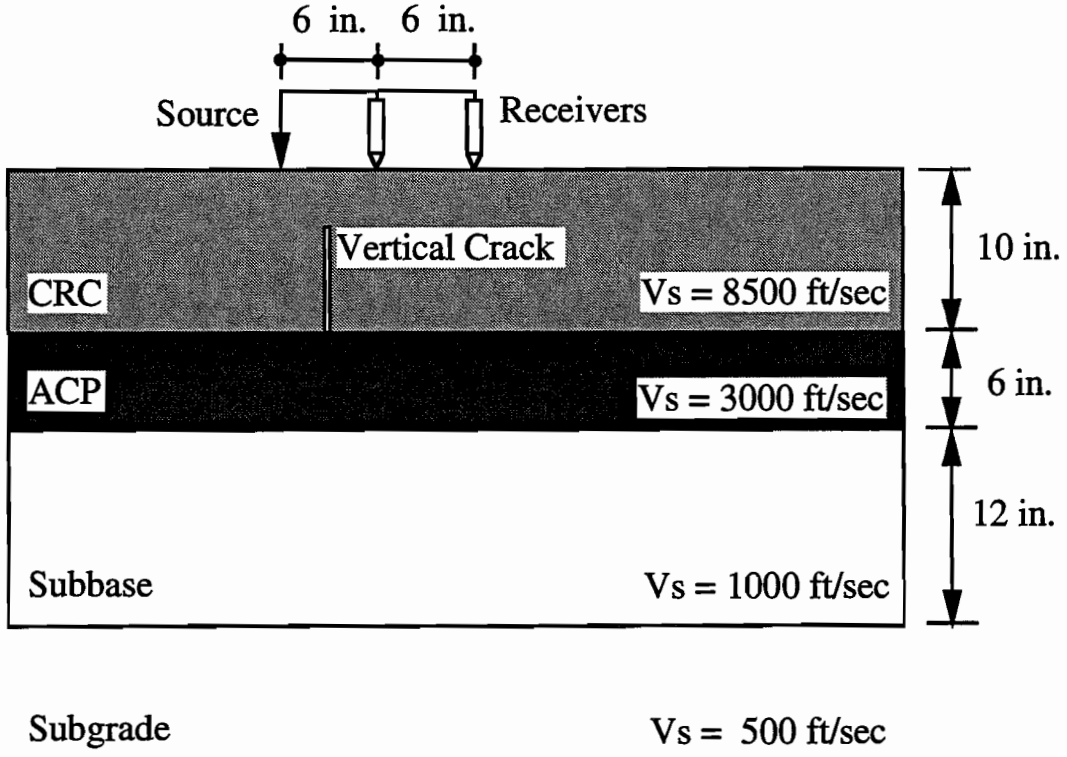


Fig. 6.20 Simulation of SASW Testing with Two Receivers on a Pavement with a Vertical Crack below Surface and between the Source and the First Receiver

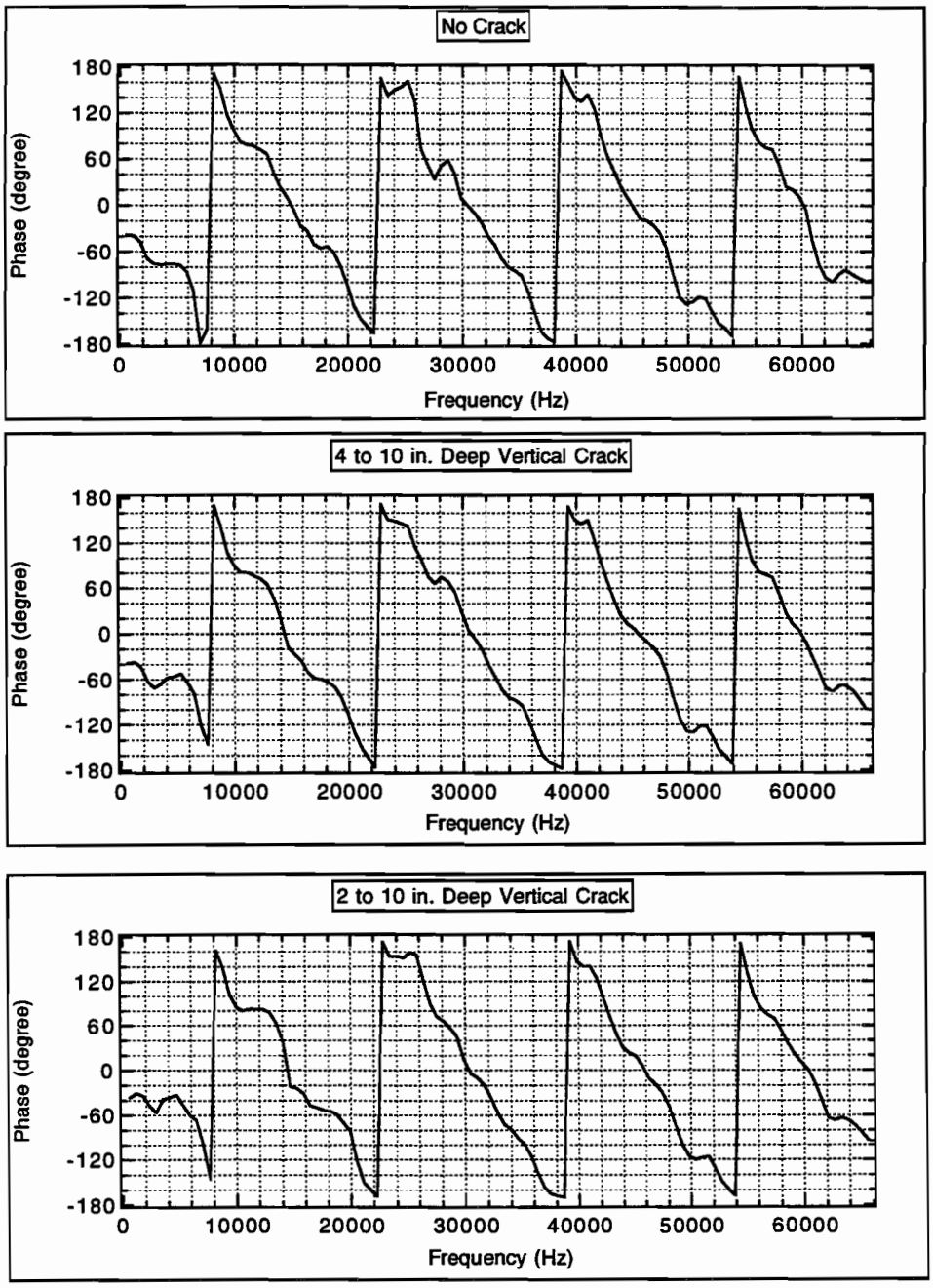


Fig. 6.21 Effect of the Depth of Subsurface Cracks, in the Middle between Source and First Receiver, on the Phase Difference

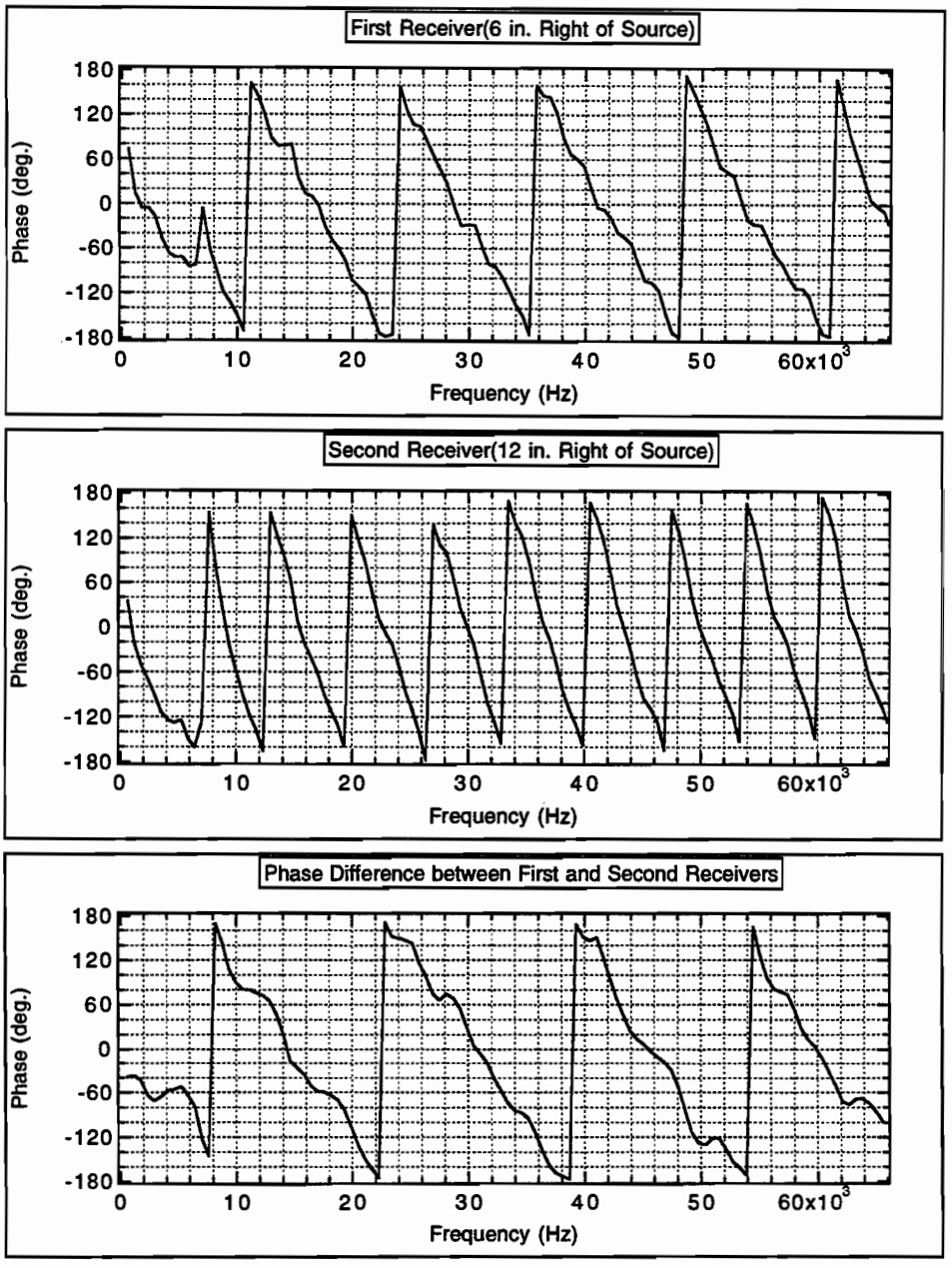


Fig. 6.22 Effect of the Depth of Subsurface Crack (4 to 10 in.), in the Middle between Source and First Receiver, on the Absolute Phases and Phase Difference

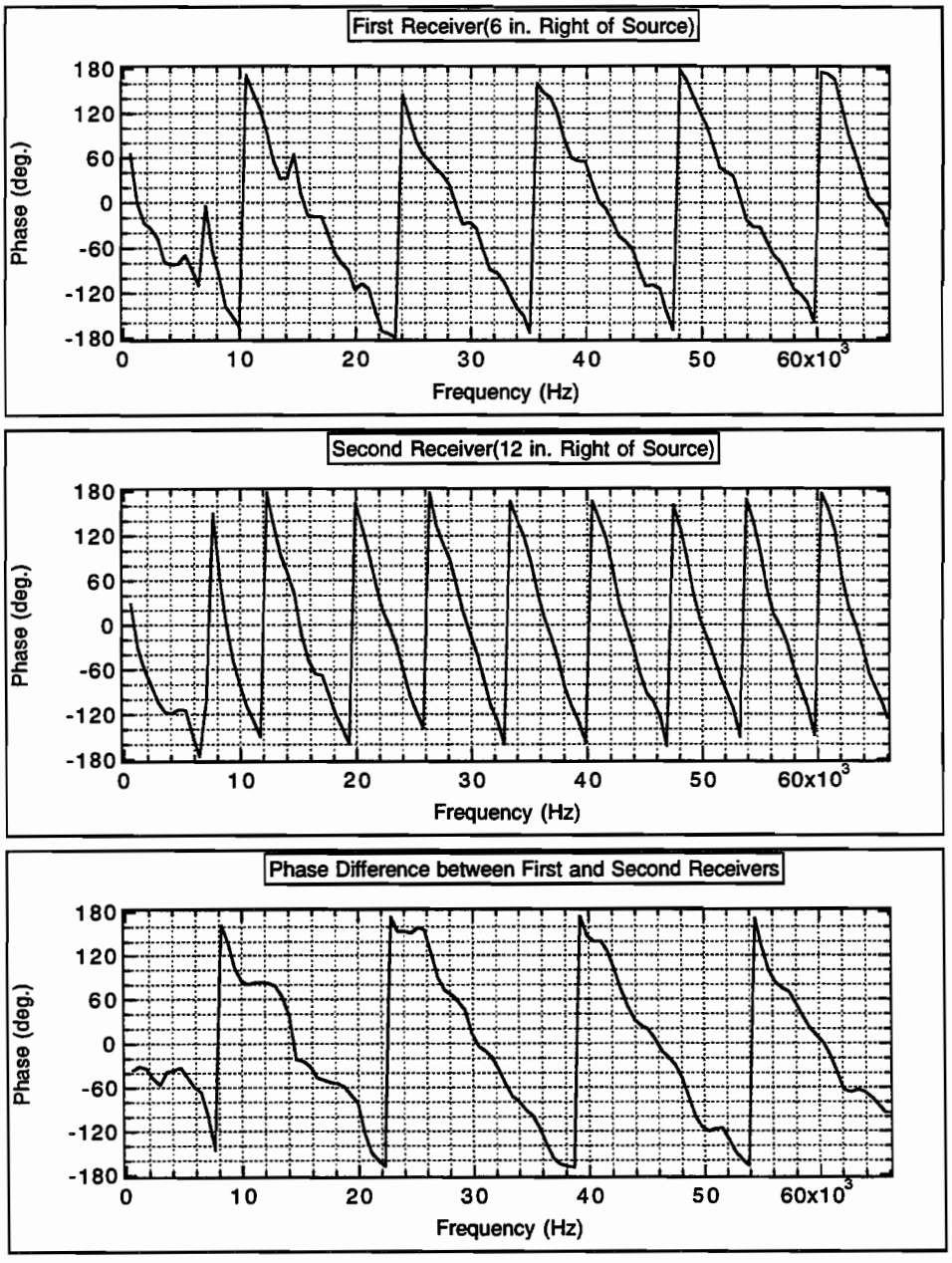


Fig. 6.23 Effect of the Depth of Subsurface Crack (2 to 10 in.), in the Middle between Source and First Receiver, on the Absolute Phases and Phase Difference

## 6.3 SOURCE-RECEIVER MOVING ACROSS CRACK

For the following studies the source is located 6 inches to the left of the receiver, as shown in Fig. 6.24. They are both moving toward the vertical crack. A triangular load with an impulse duration of 1/40000 seconds was used in the time domain FEM analyses. The steady state amplitudes of displacement in the frequency domain were obtained after the FFT was applied to the displacement time histories.

### 6.3.1 Surface-Piercing Cracks

Figures 6.25, 6.26 and 6.27 shows the amplitudes of the displacement recorded by the moving receiver at frequencies of 5, 10 and 20 kHz for crack depths of 3, 4.5 and 6 inches. At a frequency of 5 kHz the displacement amplitudes increase only to 1.2 times the amplitudes obtained in the intact pavement as the source-receiver arrives just to the left of the 3-inch crack as shown in Fig. 6.25. For a 4.5-inch crack, the ratios of the displacement amplitudes obtained in the cracked pavement to those in the intact pavement start to increase as the receiver is moving to within 5 inches from the crack. When the receiver is just to the left of the crack, the amplitude ratio reaches a peak value of 2.3. Very similar results are obtained for the 6-inch crack.

As the receiver moves across the 3-inch vertical crack but the source is still on the other side of the crack, the amplitude ratios are between 1.1 and 1.3. If the crack extends to a depth of 4.5 inches, these ratios have a sudden drop and fall into the range of 0.7 to 1.1. For the 6-inch crack, the sudden drop is even bigger

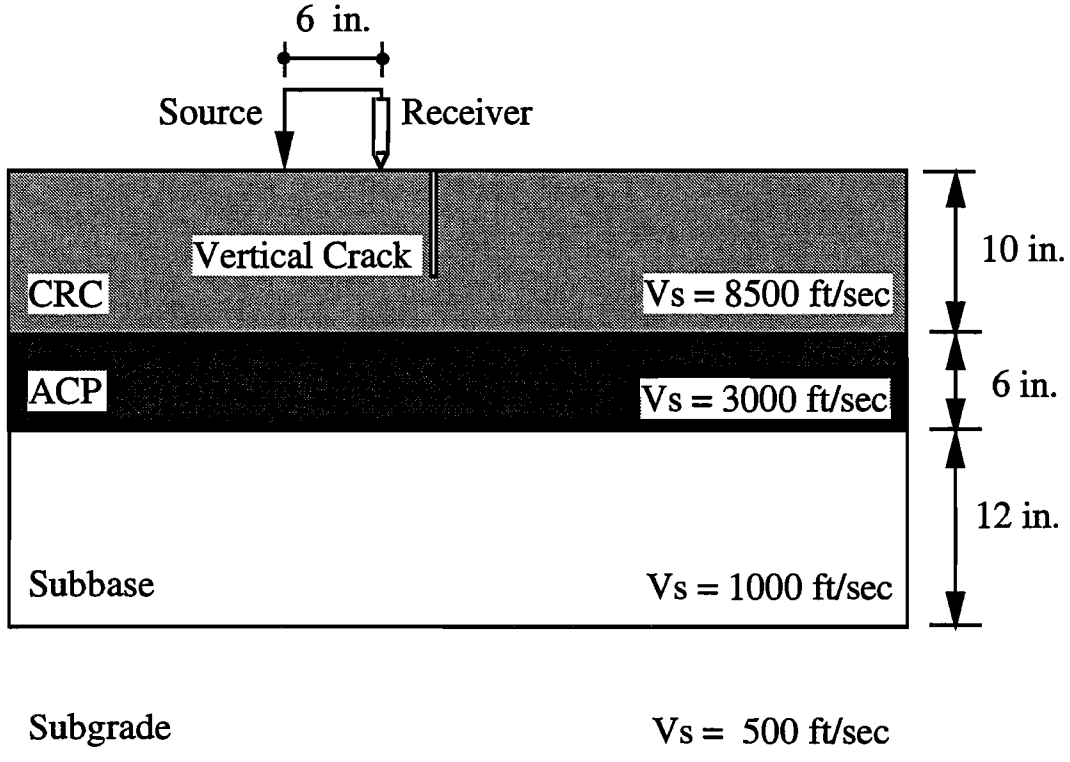


Fig. 6.24 Simulation of the Testing with One Receiver across a Vertical Crack at a Pavement

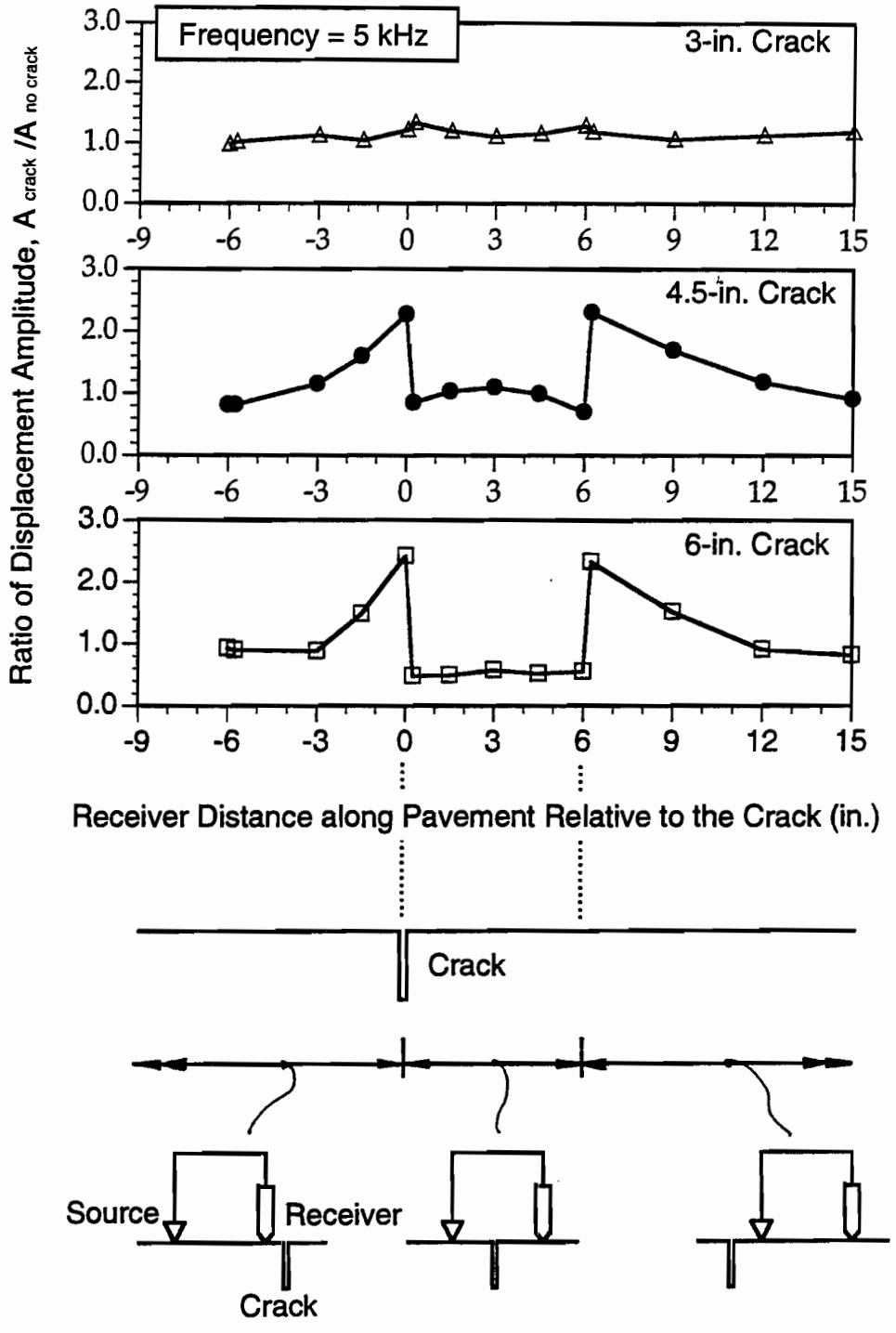


Fig. 6.25 Ratios of Displacement Amplitude for Simulation of Testing across Various Depths of Vertical Cracks at a Frequency of 5 kHz

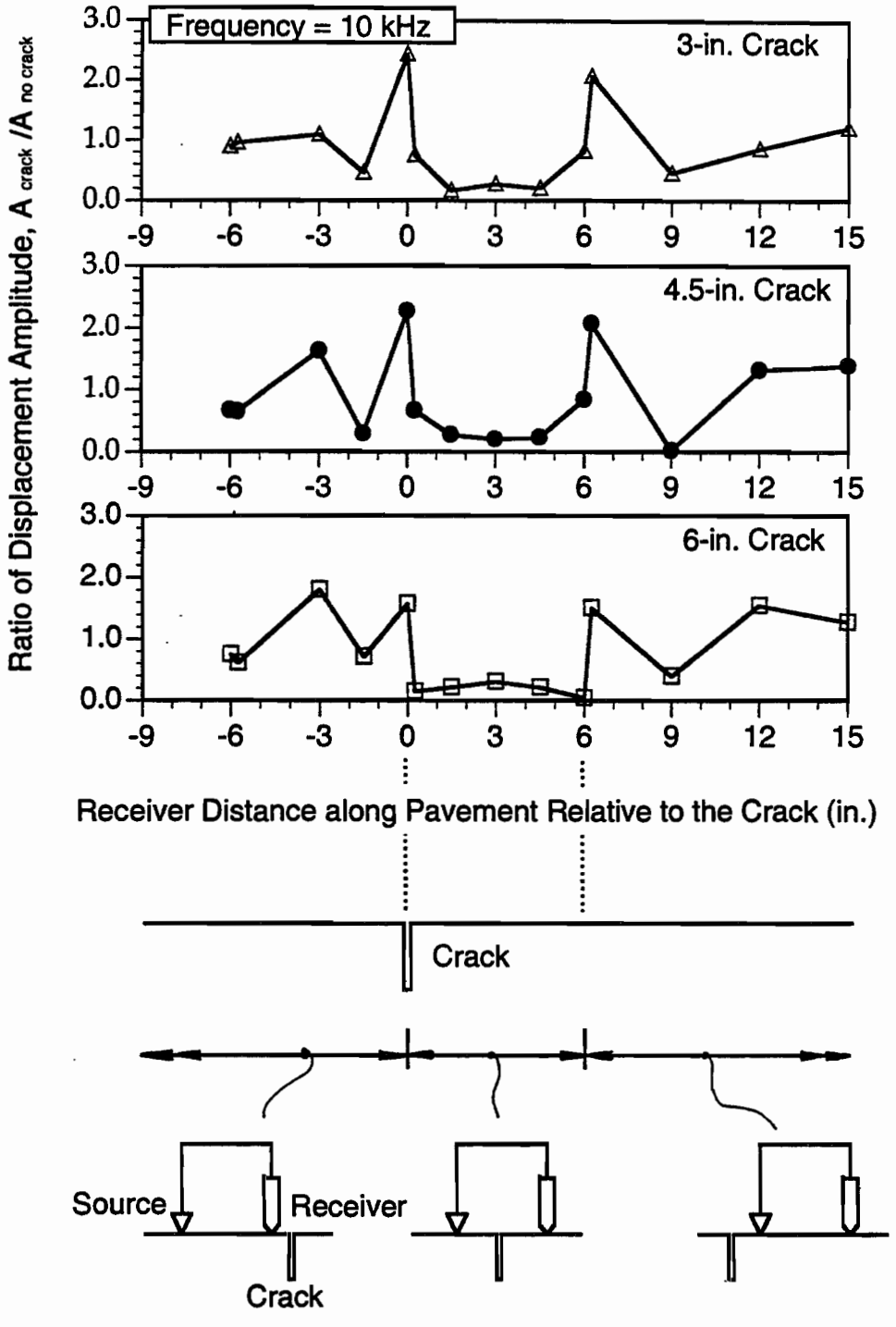


Fig. 6.26 Ratios of Displacement Amplitude for Simulation of Testing across Various Depths of Vertical Cracks at a Frequency of 10 kHz

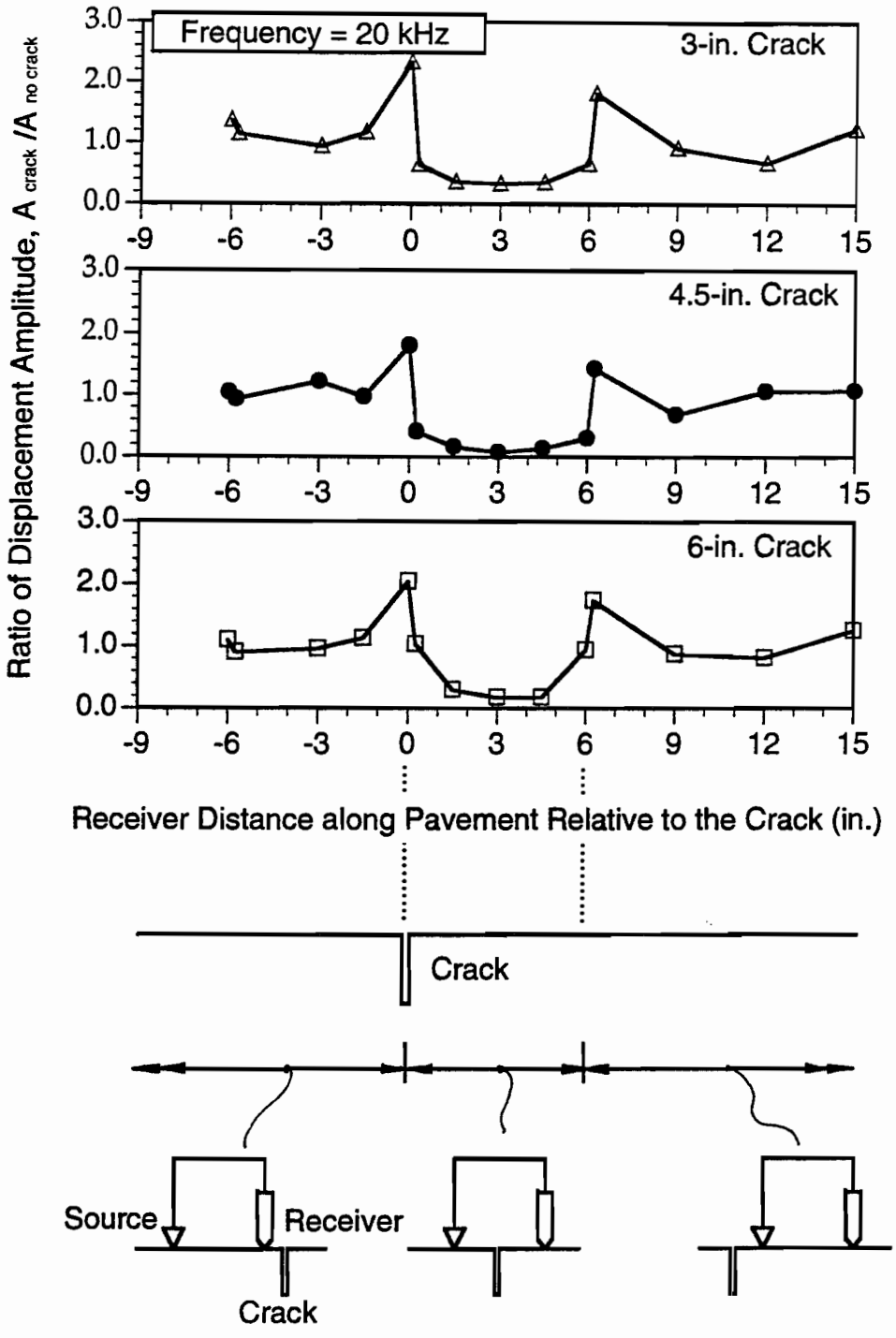


Fig. 6.27 Ratios of Displacement Amplitude for Simulation of Testing across Various Depths of Vertical Cracks at a Frequency of 20 kHz

and the ratios are within the range of 0.48 to 0.57. When the source moves across the 3-inch vertical crack, the amplitude ratios do not show again much difference. However, for the 4.5-inch and 6-inch cracks the amplitude ratios suddenly reach again the peak value and then decrease with distance from the crack.

At a frequency of 10 kHz the amplitude ratios oscillate (down to 0.46) when the source and receiver are to the left of the crack, as shown in Fig. 6.26. When the receiver is just to the left of the crack, the amplitude ratio reaches a peak value of 2.4 for the 3-inch and 4.5-inch cracks and only 1.8 for the 6-inch crack.

As the receiver moves across the vertical crack but the source is still on the other side of crack, the amplitude ratios have a sudden drop to about 0.16 for the 3-inch crack, 0.2 for the 4.5-inch crack and 0.04 to 0.3 for the 6-inch crack. When the source moves across the crack, the amplitude ratios reach again suddenly the peak value and fluctuate afterwards.

The ratios of displacement amplitude at a frequency of 20 kHz exhibit the same general trends of behavior as shown in Fig. 6.27. When the receiver is just to the left of the crack, the amplitude ratio has a peak value of 2.33 for the 3-inch crack, 1.8 for the 4.5-inch crack and close to 2 for the 6-inch crack.

As the receiver moves across the vertical crack but the source is still on the other side of crack, the amplitude ratios have again a sudden drop with a minimum value of about 0.33 for the 3-inch crack, 0.07 to 0.4 for the 4.5-inch crack and 0.17 for the 6-inch crack. As the source moves across the crack, the ratios reaches again a peak, then decrease.

In order to compare the effects of the depth of the crack, the three plots in Figs. 6.25, 6.26 and 6.27 were superimposed in Figs. 6.28, 6.29 and 6.30. The results at a frequency of 5 kHz shown in Fig. 6.28 indicate that the 3-inch crack has little effects on the amplitude ratios, while the 4.5-inch and 6-inch crack cause the ratios to jump just before the receiver crosses the crack and just after the source goes across the crack. It is interesting to note that the amplitude ratios seem to form three groups as the crack is located between the source and the receiver. The deeper the vertical crack, the lower the amplitude ratios. In Figs. 6.29 and 6.30 the results at the frequencies of 10 and 20 kHz show similar jumps as the receiver is just to the left of the crack and the source is just to the right of crack. However, the results for 10 kHz exhibit more fluctuations as the receiver is moving close to 3 inches from the crack and passing the crack by 9 inches. While the crack is located between the source and the receiver, the trend in the ratios observed in Fig. 6.28 can no longer be seen in Figs. 6.29 and 6.30.

The details of the peak amplitude ratios for each frequency are shown in Fig. 6.31. Similar relationships between amplitude ratios and crack depths can be seen when the source is just about to cross the crack and when the source is just past the crack. With a frequency of 5 kHz the deeper the vertical crack, the higher the amplitude ratio, but for the higher frequencies, such as 10 and 20 kHz, this trend does not appear (Fig. 6.31).

When the crack is located between the source and the receiver, at a frequency of 5 kHz the amplitude ratios fall into different ranges for various depths of crack as shown in Fig. 6.32. The amplitude ratios for the 3-inch crack are between 1.1 and 1.33, while the amplitude ratios are smaller, within 0.7 to 1.1,

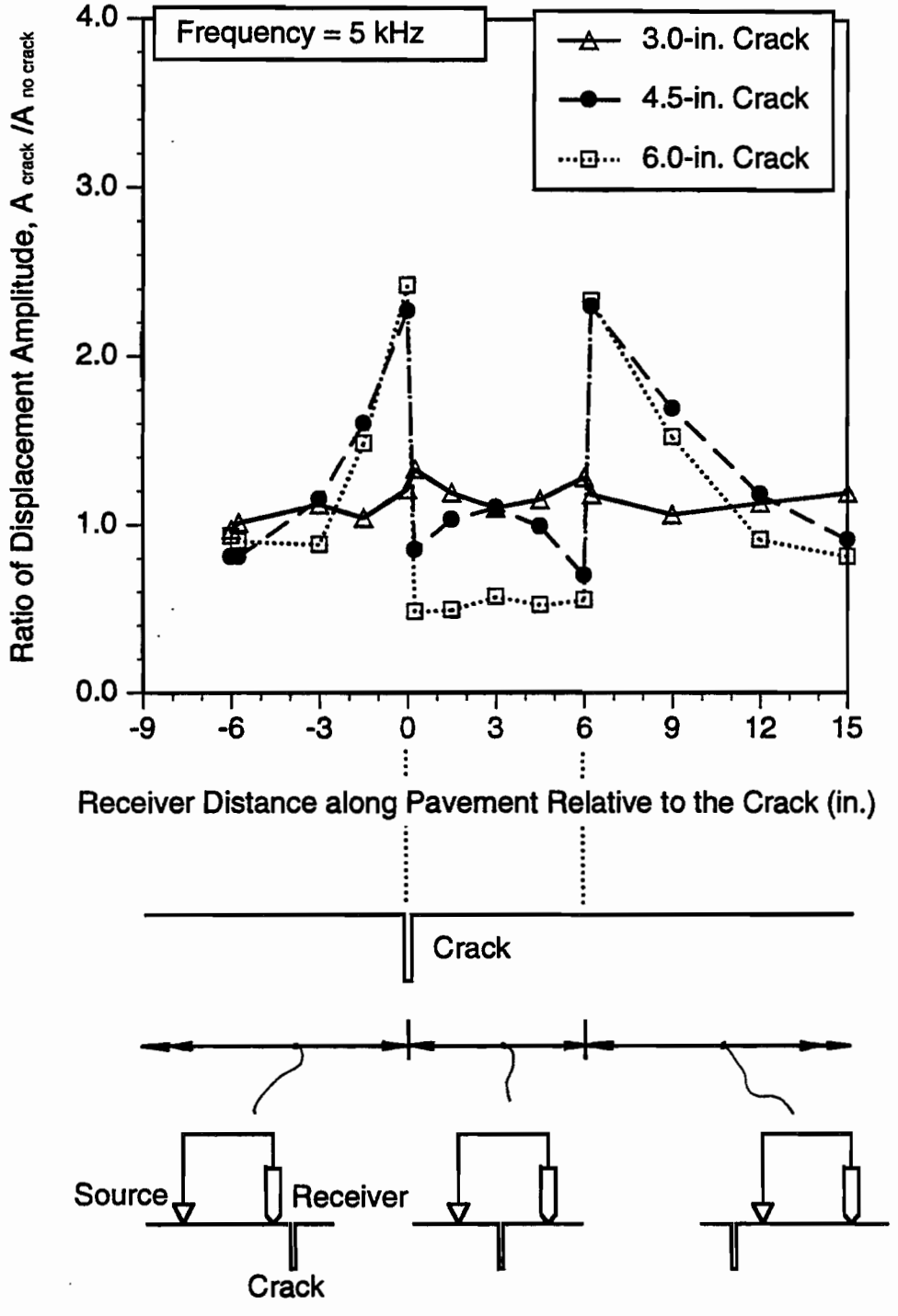


Fig. 6.28 Comparison of Ratios of Displacement Amplitude for Testing across Vertical Cracks at a Frequency of 5 kHz

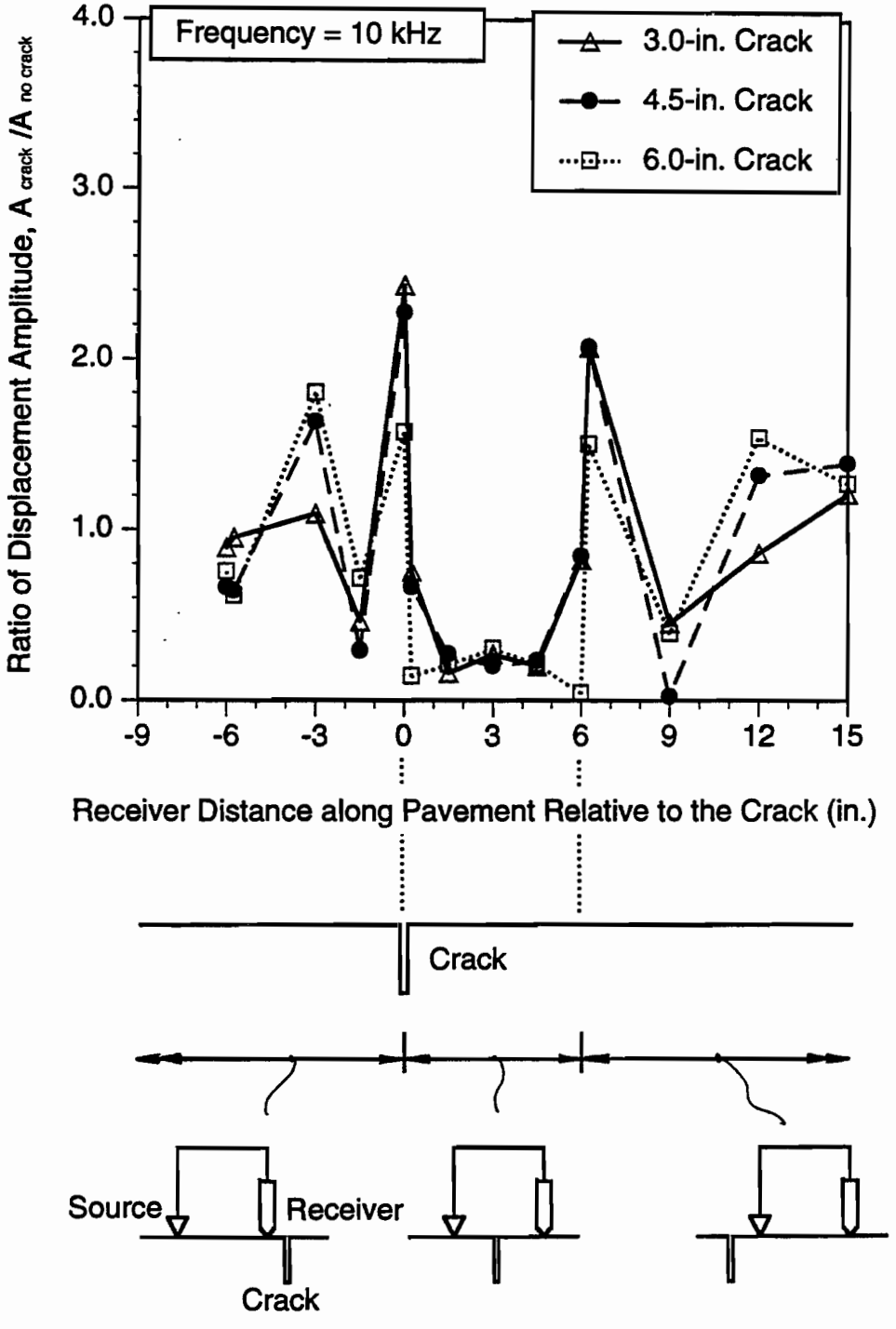


Fig. 6.29 Comparison of Ratios of Displacement Amplitude for Testing across Vertical Cracks at a Frequency of 10 kHz

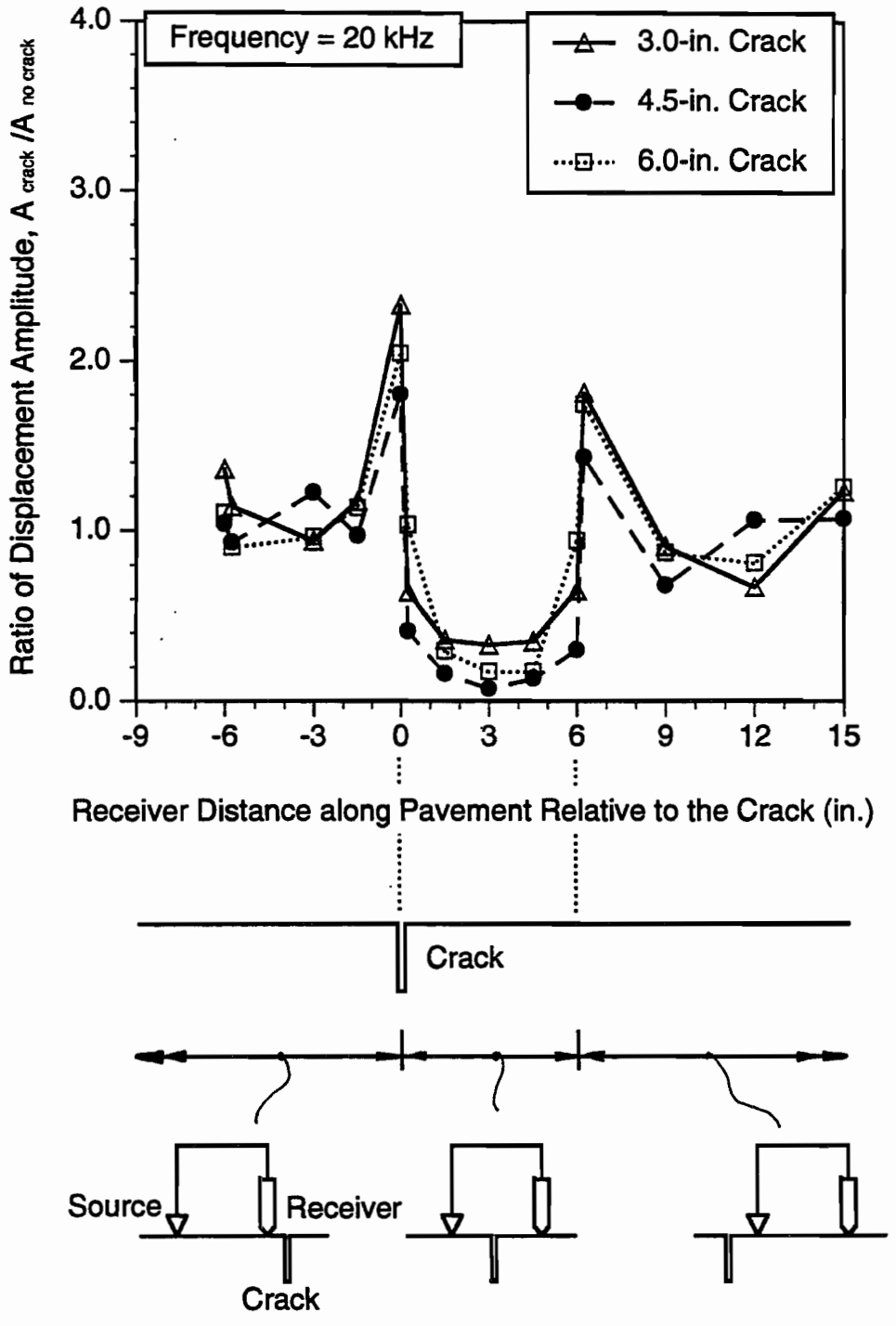


Fig. 6.30 Comparison of Ratios of Displacement Amplitude for Testing across Vertical Cracks at a Frequency of 20 kHz

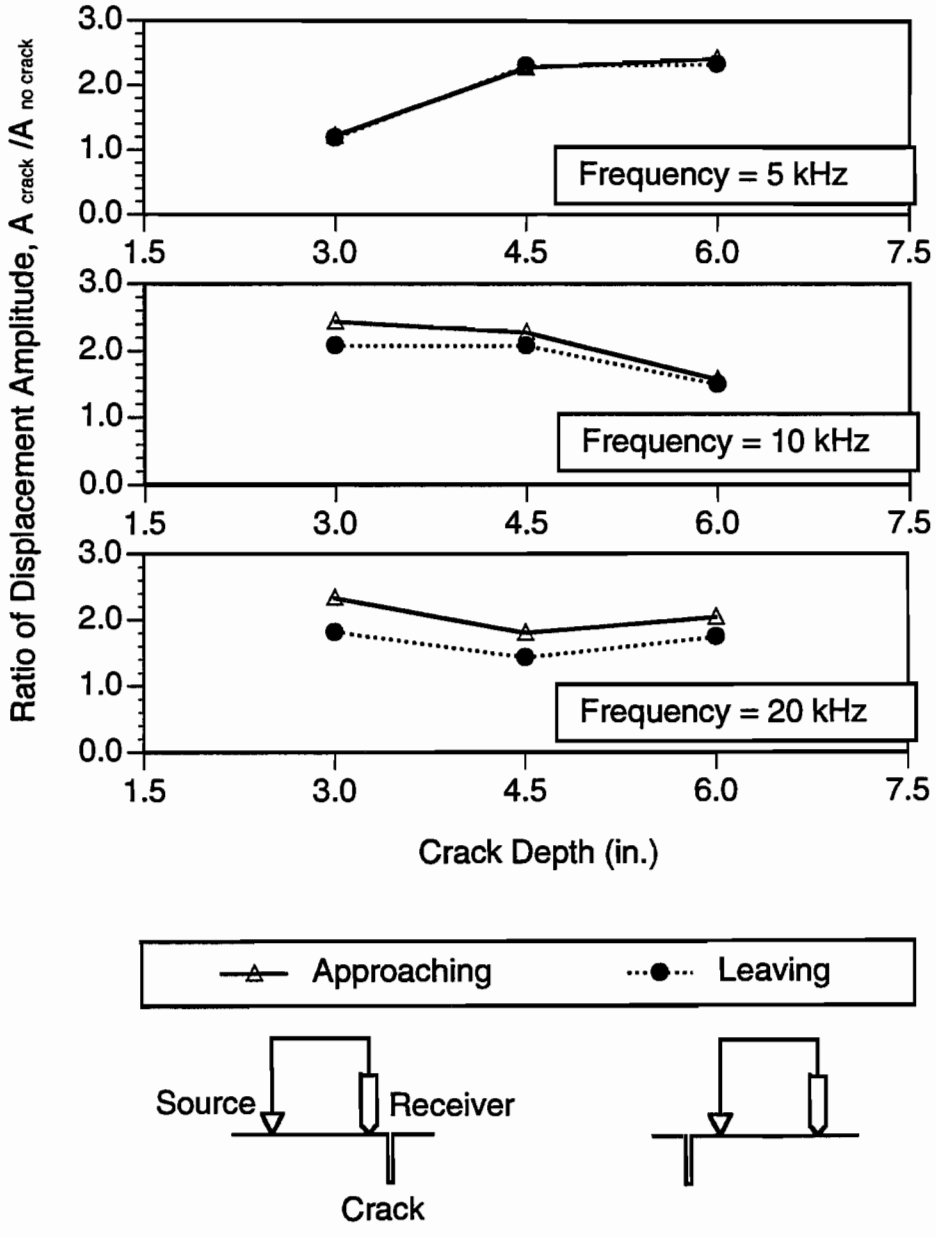


Fig. 6.31 Effect of Crack Depth on the Ratios of Displacement Amplitude just before Receiver Crosses the Crack (Approaching) and just after Source Crosses the Crack (Leaving)

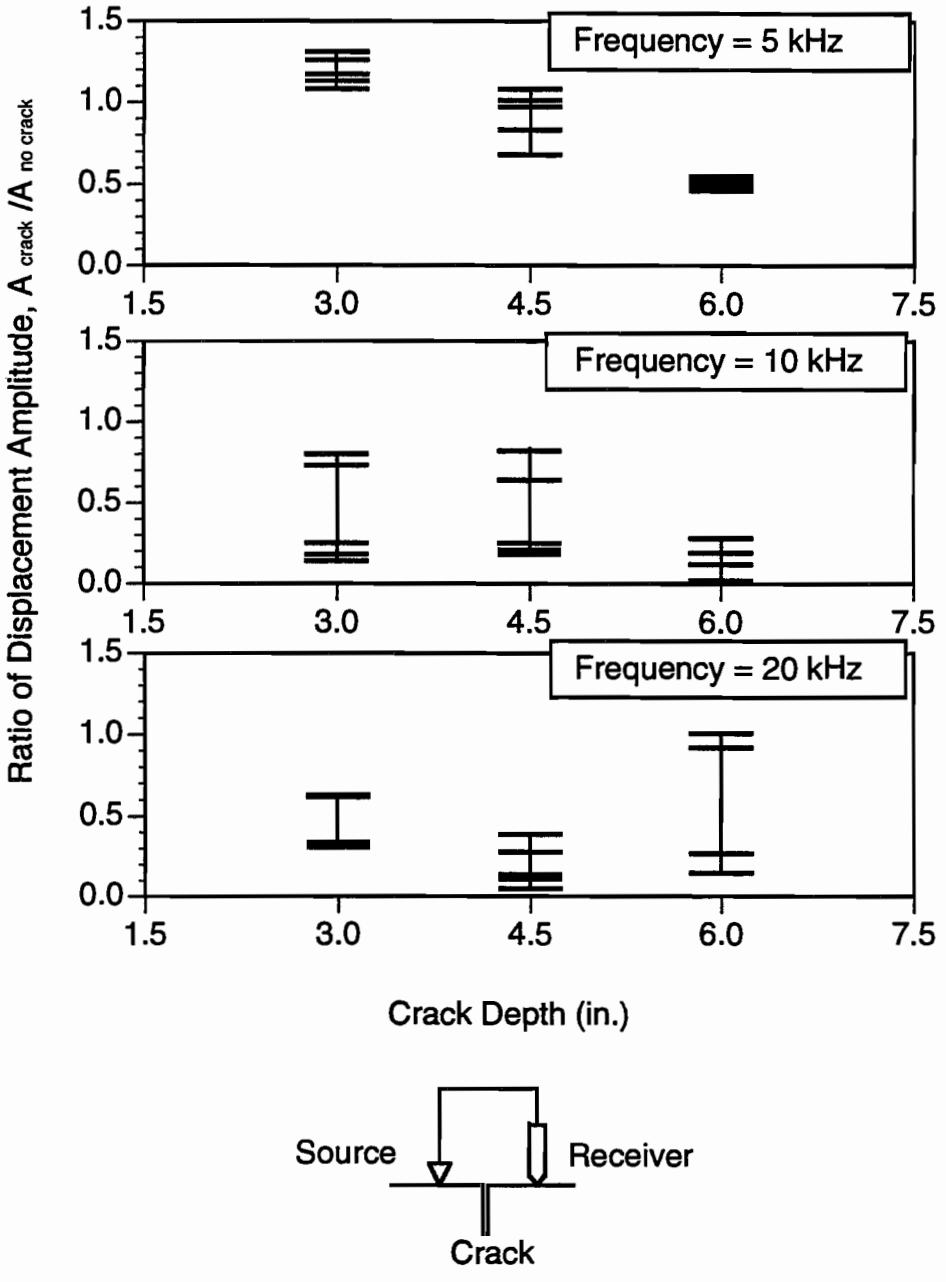


Fig. 6.32 Effect of Crack Depth on the Ratios of Displacement Amplitude while the Crack is between the Source and the Receiver

for the 4.5-inch crack. As the crack extends to 6 inches these amplitude ratios fall into the range of 0.48 and 0.57. However, the amplitude ratios at a frequency of 10 kHz for the 3-inch and 4.5-inch cracks are similar and much lower for the 6-inch crack. For a frequency of 20 kHz the amplitude ratios do not seem to be related to crack depths.

In Fig. 6.33 the effects of crack depths on the percent change of displacement amplitudes as the receiver is crossing above the crack are investigated. At a frequency of 5 kHz the displacement amplitudes for a pavement with 3-inch crack range from a 10 % increase to a 9 % reduction when the receiver is crossing the crack. These amplitudes at a frequency of 5 kHz decrease more with the depth of the crack. As shown in Fig. 6.33, the amplitudes for a pavement with 4.5-inch and 6-inch cracks decrease 51 to 70 % and 77 to 80 % respectively. However, these percent changes at a frequency of 10 kHz appear to be similar for the various depths of crack. At a frequency of 20 kHz, the percent changes seem not to be associated with crack depths.

Thus while the presence of the crack can be seen very clearly for all three frequencies the depth of the crack would be hard to determine. There would appear to be a trend at 5 kHz but this would need further study and experimental verification.

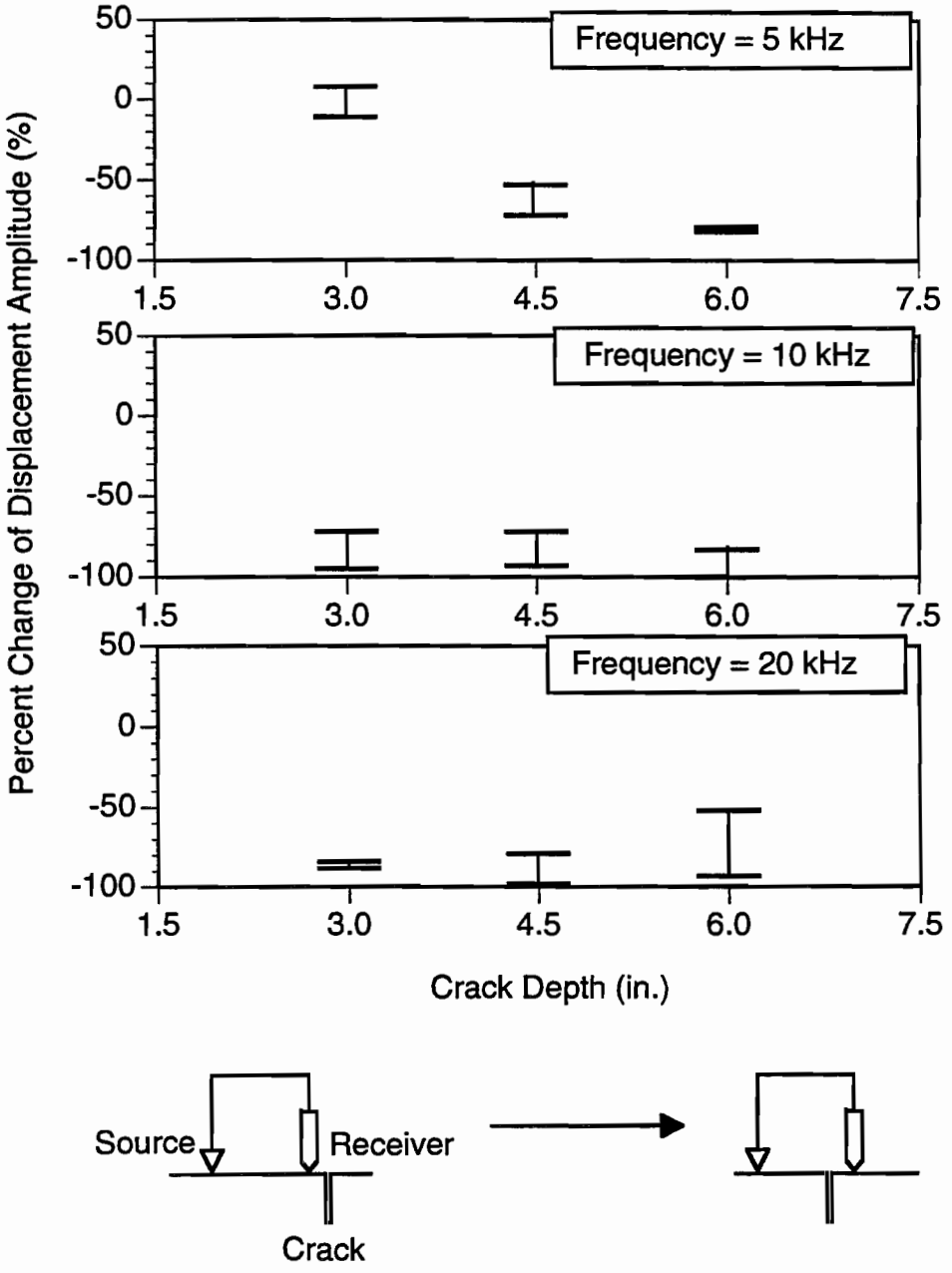


Fig. 6.33 Effect of Crack Depth on the Percent Change of Displacement Amplitude As the Receiver Crosses the Crack

### 6.3.2 Subsurface Cracks

The effects of crack depths and location on the displacement amplitudes of the receiver moving along the pavement for subsurface cracks were studied next (Fig. 6.34).

The ratios of displacement amplitude obtained in the pavement with a subsurface crack to that in the intact pavement are all smaller than 1.2 for the two cracks studied here. In the first case the crack is located from 4 to 10 inches below the surface. At a frequency of 5 kHz the amplitude ratios start to decrease as the receiver approaches the crack and the lowest ratio, 0.57, occurs when the crack is in the middle between the source and the receiver as shown in Fig. 6.35. On the contrary, at a frequency of 10 kHz the amplitude ratios start to increase as the receiver approaches the crack and the highest ratio, 1.14, occurs when the crack is in the middle between the source and receiver. This subsurface crack has very little effects on the displacement amplitude ratio at a frequency of 20 kHz.

In the second case the subsurface crack extends up to 2 inches below the surface. The amplitude ratios at both frequencies of 5 and 20 kHz exhibit the same trend of the first case with a frequency of 5 kHz. Their amplitude ratios start to decrease as the receiver approaches the crack and the lowest ratios, 0.46 for 5 kHz and 0.55 for 20 kHz, occur when the crack is half way between the source and the receiver (Fig. 6.36). This subsurface crack has little effect on the displacement amplitude of the receiver at a frequency of 10 kHz.

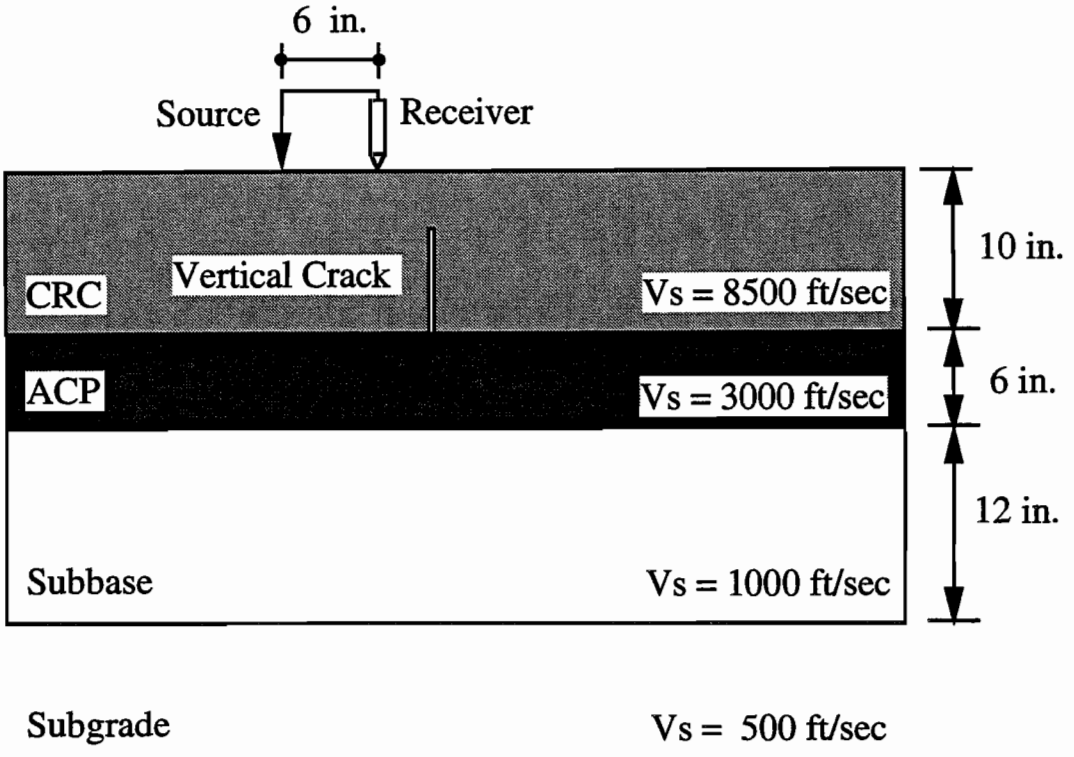


Fig. 6.34 Simulation of the Testing with One Receiver across a Vertical Crack below Surface at a Pavement

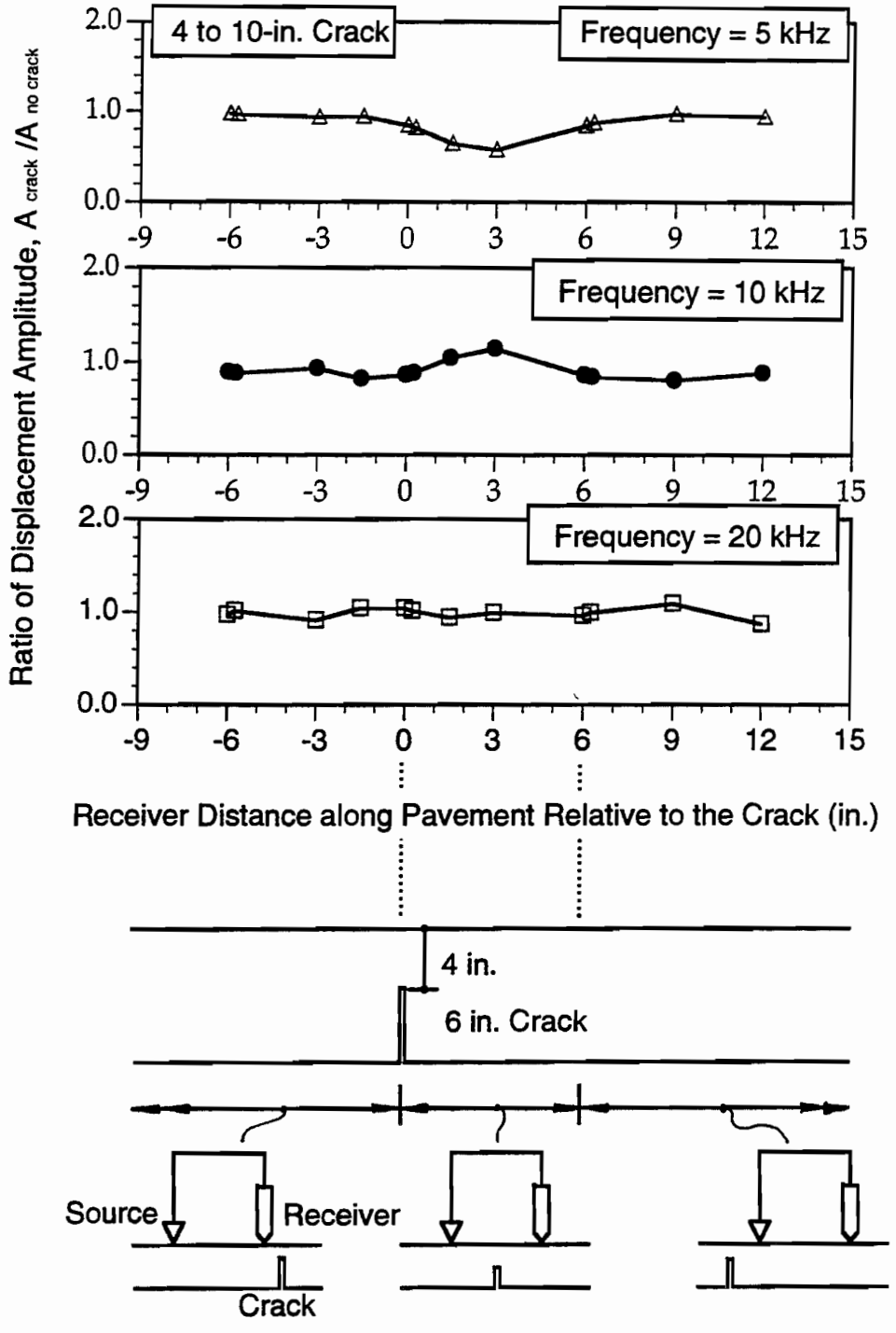


Fig. 6.35 Ratios of Displacement Amplitude for Simulation of Testing across Vertical Cracks 4 in. below the Surface

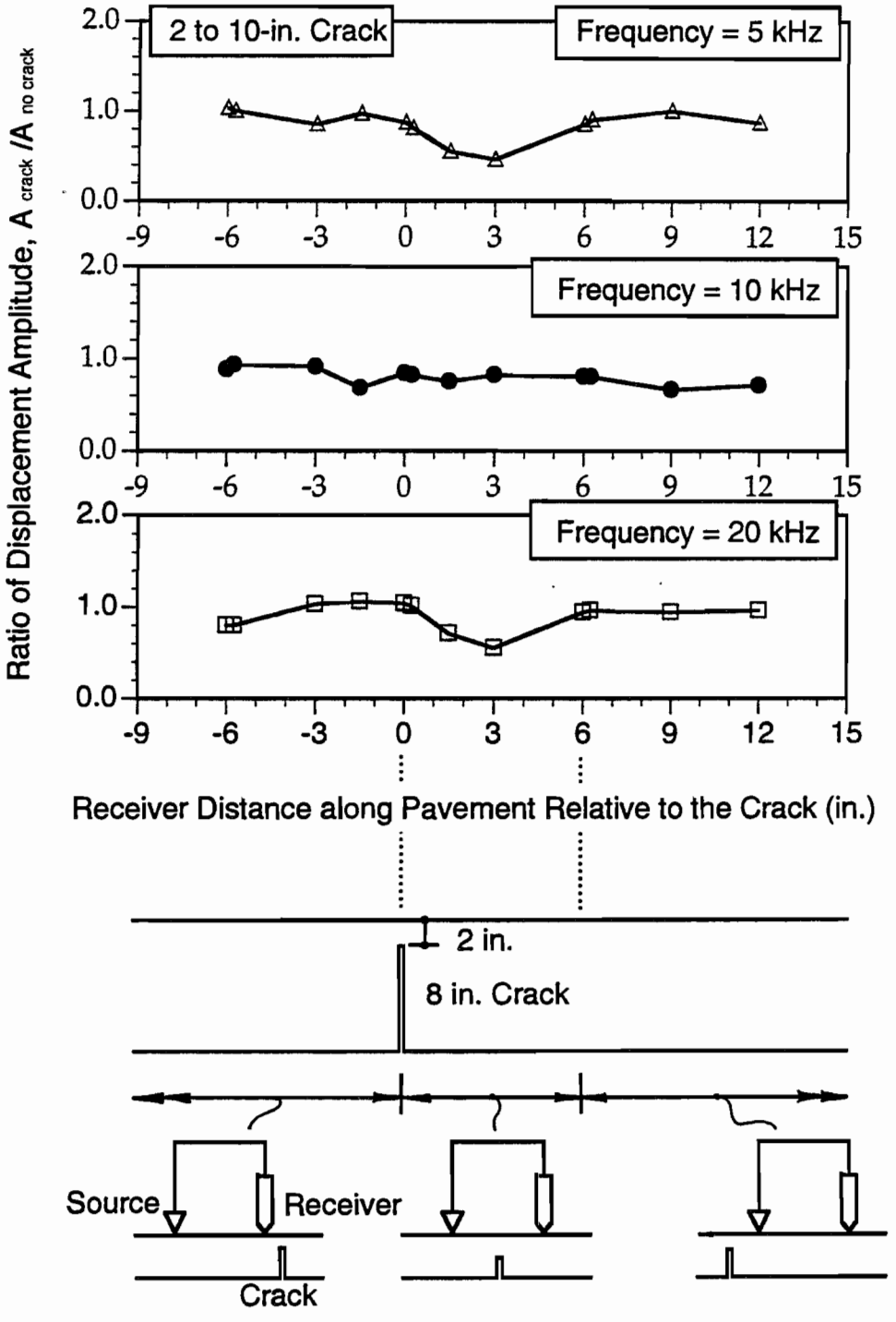


Fig. 6.36 Ratios of Displacement Amplitude for Simulation of Testing across Vertical Cracks 2 in. below the Surface

## 6.4 SUMMARY

The existence of surface cracks can be easily detected from the phase diagrams (or phase velocity) as well as from the amplitudes of the recorded motions (at various frequencies). The depth of the crack is however more difficult to determine.

Subsurface cracks are also much harder to locate from surface measurements producing changes of only 20 % or so in the amplitudes of displacements and only small variations in the phase diagrams.

# CHAPTER SEVEN

# SUMMARY, CONCLUSIONS, AND RECOMMENDATIONS

## 7.1 SUMMARY

Several methods have been developed to assess in a non-destructive way the condition of pavements or the need for repairs. Among these are the Falling Weight Deflectometer (FWD) and the Dynaflect. Neither of these two techniques is well equipped, however, for identification of delaminations, debonding, voids, or cracks in pavement systems, although these are very important features which should be discovered early for a good maintenance program.

In this work a computer model using finite elements was developed to simulate the response of pavements with horizontal delaminations, voids or vertical cracks of different sizes to dynamic loads applied at the free surface. The solution of the finite element model was carried out in the time domain to obtain both transient responses and steady state amplitudes of displacements. From the transient responses computed in the time domain the steady state amplitudes could be predicted using the Fast Fourier Transform. The effects of different irregularities on various response quantities were investigated for variable dimensions and locations in order to determine optimum ways to detect them.

The accuracy of the model was verified by comparing results obtained with three different models: a boundary element formulation in the frequency domain, a finite element model with a solution in the time domain under a steady state excitation, and the finite element model subjected to a transient impulse with

a step by step integration of the equations of motion in the time domain, used for most of the analyses.

In addition, the analytical results were compared to some experimental data collected on a pavement with known voids.

Parametric studies were conducted for intact pavements and pavements with delaminations (Chapter 4), voids (Chapter 5) and vertical cracks (Chapter 6) to assess what response parameters allow best to identify the existence of irregularities.

## 7.2 CONCLUSIONS

From the investigation of the effects of irregularities on the dynamic response of pavements which has been conducted. One can derive some general conclusions of a practical nature, related to the optimum way to detect these irregularities, and some more specific conclusions, related to the methods of analysis used and the observed results.

### 7.2.1 General Conclusions

From the studies conducted in this work it can be concluded that delaminations can be better detected using impact loads with predominant frequencies (inverse of the load duration) of the order of 1000 to 10000 Hz. This frequency range is much higher than that associated with the FWD (or Dynaflect) tests which explains why these devices are not successful at locating cavities or delaminations. Within this range there are likely to be two peaks appearing in the

amplitude response in the frequency domain. A "P-wave peak" usually associated with high frequencies, and a "flexural peak" usually in the lower frequency range. The "P-wave peak" is related to P-wave reflections. The "flexural peak" is associated with flexural vibrations of the layer above the defect. For shallow delaminations and voids where the "P-wave peak-frequency" is too high to measure in practice, will be obtained looking at the better results of "flexural oscillation" and "flexural peak". For deeper delaminations or voids the "P-wave peak" will be easier to detect.

The detection of delaminations, voids or vertical cracks will be much easier and more accurate when using a moving load and receiver system. As the source-receiver arrangement goes over the damaged area, there will be a clear variation in the observed results, either in the time domain or in the frequency domain. Detection of vertical cracks that do not reach the surface is however difficult with the mechanisms explored in this work.

### 7.2.2 Specific Conclusions

1. Without internal soil damping it can take a considerable amount of time to reach a steady state condition in time domain solutions using a finite element model subjected to a harmonic load. A better alternative is to obtain the solution due to a transient load. With this approach the duration of the transient impulse must be properly selected to obtain reliable results.

2. A good resolution in the frequency domain is very important for locating response peaks. This is controlled by the sampling rate, $\Delta t$, and the number of points used in the Fast Fourier Transform. Since the mesh size around a void or a crack must be much smaller than that used for intact layers, a larger number of points are required to obtain good resolution.

3. There are two significant frequency ranges for a pavement with a horizontal delamination, a "P-wave peak-frequency" usually associated with high frequencies, and a "flexural peak-frequency" usually in the lower frequency range. Detection of voids or delaminations is easier comparing the amplitudes of the motion in these frequency ranges. The deeper the delamination, the lower the "P-wave peak-frequency" and the higher the "flexural peak-frequency". The length of the delamination has no effect on the "P-wave peak-frequency", but as it increases the "flexural peak-frequency" decreases. The "P-wave peak-frequency" is related to P-wave reflections, which can be estimated from $V_p$ / 2d, where $V_p$ is the velocity of propagation of P-waves in the material considered and d is the depth of the delamination from the surface. The "flexural peak-frequency" is associated with flexural vibrations of the layer above the defect. Basically this peak-frequency is a function of the depth but mostly the size of the delamination. If one obtains both the "P-wave peak-frequency" and the "flexural peak-frequency", one could estimate the depth of the delamination from the "P-wave peak-frequency" and assess the size of the delamination from the "flexural peak-frequency".

4. The results of displacement histories and displacement amplitudes are almost identical for voids and delaminations with the same length as long as the depth from the surface to the top face of the void equals the depth to the delamination.

5. The existence of surface cracks can be easily detected from the phase diagrams (or phase velocity) as well as from the amplitudes of the recorded motions (at various frequencies). The depth of the crack is however more difficult to determine. Subsurface cracks are also much harder to locate from surface measurements producing changes of only 20 % or so in the amplitudes of the displacements and only small variations in the phase diagrams.

6. Since the amplitude of the "P-wave peak" attenuates very fast, it is desirable to place the receiver as close to the source as possible when using the P-wave technique.

7. In real world some noise from the equipment and traffic may be involved and the problem becomes more complicated.

8. The inhomogeneity of the materials may contribute to the difference between field results and analytical predictions.

## 7.3 RECOMMENDATIONS

The following recommendations include also some general recommendations of a practical nature and recommendations for future theoretical research:

### 7.3.1 General Recommendations

In order to detect delaminations or voids, it is recommended to have preferably a moving source-receiver configuration which applies an impulse load with a predominant frequency (inverse of the duration) between 1000 and 10000 Hz. The apparatus should have a monitor system capable of displaying the time histories in the time domain as they are recorded or to convert these histories into Fourier amplitude spectra automatically displaying them in this form. In either case the operator should be able from inspection of these figures on the screen to detect immediately the existence of a damaged area, with delaminations, voids or cracks, from the sudden variations in the amplitudes of the recorded motions. Once the existence of potential damage is recognized it would be possible to conduct more detailed tests of that area in order to define better the nature of the irregularity or its extent.

### 7.3.2 Recommendations for Future Research

During this research the irregularities considered were relatively simple in order to reduce the complexity the problem. It would be useful to pursue the following topics for future research:

1. In this research a totally separated delamination or vertical crack was considered. It would be interesting to study the response when a delamination or a vertical crack is in partial contact.

2. In the present study it was also assumed that the delamination or crack remained always open. The effect of the two edges getting in contact during the test should be investigated. This would give rise to some high frequency components.

3. In the high frequency range, the effect of aggregate size and reinforcement needs to be studied.

4. The delamination was assumed to be level (horizontal) in this study. It would be desirable to investigate the response of a pavement with an inclined or curved delamination.

5. For simplicity in this study delaminations, voids or cracks were assumed to occur separately, one at a time. In future work it would be desirable to study the effects of multiple delaminations, multiple voids, and multiple cracks, as well as combinations of these three types of irregularities.

# Bibliography


Bowen, B.R. (1992). "Damage Detection in Concrete Elements with Surface Wave Measurements." Dissertation submitted in partial fulfillment of the Doctor of Philosophy Degree, The University of Texas at Austin.

Chang, D.-W. (1991). "Nonlinear Effects on Dynamic Response of Pavements Using the Non-Destructive Testing Techniques." Dissertation submitted in partial fulfillment of the Doctor of Philosophy Degree, The University of Texas at Austin.

Chiang, C.C., J.M. Roësset and K.H. Stokoe, II (1994). "Effects of Irregularities on the Dynamic Response of Pavements in Non-Destructive Tests." *Proc. 8th IACMAG.*

Cotton, B.E. (1992). "Development of a Trailer-Mounted System to Delineate Irregularities in Rigid Pavements." Thesis submitted in partial fulfillment of the Master of Science Degree, The University of Texas at Austin.

Hinton, E., T. Rock and O.C. Zienkiewicz (1976). "A Note on Mass Lumping and Related Processes in the Finite Element Method." *Earthquake Engineering and Structural Dynamics*, Vol. 4, pp. 245-249.

Hirose, S. and M. Kitahara (1990). "BIEM for Solving the Scattering Problem by a Crack with Spring-Mass Contact." *BIEM* , Vol. 4, pp. 167-176.

Kang, Y.V. (1990). "Effect of Finite Width on Dynamic Defections of Pavements." Dissertation submitted in partial fulfillment of the Doctor of Philosophy Degree, The University of Texas at Austin.

Nogueira, A.C. (1986). "Effect of Cavities on the Propagation of Surface Waves." Thesis submitted in partial fulfillment of the Master of Science Degree, The University of Texas at Austin.

Nogueira, A.C., J.M. Roësset and J.L. Tassoulas (1994). "Effect of Cavities on the Propagation of Surface Waves." *Proc. 8th IACMAG.*

Roësset, J.M. (1980). "Computer Model for Soil Structure Interaction Analyses." *Proc. Century 2 Pressure Vessels & Piping Conference.*

Roësset, J.M., C.C. Chiang and A.C. Nogueira (1994). "Effect of Cavities on Wave Propagation: Formulation." *Proc. 8th IACMAG.*

Rosenblad, B.L. (1994). "Development of a Mobile Profiler Utilizing Stress Waves for Detection of Flaws in Rigid Pavements." Thesis submitted in partial fulfillment of the Master of Science Degree, The University of Texas at Austin (in progress).

Rosenblad, B.L., C.C. Chiang, K.H. Stokoe, II and J.M. Roësset (1994). "Nondestructive Evaluation of Subsurface Flaws in Rigid Pavements with Stress Waves." 1995 Annual Meeting of the Transportation Research Board (summitted for review).

Sansalone, M., and N.J. Carino (1988). "Impact-Echo Method." *Concrete International: Design and Construction,* Vol. 10, No. 4, April, pp. 38-46.

Sansalone, M., and N.J. Carino (1988). "Laboratory and Field Studies of the Impact-Echo Method for Flaw Detection in Concrete." *Nondestructive Testing,* SP-112, American Concrete Institute, Detroit, pp. 1-20.

Sansalone, M., and N.J. Carino (1989). "Detecting Delaminations in Concrete Slabs with and without Overlays Using the Impact-Echo Method." *ACI Materials Journal,* Vol. 86, No. 2, March-April, pp. 175-184.

Seng, C.-R. (1992). "Effect of Depth to Bedrock on Accuracy of Backcalculation Layer Moduli Obtained with Dynaflect and FWD Tests." Thesis submitted in partial fulfillment of the Master of Science Degree, The University of Texas at Austin.